Signal transmission in stochastic neuron models with non-white or non-Gaussian noise

D I S S E R T A T I O N

zur Erlangung des akademischen Grades

doctor rerum naturalium
(Dr. Rer. Nat.)
im Fach Physik
Spezialisierung: Theoretische Physik

eingereicht an der
Mathematisch-Naturwissenschaftlichen Fakultät
Humboldt-Universität zu Berlin

von
Dipl. Phys. Felix Droste

Präsident der Humboldt-Universität zu Berlin:
Prof. Dr. Jan-Hendrik Olbertz

Dekan der Mathematisch-Naturwissenschaftlichen Fakultät:
Prof. Dr. Elmar Kulke

Gutachter:
1. Prof. Dr. Benjamin Lindner (HU Berlin)
2. Prof. Dr. Lutz Schimansky-Geier (HU Berlin)
3. Prof. Dr. Magnus Richardson (U Warwick, GB)

Tag der mündlichen Prüfung: 8. Juli 2015

Zusammenfassung

Die vorliegende Arbeit befasst sich mit dem Einfluss von nicht-weißem oder nicht-Gauß'schem synaptischen Rauschen auf die Informationsübertragung in stochastischen Neuronenmodellen. Ziel ist es, zu verstehen, wie eine Nervenzelle (Neuron) ein Signal in ihrer Pulsaktivität kodiert. Synaptisches Rauschen beschreibt hier den Einfluss anderer Nervenzellen, die nicht das interessierende Signal tragen, wohl aber seine Übertragung durch ihre synaptische Wirkung auf die betrachtete Zelle beeinflussen. In stochastischen Neuronenmodellen werden diese zahlreich und scheinbar zufällig auftretenden Pulse durch einen stochastischen Prozess mit geeigneter Statistik beschrieben. Ist die Rate, mit der präsynaptische Pulse auftreten, hoch und zeitlich konstant, die Wirkung einzelner Pulse aber verschwindend gering, so wird das synaptische Rauschen durch einen Gauß'schen Prozess beschrieben. Um ein mathematisch handhabbares Modell zu erhalten wird oft zudem die sogenannte Diffusions-Approximation (DA) benutzt, d.h. angenommen, dass das Rauschen unkorreliert (weiß) ist. In der vorliegenden Arbeit wird neuronale Signalübertragung in dem Fall untersucht, dass eine solche Näherung nicht mehr gerechtfertigt ist, d.h. wenn der synaptische Hintergrund durch einen stochastischen Prozess beschrieben werden muss, der nicht weiß, nicht Gauß'sch, oder weder weiß noch Gauß'sch ist.

Mittels Simulationen und analytischer Rechnungen werden drei Szenarien behandelt: Zunächst betrachten wir eine Zelle, die nicht ein, sondern zwei Signale empfängt, welche zusätzlich durch synaptische Kurzzeitplastizität (*synaptic short-term plasticity*; STP) gefiltert werden. In diesem Fall muss der Hintergrund durch ein farbiges Rauschen beschrieben werden. Im zweiten Szenario betrachten wir den Fall, dass der Effekt einzelner Pulse nicht mehr als schwach angenommen werden kann. Das Rauschen ist dann nicht mehr Gauß'sch, sondern ein Schrotrauschen (*shot noise*; SN). Schließlich untersuchen wir den Einfluss einer präsynaptischen Population, deren Feuerrate nicht zeitlich konstant ist, sondern zwischen Phasen hoher und niedriger Aktivität, sogenannten *up* und *down states*, springt. In diesem Fall ist das Rauschen weder weiß noch Gauß'sch.

In allen drei Fällen interessieren wir uns für den Einfluss des Hintergrunds auf die Informationsübertragung, welche wir mittels der Kohärenzfunktion, einem frequenzaufgelösten Maß, quantifizieren. Diese erlaubt es zu beurteilen, wie verschiedene Frequenzkomponenten des Signals im neuronalen Pulszug kodiert werden. Sie ermöglicht außerdem, eine untere Schranke für die Transinformationsrate zu bestimmen.

Im ersten Teil untersuchen wir ein Neuron, das gleichzeitig zwei Signale empfängt. Wir nehmen an, dass die Synapsen des Neurons unterschiedliche Arten von Kurzzeitplastizität aufweisen: Die Pulszüge, in denen das erste Signal kodiert ist, beeinflussen die Zelle durch faszilitierende Synapsen, jene, in denen das zweite Signal kodiert ist, durch deprimierende Synapsen. Da die Signale eine zeitliche Struktur aufweisen und zudem durch die STP-Dynamik gefiltert werden, haben wir es hier mit einem farbigen Rauschen zu tun. Wie wir zeigen, kann die Anwesenheit eines zweiten Signals die Filtereigenschaften des Neuron ändern (hin zu einem frequenzselektiven Verhalten). Das zweite Signal kann der Übertragung des ersten sogar förderlich sein. Dies ist eine neuartige Form von stochastischer Resonanz (SR).

Im Folgenden leiten wir analytische Resultate für Integratorneurone (*integrate-and-fire* oder IF-Neurone) her, die durch Markov'sches dichotomes Rauschen (einen Zwei-Zustands-Prozess) getrieben werden. Diese stellen den seltenen Fall eines exakt lösbaren, von farbigem, nicht-Gauß'schem Rauschen getriebenen Systems dar. Wir erhalten Ausdrücke für die stationäre Spannungsverteilung und die Momente der Interspike-Intervall-Verteilung (der Verteilung der Intervalle zwischen Pulsen). Für

den Fall von Integratorneuronen mit Leckstrom (*leaky integrate-and-fire* oder LIF-Neurone) berechnen wir das Leistungsspektrum und die Suszeptibilität, zwei spektrale Maße, die es ermöglichen, mittels der Kohärenzfunktion die Informationsübertragung zu studieren. Diese Resultate bilden die Grundlage für die theoretischen Untersuchungen der verbleibenden zwei Szenarien.

Dichotomes Rauschen schließt als Grenzfall weißes, exzitatorisches Schrotrauschen mit exponentiell verteilten Gewichten ein. Dies machen wir uns zunutze, um zu untersuchen, wie nicht verschwindende synaptische Gewichte die Signalübertragung beeinflussen (verglichen mit der DA). Als einen Haupteffekt von SN finden wir eine Zu- oder Abnahme der Ausgangsfeuerrate, welche für niedrigen mittleren Eingangsstrom höher, für hohen mittleren Eingangsstrom hingegen niedriger ist als in der DA. Außerdem ist die Antwort auf hochfrequente strommodulierte Signale qualitativ von der DA verschieden: mit einem SN-Hintergund fällt die Suszeptibilität schneller ab. Dennoch kann ein solcher, aufgrund der erhöhten Feuerrate bei niedrigem mittleren Eingangsstrom, vorteilhaft für die Informationsübertragung sein.

Wir verallgemeinern die Resultate für dichotomes Rauschen mittels einer quasistatischen Näherung auf den realistischeren Fall, dass zusätzliche schnelle Fluktuationen um die Zustände auftreten. Hierdurch erhalten wir analytische Ausdrücke für ein Neuron, dessen Eingangsfeuerrate zwischen zwei diskreten Niveaus springt – ein einfaches Modell für up und down states. Wir betrachten die Übertragung eines schwachen Signals vor einem solchen up-down (UD) Hintergrund und vergleichen sie mit einem Hintergrund mit zeitlich konstanter Feuerrate. Hier finden wir, dass ein UD-Hintergrund zu einem Bandpass-Informationsfilter führt. Wenn die zeitlich gemittelte Feuerrate des Hintergrunds niedrig ist, kann ein UD-Hintergrund auch vorteilhaft für die Informationsübertragung sein. Wir zeigen, dass dies mit einer Erhöhung der Ausgangsfeuerrate einhergeht und als SR-Effekt interpretiert werden kann, und diskutieren, unter welchen Bedingungen ein UD-Hintergrund sogar bei festgehaltener Ausgangsfeuerrate vorteilhaft sein könnte.

Abstract

This thesis is concerned with the effect of non-white or non-Gaussian synaptic noise on the information transmission properties of single neurons. Synaptic noise subsumes the massive input that a cell receives from thousands of other neurons. In the framework of stochastic neuron models, this input is described by a stochastic process with suitably chosen statistics. If the overall arrival rate of presynaptic action potentials is high and constant in time and if each individual incoming spike has only a small effect on the dynamics of the cell, the massive synaptic input can be modeled as a Gaussian process. For mathematical tractability, one often assumes that furthermore, the input is devoid of temporal structure, i.e. that it is well described by a Gaussian white noise. This is the so-called diffusion approximation (DA). The present thesis explores neuronal signal transmission when the conditions that underlie the DA are no longer met, i.e. when one must describe the synaptic background activity by a stochastic process that is not white, not Gaussian, or neither.

We explore three distinct scenarios by means of simulations and analytical calculations: First, we study a cell that receives not one but two signals, additionally filtered by synaptic short-term plasticity (STP), so that the background has to be described by a colored noise. The second scenario deals with synaptic weights that cannot be considered small; here, the effective noise is no longer Gaussian and the shot-noise nature of the input has to be taken into account. Finally, we study the effect of a presynaptic population that does not fire at a rate which is constant in time but instead undergoes transitions between states of high and low activity, so-called up and down states.

In all cases, we are interested in the information transmission properties of the neuron, which we quantify using a frequency-resolved measure, the spectral coherence between a signal and the cell's output spike train. This allows to assess how different frequency components of the signal are encoded in the output spike train. It also provides a lower bound on the total rate of information transmission about the signal and allows to explore how this rate depends on the properties of the synaptic noise.

In a first part, we study a neuron that simultaneously receives two signals. We assume that synapses differ in the kind of STP they exhibit: One signal is encoded in spike trains impinging on the neuron through facilitating synapses, the other through depressing synapses. Here, either signal can be considered a source of noise with respect to the transmission of the other signal. As signals are temporally structured and additionally filtered by STP, this noise is not white but colored. We find that the presence of a second signal can switch the coherence from broadband to frequency selective and that a second signal may help the transmission of the first, a novel form of stochastic resonance (SR).

Subsequently, we derive analytical results for integrate-and-fire (IF) neurons driven by Markovian dichotomous noise, a two-state process and the rare case of a non-Gaussian colored noise that allows exact solution. Specifically, we derive expressions for the stationary voltage density, the moments of the interspike interval density, and, in the case of leaky IF neurons, for the power spectrum and the susceptibility, two spectral measures that allow to study information transmission using the coherence. These results form the basis for the theoretical study of the two remaining scenarios.

We exploit a limit case of dichotomous noise to derive exact expressions for an IF neuron driven by excitatory shot noise (SN) with exponentially distributed weights. These expressions are then used to investigate how finite spike weights change information transmission properties compared to the DA. We find that SN input leads to firing rates that are increased when the mean input is low, but decreased when it is high. Additionally, the response to high frequency components of a current-

modulated signal is qualitatively different from the DA: with an SN background, the susceptibility decays faster. Nevertheless, due to the increased firing rates at low mean input, a background with non-vanishing spike weights can be advantageous for information transmission.

Employing a quasi-static approximation, we extend the results for dichotomous noise to a more realistic case that takes fluctuations around the two states into account. We thereby obtain expressions for a neuron that receives synaptic background input with a firing rate that switches between two levels – a simple model of up and down states. Considering a setup where a sensory signal is transmitted either with an up-down (UD) background or a background with a firing rate that is constant in time, we find that an UD background leads to a band-pass coherence and can yield higher information rates when input firing rates are low. We show that this is due to an increase in output firing rate and can be considered an SR effect. Further, we briefly discuss under which conditions an UD background could be beneficial to information transmission even at fixed output firing rates.

Contents

Chapter 1.

Introduction

It is a central tenet of neuroscience that neurons communicate via stereotypical pulses, so called *spikes*. Spikes are excursions of the electrical potential that nerve cells maintain across their membrane, and the effect that a cell exerts upon others through these pulses is thought to underlie all neuronal information processing, from the forwarding of sensory input to the emergence of conscious thought. As shape and amplitude of spikes are stereotypical, information must be carried in their timing. How this "language of the brain" is to be deciphered, how, for example, a certain stimulus is encoded in the spiking activity of single neurons or complex neural networks, is a largely unsolved problem.

A theoretical framework that allows to investigate neuronal signal transmission in a model-free way is provided by information theory, pioneered by Shannon. It allows to infer transmission properties of neurons without the need to assume a particular code. Information-theoretical measures have been applied successfully to the study of signal transmission in single neurons both in models and experiments. The basic setting is the following: An input signal is presented (an animal is shown a certain stimulus, a time varying signal is fed into a simulated neuron) and the output of the neuron – the spike train – is recorded. One can then calculate the mutual information between the signal and the spike train. This allows to judge which system parameters or signal statistics have an impact on information transmission and to test hypotheses about the neural code.

Most studies that use information-theoretical measures to assess signal transmission through a single neuron have concentrated on neurons in the sensory periphery, which receive no synaptic inputs from other neurons. In this case, signal transmission is only hampered by noise that is intrinsic to the neuron and which can usually be well described by Gaussian white noise. Similarly, studies that consider information transmission in later processing stages, in which neurons receive massive synaptic input from other cells, often use the so-called diffusion approximation: They assume that the network activity that is unrelated to the signal can be described as Gaussian white noise.

The aim of the present thesis is to extend the analysis of neural information transmission to some scenarios where the background noise is *not* well described by a Gaussian white noise. We consider the transmission of a signal in three different scenarios:

1. The background includes a second signal. This is certainly a common situation, arising for instance in so-called multisensory integration, the combined processing of stimuli from different sensory modalities such as seeing and hearing. In general, such a signal has a temporal structure and the background can thus not be considered white.
2. The contribution of individual background spikes is not negligibly small. In this case, the assumptions underlying the diffusion approximation are no longer met,

and the shot-noise nature of the background has to be taken into account — the background is non-Gaussian.

3. The population of neurons that provide the background input switches stochastically between two different levels of activity, so-called up and down states. In this case, the background is neither white nor Gaussian.

The tools we use to gain insights into these scenarios stem mostly from statistical physics; in particular, we describe signals and neuronal firing by stochastic processes. Stochastic processes suggest themselves as an adequate level of description because information theory is formulated in terms of statistical ensembles and neuronal firing has been shown to be highly variable (even when the input is fixed). Our aim is to build models that are simple enough to allow insights into general phenomena and mechanisms. Wherever possible, we strive for analytical tractability; in other cases as well, as for the verification of theoretical results, we use computer simulations. Framed in the language of statistical physics, our objective lies in studying signal transmission through non-linear systems driven by certain kinds of colored or non-Gaussian noise. This perspective does not only open up a rich literature to be used, but also suggests that analytical results may be of relevance in other areas of statistical physics.

This thesis is organized as follows: The remainder of this chapter consists of brief introductions to basic neurophysiological facts and concepts (neuronal spiking, synaptic transmission, neural variability, rate coding of signals), theoretical approaches to modeling and classifying neural activity, elementary concepts of information theory, and the functional role of neuronal noise. Introductions to the more specific neurobiological topics – multisensory integration, short-term synaptic plasticity, cortical up and down states – will be given in the chapters where they are relevant.

In Chapter 2, we consider a neuron that simultaneously receives two signals, encoded in the instantaneous firing rates of two presynaptic populations that connect to the target cell via synapses with different kinds of short-term synaptic plasticity. Here, we find that the presence of a second signal can non-trivially change neuronal information filtering properties. Furthermore, the presence of a second signal may be advantageous to the transmission of the first, through a novel form of stochastic resonance.

In Chapter 3, we develop a theory for integrate-and-fire (IF) neurons driven by asymmetric dichotomous noise, a non-Gaussian colored noise. We derive exact expressions for the stationary probability density, moments of the interspike interval density, as well as (for leaky IF neurons) the power spectrum and the susceptibility. These results form the theoretical backbone of the studies carried out in the following chapters.

Chapter 4 is concerned with information transmission in a leaky integrate-and-fire (LIF) neuron that is subject to excitatory shot noise with exponentially distributed weights. Building upon the results derived in the previous chapter, we compare this setting to the diffusion approximation and discuss the effect that such a non-Gaussian noise has on signal transmission.

As a preparatory step for the modeling of up and down states, we develop in Chapter 5 approximations for two-state input with additional stochasticity within the states. We extensively compare various approximations to simulations and find them to yield decent results for realistic ranges of parameter values.

Finally, in Chapter 6, we consider the transmission of a weak signal in the face of a

background that undergoes transitions between up and down states. We contrast this case to a background in an asynchronous-irregular regime and find that at low mean input rates, an up-down regime may be favorable to information transmission.

Some of the results in this thesis have been published in two papers. The results in Chap. 2 have been published in (Droste et al., 2013). The results on general IF neurons driven by asymmetric dichotomous noise (Chapter 3) have been published in (Droste and Lindner, 2014). The expressions for power spectrum and susceptibility in Chap. 3, the results on signal transmission in the presence of up/down states (Chapter 5 and Chapter 6), and the theory for exponentially correlated shot noise input (Chapter 4) are so far unpublished (note, however, that some of the latter results have been obtained by Richardson and Swarbrick (2010) using a different approach).

1.1. Neurophysiological background

Here, we give a very short overview over some central biological facts. Much more detailed introductions can, for instance, be found in the text books by Johnston et al. (1995) and Kandel et al. (2000).

Neural spiking and synaptic transmission

Neurons maintain an electrical potential across their membrane. This is achieved by means of ion pumps – proteins that transport ions across the cell membrane (and across a concentration gradient) in exchange for metabolic energy, leading to a net negative charge of the cell's interior. Other proteins, voltage-gated ion channels, make the neuron excitable: When a depolarization makes the voltage cross a certain threshold, it leads to a large excursion of the membrane potential, the so-called *action potential* or spike.

The morphology of neurons can be very complex (see Fig. 1.1 for a simplified sketch). On a coarse level, three parts can be distinguished: The *soma* (cell body), a *dendritic arbor*, and the *axon*. A spike that originates in the soma travels along the axon until it reaches the axon terminals. Most axon terminal are located close to a dendrite of another neuron, forming part of a *synapse*, the (one-way) connection between two neurons.

An action potential arriving in the *presynaptic* axon terminal may lead to the release of vesicles filled with neurotransmitter into the *synaptic cleft* (see Fig. 1.2). The release of neurotransmitter is not deterministic – an action potential may fail to release vesicles – and the probability of release depends on the history of presynaptic spikes in the immediate past. This usage-dependence of synaptic efficacy is termed *synaptic short-term plasticity*; it will be introduced in detail in Chapter 2. Once neurotransmitter is released into the synaptic cleft, it may dock onto channels in the *postsynaptic* neuron's cell membrane, causing them to open and increase the membrane's permeability with respect to a particular type of ion. Depending on the type of synapse and the postsynaptic voltage, this leads to a depolarization or a hyperpolarization of the postsynaptic cell, either exciting or inhibiting it.

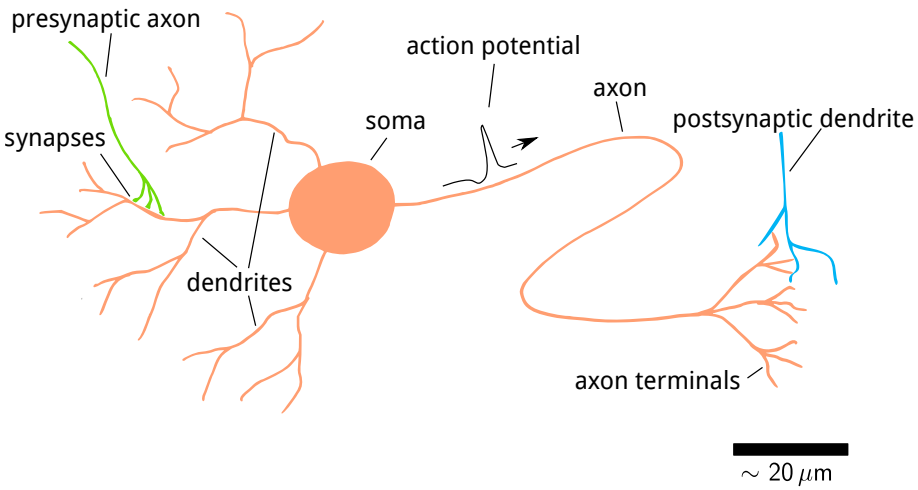

Figure 1.1.: Sketch of a neuron. Action potentials that travel along presynaptic axons impinge via synapses on the dendrites of the cell. The induced changes in membrane voltage propagate to the soma. If the voltage at the soma crosses a certain threshold, a new action potential is generated and travels along the axon. In the axon terminals, it can induce the release of neurotransmitter and thereby synaptically exert an effect on postsynaptic cells.

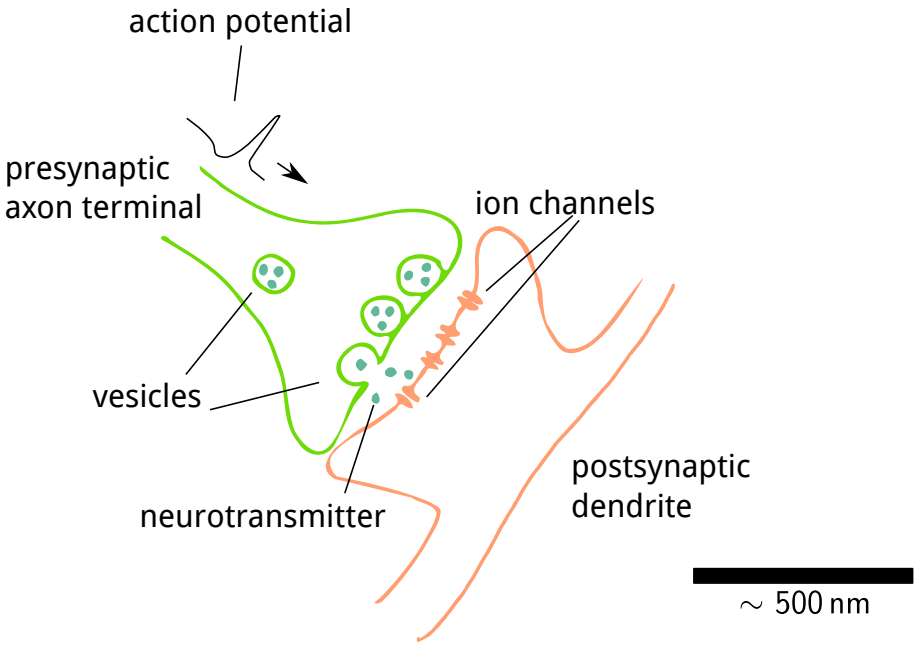

Figure 1.2.: Sketch of a synapse. Upon the arrival of a presynaptic action potential, docked (release-ready) vesicles may fuse with the cell membrane, releasing neurotransmitter into the synaptic cleft. When this neurotransmitter docks onto receptors in the postsynaptic membrane, it causes ion channels to open and may thereby affect the postsynaptic membrane voltage.

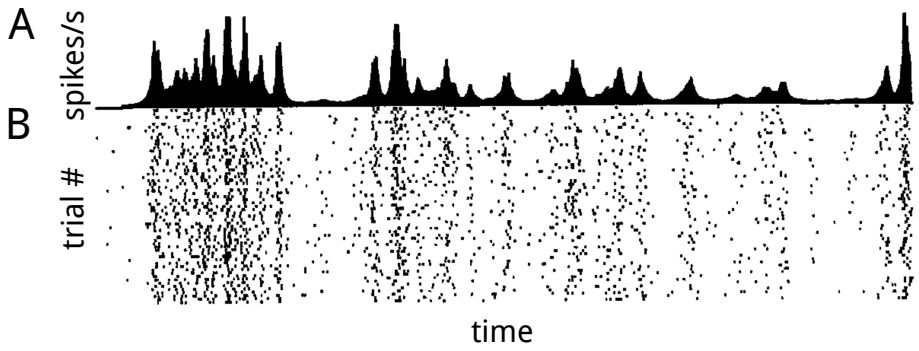

Figure 1.3.: Neural firing is variable: Response of a neuron in cortical area MT of the macaque to repeated trials of the same moving visual stimulus. The spike times for different trials are marked as dots in B, the rate of their of spiking in short time bins is shown in A. Adapted from (Bair and Koch, 1996). © 1996, Massachusetts Institute of Technology.

Neural variability

Various electrophysiological techniques enable an experimenter to measure the spiking activity of a cell (potentially while injecting a current). Measuring such activity – either in vivo or in vitro – over repeated trials shows neural spiking to be highly variable, within or across trials (for an example see Fig. 1.3) It is intriguing that brains are capable of fast and precise computation, even though neurons are noisy.

There are three main sources of *neural noise*: Channels in the cell membrane open and close stochastically (with rates that depend on quantities such as the membrane voltage or the concentration of neurotransmitter). As there is a finite number of channels, each of which contributes a finite conductance when it is open, this leads to fluctuations in the total conductance; it is referred to as *channel noise* (White et al., 2000). Two other important sources of noise are related to synaptic input: When an action potential arrives at a presynaptic terminal, the number of vesicles it releases is random, and it may fail to release any vesicles at all; one speaks of *synaptic unreliability* (Allen and Stevens, 1994). Further, a typical cortical neuron is subject to a constant *bombardment* of synaptic input from thousands of other neurons. In most situations, the arrival times of spikes can be considered stochastic. This is called *synaptic noise*[1] and is the dominant source of noise in cortical neurons (Destexhe and Rudolph-Lilith, 2012). We will revisit it in Sec. 1.2.2 when we discuss the modeling of neuronal input.

Spike trains and signals

The sequence of action potentials emitted by a cell is called its *spike train*. A useful quantity to characterize a spike train is the firing rate. This is sometimes understood with respect to a time window of length T; the rate is then the number of spikes in that time window divided by T. Following Dayan and Abbott (2001), we call this the *spike-count rate*.

Alternatively, one can consider a *time-dependent* or *instantaneous firing rate*. In an exper-

[1] The name is somewhat unfortunate as it invites confusion with synaptic unreliability; it is, however, the established terminology.

iment, this can be estimated by presenting the same stimulus over multiple trials. One may then discretize the time axis into sufficiently short bins. The rate in a given bin then corresponds to the fraction of trials in which the neuron has fired within that bin divided by the bin length (see Fig. 1.3A).

It has long been known that neurons can encode stimuli in their firing rate. Adrian and Zotterman (1926) hung weights on frog muscles and observed that the spike-count rate was a monotonic function of the weight. Following the seminal works by Barlow (1953) and Hubel and Wiesel (1962), countless researchers have mapped out visual receptive fields, i.e. they have measured the spike-count rate of neurons in response to the presentation of different classes of visual stimuli (see the textbook by Rieke et al. (1996) for a historic account).

Owing to their respective experimental paradigms, the above studies found information to be coded in the spike-count rate (because they considered static stimuli); however the concept of rate-coding can naturally be extended to time-varying stimuli, by assuming that the signal is encoded (uniquely) in the time-dependent firing rate. Information theoretic measures, which we will introduce below, provides a way to investigate the encoding of a signal without making such an assumption (de Ruyter van Steveninck et al., 1997; Rieke et al., 1996).

1.2. Mathematical modeling of stochastic neural activity

In this section, we introduce theoretical concepts that allow to classify and model neural activity. We start by defining useful measures in the framework of stochastic processes and afterwards introduce models for spiking neurons. We take the liberty to disregard this clear separation by introducing a simple model of neural spiking right away: the inhomogeneous Poisson process, which will be useful to illustrate the measures as we introduce them. In-depth introductions to concepts and methods used in theoretical neuroscience can, for example, be found in the text books by Rieke et al. (1996); Dayan and Abbott (2001); Gerstner et al. (2014).

1.2.1. Definition of some important measures

The output of a neuron, its spike train, is completely determined by the spike times. Mathematically, it is convenient to model a spike train as a superposition of Dirac delta functions,

$$x(t) = \sum_i \delta(t - t_i), \tag{1.1}$$

where $\{t_i\}$ are the spike times. Motivated by the observed variability of neural spiking, it is useful to consider a spike train a stochastic process (a point process). A particular set of spike times is then a realization of that process (out of an ensemble).

The *instantaneous firing rate* can be written as the first moment of the spike train,

$$r(t) = \langle x(t) \rangle , \tag{1.2}$$

where $\langle \cdot \rangle$ denotes ensemble averaging.

One of the simplest models of neural spiking is the *inhomogeneous Poisson process*. This process is completely defined by prescribing a time-dependent firing rate $r(t)$ and demanding that the probability that a spike occurs at a given time is independent of whether or not spikes occur at other times. A way to approximate such a process is to discretize the time axis into bins of length Δt, drawing a uniformly distributed random number $R_i \sim \mathcal{U}(0,1)$ for each bin and registering a spike whenever $R_i < \Delta t \cdot r(i \cdot \Delta t)$. For $\Delta t \to 0$, this yields an inhomogeneous Poisson Process. A *homogeneous* Poisson process is obtained when the firing rate is constant in time, $r(t) \equiv r_0$.

A stochastic process is called *stationary* if its moments do not depend on absolute time (but only time differences). Clearly, an inhomogeneous Poisson process that encodes a time-varying signal is not stationary. We can, however, consider the signal a stochastic process as well: Usually, we do not know which particular realization of a stimulus a neuron is bound to encounter; we can, at best, make statements about the statistics the stimulus will obey. If the signal process is stationary, then, by considering not only the spike-train ensemble (conditioned on a particular stimulus) but also the ensemble of stimuli, we are again dealing with a stationary process.

A stationary spike train with spike times $\{t_i\}$ can also be thought of as a sequence of *interspike intervals* (ISIs),

$$T_i = t_i - t_{i-1}, \tag{1.3}$$

that are drawn from a certain distribution $\rho(T)$. ISIs in a sequence will in general be correlated; if, by contrast, they are independent, then the spike train is a *renewal process*. The mean ISI is related to the *stationary firing rate* r_0,

$$\langle T \rangle = \frac{1}{r_0}. \tag{1.4}$$

A useful measure to quantify the irregularity of a spike train is the *coefficient of variation* (CV)

$$C_V = \frac{\sqrt{\langle \Delta T^2 \rangle}}{\langle T \rangle}, \tag{1.5}$$

with $\Delta T = T - \langle T \rangle$.

Turning back to the example of a (homogeneous) Poisson process, it is straightforward to show that the ISI distribution is exponential,

$$\rho(T) = r_0 e^{-r_0 T}, \tag{1.6}$$

and that the $C_V = 1$. The Poisson process thus often serves as a reference when assessing the regularity of spiking – spike trains with a $C_V < 1$ ($C_V > 1$) are more (less) regular than a Poisson process.

The *auto-correlation function* of a stationary spike train is defined as

$$\mathcal{K}_{xx}(\tau) := \langle x(t)x(t+\tau) \rangle - \langle x(t) \rangle^2 . \tag{1.7}$$

This can expressed via the joint probability density $P(t_1, t_2)$, where $P(t_1, t_2)dt^2$ gives the

probability to observe a spike in the time interval $(t_1, t_1 + dt)$ and a spike in $(t_2, t_2 + dt)$ (the marginal probability density $P(t_1)$ and the conditional density $P(t_1|t_2)$ are defined analogously). One has

$$\begin{aligned}
\mathcal{K}_{xx}(\tau) &= P\Big(\text{spike at } t \text{ , spike at } t+\tau\Big) - r_0^2 \\
&= P\Big(\text{spike at } t\Big)\, P\Big(\text{spike at } t+\tau \;\Big|\; \text{spike at } t\Big) - r_0^2 \\
&= r_0 \left[\delta(\tau) + P\Big(\text{different spike at } t+\tau \;\Big|\; \text{spike at } t\Big)\right] - r_0^2 \\
&= r_0 \left[\delta(\tau) + m(\tau)\right] - r_0^2,
\end{aligned} \tag{1.8}$$

where $m(\tau)$ is the *spike-triggered rate*, i.e. the probability that after a reference spike at time t, there is a different spike at time $t + \tau$ (this does not need to be the first spike after the reference spike). For a (homogeneous) Poisson process, $m(\tau) = r_0$, and thus $\mathcal{K}_{xx}(\tau) = r_0\delta(\tau)$.

One can also study second-order statistics in the Fourier domain. For a stationary process, the *power spectrum* is the Fourier transform of the correlation function,

$$S_{xx}(f) = \int_{-\infty}^{\infty} d\tau\; e^{2\pi i f \tau} \mathcal{K}_{xx}(\tau). \tag{1.9}$$

This relation is the so-called Wiener-Khinchin theorem (Gardiner, 1985; Risken, 1989). A different definition of the power spectrum, which is more easily calculated in simulations, is

$$\delta(f - f') S_{xx}(f) = \left\langle \widetilde{x}(f) \widetilde{x}^*(f') \right\rangle, \tag{1.10}$$

where the tilde denotes the Fourier transform (defined as in eq. (1.9)), and the asterisk denotes complex conjugation. In simulations we have to use finite time windows; there, we use the Fourier transform

$$\widetilde{x}_T(f) = \int_0^T dt\; e^{2\pi i f t} x(t) \tag{1.11}$$

and approximate the power spectrum as

$$S_{xx}(f) = \frac{1}{T} \left\langle \widetilde{x}_T(f) \widetilde{x}_T^*(f') \right\rangle. \tag{1.12}$$

For a renewal spike train, the power spectrum is related to the Fourier transform of the

ISI density (Stratonovich, 1967),

$$S_{xx}(f) = r_0 \frac{1 - |\widetilde{\rho}(f)|^2}{|1 - \widetilde{\rho}(f)|^2}. \tag{1.13}$$

From eq. (1.13), it can be shown that the limit of vanishing frequency of a renewal spike train is given by

$$\lim_{f \to 0} S_{xx}(f) = r_0 C_V^2. \tag{1.14}$$

For spike-train auto-correlation functions which contain no δ-peak except the one at $\tau = 0$ [2], the high-frequency limit of the power spectrum is

$$\lim_{f \to \infty} S_{xx}(f) = r_0. \tag{1.15}$$

Turning again to the example of a (homogeneous) Poisson spike train, the power spectrum is

$$S_{xx}(f) \equiv r_0 \tag{1.16}$$

(the process has equal power at all frequencies, it is *white*), which is consistent with the two limits.

The definitions eq. (1.7), eq. (1.9), eq. (1.10), and eq. (1.12) generalize to the case where one considers *two* processes $s(t)$ and $x(t)$. One has the *cross-correlation*,

$$\mathcal{K}_{sx}(\tau) = \langle s(t)x(t+\tau)\rangle - \langle s(t)\rangle \langle x(t)\rangle , \tag{1.17}$$

and the corresponding *cross spectrum*,

$$\delta(f - f')S_{sx}(f) = \left\langle \widetilde{s}(f)\widetilde{x}^*(f')\right\rangle . \tag{1.18}$$

When the influence of a signal $s(t)$ on the spike train $x(t)$ is weak, one may use linear response theory to calculate the cross spectrum: Conditioned on the signal, the first moment of $x(t)$ (the firing rate) is time-dependent. Linear response theory assumes that the effect of the signal on this rate is captured by convolution with a kernel $K(\tau)$,

$$r(t) = \langle x(t)\rangle \approx r_0 + \int_{-\infty}^{\infty} d\tau \; K(\tau)s(t-\tau), \tag{1.19}$$

where $K(\tau)$ is causal, i.e. $K(\tau < 0) = 0$. In Fourier space, the convolution turns into a multiplication, so that, for $f \neq 0$,

$$\widetilde{r}(f) = \langle \widetilde{x}(f)\rangle = \chi(f)\widetilde{s}(f) \tag{1.20}$$

where $\chi(f)$ is the *susceptibility*. From eq. (1.18) and eq. (1.20), one finds that in linear

[2] In Chapter 3, we will encounter a spike-train correlation function that falls outside of this class.

response

$$S_{sx}(f) \approx \chi^*(f) S_{ss}(f), \tag{1.21}$$

where $S_{ss}(f)$ is the signal power spectrum.

A measure that will be widely used in the present thesis is the *coherence function*,

$$C_{sx}(f) = \frac{|S_{sx}(f)|^2}{S_{xx}(f) S_{ss}(f)}. \tag{1.22}$$

The coherence is a measure between zero and one; it can be thought of as a correlation coefficient in frequency space. In the neural context, it quantifies how well certain frequency components of the signal can be linearly reconstructed from the spike train. We will come back to this measure when introducing information-theoretic concepts.

1.2.2. Spiking neuron models

Conductance-based models

A very successful approach in modeling neuron dynamics, going back to the seminal work of Hodgkin and Huxley (1952), consists in modeling the currents through a small patch of cell membrane. The time evolution of the membrane potential v is governed by

$$C\dot{v} = \sum_k I_k, \tag{1.23}$$

where C is the membrane capacitance and the sum on the r.h.s. runs over the different populations of ion channels. The current through a particular population is given by

$$I_k = -g_k(v - E_k). \tag{1.24}$$

The current depends on the conductance and the *driving force* $v - E_k$, where E_k is the *reversal potential* at which the flux of ions due to diffusion is exactly balanced by the flux due to the electric field. The conductance g_k reflects the number of open channels and their inherent conductance; it will in general nonlinearly depend on v or the concentration of neurotransmitter. The model by Hodgkin and Huxley (1952), for example, consists of a set of four differential equations which, aside from the voltage, model the dynamics of potassium (K^+) and sodium (Na^+) conductances that are responsible for the generation of the action potential.

A simple model for the currents due to synaptic inputs assumes that the release of neurotransmitter leads to an instantaneous jump in conductance, followed by an exponential decay (channels are assumed to open rapidly and then close at a fixed rate). Assuming that synapses are perfectly reliable and only differ in being either excitatory or inhibitory one has

$$I_{syn} = -g_E(v - E_E) - g_I(v - E_I), \tag{1.25}$$

$$\tau_E \dot{g_E} = -g_E + \tau_E c_E \sum_i \delta(t - t_i), \tag{1.26}$$

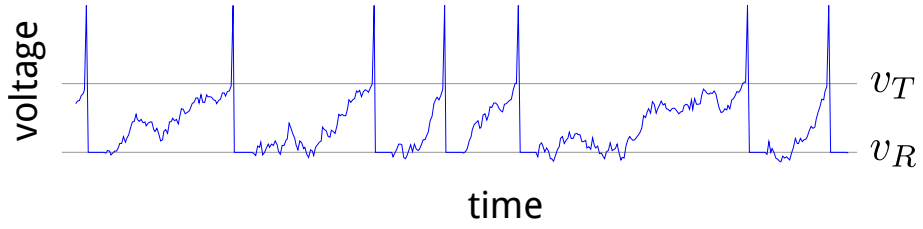

Figure 1.4.: Voltage time-course of an LIF neuron. The spikes at threshold crossings are shown for the purpose of illustration; the model does not dynamically generate spikes.

$$\tau_I \dot{g_I} = -g_I + \tau_I c_I \sum_j \delta(t - t_j). \tag{1.27}$$

Here, $\{t_i\}$ ($\{t_j\}$) is the set of spike times of presynaptic excitatory (inhibitory) neurons, c_E (c_I) the jump in conductance induced by a presynaptic AP, τ_E (τ_I) the synaptic time constant and E_E (E_I) the reversal potential. Note that eq. (1.25) to eq. (1.27) represent an effectively one-dimensional model; the evolution equations for the conductances are just filters that implement the convolution of presynaptic δ-spikes trains with exponentials.

The expression for the synaptic current can be combined with a leak current to yield the description of a *passive* patch of membrane

$$C\dot{v} = -g_L(v - E_L) - g_E(v - E_E) - g_I(v - E_I). \tag{1.28}$$

Here, passive refers to the absence of the voltage-gated ion channels that are responsible for the generation of the action potential. In the absence of synaptic inputs, ions can still cross the membrane (captured by the constant leak conductance) and the voltage exponentially decays to its resting potential (the leak reversal potential E_L). The leak potential is typically far below the excitatory reversal potential and somewhat above the inhibitory reversal potential, so that an excitatory input depolarizes the membrane potential while an inhibitory input hyperpolarizes it.

Integrate-and-fire models

The simple yet surprisingly successful class of IF models is based on two drastic assumptions:

1. The spatial organization of the neuron can be neglected; channels (and synaptic inputs) are distributed isotropically. Effectively, one deals with a *point neuron* that is fully described by its membrane voltage.
2. The voltage-gated ion channels (and thus the generation of the AP) do not need to be modeled explicitly; instead, APs are introduced into the model through a fire-and-reset rule: whenever a threshold voltage v_T is crossed, a spike is registered. The voltage is then reset to a value v_R and, after an absolute *refractory period* τ_{ref}, the sub-threshold dynamics continue (see Fig. 1.4).

IF models can be traced back to Lapicque (1907), and have since played a crucial role in shaping the way we think about neuronal integration of inputs. They have been used in numerous studies, both in simulations and analytical work (reviewed by Burkitt

(2006a,b)). IF neurons have allowed to obtain insights into the spontaneous activity of single neurons (Gerstein and Mandelbrot, 1964; Stein, 1965; Lindner et al., 2002), the effect of input correlations on firing statistics (Brunel and Sergi, 1998; Fourcaud and Brunel, 2002; Salinas and Sejnowski, 2002; Brunel and Latham, 2003; Middleton et al., 2003; Moreno et al., 2002; Schwalger and Schimansky-Geier, 2008), the signal transmission properties of single neurons (Stein et al., 1972; Brunel et al., 2001; Lindner and Schimansky-Geier, 2001; Fourcaud and Brunel, 2002; Richardson, 2007), the transmission of synchronous pulses or rate-coded signals through networks (Diesmann et al., 1999; Kumar et al., 2010; Vogels and Abbott, 2005), or the different dynamical regimes of large neural networks (Brunel, 2000). IF models have also proven able to reproduce experimentally measured statistics (Gerstein and Mandelbrot, 1964; Fisch et al., 2012; Bauermeister et al., 2013) and even individual voltage traces and spike times (Badel et al., 2008).

The *conductance-based LIF* model (Destexhe et al., 2001) consists in starting from the evolution equation for the passive patch of membrane eq. (1.28), adding a fire-and-reset rule and proclaiming that the equations describe not only a patch of membrane but the whole neuron. This model (along with additional synaptic dynamics) will be used for the numerical simulations in Chapter 2.

An even more minimalist neuron model that is easier to treat analytically is the *current-based* LIF neuron. Here, the effect of incoming spikes is independent of the membrane voltage,

$$\tau_m \dot{v} = \mu - v + \tau_m X_{\text{in}}(t), \tag{1.29}$$

where τ_m is the *membrane time constant*, μ is the base current[3] and $X_{\text{in}}(t)$ captures the input to the cell.

Frequently, one considers the limit of infinitely fast synapses (the incoming spike train is not convolved with exponentials), yielding

$$X_{in}(t) = a_E \sum_i \delta(t - t_i) - a_I \sum_j \delta(t - t_j). \tag{1.30}$$

Here, each excitatory (inhibitory) spike directly leads to a jump in the membrane voltage by a_E (a_I).

As a further abstraction, one may consider more general forms of subthreshold dynamics,

$$\tau_m \dot{v} = f(v) + \tau_m X_{\text{in}}(t). \tag{1.31}$$

Choosing a nonlinear $f(v)$ may help to better model the spike generation. Besides the LIF neuron (with $f(v) = \mu - v$), common choices are the *perfect integrate-and-fire* neuron (PIF; with $f(v) = \mu$), the *quadratic integrate-and-fire* neuron (QIF; $f(v) = \mu + v^2$) or the *exponential integrate-and-fire* neuron (EIF) (Fourcaud and Brunel, 2002).

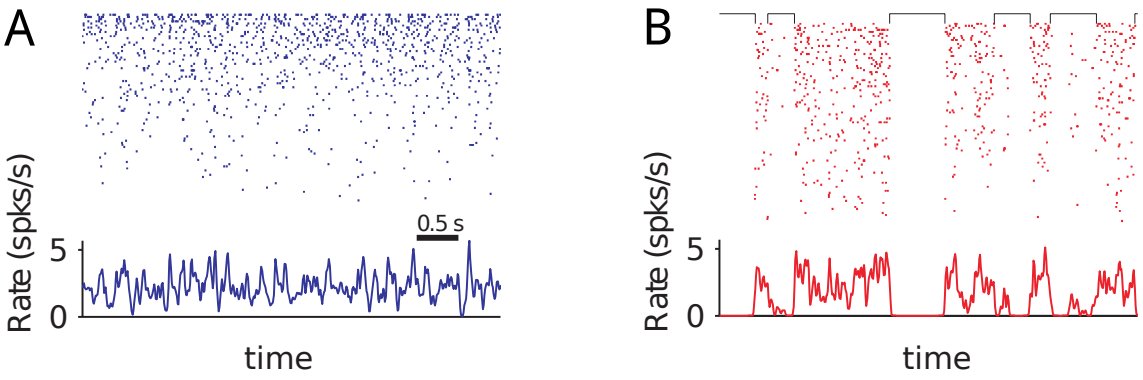

Figure 1.5.: Network states in rat neocortex in vivo. Each line in the raster plots shows the spike train of one of 100 simultaneously recorded neurons (sorted by spike-count rate). A: The asynchronous-irregular regime assumed in the diffusion approximation. B: Transitions between up and down states. This regime is outside the scope of the diffusion approximation and will be treated in Chapter 6. Adapted from (Renart et al., 2010). Reprinted with permission from AAAS.

Modeling of neural input

To gain analytical insights into the behavior of IF neurons, one has to make assumptions about the statistics of the input. In the following, we will refer to IF neurons with instantaneous current synapses [eq. (1.31)]; the approximations for the input can also be used for conductance based neurons (Richardson, 2004), but it is more difficult to treat them analytically.

For cortical neurons, it is common to assume that the background population is in an *asynchronous-irregular* (AI) state, i.e. that cross-correlations between presynaptic neurons vanish and that individual neurons fire irregularly (see Fig. 1.5A). In this case, the total background input has often been described by a Poisson process (Stein, 1965). Note that this is not strictly justified, as individual spike trains are in general non-Poissonian and the superposition of many such spike trains is not a Poisson process (Lindner, 2006).

In analytical studies, the assumption of Poissonian input is often but a step toward the *diffusion approximation* (Ricciardi and Sacerdote, 1979; Lánský and Lánská, 1987): The effect of individual incoming spikes is assumed to be negligibly small and the rate of their occurrence very large. In this case the increment to the voltage is Gaussian distributed. One can then write down a Langevin equation for the voltage,

$$\tau_m \dot{v} = f(v) + \sqrt{2D}\xi(t), \tag{1.32}$$

where $\xi(t)$ is a Gaussian white noise and D is the noise intensity. Using the Fokker-Planck formalism (Gardiner, 1985; Risken, 1989) then allows to calculate spontaneous-activity statistics of the output spike train (Ricciardi and Sacerdote, 1979; Lindner et al., 2002) as well as its (linear) response to a signal (Brunel et al., 2001; Lindner and Schimansky-Geier, 2001).

[3] The membrane time constant τ_m and the base current μ can be related to the physiological parameters in the conductance-based neuron through the so-called effective time constant approximation (ECA), see e.g. (Richardson and Gerstner, 2005).

Analytical results for input that is not white or not Gaussian are harder to come by; most studies of colored noise have considered exponentially correlated Gaussian noise (that arises for example due to an AI background with non-instantaneous synaptic dynamics), either in the limit of short or long correlation times (Brunel and Sergi, 1998; Fourcaud and Brunel, 2002; Moreno et al., 2002; Brunel and Latham, 2003; Middleton et al., 2003; Schwalger and Schimansky-Geier, 2008). Some results exist for white shot noise, for passive membranes (Richardson and Gerstner, 2005; Wolff and Lindner, 2008) and spiking LIF neurons (Richardson and Swarbrick, 2010).

Most studies that consider Gaussian noise that is not exponentially correlated (Bauermeister et al., 2013; Schwalger et al., 2015) or a non-Gaussian, exponentially correlated noise (dichotomous noise) (Salinas and Sejnowski, 2002; Lindner, 2004a; Droste and Lindner, 2014; Müller-Hansen et al., 2015) do not explicitly use the noise to model massive input from a network. Recently, a theory for PIF neurons driven by weak but arbitrarily colored Gaussian noise was put forward (Schwalger et al., 2015); there, examples of how different colored noises arise in realistic network scenarios are given. In Chapter 6, we will build upon a dichotomous noise to model a network regime that undergoes transitions between up and down states (see Fig. 1.5B).

1.3. Information theory

Information theory was developed in the 1940s, chiefly by Claude Shannon (Shannon, 1948, 1949), based on earlier work by Nyquist (1924) and Hartley (1928). A review of the use of information theory in neuroscience can, for instance, be found in the text book by Rieke et al. (1996) or in the papers by Borst and Theunissen (1999) and Dimitrov et al. (2011).

The main goal of Shannon's original work was to understand and optimize the transmission of signals through telephone lines or wireless channels. It is important to note that "information" here is to be distinguished from the common understanding of the term, where it includes a sense of meaning that depends on the receiving subject. Instead, Shannon proposes an objective measure; he is mostly interested in the amount of information that can be maximally transmitted over a given line and the encoding that is necessary to achieve optimal transmission, regardless of whether the received message ultimately makes sense to the recipient.

Entropy and mutual information

In Shannon's framework, the *information source* selects one out of many possible messages. If a particular message x is selected with probability $\Pr(x)$, the average amount of information conveyed by a message is given by the *entropy*

$$H = -\sum_x \Pr(x) \log_2[\Pr(x)], \tag{1.33}$$

where the sum runs over all possible messages.

The entropy measure is most easily understood for the case of equiprobable messages.

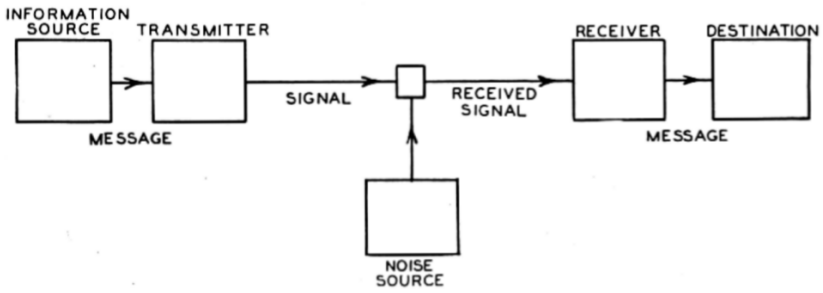

Figure 1.6.: A communications system after Shannon: The message source selects a message which is encoded by the transmitter, passes through the channel where it is subject to noise, and is decoded by the receiver before reaching its destination. © 1949 IEEE. Reprinted, with permission, from Shannon (1949)

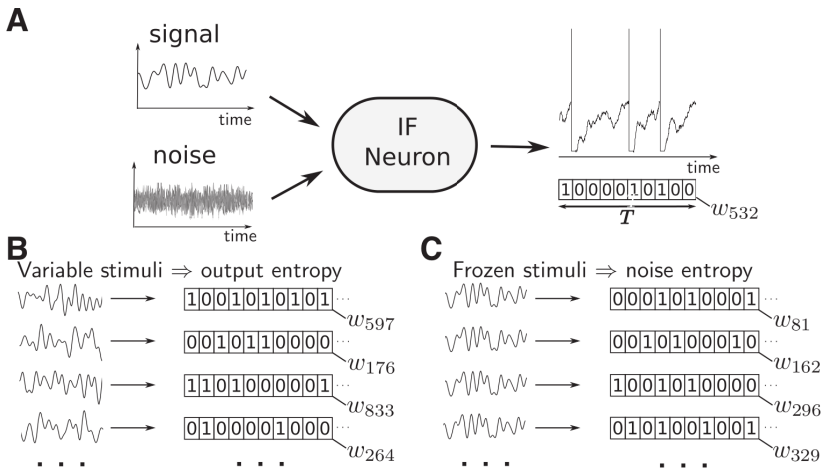

Figure 1.7.: Estimating mutual information in a neuron (model) using the direct method. Reproduced from Bernardi and Lindner (2015). © 2014, The American Physiological Society.

In this case, one has $H = \log_2(N_r)$, where N_r is the number of possible messages. It it plausible that, say, picking a certain message out of thousands allows to convey more information than picking one out of two. The logarithm further ensures that the measure behaves as one would expect: With only one possible message, no information can be transmitted (and $H = 0$ bits); two possible messages can convey one bit of information; combining two independently selected messages doubles the amount of information. In general, H can be thought of as the mean number of yes/no questions that have to be asked to identify one of the possible messages. It can also be seen as a measure of the variability in the ensemble of possible messages.

In communication over a noisy channel (see Fig. 1.6), the important question is how much information the received message conveys about the originally selected one. Or, phrased in terms of the neural setting we are interested in, how much can be learned about the stimulus by looking at the spike train. Consider the setup in Fig. 1.7A. By repeated application of the "experimental" procedure – select a stimulus, feed it into the neuron, record a spike train – one can generate many realizations of spike trains, and, in principle, measure the statistics of their occurrence to estimate their entropy (Fig. 1.7B).

However, due to the presence of noise, not all variability in the spike train is informative about a change in the stimulus. To estimate the amount of entropy that is due to noise, one defines a conditional entropy,

$$H_{x|s} = -\sum_x \Pr(x|s) \log_2[\Pr(x|s)], \tag{1.34}$$

where $\Pr(x|s)$ is the probability of obtaining the spike train x for a fixed stimulus s. Averaging this quantity over the stimulus ensemble yields the *noise entropy* (Fig. 1.7C),

$$H_n = \sum_{s,x} \Pr(s) \Pr(x|s) \log_2[\Pr(x|s)], \tag{1.35}$$

which quantifies the variability in the output that is not due to the signal. The *mutual information* is then given by

$$I = H - H_n = \sum_{x,s} \Pr(x,s) \log_2 \left[\frac{\Pr(x,s)}{\Pr(x) \Pr(s)} \right]. \tag{1.36}$$

The last line shows that the mutual information is symmetric (so an equivalent question to the above would have been "how much information about the spike train does the stimulus carry?").

The entropy can also be defined for continuous variables, thinking, for example, of signals that are continuous functions. Taking the sum in eq. (1.33) to a continuum limit introduces an additive divergent term. This is not surprising, since a continuous variable can encode an infinite amount of information. However, the divergent terms cancel when considering the difference of two entropies, as in the calculation of the mutual information.

Instead of the information source selecting a whole message, one can think of the message as a sequence of symbols – for example, the values of a signal at discrete points in time. The information source then selects one symbol at each time step. The probability of choosing a particular symbol may of course depend on the symbols chosen in the past. In other words, the information source is a stochastic process. Especially when dealing with stationary stochastic processes, it makes more sense to consider the *mutual information rate*

$$\mathcal{R}_{\text{info}} = \lim_{T \to \infty} \frac{I}{T}, \tag{1.37}$$

i.e. the number of bits transmitted per second.

Lower bound to the mutual information rate

In principle, the mutual information can be calculated directly, basically by using the steps in the above definition as a recipe: The same fixed signal $s(t)$ is presented many times to estimate the conditional entropy $H(x|s)$; this step is then repeated with many

signals in order to estimate the noise entropy H_n by averaging. The latter is then subtracted from the full entropy of the spike train (estimated from many runs with different signals) to yield the mutual information. In practice, however, this so-called *direct method* is computationally extremely expensive and in many cases not feasible. When the stimulus is Gaussian, there exists a rigorous lower bound to the mutual information rate. It is based on spectral measures that are much easier to obtain.

For a Gaussian stimulus $s(t)$ and output $x(t)$, the lower bound to the mutual information rate is given by (Bialek et al., 1993; Rieke et al., 1996):

$$\mathcal{R}_{\text{info}} \geq \mathcal{R}_{\text{info}}^{LB} = -\int_0^{f_c} df \log_2[1 - C_{sx}(f)]. \tag{1.38}$$

Recently, Bernardi and Lindner (2015) have compared this lower bound to direct measurements of the mutual information and found close agreement for weak signals fed into single integrate-and-fire neurons.

1.4. Information transmission in the face of neural noise

Now that basic theoretical concepts have been introduced, we return to the topic of neural noise and its effect on information transmission. We concentrate on two questions:

1. Is there a functional role of neuronal noise, or is it a mere nuisance?
2. Is it necessary to clearly distinguish between signal and noise and is such a distinction always possible?

Given the ubiquity of neuronal variability, various functional roles of noise in the brain have been discussed: It has, for example been suggested that noise is vital for probabilistic decision making and to enable efficient learning in changing environments (Rolls and Deco, 2010) and that noisy activity may encode probability distributions that are important in inference (Ma et al., 2006). Here, we concentrate on a beneficial role in the transmission of weak signals: Stochastic resonance, a concept that has its origins in statistical physics and has since widely been studied in neural systems.

1.4.1. Stochastic resonance

Stochastic resonance (SR) (Gammaitoni et al., 1998) refers to an enhancement in the detection or transmission of a weak signal by a certain optimal amount of noise. The term was coined by Benzi et al. (1981, 1982), who considered an overdamped particle in a double-well potential, driven by a sinusoidal signal. In the absence of noise, the weak signal is unable to push the particle from one well to the other. In this case, adding some noise helps to cross the potential barrier and may allow the system to track the periodic driving better than before. This can be quantified by considering the signal-to-noise ratio – the system's power spectrum at the driving frequency divided by the power spectrum in the absence of a signal. Plotting this signal-to-noise ratio over the noise intensity reveals a maximum, indicative of an optimal noise intensity (see Fig. 1.8A).

In the original model (Benzi et al., 1982), SR was used to explain the periodicity in

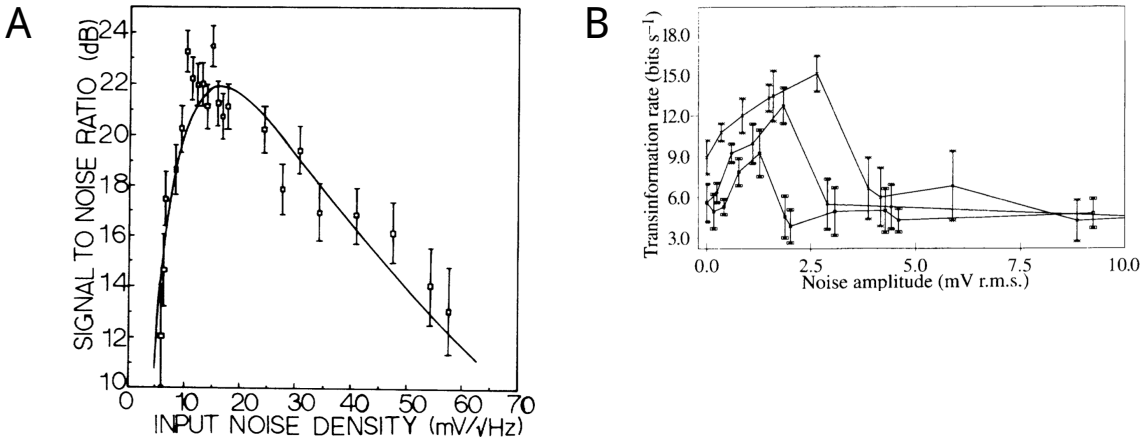

Figure 1.8.: Examples of stochastic resonance. A: SR in a ring laser. This is an example of the classical setup in which a bistable system is periodically driven and the signal-to-noise ratio is measured (reprinted figure with permission from (McNamara et al., 1988). © (1988) by the American Physical Society; URL: http://dx.doi.org/10.1103/PhysRevLett.60.2626). **B: SR in a sensory neuron in the cricket.** Here, an excitable system transmits a broadband signal optimally at a given noise intensity, as quantified by the mutual information rate (adapted by permission from Macmillan Publishers Ltd: Nature (Levin and Miller, 1996); © 1996).

the occurrence of ice ages in the earth's climate, but in a more general sense, SR can be considered a beneficial effect of noise on the transmission of a weak signal. It is not restricted to bistable systems, but has also been observed in excitable systems (Longtin, 1993; Lindner et al., 2004), or, in general, systems that contain some kind of threshold. Further, it is not restricted to sinusoidal stimuli but can be observed for arbitrary signals (so-called aperiodic SR (Collins et al., 1995)). In this case, the mutual information rate between the signal and the system's output suggests itself as a suitable measure (Levin and Miller, 1996; Heneghan et al., 1996; Bulsara and Zador, 1996) (see Fig. 1.8B).

The relevance of SR for the signal transmission in threshold systems has prompted the question whether a functional role of neural noise may be the amplification of weak signals. This idea has been explored in an ever-growing number of experimental and theoretical studies (reviewed by Hänggi (2002); Moss et al. (2004); Faisal et al. (2008); McDonnell and Abbott (2009)).

1.4.2. Signal vs noise

It has been argued that the trial-to-trial variability of higher-order neurons (that is, neurons that are not in the sensory periphery or motor areas) is not really due to noise, but rather due to internal spiking activity that is neither controlled nor understood by the experimenter (Masquelier, 2013) or due to suboptimal inference (Beck et al., 2012). Indeed, synaptic noise, the dominant noise source for cortical neurons, is caused by the spikes from other neurons, and it is natural to assume that many of these spikes carry information (about attention, working memory, internal predictive signals, to name but a few possibilities). Are these "deterministic, but uncontrolled, internal variables" (Masquelier, 2013) that we called synaptic noise not rather signal than noise?

The perceived contradiction lies in the understanding of the term noise. If noise is

understood as something intrinsic, caused by "truly random" events, unable to carry information, then what we called “synaptic noise” can in general not be considered noise at all (note, however, that work about the chaotic nature of cortical networks (London et al., 2010) suggests that at least part of the synaptic input is, for all practical purposes, noise). The above definition might, however, be an unnecessarily narrow definition of the term. If one rather sees noise – or stochastic processes – as a means to incorporate influences of which the precise causes are unknown to us, but which lend themselves to a statistical description, then synaptic noise can be a fruitful concept.

In Chapter 6, for example, we use a stochastic process to model up and down states. We do not suggest that such activity is at its basis random and carries no information; rather, we consider it an adequate description of our ignorance about the complex processes that produce this activity. The situation that the background contains a signal is made explicit in the setup we consider in Chapter 2.

Chapter 2.

Interplay of two signals shaped by short-term plasticity

The thousands of synaptic inputs that a neuron typically receives may encode more than one signal, and these signals may interact in a non-trivial way. An especially clear-cut case is *multisensory integration*, the phenomenon that two signals from different sensory modalities (e.g. an auditory and a visual stimulus), presented simultaneously, may evoke a response that goes beyond a mere superposition of the responses to each signal in isolation.

Multisensory integration (Shimojo and Shams, 2001; Driver and Noesselt, 2008) has been observed in diverse experimental setups, ranging from behavioral studies (Sekuler et al., 1997; Shams et al., 2000) over fMRI (Macaluso et al., 2000) and EEG studies (Giard and Peronnet, 1999) down to single-cell measurements (Meredith and Stein, 1983; Stein and Stanford, 2008). Most of the experimental as well as theoretical work (Deneve et al., 2001; Patton et al., 2002; Rowland et al., 2007; Ma and Pouget, 2008; Elliott et al., 2009) focuses on static stimuli: At each modality, a stimulus is either present or absent, and the response (on a cellular level) is quantified by a certain (constant) firing rate. The interaction of two time-dependent signals has, to our knowledge, not previously been investigated.

While a hot-spot of multisensory integration is the superior colliculus (Meredith and Stein, 1983; Stein and Stanford, 2008), it has recently been observed in cortical areas (Foxe et al., 2000; Ghazanfar and Schroeder, 2006). Arguably even more widespread is the interaction between one external (sensory) signal and an internally generated signal. This internal signal could for instance be modulatory in nature, or it could be a running prediction of the sensory input.

Different signals, stemming for example from different brain regions, will in general enter a neuron through different channels. Cortical pyramidal neurons, for example, receive synaptic connections in different cortical layers, depending on the source of the connection (Yamamoto et al., 1992), and input to these layers can be coupled non-trivially (Larkum et al., 1999). Another difference between two streams of input may lie in the kind of short-term plasticity (STP) exhibited by the respective populations of synapses. STP refers to changes in a synapse's efficacy that depend on its usage in the immediate past. There is evidence that synapses may systematically differ in their STP properties depending on the type of target cell or the source of the connection (Stratford et al., 1996; Markram et al., 1998b; Gupta et al., 2000; Boudreau and Ferster, 2005).

In this chapter, we study the interplay of two signals that impinge on a target neuron. We focus on the second scenario: The two presynaptic neural populations that encode

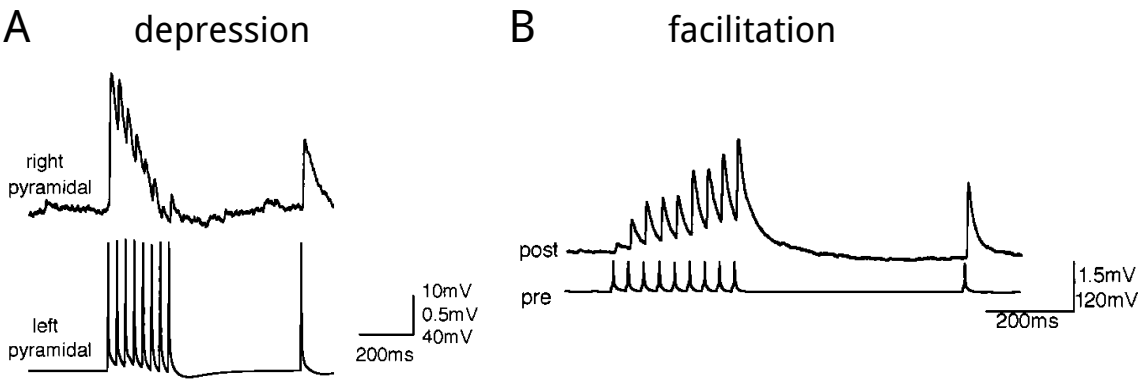

Figure 2.1.: Experimentally measured excitatory postsynaptic potentials (EPSPs) in cells connected by depressing (A) or facilitating (B) synapses. The bottom row shows EPSPs in the presynaptic, the top row in the postsynaptic cell. Adapted from (Markram et al., 1998b). © 1998, The National Academy of Sciences.

the signals differ in the kind of synaptic connection they make onto the target cell; one population is connected via facilitating, the other via depressing synapses. We ask how the transmission of one signal depends on the presence or absence of the other.

In the following, we give a brief introduction to synaptic short-term plasticity in Sec. 2.1, before introducing the setup we consider in Sec. 2.2. We then discuss two main findings: The presence of a second signal may switch the neuron's information filter properties from broadband to frequency selective (Sec. 2.3), and it may be beneficial for the transmission of the first signal (Sec. 2.4).

2.1. Synaptic short-term plasticity

Short-term synaptic plasticity (reviewed by Zucker and Regehr (2002)) refers to a usage-dependence of synaptic efficacy. Presynaptic action potentials, arriving in close succession, will in general differ in the magnitude of postsynaptic potentials (EPSPs) they evoke. We speak of synaptic *depression* if the second of two subsequent action potentials elicits on average a smaller response than the first one, and of *facilitation* in the opposite case. In general, both phenomena can occur in the same synapse on different timescales. These timescales are typically on the order of 100 ms, which distinguishes STP from other kinds of synaptic plasticity that act on longer timescales and are thought to underlie learning. Examples of evoked postsynaptic potentials after depressing/facilitating synapses (from Markram et al. (1998b)) can be found in Fig. 2.1.

Both facilitation and depression are presynaptic effects. Depression can be explained by a depletion of presynaptic neurotransmitter-filled vesicles: Each presynaptic action potential (AP) releases docked vesicles with a certain probability. Once a vesicle has been released, it takes some time until it is replaced. If the next presynaptic AP occurs shortly after the previous one, there may thus be fewer vesicles docked, leading to a reduced response.

When an AP arrives in the presynaptic terminal, it causes voltage-gated calcium channels to open, and the influx of calcium is what causes vesicle release. After an AP, el-

evated calcium levels may persist for hundreds of milliseconds. This *residual calcium*, which may increase the probability that a subsequent AP releases vesicles, is believed to be the cause of facilitation (Katz and Miledi, 1968; Dittman et al., 2000; Zucker and Regehr, 2002).

Functional roles of STP

Short-term plasticity endows synapses with computational capabilities (Abbott and Regehr, 2004) and many functional roles have been studied: STP can implement gain control (Abbott et al., 1997; Banitt et al., 2007), lead to decorrelation of inputs (Goldman et al., 2002), allow efficient detection of transients (Lewis and Maler, 2002; Abbott et al., 1997), and enable selectivity for bursts (Lisman, 1997) or for a given level of presynaptic synchrony (Bird and Richardson, 2014).

Especially the role of STP-endowed synapses as a temporal filter has received much attention (Fortune and Rose, 2001). Most studies concerning filtering consider the response at a given frequency of presynaptic firing (Fortune and Rose, 2001; Dittman et al., 2000; Lewis and Maler, 2002; Klyachko and Stevens, 2006; Rotman et al., 2011), while others focus on frequency components of a signal by which the firing rate is modulated (Lindner et al., 2009; Merkel and Lindner, 2010; Rosenbaum et al., 2012; Droste et al., 2013). In order to distinguish the two, we will use *frequency* only to refer to signal frequency, not the rate of presynaptic firing.

Lindner et al. (2009) used spectral measures such as the coherence to investigate signal transmission through a population of synapses that was either facilitation- or depression-dominated. Remarkably, they found that, over a wide range of parameters, information transmission is frequency independent, even though STP does induce a strong frequency dependence both in the power spectrum of the point process that models synaptic vesicle release and in the cross spectrum between the signal and this process. This effect was further studied by Merkel and Lindner (2010), who derived analytical approximations to the cross and power spectra for single synapses (subject to inhomogeneous Poisson input that carries a rate-modulated signal). Rosenbaum et al. (2012) considered a model of short-term depression that incorporates the stochasticity of vesicle release and recovery and found that broadband transmission only occurs for large numbers of release sites or presynaptic cells, while otherwise, the depressing synapse acts as a high-pass filter for information.

Stochastic model

A simple stochastic model for synaptic depression, which has been (with minor alterations) widely used (Vere-Jones, 1966; Fuhrmann et al., 2002; Loebel et al., 2009; Rosenbaum et al., 2012; Bird and Richardson, 2014), assumes that there are N_{rs} independent *release sites*[1] where vesicles can be docked and that, at a given time, K of them are occupied. Upon arrival of a presynaptic AP, release gets triggered at each occupied site with a constant probability F_0. Between APs, each unoccupied site recovers a vesicle at the rate

[1] Physiologically, a presynaptic neuron may make multiple synaptic contacts onto a postsynaptic cell, each of which may contain a number of release-ready vesicles. As we assume independence of vesicle release events, we understand the number of release sites as the total number of release-ready vesicles.

$1/\tau_D$.

Facilitation can be added to this stochastic model via a modification of the release probability F. Following (Dittman et al., 2000; Lewis and Maler, 2002; Merkel and Lindner, 2010), the release probability is now time-dependent and takes the form

$$F(t) = F_0 + \left(\frac{1}{1 - F_0} + \frac{1}{F_C(t)} \right)^{-1}, \tag{2.1}$$

where $F_C(t)$ is proportional to the concentration of a hypothesized calcium-binding molecule. One assumes that this concentration is instantaneously increased by presynaptic APs and otherwise decays exponentially,

$$\dot{F}_C(t) = -\frac{F_C(t)}{\tau_F} + \Delta \cdot \sum_{\{t_i\}} \delta(t - t_i), \tag{2.2}$$

where $\{t_i\}$ are the times of presynaptic APs.

Deterministic model

When the number of release sites is large, or when fitting to trial-averaged data (such as shown in Fig. 2.1), it may be convenient to use a deterministic model. Here, we use an averaged version of the stochastic model presented above; such so-called FD models and similar models have been widely used (Tsodyks and Markram, 1997; Markram et al., 1998a; Dittman et al., 2000; Lewis and Maler, 2002, 2004; Lindner et al., 2009; Merkel and Lindner, 2010; Droste et al., 2013). Each AP releases on average $F(t) \cdot D(t) \cdot N_{\mathrm{rs}}$ vesicles, where $D(t)$ is the mean fraction of occupied release sites, $D(t) = \langle K(t) \rangle / N_{\mathrm{rs}}$. Between APs, vesicles are recovered at the rate $1/\tau_D$, so that $D(t)$ is governed by

$$\dot{D}(t) = \frac{1 - D(t)}{\tau_D} - F(t^-)D(t^-) \cdot \sum_{\{t_i\}} \delta(t - t_i), \tag{2.3}$$

where the "-" superscript indicates that the value is to be taken immediately before it is itself influenced by the AP.

In this chapter, we will mostly use idealized synapses that are either purely facilitating or purely depressing. For purely facilitating synapses, we assume infinitely fast recovery of vesicles (we set $D(t) \equiv 1$), while for purely depressing synapses, we assume a constant release probability, $F(t) \equiv F_0$.

2.2. Model and setup

The setup we consider is sketched in Fig. 2.2: A cell receives input from two excitatory populations of presynaptic neurons, each population encoding a signal. The populations

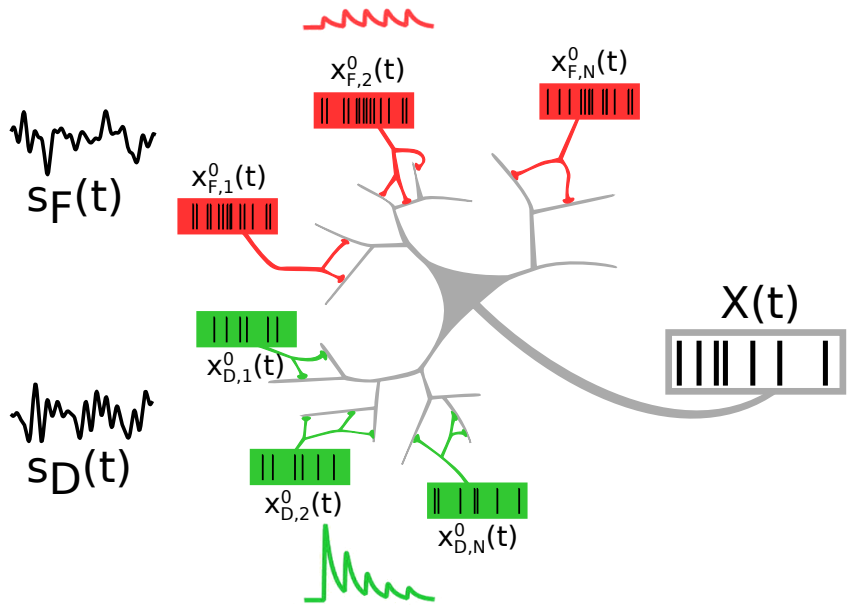

Figure 2.2.: The setup considered in this chapter: A neuron receives two signals, one entering via facilitating synapses (the "F signal" $s_F(t)$), the other via depressing synapses (the "D signal" $s_D(t)$). We study how information about different frequency components of the signals is encoded in the output spike train $X(t)$ and how the presence of one signal affects the transmission of information about the other.

differ in their synaptic connections to the target cell; one is connected via facilitating, the other via depressing synapses. We will refer to the population connected via facilitating synapses as the F population and to the signal it encodes as the F signal (and analogously: D population, D signal).

The signals $s_F(t)$ and $s_D(t)$ are two independent sources of band-limited Gaussian white noise, with a cutoff frequency $f_c = 10\,\mathrm{Hz}$ and unit variance.

Each presynaptic population consists of $N = 500$ neurons, each of which is modeled by an independent inhomogeneous Poisson process. All neurons within the population P (where P is either F or D) share a common firing rate; it may either be a low and constant background rate,

$$R_P(t) \equiv r_0 = 1\,\mathrm{Hz}, \tag{2.4}$$

when the population is inactive, or a time dependent rate

$$R_P(t) = r_P\left(1 + \epsilon_P s_P(t)\right), \tag{2.5}$$

when the population is encoding a signal (where $r_P = 20\,\mathrm{Hz}$ for both populations).

The spike train generated by the nth neuron in population P is

$$x^0_{P,n}(t) = \sum_{\{t_{P,n,i}\}} \delta(t - t_{P,n,i}), \tag{2.6}$$

where $t_{P,n,i}$ is the time of the ith spike emitted by that neuron and

$$\left\langle x^0_{P,n}(t) \right\rangle = R_P(t). \tag{2.7}$$

This spike train impinges on a synapse that is either purely facilitating or purely depressing.

The dynamics of the nth facilitating synapse are described by

$$F_n(t) = F_{0,F} + \left(\frac{1}{1 - F_{0,F}} + \frac{1}{F_{C,n}(t)} \right)^{-1}, \tag{2.8}$$

$$\dot{F}_{C,n}(t) = -\frac{F_{C,n}(t)}{\tau_F} + \Delta \cdot x^0_{F,n}(t), \tag{2.9}$$

and of the kth depressing synapse by

$$\dot{D}_k(t) = \frac{1 - D_k(t)}{\tau_D} - F_{0,D} D_k(t^-) \cdot x^0_{D,k}(t). \tag{2.10}$$

For an input $x^0_{P,n}(t)$, the synapses output a weighted spike train,

$$x_{F,n}(t) = F_n(t) x^0_{F,n}(t) \quad x_{D,k}(t) = F_0 D_k(t) x^0_{D,k}(t). \tag{2.11}$$

The total (weighted) input

$$X_{\text{in}}(t) = \sum_n^N x_{F,n}(t) + \sum_k^N x_{D,k}(t) \tag{2.12}$$

enters the conductance of the target cell,

$$\dot{g}_e = -\frac{g_e}{\tau_e} + c X_{\text{in}}(t), \tag{2.13}$$

where c is the jump in conductance if all functional contacts belonging to a presynaptic neuron release their vesicles. The target cell is a leaky integrate-and-fire neuron,

$$C\dot{v} = -g_L(v - E_L) - g_e(v - E_e) + I_i. \tag{2.14}$$

Whenever v crosses as threshold v_T, a spike is added to the output spike train $X(t)$ and the voltage is reset to v_R, where it remains clamped for a refractory period τ_{ref}. All inhibitory input is approximated by the constant inhibitory current I_i, which allows us to control the firing regime (subthreshold vs suprathreshold).

The parameters used are summarized in Table 2.1.

Parameter	Value	Description
f_c	10 Hz	signal cut-off frequency
ϵ_F	0.05	amplitude of the F signal
ϵ_D	0.05	amplitude of the D signal
N	500	neurons per (F/D) population
r_P	20 Hz	baseline firing rate of an active population
r_0	1 Hz	baseline firing rate of a passive population
$F_{0,F}$	0.05	intrinsic release probability for facilitating synapses
$F_{0,D}$	0.4	intrinsic release probability for depressing synapses
Δ	0.175	per-spike increment for facilitation dynamics
τ_F	0.05 s	timescale of facilitation dynamics
τ_D	0.05 s	timescale of depression dynamics
τ_e	0.003 s	timescale of conductance dynamics
c	10 nS	synaptic weight
C	300 pF	membrane capacitance
g_L	15 nS	leak conductance
E_L	−62.5 mV	leak reversal potential
E_E	0 mV	excitatory reversal potential
I_i	−2.25 nA	(inhibitory) base current
v_R	−62.5 mV	reset voltage
v_T	−50 mV	threshold voltage
τ_{ref}	0.001 s	refractory period

Table 2.1.: Model parameters used in this chapter where not indicated differently.

2.2.1. Analytical approximation for the spectral coherence function

Here, we derive an analytical expression for the coherence between either of the signals and the total weighted input (see sketch in Fig. 2.3),

$$C_{sX_{\text{in}}}(f) = \frac{|S_{sX_{\text{in}}}(f)|^2}{S_{ss}(f)S_{X_{\text{in}}X_{\text{in}}}(f)}. \tag{2.15}$$

Our goal is to express the cross and power spectra $S_{sX_{\text{in}}}(f)$ and $S_{X_{\text{in}}X_{\text{in}}}(f)$ in terms of the spectra for a single synapse. These have been derived by Merkel and Lindner (2010) and read

$$S_{s_F x_F}(f) = \frac{r_F \epsilon_F}{2f_c}\left(F_{0,l} + \Delta_l r_F \tau_F \left(1 + \frac{1}{1 - 2\pi i f \tau_F}\right)\right), \tag{2.16}$$

$$S_{x_F x_F}(f) = r_F \frac{\left(F_{1,l} + \Delta_l r_F \tau_F\right)^2 + (2\pi f \tau_F)^2 F_{1,l}^2}{1 + (2\pi f \tau_F)^2} + \frac{1}{2}\Delta_l^2 r_F^2 \tau_f, \tag{2.17}$$

$$S_{s_D x_D}(f) = F_{0,D}\frac{r_D \epsilon_D}{2f_c}\left(1 - \frac{F_{0,D} r_D \tau_D/\beta_D}{1 - 2\pi i f \tau_D/\beta_D}\right), \tag{2.18}$$

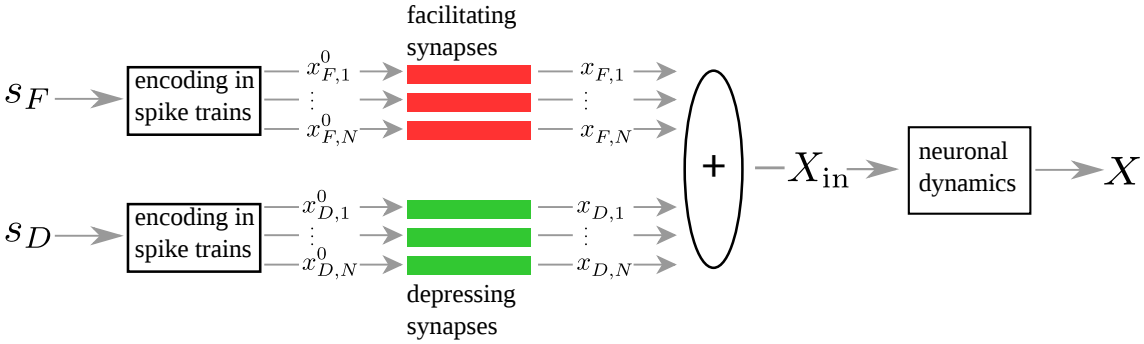

Figure 2.3.: A more schematic depiction of the setup considered: the F (D) signal is encoded in N spike trains, each of which gets filtered by a facilitating (depressing) synapse. The sum of all weighted spike trains from both populations, $X_{\text{in}}(t)$, enters the neuronal (conductance) dynamics, producing an output spike train $X(t)$.

$$S_{x_D x_D}(f) = \frac{r_D F_{0,D}^2}{\beta_D^3 (1 + F_{0,D} r_D \tau_D - F_{0,D}^2 r_D \tau_D / 2)} \cdot \frac{1 + (2\pi f \tau_D)^2}{1 + (2\pi f \tau_D / \beta_D)^2}, \tag{2.19}$$

where

$$F_{0,I} := F_{0,F} + \frac{(\Delta r_F \tau_F)^2 (1 - F_{0,F})}{\gamma^2} + \frac{\Delta^2 r_F \tau_F (1 - F_{0,F})^2}{6\gamma^3} \left(1 - \frac{\Delta (1 + 9 r_F \tau_F)}{\gamma}\right), \tag{2.20}$$

$$\Delta_I := \frac{\Delta (1 - F_{0,F})^2}{\gamma^2} \cdot \left(1 - \frac{2\Delta}{3\gamma} + \frac{\Delta^2 (1 + 3 r_F \tau_F)}{2\gamma^2}\right), \tag{2.21}$$

$$\gamma := 1 - F_{0,F} + \Delta r_F \tau_F, \tag{2.22}$$

$$F_{1,I} := F_{0,I} + \Delta_I r_F \tau_F, \tag{2.23}$$

$$\beta_D := 1 + F_{0,D} r_D \tau_D. \tag{2.24}$$

In the following, we present a derivation for $C_{s_F X_{\text{in}}}(f)$, the coherence between the F signal and the total input; a derivation for the D signal is completely analogous, it suffices to swap all F and D subscripts.

In order to calculate the cross spectrum between $s_F(t)$ and $X_{\text{in}}(t)$, we exploit the independence of the F signal and the spike trains emitted by the D population as well as the stationarity of all considered processes. We obtain

$$\delta(f - f') S_{s_F X_{\text{in}}}(f) = \left\langle \tilde{s}_F(f) \tilde{X}_I^*(f') \right\rangle_{\xi,s} \tag{2.25}$$

$$= \left\langle \tilde{s}_F(f) \left(\sum_n^N \tilde{x}_{F,n}^*(f') + \sum_k^N \tilde{x}_{D,k}^*(f') \right) \right\rangle_{\xi,s} \tag{2.26}$$

$$= \sum_n^N \left\langle \tilde{s}_F(f) \tilde{x}_{F,n}^*(f') \right\rangle_{\xi,s} + \sum_k^N \left\langle \tilde{s}_F(f) \right\rangle_s \left\langle \tilde{x}_{D,k}^*(f') \right\rangle_\xi \tag{2.27}$$

$$= N \left\langle \tilde{s}_F(f) \tilde{x}_F^*(f') \right\rangle_{\xi,s}. \tag{2.28}$$

Here, $\langle . \rangle_s$ refers to an average over the stimulus ensemble and $\langle . \rangle_\xi$ to one over the ensemble of (inhomogeneous Poisson) spike trains. Thus, we have

$$S_{s_F X_{\text{in}}}(f) = N S_{s_F x_F}(f). \tag{2.29}$$

The power spectrum can be written as

$$\delta(f - f') S_{X_{\text{in}} X_{\text{in}}}(f) = \left\langle \tilde{X}_I(f) \tilde{X}_I^*(f') \right\rangle_{\xi,s} \tag{2.30}$$

$$= \sum_{i,j}^{N} \left\langle \tilde{x}_{F,i}(f) \tilde{x}_{F,j}^*(f') \right\rangle_{\xi,s} + \sum_{i,j}^{N} \left\langle \tilde{x}_{D,i}(f) \tilde{x}_{D,j}^*(f') \right\rangle_{\xi,s}, \tag{2.31}$$

where, again, we have exploited stationarity and the independence between spike trains entering through facilitating and depressing synapses. This can be further simplified, using

$$\left\langle \tilde{x}_{F,i}(f) \tilde{x}_{F,j}^*(f') \right\rangle_{\xi,s} = \left\langle \tilde{x}_{F,i}(f) \tilde{x}_{F,j}^*(f') \right\rangle_{\xi,s} \delta_{ij} + \left\langle \left\langle \tilde{x}_{F,i}(f) \right\rangle_\xi \left\langle \tilde{x}_{F,j}(f') \right\rangle_\xi^* \right\rangle_s \tag{2.32}$$

$$= \left\langle \tilde{x}_{F,i}(f) \tilde{x}_{F,j}^*(f') \right\rangle_{\xi,s} \delta_{ij} + |\chi_F(f)|^2 \left\langle \tilde{s}_F(f) \tilde{s}_F^*(f') \right\rangle_s \tag{2.33}$$

(and likewise for the depressing synapses). Here, we have assumed (as done by Merkel and Lindner (2010)) that signals are weak, so that a linear response ansatz,

$$\left\langle \tilde{x}_F(f) \right\rangle_s = \chi_F(f) \tilde{s}_F(f), \tag{2.34}$$

can be used. The susceptibility $\chi_F(f)$ is given by eq. (2.16), which can be written as

$$S_{s_F x_F}(f) = \chi_F^*(f) S_{s_F s_F}(f). \tag{2.35}$$

The power spectrum thus reads

$$\begin{aligned} S_{X_{\text{in}} X_{\text{in}}}(f) = N \Big(& S_{x_F x_F}(f) + S_{x_D x_D}(f) \Big) \\ & + N(N-1) \cdot \Big(|\chi_F(f)|^2 S_{s_F s_F}(f) + |\chi_D(f)|^2 S_{s_D s_D}(f) \Big). \end{aligned} \tag{2.36}$$

Plugging eq. (2.29) and eq. (2.36) into eq. (2.15) yields

$$C_{s_F X_{\text{in}}}(f) = \left[\frac{1}{N} \frac{1}{C_{s_F x_F}(f)} \left(1 + \frac{S_{x_D x_D}(f)}{S_{x_F x_F}(f)} \right) + \frac{N-1}{N} + \frac{N-1}{N} \frac{|S_{s_D x_D}(f)|^2}{|S_{s_F x_F}(f)|^2} \right]^{-1}, \tag{2.37}$$

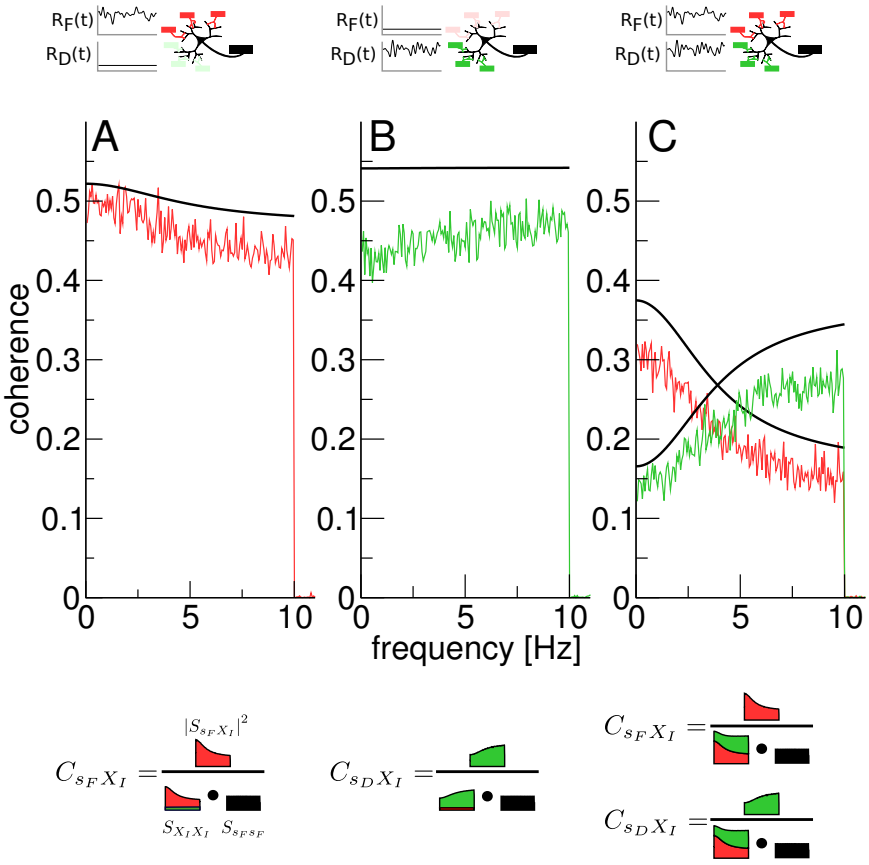

Figure 2.4.: Coherence curves between signals and output spike train in three scenarios. In A, only the F population is active and transmitting a signal ($R_F(t) = r_F\,(1 + \epsilon_F s_F(t))$, with $r_F = 20\,\text{Hz}$ and $\epsilon_F = 0.05$), while the D population is firing at a low background rate ($R_D(t) \equiv 1\,\text{Hz}$). In B, only the D population is active and transmitting a signal ($R_F(t) \equiv 1\,\text{Hz}$). In C, both populations are active. Red lines show the coherence between the F signal and the output spike train, green lines between the D signal and the output spike train, black lines the approximation eq. (2.37).

where $C_{s_F x_F}(f)$ is the single-synapse coherence.

2.3. Spectral separation of information

In Fig. 2.4, we plot the coherence curves between either of the signals and the output spike train for three different situations. When only the F signal is present and the D population is firing at a low background rate ($\epsilon_D = 0, R_D(t) \equiv 1\,\text{Hz}$), the coherence between the F signal and the output spike train is rather flat (Fig. 2.4A). The same is observed for the coherence between the D signal and the output spike train when only the D signal is present (Fig. 2.4B, where $\epsilon_F = 0, R_F(t) \equiv 1\,\text{Hz}$). This means that in these cases, information transmission is approximately broadband, i.e frequency-independent. This effect was first reported by Lindner et al. (2009).

In contrast, when both populations are transmitting a signal (Fig. 2.4C), the picture changes drastically: The coherence over the F signal becomes low-pass, while the coher-

ence over the D signal is now high-pass. In other words, the neuron now preferentially encodes information about slow components of the F signal and fast components of the D signal. This *spectral separation* effect constitutes a non-trivial interaction between the two signals.

In order to understand these effects, consider how the coherence is calculated. This is graphically sketched in the bottom row of Fig. 2.4. In A, the power that enters the system is dominated by the facilitating synapses. Facilitating synapses lead to a low-pass filtering of power. However, the squared cross spectrum exhibits a very similar frequency dependence, so that, in the calculation of the coherence, they cancel, resulting in a flat coherence. The same (non-trivial) cancellation occurs for B. When both populations are transmitting a signal (C), the cross spectrum between a given signal and the output spike train retains its frequency dependence. Now, however, both populations contribute substantially to the input power, and adding up the respective power spectra results in an approximately flat spectrum. Thus, the frequency dependence in the cross spectrum no longer cancels, leading to the spectral separation effect.

The theory, eq. (2.37), is shown as black lines in Fig. 2.4. It can be seen to be qualitatively a decent match, which is surprising as it describes only the coherence between a signal and the total input to the cell, i.e. it neglects the dynamics of the spiking neuron. An explanation is that the firing rates in Fig. 2.4 are rather high [90 Hz (A), 144 Hz (B), and 226 Hz (C)]. IF neurons constitute a low-pass coherence filter (Vilela and Lindner, 2009), with a cut-off approximately determined by the firing rate. Here, the signals are slow with respect to the firing rate, and the neuron thus acts approximately as a linear system.

2.3.1. Robustness under variation of parameters

In order to quantify whether spectral separation occurs for a given set of parameters or not, we introduce the separation factor (see the sketch in Fig. 2.5)

$$\Gamma := \frac{h - l}{l}, \tag{2.38}$$

where

$$h = \max_{0 \le f \le f_c} C_{sX}(f), \quad l = \min_{0 \le f \le f_c} C_{sX}(f). \tag{2.39}$$

This factor is zero for a flat coherence; a non-zero value is (in the present setup) indicative of a high or low-pass coherence.

In Fig. 2.5, we plot the separation factor under variation of twelve parameters. In each panel, we vary one parameter and plot four separation factors: the factor for the F (D) coherence when only the F (D) population is transmitting a signal (thin lines), and the factor for the F (D) coherence when both populations are transmitting a signal (thick lines). The effect of spectral separation described above occurs when the separation factors are low for one signal in isolation, but high when both signals are present.

It can be seen that the spectral separation effect is present over a wide range of parameters. From this analysis, we may expect it to occur for presynaptic populations of 400 and more neurons, and for rather fast synaptic dynamics (100 ms and less, as reported

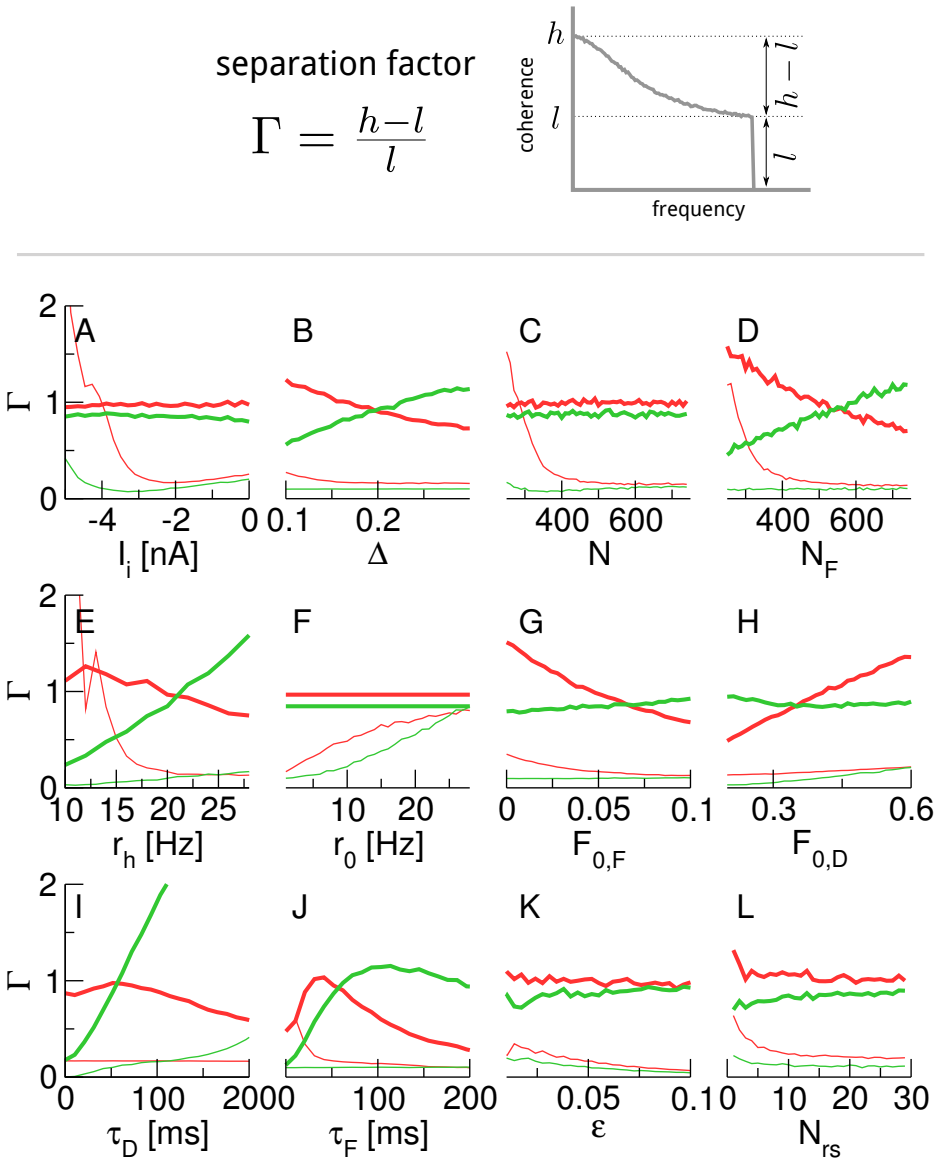

Figure 2.5.: Separation factors for the three scenarios when varying system parameters. Thick lines mark the factors for the F (red) and D (green) coherence when both signals are present, thin lines for the case where only one signal is present. In panel D, we vary the number of neurons in the F population, while keeping the number of neurons in the D population constant, $N_D = 500$. In panel E, we vary the baseline rate of an active population. This means we vary either r_F or r_D (or both of them simultaneously). Similarly, in F, we vary the background rate at which inactive populations fire.

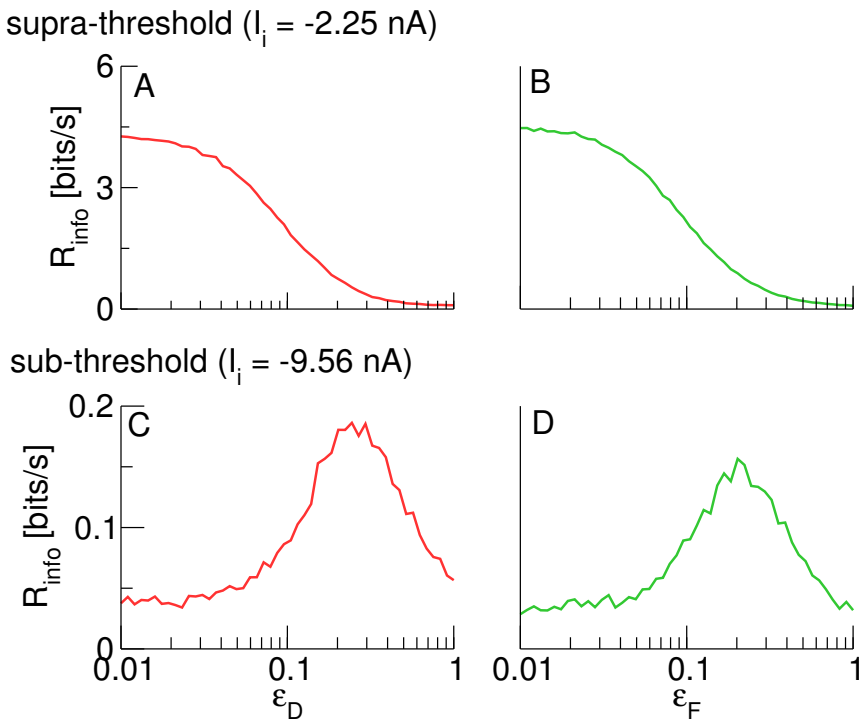

Figure 2.6.: Mutual information rates (lower bound) about one signal as a function of the other signal's strength. Red lines: Information about the F signal; green lines: information about the D signal. In A and C (B and D) ϵ_F (ϵ_D) is kept fixed. In the supra-threshold case (A, B; $I_i = -2.25\,\mathrm{nA}$), increasing the respective second signal leads to a decrease in information transmission. In contrast, in the subthreshold regime (C, D; $I_i = -9.56\,\mathrm{nA}$), one observes optimal information transmission at a non-vanishing strength of the respective other signal.

for instance by Lewis and Maler (2002)).

In addition, we also plot the separation factors for stochastic synapses. Recall that the stochastic model (see Sec. 2.1) approaches the deterministic model as the number of release sites goes to infinity, i.e. $N_{\mathrm{rs}} \to \infty$. In the bottom-right panel of Fig. 2.5, we see that the spectral separation effect is already pronounced for a relatively moderate number of release sites of about $N_{\mathrm{rs}} \approx 10$.

2.4. Signal-mediated stochastic resonance

One may also ask how the total amount of information transmitted about one signal is affected by the presence or absence of the other. Intuitively, one would expect a second signal to be detrimental to information transmission. Indeed, for the parameters studied in the previous section, this is the case. In Fig. 2.6A (B), we plot the lower bound for the mutual information rate over the F signal (D signal) when ϵ_D (ϵ_F), the modulation amplitude of the other signal, is varied (the baseline firing rates are kept constant). It is apparent that increasing the strength of the respective other signal leads to a decrease in information transmission. This is plausible, as increasing the strength of one signal can be considered an increase in noise with respect to the other signal.

However, it is known that in nonlinear systems, noise can also have beneficial effects on

signal transmission through stochastic resonance (SR). In Fig. 2.6B and C, we again plot the lower bound for the mutual information rates, but this time at a stronger inhibitory current. By increasing inhibition, we put the neuron in a subthreshold regime, a known prerequisite for SR. Indeed, both curves now show a maximum at a non-vanishing value of the respective other signal's strength. This is a new form of stochastic resonance, in which the role of the beneficial noise is played by a signal that is itself encoded in the output spike train.

2.4.1. Comparison of different noise sources

It is worthwhile to compare the SR effect in our setup to other scenarios of stochastic resonance. In a neuroscientific context, both channel noise (Goychuk and Hänggi, 2000; Schmid et al., 2001) and synaptic noise (Rudolph and Destexhe, 2001; Torres et al., 2011) have been shown to cause stochastic resonance. Synaptic noise, due to the stochastic bombardment by presynaptic spikes, can be controlled by changing the baseline firing rate of presynaptic populations; it is thus already present in our model. We model fast ion channel noise by explicitly adding a Gaussian white noise term $\sqrt{2D}\xi(t)$ (with $\langle\xi(t)\rangle = 0$ and $\langle\xi(t)\xi(t')\rangle = \delta(t-t')$) to the r.h.s of eq. (2.14), the voltage dynamics.

In order to be able to compare these different noise sources, we plot in Fig. 2.7 the mutual information rate for the D signal as a function of the output firing rate. Starting from $\epsilon_F = 0$, $D = 0\,\mathrm{nA^2s}$, and $r_F = 20\,\mathrm{Hz}$, we increase either the modulation amplitude, the noise strength, or the F population's baseline rate. It can be seen that the signal-mediated stochastic resonance (solid green line) is less efficient than either the classical variant with a white noise source (dashed green line) or the variant with synaptic noise (dotted green line). The variant with synaptic noise achieves the highest mutual information rates because in this case, one also increases the mean input, as mentioned above.

An important difference to both channel noise and synaptic noise as a beneficial factor in SR is that for our scenario of signal-mediated SR, the F signal that plays the role of the helpful noise is also encoded in the output spike train; we thus also plot the mutual information rate about the F signal (solid red line) and the sum of F and D signal (solid black line).

To understand why for example white-noise-mediated SR is more efficient than our signal-mediated SR, recall that the beneficial F signal has power in exactly the same frequency range as the D signal about which we measure information transmission. Thus, all helpful power (in the sense that it leads to an increase in output firing rate) lies also in the frequency range where it is conceivably most detrimental to information transmission. In contrast, in the white noise case, there are high-frequency components that may help to increase the firing rate without contaminating the signal frequency range.

The benefit of noise (or a second signal) that only has power outside the signal's frequency range is explicitly illustrated in Fig. 2.8, where, in addition to the curve from Fig. 2.6D, we also plot the mutual information rate about the D signal for an F signal that is shifted in frequency space ($f_0 = 10\,\mathrm{Hz}$, $f_c = 20\,\mathrm{Hz}$). One sees indeed that signal mediated SR is more effective in this *detuned* case.

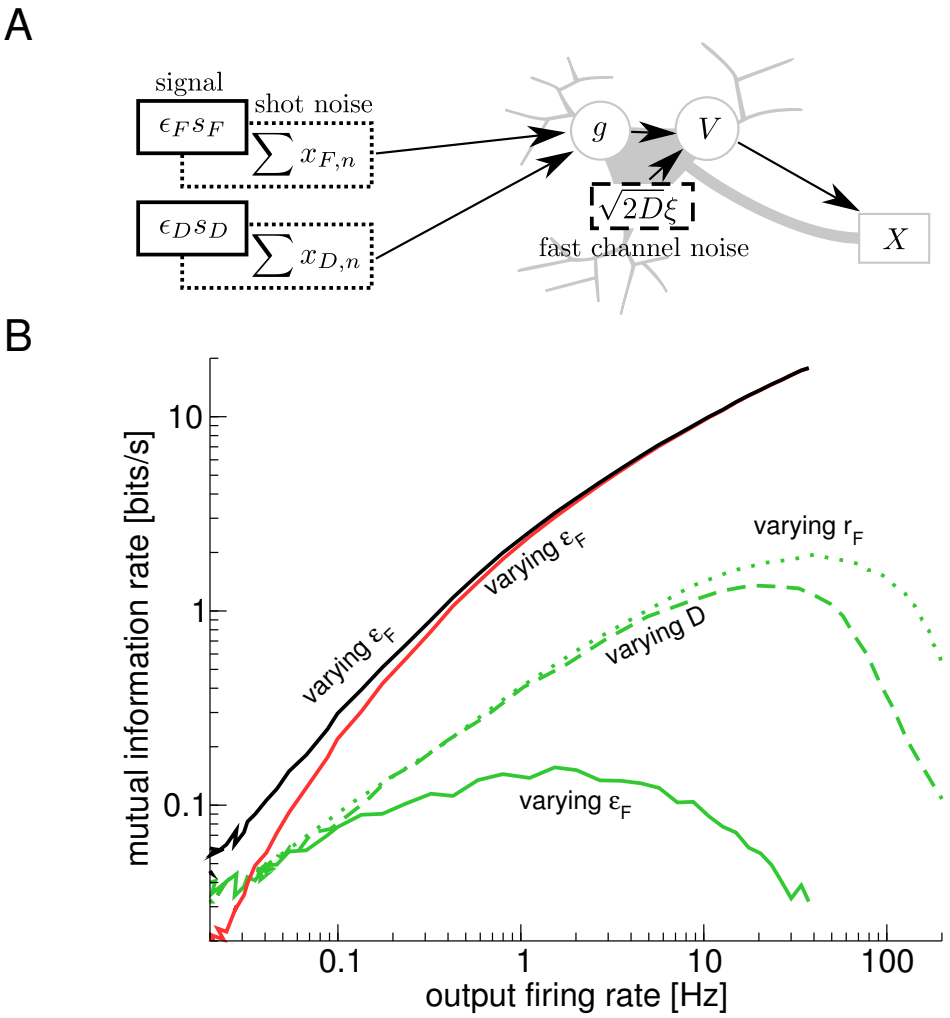

Figure 2.7.: Stochastic resonance with different noise sources. The different noise sources are sketched in A: In addition to the fluctuating signals (solid lines), noise is introduced by the stochastic encoding in spike trains (synaptic noise, dotted lines) and explicitly by adding a Gaussian white noise term to the voltage dynamics (dashed lines). In order to make the different scenarios comparable, we plot the mutual information rate (lower bound) over the output firing rate in B. Here, the color of the line refers to the signal about which we show the mutual information rate (green: D signal, red: F signal, black: sum of the two mutual information rates).

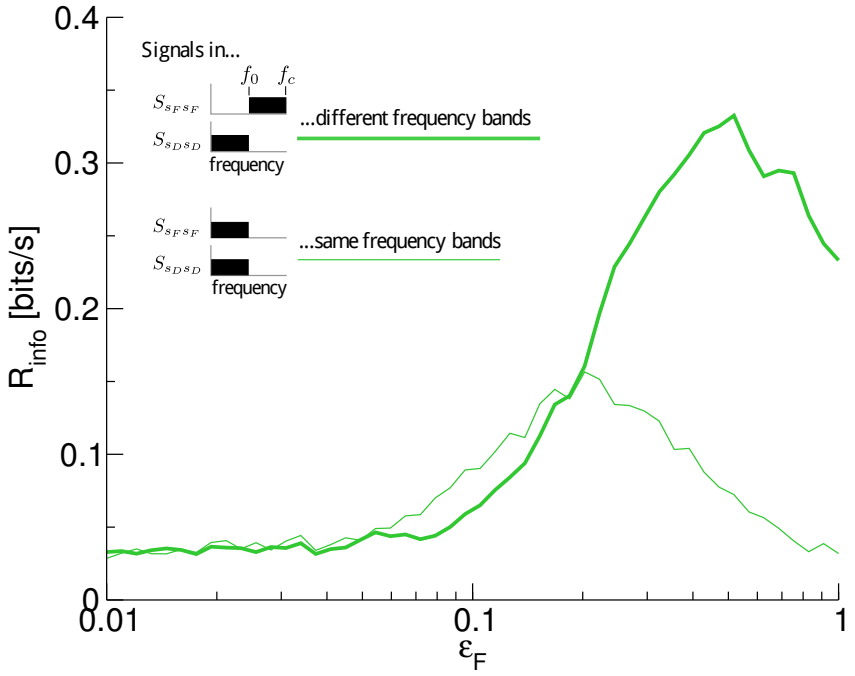

Figure 2.8.: Mutual information rate (lower bound) between D signal and output spike train when ϵ_F is varied. The thin line corresponds to the parameters in Fig. 2.6D and Fig. 2.7, while for the thick line, the F signal has been shifted in frequency space ($f_0 = 10\,\mathrm{Hz}$, $f_c = 20\,\mathrm{Hz}$).

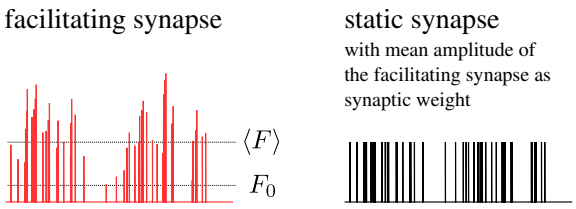

Figure 2.9.: Weights of the static synapses are chosen to equal the mean of their dynamic counterparts, here shown for a facilitating synapse.

2.4.2. Comparison to a setup with static synapses

In signal-mediated SR, the second signal helps the transmission of the first because it leads to an increase in output firing rate. Thus, in contrast to the spectral separation effect, the signal-mediated SR effect is not a consequence of synaptic dynamics. To better understand the influence of dynamic synapses on SR, we study the same setup with static synapses.

We choose the weights of the static synapses so that they equal the mean amplitudes of the respective dynamic synapse (note that more elaborate schemes exist (Lindner et al., 2009)). This choice is sketched in Fig. 2.9. The mean amplitudes are (Merkel and Lindner, 2010)

$$\langle F(t) \rangle = F_{0,I} + \Delta_I r_0 \tau + F, \tag{2.40}$$

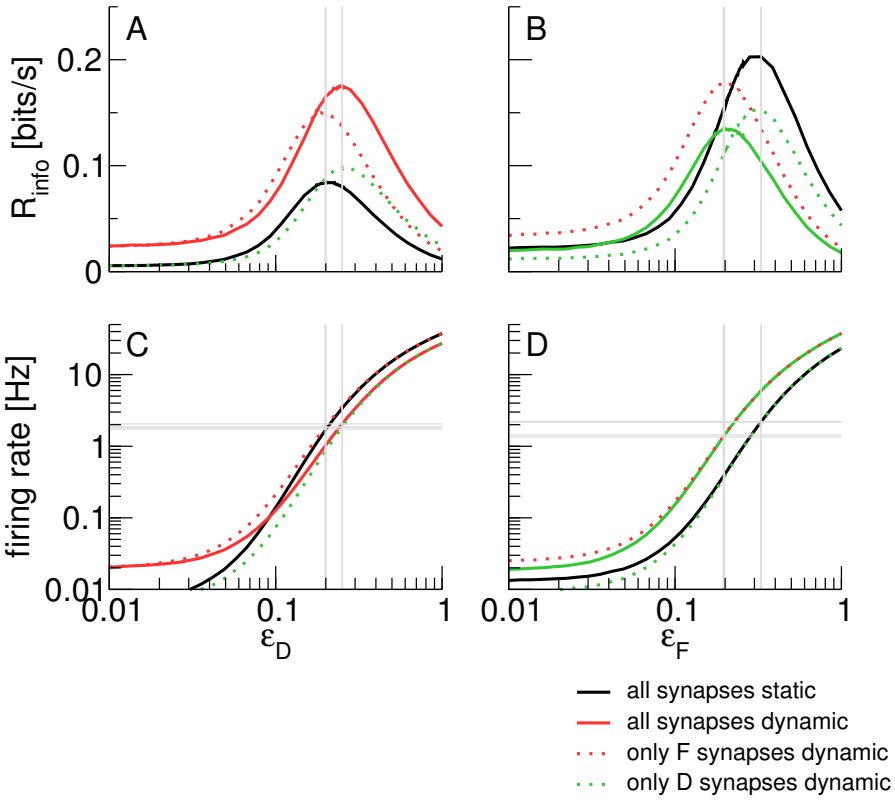

Figure 2.10.: Dependence of the SR peak on the nature of synaptic dynamics. Solid lines: both synaptic populations dynamic; red dotted lines: only facilitating synapses dynamic; green dotted lines: only depressing synapses dynamic; black solid lines: all synapses static. Static synapses for the F population have the weight set to $A = 0.19$, static synapses for the D population to $A = 0.29$. Other parameters as in Fig. 2.6.

$$\langle D(t) \rangle = \frac{F_0}{1 + F_0 r_0 \tau_D}, \tag{2.41}$$

with $F_{0,I}$ and Δ_I defined in eqs. (2.20, 2.21).

In Fig. 2.10, we plot the lower bound for the mutual information rate over the F (D) signal when ϵ_D (ϵ_F) is varied for different combinations of static and dynamic synapses. Indeed, all curves display an SR peak, irrespective of the nature of the synapses. There are, however, quantitative differences: The peak value is higher for dynamic than for static synapses in case of the F signal and vice versa in case of the D signal. When the synapses connecting the D population are static (solid black and dotted red line), the SR peak is shifted to lower values of ϵ_D, while it is shifted to higher values of ϵ_F when the F synapses are static (solid black and dotted green lines).

In the following, we refer to the synapses through which the signal-carrying spike trains enter as the "signal synapses" and to the other synapses as the "noise synapses". It is apparent that for the F signal, peak information transmission is higher with dynamic signal synapses than with static ones, while for the D signal, the opposite is true. This can be made plausible as follows: In the regime considered, fluctuations in the system are dominated by the noise synapses. The effect of changing the nature of the signal

synapses on the coherence is thus mainly due to the change in the cross spectrum between signal and output, because the noise power spectrum changes comparatively little. If the signal synapses are facilitating, their output has a higher cross-correlation with the signal than for static synapses, as the amplitudes of spikes change in parallel with signal modulations. For depressing synapses, by contrast, the change in amplitude is in the opposite sense, leading to a smaller cross-correlation than with static synapses. Thus, the coherence about the F signal decreases when facilitating synapses are replaced by static ones, while the opposite is true for the D signal.

We now give an explanation for the shifting of the peak. We see that the position of the peak depends on the nature of the noise synapses. To understand this, recall that the beneficial effect of noise in SR lies in an increase in firing rate. Tracing the gray vertical lines marking peak position to the bottom panels in Fig. 2.10, it becomes apparent that the SR maximum is attained when the output firing rate is around 2 Hz. A spike train that has passed through a facilitating synapse has more power than one that has passed through a static synapse (if mean weights are the same), while the situation is reversed for the case of depression. In Fig. 2.10A and C, replacing the (depressing) noise synapses by static ones thus feeds more power into the system, which in turn means that the firing rate of 2 Hz is already obtained at a lower ϵ_D. Conversely, in Fig. 2.10B and D, using static synapses reduces the power in the system, leading to a shift to higher values of ϵ_F. Changing the nature of the signal synapses has no noticeable effect on the peak positions, because in the regime displayed, fluctuations in the system are dominated by the noise synapses.

2.5. Summary

In this chapter, we have studied the interaction of two signals in a single neuron. The signals were encoded in the instantaneous firing rate of two presynaptic populations, one of which was connected to the target cell via facilitating, the other via depressing synapses. We used the coherence and the lower bound for the mutual information rate to address the question how one signal affects the transmission of the other and found two main effects: First, while for one signal in isolation, the coherence is flat (i.e. information transmission is broadband), the simultaneous presence of both signals leads to a spectral separation effect – the neuron now preferentially encodes information about slow components of the signal that enters through facilitating synapses, and fast components of the signal that enters via depressing synapses. Second, we observe a novel kind of stochastic resonance, in which the role of the helpful noise is played by the second signal: In a sub-threshold regime, there is a non-vanishing modulation amplitude for one signal that is optimal for the transmission of the other.

Chapter 3.

Theory for integrate-and-fire neurons driven by dichotomous noise

In this chapter, we lay the theoretical groundwork for the investigation of signal transmission in the presence of non-Gaussian (and, potentially, non-white) background noise that will be carried out in the following chapters. We consider IF neurons driven by Markovian dichotomous noise, a two-state process. The expressions we derive for IF neurons driven by such a process will then be used to explore the effect of finite synaptic weights (Chapter 4) and up-down states (Chapter 6) on information transmission.

We start by introducing dichotomous noise and listing some of its properties in Sec. 3.1. In Sec. 3.2, we define the dynamics of the model and discuss the master equation associated with it; here, we discuss initial and boundary conditions that are relevant to all of the subsequent sections. We calculate the stationary density for general IF neurons driven by dichotomous noise and discuss some differences to the case of Gaussian white noise in Sec. 3.3. In Sec. 3.4, we derive recursive relations for the ISI moments. We then turn to the calculation of spectral quantities that are relevant to assess information transmission: For the special case of an LIF neuron, we calculate the power spectrum in Sec. 3.5.1 and the susceptibility with respect to a current-modulated signal in Sec. 3.5.2. Finally, we derive an expression for the susceptibility with respect to the modulation of a switching rate of the noise in Sec. 3.5.3.

3.1. Dichotomous noise and its properties

Here, we introduce dichotomous noise and list some of its properties. These are known results; see, for instance, the works by Fitzhugh (1983); Horsthemke and Lefever (1984); Lindner (2009).

The dichotomous Markov process (DMP) $\eta(t)$ jumps between a *"+" state* ($\eta(t) = \sigma_+$) and a *"-" state* ($\eta(t) = \sigma_-$) (see Fig. 3.1). We denote the (constant) rate at which jumps *out of* the "+" state occur by k_+ and the rate of jumps out of the "-" state by k_-. Owing to the constant rates, the residence time in a given state is an exponentially distributed random variable.

We denote by $P_\pm(t)$ the probability to find the noise in "+" state/"-" state at time t, $P_\pm(t) := \Pr(\eta(t) = \sigma_\pm)$. The time evolution of these probabilities is given by the master

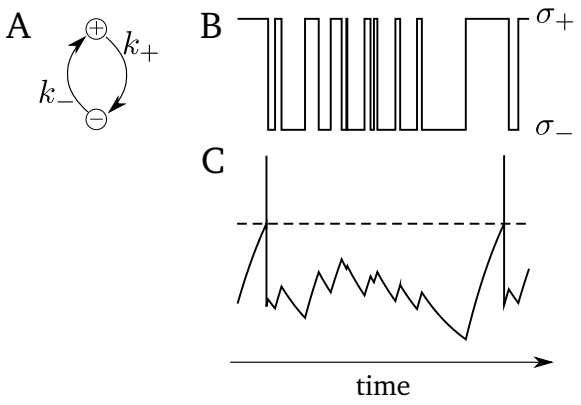

Figure 3.1.: Dichotomous noise jumps between a "+" and a "-" state at constant rates k_+ and k_- (A). A realization of such a process (where the "+" state is assigned the value σ_+ and the "-" state the value σ_-) is shown in B. C shows the voltage time-course of an LIF driven by this realization.

equation,

$$\frac{d}{dt}P_+ = -k_+P_+ + k_-P_-, \tag{3.1}$$

$$\frac{d}{dt}P_- = k_+P_+ - k_-P_-. \tag{3.2}$$

The solution of this system of equations is straightforward and allows, for instance, to calculate the transition probabilities

$$P_{i|j}(\tau) := \Pr\left[\eta(t+\tau) = \sigma_i | \eta(t) = \sigma_j\right], \tag{3.3}$$

where $i, j \in \{+, -\}$:

$$P_{+|+}(\tau) = \frac{k_+ e^{-(k_+ + k_-)\tau} + k_-}{k_+ + k_-}, \tag{3.4}$$

$$P_{+|-}(\tau) = \frac{k_-}{k_+ + k_-}\left(1 - e^{-(k_+ + k_-)\tau}\right), \tag{3.5}$$

$$P_{-|+}(\tau) = \frac{k_+}{k_+ + k_-}\left(1 - e^{-(k_+ + k_-)\tau}\right), \tag{3.6}$$

$$P_{-|-}(\tau) = \frac{k_- e^{-(k_+ + k_-)\tau} + k_+}{k_+ + k_-}. \tag{3.7}$$

One directly finds the stationary probabilities,

$$P_{0,+} := \frac{k_-}{k_+ + k_-}, \quad P_{0,-} := \frac{k_+}{k_+ + k_-}. \tag{3.8}$$

In general, a DMP has non-vanishing mean,

$$\langle \eta(t) \rangle = \frac{k_- \sigma_+}{k_+ + k_-} + \frac{k_+ \sigma_-}{k_+ + k_-}. \tag{3.9}$$

The variance is given by

$$\mathrm{var}(\eta(t)) = \frac{k_+ k_- (\sigma_+ - \sigma_-)^2}{(k_+ + k_-)^2}. \tag{3.10}$$

Dichotomous noise is a colored noise; it is exponentially correlated, with the correlation time τ_c given by

$$\tau_c = \frac{1}{k_+ + k_-}. \tag{3.11}$$

Another useful measure is the noise intensity,

$$D = \tau_c \mathrm{var}(\eta(t)) = \frac{k_+ k_- (\sigma_+ - \sigma_-)^2}{(k_+ + k_-)^3}. \tag{3.12}$$

The power spectrum of dichotomous noise is a Lorentzian,

$$S_{\eta\eta}(\omega) = \frac{2 k_+ k_-}{k_+ + k_-} \frac{(\sigma_+ - \sigma_-)^2}{\omega^2 + (k_+ + k_-)^2}. \tag{3.13}$$

3.2. Model and governing equations

Our aim is to derive analytical expressions for IF neurons driven by asymmetric dichotomous noise and a weak additive signal. The time evolution of the neuron's membrane potential v between spikes is given by the stochastic differential equation

$$\dot{v} = f(v) + \epsilon s(t) + \eta(t). \tag{3.14}$$

Here, $f(v)$ is a continuous, potentially nonlinear function, $s(t)$ is a time-dependent signal (with $\epsilon \ll 1$), and $\eta(t)$ is dichotomous noise. For ease of notation, we use non-dimensionalized dynamics, i.e. time is measured in units of the membrane time constant.

Spiking is implemented through a fire-and-reset rule: Once the membrane voltage hits

the firing threshold v_T, it is reset to the reset voltage v_R. There it is clamped for an absolute refractory period τ_{ref} before it continues to evolve according to eq. (3.14).

Most of the statistics we derive, such as the stationary distribution of the voltage, the firing rate, the coefficient of variation, or the power spectrum, describe the neurons *spontaneous activity*. Spontaneous activity refers to the absence of sensory input (the signal), not the absence of inputs in general — the DMP, thought to model, for example, input from a network undergoing transitions between up and down states, is still present. Thus, we set $\epsilon = 0$, except for Sec. 3.5.2, where we calculate the neuron's susceptibility to the signal.

The difference between the various types of IF neurons used in the literature lies in the choice of $f(v)$. The most simple case, for instance, is the perfect IF neuron (PIF), where $f(v) = \mu$ (where μ is a constant driving). The famous leaky IF neuron (LIF) owes its name to an additional linear leak term, $f(v) = \mu - v$. The quadratic IF neuron (QIF) has $f(v) = \mu + v^2$. Below, we will leave $f(v)$ unspecified wherever possible; only the calculations for power spectrum and susceptibility are restricted to LIF neurons. In all other cases, the general theoretical results are compared to simulations for LIF and QIF neurons.

The dichotomous process $\eta(t)$ jumps between the values σ_+ and σ_-. It is always possible to consider an equivalent system with symmetric noise values $\pm\sigma$ by setting $\sigma = (\sigma_+ - \sigma_-)/2$ and using a new nonlinearity,

$$\bar{f}(v) = f(v) + \frac{\sigma_+ + \sigma_-}{2}. \tag{3.15}$$

In the following, we mostly use this symmetrized version, but return to calling the nonlinearity $f(v)$ to ease notation. Note that the rates of the DMP, k_+ and k_-, will in general still be asymmetric. Removing asymmetry in the rates is less straightforward but also possible using a Lorentz transformation (Balakrishnan and Chaturvedi, 1988; Balakrishnan and Lakshmibala, 2005; Müller-Hansen et al., 2015). Here, however, we will explicitly keep asymmetric transition rates.

The spontaneous dynamics ($\epsilon = 0$) can be described as the switching between two deterministic flows: The system jumps between the *"+" dynamics*, where $\dot{v} = f(v) + \sigma$, and the *"-" dynamics*, where $\dot{v} = f(v) - \sigma$.

Dynamical regimes

The finite support of dichotomous noise introduces some constraints on the neuronal dynamics that one does not encounter with the commonly used additive Gaussian noise. In order to understand the range of possible voltages and to classify different regimes of firing, it is instructive to study the two deterministic flows $f(v) + \sigma$ and $f(v) - \sigma$.

The flow in the "+" dynamics should be positive for all $v < v_T$. Otherwise, if it had a fixed point (FP) at which $f(v) + \sigma = 0$, it would be impossible for the system to overcome this point toward higher values of v and the voltage could never reach the threshold. As we are interested in the firing statistics, we exclude this case.

The "-" dynamics, however, may well have FPs. The system can only cross such points

toward higher values of v via the "+" dynamics. Indirectly, FPs in the "-" dynamics may also be crossed toward lower values of v if the voltage crosses the threshold (making the neuron fire) and is subsequently reset (to a value below the FP). This means that the range of possible voltages is bounded below either by the reset voltage v_R or, if $f(v_R) - \sigma < 0$ and trajectories can move toward lower values, by the first FP below v_R, if one exists. Only if $f(v_R) - \sigma < 0$ and there exists no FP below v_R (e.g. for a PIF with $\mu - \sigma < 0$) does the range of possible voltages extend to $-\infty$.

A FP may be stable or unstable, depending on whether trajectories move toward it from both below and above, or away from it. Stability can be determined by the slope of $f(v) - \sigma$: positive slope corresponds to a stable, negative slope to an unstable FP. If the lower boundary is a FP, it is always a stable one — if the first FP below v_R is unstable, it can never be reached as $f(v_R) - \sigma > 0$ in this case.

Especially when the switching between noise states is slow (compared to the time from reset to threshold in one or both deterministic flows), the presence or absence of a stable FP in the "-" dynamics may have a strong qualitative effect on firing characteristics: If the system may get stuck in a stable FP, it needs to wait for the noise to switch before the next sequence of spikes is fired, leading to burst-like behavior.

If $f(v_T) - \sigma < 0$, the threshold can only be crossed during "+" dynamics, whereas for $f(v_T) - \sigma > 0$, the neuron may fire both during "+" and during "-" dynamics. As we discuss in detail below, this distinction is important in determining self-consistent initial conditions used in the solution of the associated master equation. Furthermore, it has consequences for the statistical structure of the generated spike train: In general, the spike train of neuron models driven by colored noise is not a renewal processes — interspike intervals may be correlated through the correlations in the driving noise. If the threshold may only be crossed in "+" dynamics, however, the neuron is reset to v_R with the noise in "+" state – the length of the ISI to come thus cannot be influenced by the previous interval (there can be no memory of the length of the previous interval if each interval starts from identical conditions) and spiking will be a renewal sequence despite the colored noise driving.

Master equation

For calculating statistics of the neuron's membrane voltage and spike train, the probability density $P(v,t)$ is of particular interest. $P(v,t)dv$ is the probability to find the voltage v in the infinitesimally small interval $(v + dv, v)$ at time t.

In order to describe systems driven by dichotomous noise, an established approach (Horsthemke and Lefever, 1984; Bena, 2006) is to consider *two* probability densities, $P_+(v,t)$ and $P_-(v,t)$, where $P_+(v,t)dv$ ($P_-(v,t)dv$) is the probability to find the noise in "+" state ("-" state) and v in the interval $(v + dv, v)$ at time t. The probability density $P(v,t)$ is then just the sum $P(v,t) = P_+(v,t) + P_-(v,t)$. In the absence of switching between noise states and without the fire-and-reset rule, the change in probability in an infinitesimally small voltage interval is given by the difference of probability in- and efflux. With the *flux*

$$J_\pm(v,t) := (f(v) + \epsilon s(t) \pm \sigma) P_\pm(v,t), \tag{3.16}$$

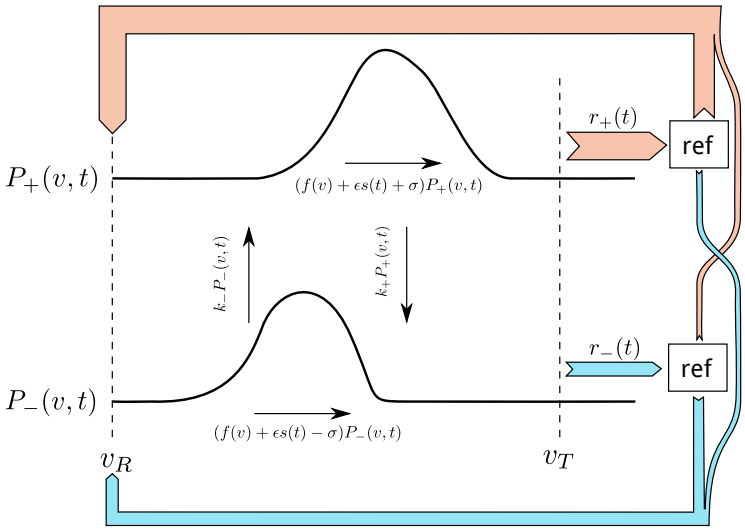

Figure 3.2.: Sketch of how the probability densities $P_+(v,t)$ and $P_-(v,t)$ evolve. Within a state, the evolution is determined by the deterministic drift, while the switching of the noise states leads to a flux between states. Trajectories that cross the threshold enter a refractory state; after the refractory period τ_{ref} has passed, a fraction of them have switched to the other noise state. Subsequently, trajectories are reset to v_R in their respective noise state.

this corresponds to the continuity equation

$$\partial_t P_\pm(v,t) = -\partial_v J_\pm(v,t). \tag{3.17}$$

Combining eq. (3.17) with the master equation for the dichotomous noise, eqs. (3.1 - 3.2), and allowing for (as of yet unspecified) inhomogeneities $\Delta_\pm(v,t)$, one obtains

$$\begin{aligned}\partial_t P_+(v,t) = &-\partial_v\left[(f(v)+\epsilon s(t)+\sigma)P_+(v,t)\right]\\ &-k_+P_+(v,t)+k_-P_-(v,t)+\Delta_+(v,t),\end{aligned} \tag{3.18}$$

$$\begin{aligned}\partial_t P_-(v,t) = &-\partial_v\left[(f(v)+\epsilon s(t)-\sigma)P_-(v,t)\right]\\ &+k_+P_+(v,t)-k_-P_-(v,t)+\Delta_-(v,t).\end{aligned} \tag{3.19}$$

This system of partial differential equations provides the starting point for all calculations in this chapter.

Like any partial differential equation, the master equations eqs. (3.18, 3.19) are not complete as long as no initial and boundary conditions have been given. Boundary and initial conditions are intimately linked to the fire-and-reset rule. In the following, we thus discuss in detail which boundary conditions are appropriate for a given problem and a specific dynamic regime. We also explain how these conditions can be simplified by properly choosing the inhomogeneities $\Delta_\pm(v,t)$.

Initial and boundary conditions

Consider the problem of calculating the probability density of interspike intervals (ISIs) of the spike train emitted by a neuron in a stationary state. As we detail below, a viable approach is to consider a corresponding first-passage-time (FPT) problem and ask how the escape times from the reset voltage v_R to the threshold are distributed. How should the initial conditions for such a problem be chosen?

For problems involving only white noise, this is easily answered — the only possibly relevant information about the beginning of a voltage trajectory is *where* it starts, leading to $P(v,0) = \delta(v - v_R)$. For colored noise, the situation is more complicated, as one also has to specify the distribution of the noise at the start of a trajectory. One could in principle choose arbitrary initial noise distributions (the noise is always in the "+" state, always in "-" state, distributed according to its stationary distribution, etc...) and would be dealing with a well-posed FPT problem. However, it would no longer be equivalent to calculating the ISI density, where the noise should, at the beginning of a trajectory, be distributed in accordance with the fact that the previous spike just occurred. When, for instance, threshold crossings are more likely in the "+" state, trajectories need to be equally more likely to start in the "+" state. The initial distribution for the noise thus needs to be the *noise upon firing*.

This changes somewhat with an absolute refractory period. In this case, the voltage stays clamped to v_R during the refractory period τ_{ref}, but the DMP (which is external to the neuron) evolves further (see sketch in Fig. 3.2). For the present case of dichotomous noise, let α be the fraction of trajectories that cross, in stationary state, the threshold while the noise is in the "+" state. We will later determine α self-consistently. Using the transition probabilities for the DMP, eq. (3.4) to eq. (3.7), the initial conditions are given by

$$\begin{aligned} P_+(v,\tau_{\mathrm{ref}}) &= \left[\alpha P_{+|+}(\tau_{\mathrm{ref}}) + (1-\alpha)P_{+|-}(\tau_{\mathrm{ref}})\right]\delta(v-v_R) \\ &= \left[\alpha e^{-\frac{\tau_{\mathrm{ref}}}{\tau_c}} + \frac{k_-}{k_+ + k_-}\left(1 - e^{-\frac{\tau_{\mathrm{ref}}}{\tau_c}}\right)\right]\delta(v-v_R) \qquad (3.20) \\ &=: \Gamma_+(\alpha,\tau_{\mathrm{ref}})\delta(v-v_R), \\ P_-(v,\tau_{\mathrm{ref}}) &= \left[\alpha P_{-|+}(\tau_{\mathrm{ref}}) + (1-\alpha)P_{-|-}(\tau_{\mathrm{ref}})\right]\delta(v-v_R) \\ &= \left[(1-\alpha)e^{-\frac{\tau_{\mathrm{ref}}}{\tau_c}} + \frac{k_+}{k_+ + k_-}\left(1 - e^{-\frac{\tau_{\mathrm{ref}}}{\tau_c}}\right)\right]\delta(v-v_R) \qquad (3.21) \\ &=: \Gamma_-(\alpha,\tau_{\mathrm{ref}})\delta(v-v_R). \end{aligned}$$

As a quick check on the plausibility of these ICs, consider the limit $\frac{\tau_{\mathrm{ref}}}{\tau_c} \to \infty$ (refractory period much larger than the correlation time of the noise). In this case, the noise upon firing should be forgotten, and indeed one finds that the initial noise distribution corresponds to the stationary distribution (see eq. (3.8)). Further, summing eqs. (3.20, 3.21)

(which corresponds to integrating out the noise variable) yields

$$P(v, \tau_{\text{ref}}) = \delta(v - v_R), \tag{3.22}$$

as expected.

We now turn to the boundary conditions. The instantaneous firing rate of the neuron, $r(t)$, corresponds to the time-dependent probability flux across the threshold,

$$r(t) = J(v_T, t), \tag{3.23}$$

provided that trajectories are removed after they have crossed the threshold (and, after a refractory period, are reinserted at the reset). This can be split into the rates conditioned on crossing in a given noise state,

$$\begin{aligned} r(t) &= r_+(t) + r_-(t) = J_+(v_T, t) + J_-(v_T, t) \\ &= [f(v_T) + \sigma]P_+(v_T, t) + [f(v_T) - \sigma]P_-(v_T, t), \end{aligned} \tag{3.24}$$

which directly gives us the boundary condition for the probability density at the threshold,

$$P(v_T, t) = \frac{r_+(t)}{f(v_T) + \sigma} + \frac{r_-(t)}{f(v_T) - \sigma}. \tag{3.25}$$

In contrast to white noise driving, for which the probability density always vanishes at an absorbing boundary, here, a non-vanishing firing rate leads to a jump in probability density. This is common to colored-noise-driven systems.

After trajectories have crossed the threshold and been removed at time t, they remain in a refractory state until, at $t + \tau_{\text{ref}}$, they are re-inserted at the reset voltage. This leads to a jump in the flux at the reset voltage,

$$J_\pm(v_R^{\leftarrow}, t + \tau_{\text{ref}}) - J_\pm(v_R^{\rightarrow}, t + \tau_{\text{ref}}) = \left[r_\pm(t) e^{-\frac{\tau_{\text{ref}}}{\tau_c}} + r(t) \frac{k_\mp}{k_+ + k_-} \left(1 - e^{-\frac{\tau_{\text{ref}}}{\tau_c}} \right) \right], \tag{3.26}$$

where $\cdot^{\leftarrow}$ ($\cdot^{\rightarrow}$) refers to a limit taken from above (below). The jump in the total flux sums to the firing rate,

$$J(v_R^{\leftarrow}, t + \tau_{\text{ref}}) - J(v_R^{\rightarrow}, t + \tau_{\text{ref}}) = r(t). \tag{3.27}$$

This gives a boundary condition for the difference between the solutions of the probability density above and below threshold,

$$P_\pm(v_R^{\leftarrow}, t + \tau_{\text{ref}}) - P_\pm(v_R^{\rightarrow}, t + \tau_{\text{ref}}) = \frac{r_\pm(t) e^{-\frac{\tau_{\text{ref}}}{\tau_c}} + r(t) \frac{k_\mp}{k_+ + k_-} \left(1 - e^{-\frac{\tau_{\text{ref}}}{\tau_c}} \right)}{f(v_R) \pm \sigma}. \tag{3.28}$$

For the stationary case, this can be rewritten by denoting the stationary firing rate by r_0

and using $\Gamma_\pm(\alpha, \tau_{\text{ref}})$ as defined in eqs. (3.20, 3.21),

$$P_\pm(v_R^{\leftarrow}) - P_\pm(v_R^{\rightarrow}) = r_0 \frac{\Gamma_\pm(\alpha, \tau_{\text{ref}})}{f(v_R) \pm \sigma}. \tag{3.29}$$

A more compact – and, physically, instructive – way of implementing these boundary conditions lies in introducing additional inhomogeneities. One can also think of the absorbing threshold as a probability *sink*, contributing the term

$$- r_\pm(t)\delta(v - v_T) \tag{3.30}$$

on the r.h.s. of the master equation, and the reset mechanism as a probability *source*, contributing

$$\left[r_\pm(t - \tau_{\text{ref}}) e^{-\frac{\tau_{\text{ref}}}{\tau_c}} + r(t - \tau_{\text{ref}}) \frac{k_\mp}{k_+ + k_-} \left(1 - e^{-\frac{\tau_{\text{ref}}}{\tau_c}}\right) \right] \delta(v - v_R). \tag{3.31}$$

By integrating the new master equations from $v_T - \epsilon$ to $v_T + \epsilon$, taking the limit $\epsilon \to 0$, and imposing the new boundary condition that the flux needs to vanish above the threshold, it is straightforward to show that the probability density satisfies the original boundary condition eq. (3.25) (and analogously for v_R).

The same approach can be taken for the initial condition. Adding the terms

$$\left[\alpha e^{-\frac{\tau_{\text{ref}}}{\tau_c}} + \frac{k_-}{k_+ + k_-} \left(1 - e^{-\frac{\tau_{\text{ref}}}{\tau_c}}\right) \right] \delta(v - v_R)\delta(t - \tau_{\text{ref}}), \tag{3.32}$$

$$\left[(1 - \alpha) e^{-\frac{\tau_{\text{ref}}}{\tau_c}} + \frac{k_+}{k_+ + k_-} \left(1 - e^{-\frac{\tau_{\text{ref}}}{\tau_c}}\right) \right] \delta(v - v_R)\delta(t - \tau_{\text{ref}}), \tag{3.33}$$

to the r.h.s. of the master equation, eqs. (3.18, 3.19), corresponds to injecting probability at the reset voltage at time t. Along with the new initial condition that there was *no* probability before τ_{ref}, this implements the initial condition discussed above.

Using source and sink terms to incorporate initial and boundary conditions makes for longer equations. However, it outsources some book-keeping from head to paper (one only has to remember the new trivial boundary/initial conditions that there is *no* probability above the threshold/before the injection) and, especially for the fire-and-reset rule, nicely fits the picture of removing and inserting trajectories.

3.3. Stationary density

To calculate the stationary probability density $P_0(v)$, we set the l.h.s. of eqs. (3.18, 3.19) to zero.

$$\begin{aligned} 0 = &- \left[(f(v)+\sigma)P_+(v)\right]' - k_+P_+(v) + k_-P_-(v) \\ &+ r_0\left[\Gamma_+(\alpha,\tau_{\text{ref}})\delta(v-v_R) - \alpha\delta(v-v_T)\right], \end{aligned} \tag{3.34}$$

$$\begin{aligned} 0 = &- \left[(f(v)-\sigma)P_-(v)\right]' + k_+P_+(v) - k_-P_-(v) \\ &+ r_0\left[\Gamma_-(\alpha,\tau_{\text{ref}})\delta(v-v_R) - (1-\alpha)\delta(v-v_T)\right], \end{aligned} \tag{3.35}$$

with $\Gamma_\pm(\alpha,\tau_{\text{ref}})$ as defined in eqs. (3.20, 3.21).

By expressing eqs. (3.34, 3.35) in terms of $P_0(v) = P_+(v) + P_-(v)$ and

$$Q(v) := P_+(v) - P_-(v) \tag{3.36}$$

and adding/subtracting one from the other, one obtains

$$0 = -\left[f(v)P_0(v) + \sigma Q(v)\right]' + r_0\left[\delta(v-v_R) - \delta(v-v_T)\right], \tag{3.37}$$

$$\begin{aligned} 0 = &- \left[f(v)Q(v) + \sigma P_0(v)\right]' - (k_+ - k_-)P_0(v) - (k_+ + k_-)Q(v) \\ &+ r_0\left[\Gamma_\Delta(\alpha,\tau_{\text{ref}})\delta(v-v_R) - (2\alpha-1)\delta(v-v_T)\right], \end{aligned} \tag{3.38}$$

where

$$\Gamma_\Delta(\alpha,\tau_{\text{ref}}) := \Gamma_+(\alpha,\tau_{\text{ref}}) - \Gamma_-(\alpha,\tau_{\text{ref}}) = (2\alpha-1)e^{-\frac{\tau_{\text{ref}}}{\tau_c}} + \frac{k_- - k_+}{k_+ + k_-}\left(1 - e^{-\frac{\tau_{\text{ref}}}{\tau_c}}\right). \tag{3.39}$$

Eq. (3.37) can be directly integrated, yielding an expression for the flux,

$$J(v) = \left[f(v)P_0(v) + \sigma Q(v)\right] = r_0\left[\theta(v-v_R) - \theta(v-v_T)\right], \tag{3.40}$$

which, as expected in the stationary state, is piecewise constant and, where it does not vanish, equal to the firing rate.

Solving eq. (3.40) for $Q(v)$ and plugging it into eq. (3.38) yields the ODE

$$\begin{aligned} G'(v) = &- \left[\frac{k_+}{f(v)+\sigma} + \frac{k_-}{f(v)-\sigma}\right] G(v) \\ &+ r_0\Bigg[\left(f(v)\left[\frac{k_+}{f(v)+\sigma} + \frac{k_-}{f(v)-\sigma}\right] - k_+ - k_-\right)\cdot\Big[\theta(v-v_R) - \theta(v-v_T)\Big] \\ &+ \sigma\Big[\Gamma_\Delta(\alpha,\tau_{\text{ref}})\delta(v-v_R) - (2\alpha-1)\delta(v-v_T)\Big]\Bigg], \end{aligned} \tag{3.41}$$

where we have used the abbreviation

$$G(v) := f(v)r_0\left[\theta(v-v_R)-\theta(v-v_T)\right]-\left(f^2(v)-\sigma^2\right)P_0(v). \tag{3.42}$$

Note that we have divided by $f^2(v)-\sigma^2$. At FPs of the "-" dynamics, where $f(v)=\sigma$, this is undefined and we cannot expect a solution of the ODE to be valid across such a point. How to handle FPs is discussed in detail below.

The ODE eq. (3.41) can be solved by variation of constants. After resubstituting $P_0(v)$ and simplifying the result using integration by parts, one obtains

$$\begin{aligned}P_0(v) = r_0\frac{e^{-\phi(v)}}{f^2(v)-\sigma^2}\Bigg[&f(c)e^{\phi(c)}\left[\theta(c-v_R)-\theta(c-v_T)\right]\\&+\Big[\theta(c-v_R)-\theta(v-v_R)\Big]\Big(\sigma\Gamma_\Delta(\alpha,\tau_{\text{ref}})-f(v_R)\Big)e^{\phi(v_R)}\\&-\Big[\theta(c-v_T)-\theta(v-v_T)\Big]\Big(\sigma(2\alpha-1)-f(v_T)\Big)e^{\phi(v_T)}\\&+\int_c^v dx\; e^{\phi(x)}\left[\theta(x-v_R)-\theta(x-v_T)\right]\left(f'(x)+k_+k_-\right)\Bigg],\end{aligned} \tag{3.43}$$

where c is a free constant and

$$\phi(v) := k_+\int^v du\;\frac{1}{f(u)+\sigma}+k_-\int^v du\;\frac{1}{f(u)-\sigma}. \tag{3.44}$$

For some common nonlinearities (PIF, LIF, QIF), closed-form expressions for $\phi(v)$ can be given. These are listed in Appendix A.1.

In order to fully understand how the free constant c as well as the firing rate r_0 and the fraction of threshold-crossings in "+" state, α, are determined, we first need to consider how the solution behaves near FPs of the "-" dynamics.

Dealing with fixed points of the "-" dynamics

It was first noted by Bena et al. (2002) that particular care needs to be taken at FPs of the deterministic flows when calculating stationary densities of DMP-driven systems. In essence, they pointed out that using one single solution across an unstable FP leads to a divergence, and that the correct procedure is to use solutions above and below the FP, with the respective free constant chosen such that the divergence vanishes. Before we follow their argument and demonstrate the symptom (the divergence) and the remedy (the proper choice of c) in our solution, it is instructive to ask what the healthy patient should look like.

At a FP of the "-" dynamics v_F, where $f(v_F)=\sigma$, the whole flux r_0 has to be mediated

by the "+" dynamics. This means (between reset and threshold)

$$J_+(v_F) = (f(v_F) + \sigma)P_+(v_F) = r_0, \tag{3.45}$$

which fixes

$$P_+(v_F) = \frac{r_0}{f(v_F) + \sigma} = \frac{r_0}{2\sigma}. \tag{3.46}$$

At v_F, the stationary master equation, eq. (3.35), thus becomes

$$0 = -f'(v_F)P_-(v_F) - \lim_{v \to v_F} \left((f(v) - \sigma)P'_-(v) \right) - k_-P_-(v_F) + k_+\frac{r_0}{2\sigma}. \tag{3.47}$$

If we assume that $P'_-(v)$ remains finite as $v \to v_F$, this simplifies to

$$0 = -f'(v_F)P_-(v_F) - k_-P_-(v_F) + k_+\frac{r_0}{2\sigma}. \tag{3.48}$$

This can be solved for $P_-(v_F)$ and one obtains

$$P_0(v_F) = \frac{r_0}{2\sigma}\left(1 + \frac{k_+}{f'(v_F) + k_-}\right). \tag{3.49}$$

Note that for stable FPs ($f'(v_U) < 0$), this expression may become negative when k_- becomes smaller than $|f'(v_U)|$. This is because for stable FPs with $k_- < |f'(v_U)|$, the probability density may diverge, violating the above assumption. Divergence at stable FPs is not a problem, as we discuss below.

To see how our solution, eq. (3.43), behaves in the vicinity of a FP v_F, we approximate $f(v) \approx f(v_F) + f'(v_F)(v - v_F) = \sigma + f'(v_F)(v - v_F)$. This means $f'(v) \approx f'(v_F)$, $f^2(v) - \sigma^2 \approx 2\sigma f'(v_F)(v - v_F)$,

$$e^{-\phi(v)} \approx \left|v - v_F\right|^{-\frac{k_-}{f'(v_F)}} \cdot \left|v - v_F + \tfrac{2\sigma}{f'(v_F)}\right|^{-\frac{k_+}{f'(v_F)}}, \tag{3.50}$$

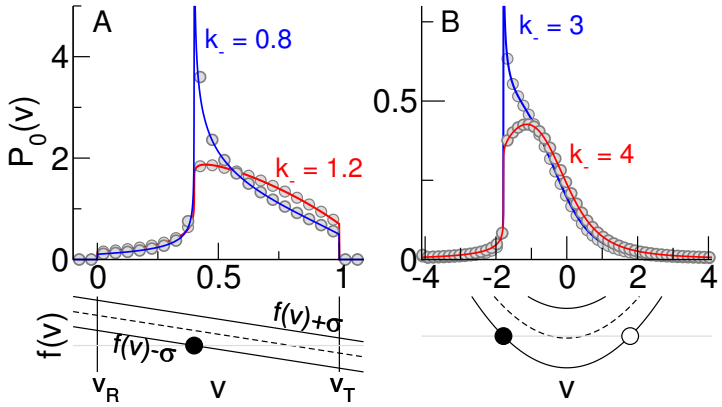

Figure 3.3.: Behavior of the stationary probability density at FPs of the "-" dynamics (lines: theory; circles: simulation results). Also shown is the nonlinearity $f(v) \pm \sigma$ and FPs (stable FPs: black dots; unstable FPs: white dots). A: LIF with $\mu = 0.8, v_R = 0, v_T = 1, \sigma = 0.4$ and $k_+ = 1.5$. Depending on the value of k_-, $p(v)$ can either be continuous at a stable FP ($k_- = 1.2$) or exhibit an integrable divergence ($k_- = 0.8$). B: QIF with $\mu = -0.2, v_R = -500, v_T = 500, \sigma = 3$ and $k_+ = 5$. Again, $p(v)$ is either continuous ($k_- = 4$) or exhibits an integrable divergence ($k_- = 3$) at the stable FP. Note that, owing to a proper choice of integration constants, it is smooth and continuous at the unstable FP.

and thus

$$
\begin{aligned}
P_0(v) \approx & \frac{\left|v - v_F\right|^{-\frac{k_-}{f'(v_F)}} \cdot \left|v - v_F + \frac{2\sigma}{f'(v_F)}\right|^{-\frac{k_+}{f'(v_F)}}}{2\sigma f'(v_F)(v - v_F)} \\
& \cdot \Bigg[f(c) e^{\phi(c)} \left[\theta(c - v_R) - \theta(c - v_T)\right] \\
& + \Big[\theta(c - v_R) - \theta(v - v_R)\Big] \Big(\sigma \Gamma_\Delta(\alpha, \tau_{\text{ref}}) - f(v_R)\Big) e^{\phi(v_R)} \\
& - \Big[\theta(c - v_T) - \theta(v - v_T)\Big] \Big(\sigma(2\alpha - 1) - f(v_T)\Big) e^{\phi(v_T)} \\
& + \int_c^v dx \, e^{\phi(x)} \left[\theta(x - v_R) - \theta(x - v_T)\right] \left(f'(x) + k_+ + k_-\right) \Bigg].
\end{aligned}
\tag{3.51}
$$

If v_U is an unstable FP, then $f'(v_U) > 0$ and $P_0(v)$ diverges,

$$
P_0(v) \sim |v - v_U|^{-\frac{k_-}{|f'(v_U)|} - 1}. \tag{3.52}
$$

As pointed out by Bena et al. (2002), this is "clearly unphysical and mathematically improper in view of the requirement of normalization". Any divergence should be integrable for $P_0(v)$ to be a probability density. Also, it should only occur at stable FPs,

where probability may accumulate, not at unstable ones, from where it is driven away.

The solution proposed by Bena et al. (2002) is to consider separate solutions above and below v_U and choose their respective integration constants so that a divergence is avoided. Here, this corresponds to setting $c = v_U$ in eq. (3.43). One may use l'Hôpital's rule to convince oneself that this does indeed lead to the finite value calculated above [eq. (3.49)],

$$\lim_{v \to v_U} P(v) = \frac{r_0}{2\sigma} \left(1 + \frac{k_+}{f'(v_U) + k_-} \right). \tag{3.53}$$

In contrast to unstable FPs, stable FPs ($f'(v_S) = -|f'(v_S)|$) pose no principal problem, the previously problematic term in eq. (3.51) becomes

$$|v - v_S|^{\frac{k_-}{|f'(v_S)|} - 1}. \tag{3.54}$$

For $k_- > |f'(v_S)|$, this does not diverge (trajectories leave toward the "+" state faster than new ones are coming in); for $k_- < |f'(v_S)|$, it diverges but can still be integrated. This is illustrated in Fig. 3.3. However, one still has to make sure that stable FPs lie outside the integration boundaries of the integral in eq. (3.43), where they would cause a divergence.

Full solution

As detailed above, the solution needs to be given separately in N intervals delimited by the threshold v_T, FPs of the "-" dynamics, and the lowest attainable voltage v_-. The free constants c_i ($i = 1 \dots N$) are then chosen as follows:

1. If the ith interval borders on an unstable FP at v_U, we have to avoid a divergence at that point. This fixes $c = v_U$, as discussed in the previous section.
2. In the rightmost interval ($i = N$), we have to ensure that the probability density vanishes beyond the threshold,

   $$P_0(v_T^{\leftarrow}) = 0. \tag{3.55}$$

   If $f(v_T) - \sigma < 0$, this fixes $c_N = v_T^{\leftarrow}$. In this case, the threshold can only be crossed during "+" dynamics, so $\alpha = 1$. If, however, $f(v_T) - \sigma > 0$, then the lower interval boundary is either an unstable FP, demanding $c_N = v_U$, or it is the reset voltage v_R, demanding $c_N = v_R^{\rightarrow}$ (see the treatment of the leftmost interval below). In this case, the boundary condition is used to determine α.
3. In the leftmost interval ($i = 1$), there are two possibilities. If $f(v_R) - \sigma < 0$, then v_- is a stable FP. In this case, the right interval boundary is either an unstable FP, fixing $c_1 = v_U$, or it is the threshold with $f(v_T) - \sigma < 0$, fixing $c_1 = v_T^{\leftarrow}$. Otherwise, if $f(v_R) - \sigma > 0$, we have to impose

   $$P_0(v_R^{\rightarrow}) = 0, \tag{3.56}$$

   which is ensured by $c_1 = v_R^{\rightarrow}$.

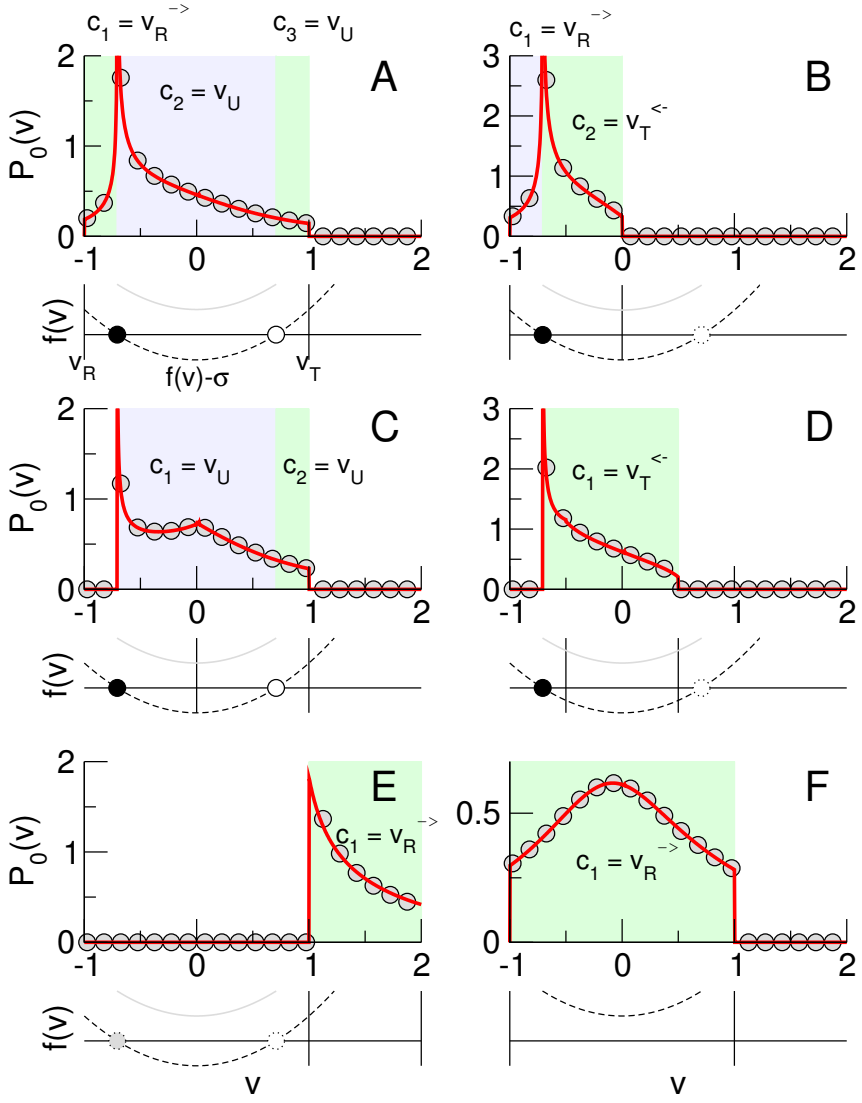

Figure 3.4.: Stationary probability density of a QIF neuron for different parameter sets (red solid lines), compared to simulation results (circles). Depending on the position of FPs of the "-" dynamics (shown as filled black or white circles) and the threshold- and reset points v_R and v_T, the solution is given in different intervals (shaded areas) according to eq. (3.57) and eq. (3.58). We show all possible interval combinations and list the choices of the integration constants c_i that satisfy the boundary conditions. Parameters: $\mu = 0.5, v_R = -1, v_T = 1$ (A), $\mu = 0.5, v_R = -1, v_T = 0$ (B), $\mu = 0.5, v_R = 0, v_T = 1$ (C), $\mu = 0.5, v_R = -0.5, v_T = 0.5$ (D), $\mu = 0.5, v_R = 1, v_T = 2$ (E), $\mu = 1.5, v_R = -1, v_T = 1$ (F); for all panels: $\sigma = 1, k_+ = 1.6, k_- = 0.9, \tau_{\text{ref}} = 0.1$. Note that threshold and reset for a QIF are usually set to $\pm\infty$ (in which case the solution would be either of the type in A or in F); here we have set them to finite values to illustrate all the different possible cases.

In Fig. 3.4, we illustrate the different possible cases and corresponding choices of c_i for a QIF neuron.

Note that for all choices of c_i, the term $f(c_i)e^{\phi(c_i)}\left[\theta(c_i - v_R) - \theta(c_i - v_T)\right]$ in eq. (3.43) vanishes. In the ith interval, we thus have the solution

$$\begin{aligned} P_0^i(v) = r_0 \frac{e^{-\phi(v)}}{f^2(v) - \sigma^2} \Bigg[& \Big[\theta(c_i - v_R) - \theta(v - v_R)\Big] \Big(\sigma\Gamma_\Delta(\alpha, \tau_{\text{ref}}) - f(v_R)\Big) e^{\phi(v_R)} \\ & - \Big[\theta(c_i - v_T) - \theta(v - v_T)\Big] \Big(\sigma(2\alpha - 1) - f(v_T)\Big) e^{\phi(v_T)} \\ & + \int_{c_i}^{v} dx\, e^{\phi(x)} \left[\theta(x - v_R) - \theta(x - v_T)\right] \left(f'(x) + k_+ + k_-\right) \Bigg], \end{aligned} \tag{3.57}$$

with

$$c_i = \begin{cases} v_R^{\rightarrow} & \text{if } i = 1 \text{ and } f(v_T) - \sigma > 0, \\ v_U & \text{if one of the interval boundaries is an unstable FP at } v_U, \\ v_T^{\leftarrow} & \text{if } i = N \text{ and } f(v_T) - \sigma < 0, \end{cases} \tag{3.58}$$

and

$$\alpha = 1 - \frac{\theta(v_R - c_N)\frac{k_+ e^{\phi(v_R)}}{k_+ + k_-}\left[1 - e^{-\frac{\tau_{\text{ref}}}{\tau_c}}\right] + k_+ \int_{c_N}^{v_T} dx\, e^{\phi(x)} \frac{\theta(x - v_R)}{f(x) + \sigma}}{e^{\phi(v_T)} - \theta(v_R - c_N) e^{-\frac{\tau_{\text{ref}}}{\tau_c}} e^{\phi(v_R)}}. \tag{3.59}$$

The above expression for α can be extracted from the condition $P_0(v_T^{\leftarrow}) = 0$. To arrive at the compact form in eq. (3.59), some simplifying steps are needed. An approach that directly yields the result in the form given above will be presented in the following section.

It remains to fix the last free parameter by calculating the firing rate r_0. This can be obtained from the normalization condition

$$r_0 \tau_{\text{ref}} + \int_{v_-}^{v_T} dv\, P_0(v) = 1. \tag{3.60}$$

An alternative derivation of the firing rate is given in the following, where we calculate the moments of the ISI density. As the general result is somewhat lengthy, we do not reproduce it here but refer to eq. (3.74) below.

We have already discussed qualitative aspects in which the probability density of DMP-driven IF neurons differs from white-noise-driven ones: The density does not go to zero at the threshold, and there are points where it may diverge (while still being integrable) (see Fig. 3.3). The former is due to the color of the noise (see e.g. (Gerstner et al., 2014)),

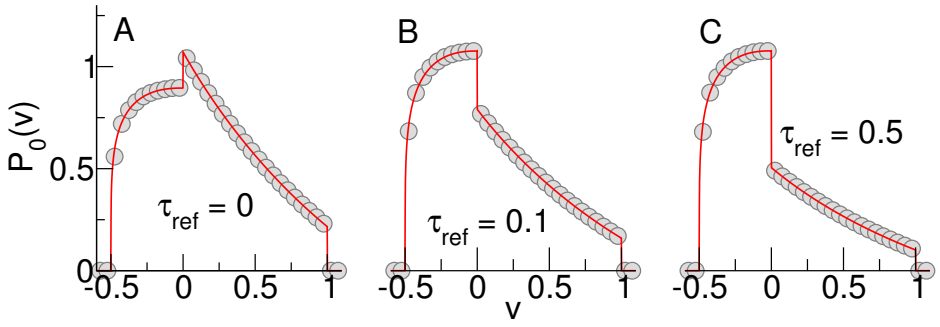

Figure 3.5.: Influence of the refractory period τ_{ref} on the stationary density of an LIF neuron. As, for the parameters used here, the threshold can only be crossed during "+" dynamics, all reset trajectories initially drift to the right for $\tau_{\text{ref}} = 0$ (A). Thus, the density jumps to higher values at v_R. As τ_{ref} is increased (B, C), the fraction of trajectories for which the noise has switched increases, so that already for $\tau_{\text{ref}} = 0.1$ (B), a majority of trajectories initially drifts to the left, leading to a downward jump in the density. Parameters: $k_+ = 3.3, k_- = 1.2, \sigma = 3, \mu = 2.5, v_R = 0, v_T = 1$.

while the latter is an effect of its stationary distribution, specifically the fact that it takes discrete values. An additional difference lies in the effect that the refractory period has on the probability density: For white noise driving, it only enters through a reduced firing rate. Here, by contrast, the refractory period has a qualitative impact on the probability density around v_R, as illustrated in Fig. 3.5.

3.4. Moments of the interspike interval density

In order to characterize neural spike train statistics, it is useful to derive expressions not only for the rate, but also for higher moments of the ISI density. A frequently used measure to quantify the regularity of spiking is the coefficient of variation (CV), which is defined in terms of the first two moments of the ISI density,

$$C_V = \frac{\sqrt{\langle T^2 \rangle - \langle T \rangle^2}}{\langle T \rangle}. \tag{3.61}$$

In this section, we derive recursive relations that allow to express the nth moment of the ISI density of IF neurons driven by a DMP in terms of quadratures.

The calculation of ISI moments corresponds to solving a FPT problem for the membrane voltage; specifically, the ISI density corresponds to the density of first-passage times from the reset voltage v_R to the threshold v_T.

For the case of one-dimensional systems driven by Gaussian white noise, recursive relations for the FPT moments have been known for a long time (Siegert, 1951). An alternative derivation was given by Lindner (2004b); here, we follow this approach and adapt it to DMP-driven IF neurons.

The starting point of our derivation is the observation that the FPT density corresponds to the time-dependent flux across the threshold of an ensemble in which all trajectories

start at v_R at time $t = \tau_{\text{ref}}$ and where, importantly, one has made sure (through appropriate boundary conditions) that no probability can flow back from above the threshold (which would mean that reentering trajectories are counted more than once).

We start by writing the master equation eqs. (3.18, 3.19) in terms of the total flux, $J(v,t) = J_+(v,t) + J_-(v,t)$, and the flux in "-" state, $J_-(v,t)$. The latter is a useful choice to obtain simple boundary conditions, because we know that $J_-(v,t)$ needs to vanish at FPs of the "-" dynamics. After some simplification, the resulting equations read

$$\partial_v J(v,t) = -\partial_t \left(\frac{J(v,t)}{f(v)+\sigma} + \frac{2\sigma J_-(v,t)}{f^2(v)-\sigma^2} \right) + \delta(t-\tau_{\text{ref}})\delta(v-v_R), \tag{3.62}$$

$$\begin{aligned} \partial_v J_-(v,t) = &- \left[\partial_v \phi(v)\right] J_-(v,t) - \frac{\partial_t J_-(v,t)}{f(v)-\sigma} + \frac{k_+}{f(v)+\sigma} J(v,t) \\ &+ \Gamma_-(\alpha,\tau_{\text{ref}})\delta(t-\tau_{\text{ref}})\delta(v-v_R), \end{aligned} \tag{3.63}$$

with $\Gamma_-(\alpha,\tau_{\text{ref}})$ as defined in eq. (3.21) and $\phi(v)$ as given in eq. (3.44).

We multiply both sides of eqs. (3.62, 3.63) by t^n and integrate them over t from $-\infty$ to ∞. For this, it is convenient to introduce the abbreviations

$$\mathcal{J}_n(v) := \int_{-\infty}^{\infty} dt\ J(v,t) t^n, \tag{3.64}$$

$$\mathcal{M}_n(v) := \int_{-\infty}^{\infty} dt\ J_-(v,t) t^n. \tag{3.65}$$

The term involving a time derivative can be integrated by parts. For eq. (3.63), for example, one has

$$-\int_{-\infty}^{\infty} dt\ t^n \partial_t \frac{J_-(v,t)}{f(v)-\sigma} = -\left[t^n \frac{J_-(v,t)}{f(v)-\sigma} \right]_{-\infty}^{\infty} + n \int_{\tau_{\text{ref}}}^{\infty} dt\ t^{n-1} \frac{J_-(v,t)}{f(v)-\sigma} \tag{3.66}$$

$$= n \frac{\mathcal{M}_{n-1}(v)}{f(v)-\sigma}. \tag{3.67}$$

Here, we have used that there is no flux before $t = \tau_{\text{ref}}$ and that all fluxes vanish for $t \to \infty$, as eventually all trajectories will have crossed the threshold. The integration by parts in eq. (3.62) is carried out analogously.

One obtains a system of ODEs,

$$\frac{d}{dv}\mathcal{J}_n(v) = n \left(\frac{\mathcal{J}_{n-1}(v)}{f(v)+\sigma} + \frac{2\sigma \mathcal{M}_{n-1}(v)}{f^2(v)-\sigma^2} \right) + \tau_{\text{ref}}^n \delta(v-v_R), \tag{3.68}$$

$$\frac{d}{dv}\mathcal{M}_n(v) = -\phi'(v)\mathcal{M}_n(v) + n\frac{\mathcal{M}_{n-1}(v)}{f(v)-\sigma} + \frac{k_+\mathcal{J}_n(v)}{f(v)+\sigma} + \tau_{\text{ref}}^n\Gamma_-(\alpha,\tau_{\text{ref}})\delta(v-v_R). \tag{3.69}$$

Eq. (3.68) can be directly integrated and eq. (3.69) can be solved by variation of constants. Keeping in mind the necessary treatment of FPs in the "-" dynamics (see the previous section), the voltage axis needs to be divided into N intervals delimited by the threshold voltage v_T, FPs in the "-" dynamics, and the lowest attainable voltage v_- (as illustrated for a QIF in Fig. 3.4). Denoting by $i(v)$ the interval containing the voltage v, and by l_i and r_i the lower and upper boundaries of the ith interval, the solutions can be given as

$$\mathcal{J}_n(v) = \sum_{i=1}^{i(v)} \int_{l_i}^{\min(v,r_i)} dx\; n\left(\frac{\mathcal{J}_{n-1}(x)}{f(x)+\sigma} + \frac{2\sigma\mathcal{M}_{n-1}^i(x)}{f^2(x)-\sigma^2}\right) + \tau_{\text{ref}}^n\delta(x-v_R), \tag{3.70}$$

$$\mathcal{M}_n^i(v) = e^{-\phi(v)}\int_{c_i}^{v} dx\; e^{\phi(x)}\left(n\frac{\mathcal{M}_{n-1}^i(x)}{f(x)-\sigma} + \frac{k_+\mathcal{J}_n(x)}{f(x)+\sigma} + \tau_{\text{ref}}^n\Gamma_-(\alpha,\tau_{\text{ref}})\delta(x-v_R)\right). \tag{3.71}$$

Here, we have already satisfied the boundary condition for $\mathcal{J}_n(v)$: The total flux needs to vanish at the lowest attainable voltage $v_- = l_1$, which implies $\mathcal{J}_n(l_1) = 0$.

The boundary conditions for $\mathcal{M}_n^i(v)$ warrant a more detailed discussion. There are three kinds of BCs:

1. If $f(v_T) - \sigma < 0$, one needs to ensure that no trajectories cross the threshold from above; this means $J_-(v_T, t) = 0$, leading to $\mathcal{M}_n^N(v_T) = 0$. This BC has to be satisfied by setting $c_N = r_N = v_T^{\leftarrow}$.
2. If $f(v_R) - \sigma > 0$, then no trajectory can cross the reset voltage toward lower values. This implies $J_-(v_R^{\rightarrow}, t) = 0$ and thus $\mathcal{M}(v_R^{\rightarrow}) = 0$, which is satisfied by choosing $c_1 = l_1 = v_R^{\rightarrow}$.
3. Finally, if the ith interval is delimited below (above) by an unstable FP in the "-" dynamics, setting $c_i = l_i$ ($c_i = r_i$) is needed for the proper behavior at the FP (vanishing instead of diverging flux $J_-(v_U, t)$).

The three BCs thus lead to the same choice in c_i as in the calculation of the stationary density above. Again, they consistently cover all cases: For example, if $f(v_T) - \sigma > 0$, then the "no backflow" condition is automatically fulfilled and cannot be used to determine c_N. However, in this case c_N is still uniquely determined by one of the other BCs: Either $f(v) - \sigma$ does not have zero crossings between v_T and v_R, in which case the left interval boundary is $v_R^{\rightarrow}$, at which $f(v_R) - \sigma > 0$ and BC 2 demands $c_N = v_R^{\rightarrow} = l_N$. Or there is a zero crossing, in which case the lower interval boundary is necessarily an unstable FP and BC 3 demands $c_N = v_U = l_N$. Note that c_i is always one of the two interval boundaries.

Our aim was to obtain an expression for the nth moment of the ISI density. As we

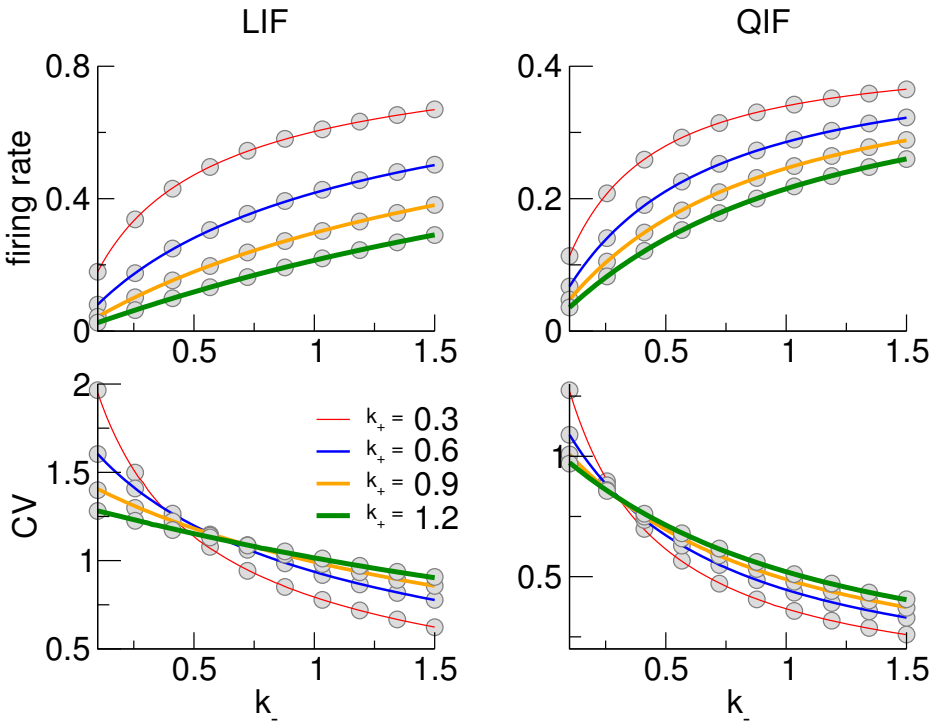

Figure 3.6.: Firing rate and CV of LIF and QIF neurons over k_- for different values of k_+. Theory (lines) is compared to simulation results (symbols). Parameters: $\mu = 0.5, \sigma = 1, v_R = 0, v_T = 1, \tau_{\text{ref}} = 0$ (LIF), $\mu = 0.5, \sigma = 1, v_R = -10, v_T = 10, \tau_{\text{ref}} = 0$ (QIF).

have argued, the ISI density corresponds to the flux across the threshold with boundary conditions as described above. To calculate the nth moment, we may thus recursively calculate $\mathcal{J}_n(v)$ and evaluate it at the threshold,

$$\langle T^n \rangle = \int_0^\infty dT\ T^n J(v_T, T) = \mathcal{J}_n(v_T). \tag{3.72}$$

From eq. (3.70), one sees directly that $\mathcal{J}_0(v_T) = 1$, consistent with the requirement that the FPT density be normalized.

Finally, eqs. (3.70, 3.71) provide a quick way to calculate α. Recall that α is the fraction of trajectories that cross the threshold in "+" state. Thus,

$$\alpha = \int_0^\infty dt\ J_+(v_T, t) = \mathcal{J}_0(v_T) - \mathcal{M}_0(v_T). \tag{3.73}$$

This can be solved for α (in general, the r.h.s. also depends on α !), yielding the expression given in eq. (3.59).

The first ISI moment reads

$$\begin{aligned}\langle T\rangle = (k_+ + k_-)\sum_{i=1}^{N}\int_{l_i}^{r_i} dx\;\theta(x-v_R)\frac{e^{\phi(x)}}{f(x)+\sigma}\int_{x}^{\bar{c}_i} dy\;\frac{e^{-\phi(y)}}{f(y)-\sigma}\\ + \tau_{\rm ref} + e^{-\phi(v_T)}\int_{c_N}^{v_T} dx\;\frac{e^{\phi(x)}}{f(x)+\sigma} \qquad (3.74)\\ + \frac{\Gamma_-(\alpha,\tau_{\rm ref})}{k_+}\left(e^{\phi(v_R)-\phi(\bar{c}_1)} - 1 + (k_+ + k_-)e^{\phi(v_R)}\int_{v_R}^{\bar{c}_1} dx\;\frac{e^{-\phi(x)}}{f(x)-\sigma}\right),\end{aligned}$$

where $\bar{c}_i$ denotes the interval boundary opposite of c_i.

As an example, we plot in Fig. 3.6 firing rate and CV for an LIF and a QIF for varying k_- and different values of k_+. It can be seen that our theory (lines) matches simulation results (symbols). For both neuron models, the firing rate (at fixed k_+) increases with k_-, which is plausible, as the DMP spends more time in the "+" state, in which the threshold can be crossed (LIF) or the stable FP overcome (QIF). Conversely, with increasing k_+ at fixed k_-, the firing rate decreases. The CV decreases with increasing k_-; for varying k_+, the situation is more complicated: At small k_-, increasing k_+ makes spiking more regular, while at larger k_-, it makes it less regular.

A detailed discussion of how firing rate and CV depend on the noise correlation time (including an expansion in the limit of small correlation times) and other model parameters can be found in (Droste and Lindner, 2014).

3.5. Power spectrum and susceptibility for the case of leaky integrate-and-fire neurons

Ultimately, our motivation for developing a theory of IF neurons driven by dichotomous noise is to understand how signal transmission is affected by up/down states. In particular, we ask how a single neuron transmits a weak signal when the dominant input consists of two-state fluctuations. In order to calculate, in linear response, the coherence between signal and output spike train of a neuron driven by a DMP, we need expressions for

- the power spectrum, quantifying the noise background that the signal has to stand out against,
- the susceptibility, quantifying the amplitude and phase with which the neuron responds to a stimulus at a given frequency.

Below, we consider the case of a *leaky* integrate-and-fire neuron driven by asymmetric dichotomous noise and derive exact expressions for the power spectrum of the neuron's

spontaneous activity[1] as well as its susceptibility with respect to a weak signal. This means we restrict ourselves to the case $f(v) = \mu - v$. The dynamics are described by

$$\dot{v} = \mu - v + \epsilon s(t) + \eta(t). \tag{3.75}$$

For the calculation of the power spectrum, we set $\epsilon = 0$.

In the following derivation, we concentrate on the regime of noise parameters where the threshold can only be crossed in "+" state ($\mu - \sigma < v_T$). During down states (which the "-" state is supposed to model), the postsynaptic membrane potential is usually strongly hyperpolarized (Steriade et al., 2001), so that this choice arises naturally. Further, we assume that the stable FP is below the reset voltage ($\mu - \sigma < v_R$). While for this particular choice of parameters, the neuronal spike train is a renewal process, we would like to stress that we do not use the renewal property in the derivation of the power spectrum. Extending our derivation to the case where $\mu - \sigma > v_T$ should thus be straightforward.

Our derivation was inspired by (Richardson, 2008), where a similar approach is used to obtain numerical integration schemes for spectra and susceptibilities of nonlinear IF neurons driven by Gaussian white noise. Conveniently, both the problem of calculating the power spectrum as well as that of calculating the susceptibility lead to a set of ODEs that have the same structure and only differ in their inhomogeneities. Below, we therefore calculate the power spectrum in detail and then re-use the results in the calculation of the susceptibility.

3.5.1. Power spectrum

The Wiener-Khinchin theorem (Gardiner, 1985; Risken, 1989),

$$S_{xx}(\omega) = \int_{-\infty}^{\infty} d\tau \; e^{i\omega\tau} \mathcal{K}_{xx}(\tau), \tag{3.76}$$

relates the power spectrum $S_{xx}(\omega)$ of a stationary process $x(t)$ to the autocorrelation function $\mathcal{K}_{xx}(\tau)$. As we have shown in the introduction (Sec. 1.2.1), the latter can be written as

$$\mathcal{K}_{xx}(\tau) = r_0 m(\tau) + r_0 \delta(\tau) - r_0^2, \tag{3.77}$$

where r_0 is the stationary firing rate and $m(\tau)$ is the *spike-triggered rate*, i.e. the rate at which spikes occur at time $t = \tau$ given that there was a (different) spike at $t = 0$. The power spectrum is then given by

$$S_{xx}(\omega) = r_0 \left(1 + 2\Re[\widetilde{m}(\omega)]\right). \tag{3.78}$$

The task is thus to calculate $\widetilde{m}(\omega)$, the spike-triggered rate, in the Fourier domain.

As we want to calculate the time-dependent rate (flux over threshold) given that a spike just occurred, the initial condition is the same as for the FPT problem. However, here we are not only interested in the rate at which the *first* spike occurs at time t (the

[1] Spontaneous activity refers to the absence of *sensory* inputs (the signal), not the absence of inputs in general. The dominant two-state input, modeled by the DMP, is, of course, still present.

FPT density) but the rate that *any spike* (be it the second, third, ...) occurs at that time. We therefore need to include the reset mechanism. The master equation reads

$$\begin{aligned}\partial_t P_+(v,t) = &-\partial_v\left((\mu - v + \sigma)P_+(v,t)\right) - k_+ P_+(v,t) + k_- P_-(v,t)\\ &+ m(t-\tau_{\text{ref}})P_{+|+}(\tau_{\text{ref}})\delta(v-v_R) - m(t)\delta(v-v_T)\\ &+ \delta(t-\tau_{\text{ref}})P_{+|+}(\tau_{\text{ref}})\delta(v-v_R),\end{aligned} \tag{3.79}$$

$$\begin{aligned}\partial_t P_-(v,t) = &-\partial_v\left((\mu - v - \sigma)P_-(v,t)\right) + k_+ P_+(v,t) - k_- P_-(v,t)\\ &+ m(t-\tau_{\text{ref}})P_{-|+}(\tau_{\text{ref}})\delta(v-v_R)\\ &+ \delta(t-\tau_{\text{ref}})P_{-|+}(\tau_{\text{ref}})\delta(v-v_R).\end{aligned} \tag{3.80}$$

One may transform this set of partial differential equations into ODEs by Fourier transform (conveniently, the quantity of interest is $\widetilde{m}(\omega)$). Using

$$\int_{-\infty}^{\infty} dt\; m(t-\tau_{\text{ref}})e^{i\omega t} = \widetilde{m}(\omega)e^{i\omega\tau_{\text{ref}}}, \tag{3.81}$$

one finds

$$\begin{aligned}-i\omega\widetilde{P}_+(v,\omega) = &-\frac{d}{dv}\left[(\mu - v + \sigma)\widetilde{P}_+(v,\omega)\right] - k_+\widetilde{P}_+(v,\omega) + k_-\widetilde{P}_-(v,\omega)\\ &+\widetilde{\Delta}_+(v,\omega),\end{aligned} \tag{3.82}$$

$$\begin{aligned}-i\omega\widetilde{P}_-(v,\omega) = &-\frac{d}{dv}\left[(\mu - v - \sigma)\widetilde{P}_-(v,\omega)\right] + k_+\widetilde{P}_+(v,\omega) - k_-\widetilde{P}_-(v,\omega)\\ &+\widetilde{\Delta}_-(v,\omega),\end{aligned} \tag{3.83}$$

where

$$\begin{aligned}\widetilde{\Delta}_+(v,\omega) = &\widetilde{m}(\omega)\left[e^{i\omega\tau_{\text{ref}}}P_{+|+}(\tau_{\text{ref}})\delta(v-v_R) - \delta(v-v_T)\right]\\ &+ e^{i\omega\tau_{\text{ref}}}P_{+|+}(\tau_{\text{ref}})\delta(v-v_R),\end{aligned} \tag{3.84}$$

$$\widetilde{\Delta}_-(v,\omega) = \widetilde{m}(\omega)e^{i\omega\tau_{\text{ref}}}P_{-|+}(\tau_{\text{ref}})\delta(v-v_R) + e^{i\omega\tau_{\text{ref}}}P_{-|+}(\tau_{\text{ref}})\delta(v-v_R). \tag{3.85}$$

To unburden notation, we will omit the ω argument in the following.

One may transform the system of two first-order ODEs to one second-order ODE for

the total flux $\widetilde{J}(v)$ (the calculation can be found in Appendix A.2):

$$\begin{aligned} 0 = {} & \widetilde{J}''(v) + p(v)\widetilde{J}'(v) + q(v)\widetilde{J}(v) \\ & - \left(p(v) + \frac{i\omega}{\mu - v + \sigma}\right)\widetilde{\Delta}_+(v) - \left(p(v) + \frac{i\omega}{\mu - v - \sigma}\right)\widetilde{\Delta}_-(v) \\ & - \widetilde{\Delta}'_+(v) - \widetilde{\Delta}'_-(v), \end{aligned} \tag{3.86}$$

where

$$p(v) := -\frac{(\mu - v)\,(2 - k_+ - k_- + 2i\omega) + \sigma\,(k_+ - k_-)}{(\mu - v)^2 - \sigma^2}, \tag{3.87}$$

$$q(v) := \frac{i\omega\,(1 - k_+ - k_- + i\omega)}{(\mu - v)^2 - \sigma^2}. \tag{3.88}$$

In the following, we solve this ODE and then exploit that the flux has to vanish at the lowest possible voltage to calculate the spike-triggered rate.

To find solutions to the homogeneous equation $0 = \widetilde{J}''(v) + p(v)\widetilde{J}'(v) + q(v)\widetilde{J}(v)$, one needs to characterize its singular points (Morse and Feshbach, 1953), i.e. points where $p(v)$ and/or $q(v)$ diverge. A singular point v_0 is called regular if $(v - v_0)p(v)$ and $(v - v_0)^2 q(v)$ remain finite as $v \to v_0$.

In our case, there are three regular singular points; they lie at $\mu \pm \sigma$ and ∞ (the behavior at ∞ is judged by performing a change of variables $v \to 1/u$ and considering $u \to 0$). Any second-order ODE with at most three regular singular points can be transformed into the hypergeometric differential equation (Morse and Feshbach, 1953), for which solutions are known in terms of hypergeometric functions. The regular singular points of the hypergeometric differential equation lie at 0, 1 and ∞, suggesting a change of variables from v to z,

$$v = 2\sigma z + \mu - \sigma. \tag{3.89}$$

Performing this change of variables on eq. (3.86) leads to

$$\begin{aligned} 0 = {} & \widetilde{J}''(z) + p(z)\widetilde{J}'(z) + q(z)\widetilde{J}(z) \\ & - \left(p(z) + \frac{i\omega}{1 - z}\right)2\sigma\widetilde{\Delta}_+(z) - \left(p(z) - \frac{i\omega}{z}\right)2\sigma\widetilde{\Delta}_-(z) \\ & - 2\sigma\left[\widetilde{\Delta}'_+(z) + \widetilde{\Delta}'_-(z)\right], \end{aligned} \tag{3.90}$$

where all derivatives are now to be understood with respect to z and where

$$p(z) = \frac{-z\,(2 - k_+ - k_- + 2i\omega) + (1 - k_- + i\omega)}{z(1 - z)}, \tag{3.91}$$

$$q(z) = \frac{-i\omega\left(1 - k_+ - k_- + i\omega\right)}{z(1-z)}. \tag{3.92}$$

By comparison, one finds that the homogeneous part corresponds to the hypergeometric differential equation (Morse and Feshbach, 1953),

$$z(1-z)\widetilde{J}''(z) + \left(c - z(1+a+b)\right)\widetilde{J}'(z) - ab\widetilde{J}(z) = 0, \tag{3.93}$$

with the parameters

$$a = i\omega, \tag{3.94}$$
$$b = 1 - k_+ - k_- + i\omega, \tag{3.95}$$
$$c = 1 - k_- + i\omega. \tag{3.96}$$

Between the singular points 0 and 1 (the region between stable FP and threshold that we are interested in), linearly independent solutions to this equation are given by

$$\widetilde{J}_1(z) = {}_2F_1\left(a, b; c; z\right) \tag{3.97}$$
$$= {}_2F_1\left(i\omega, 1 - k_+ - k_- + i\omega, 1 - k_- + i\omega, z\right), \tag{3.98}$$

$$\widetilde{J}_2(z) = z^{1-c}{}_2F_1\left(1 + a - c, 1 + b - c; 2 - c; z\right) \tag{3.99}$$

$$= z^{k_- - i\omega}{}_2F_1\left(k_-, 1 - k_+; 1 + k_- - i\omega; z\right), \tag{3.100}$$

where ${}_2F_1\left(a, b; c, z\right)$ is the hypergeometric function (Abramowitz and Stegun, 1972) .

It remains to calculate the full solution for given inhomogeneities $\widetilde{\Delta}_+(v)$ and $\widetilde{\Delta}_-(v)$. Once two linearly independent solutions to the homogeneous equation are known, a particular solution $J_p(z)$ to the inhomogeneous ODE

$$\widetilde{J}''(z) + p(z)\widetilde{J}'(z) + q(z)\widetilde{J}(z) = \widetilde{\Delta}(z) \tag{3.101}$$

is known at least formally (Morse and Feshbach, 1953):

$$J_p(z) = \int_z^\infty du\ \widetilde{\Delta}(u)\frac{\widetilde{J}_2(u)\widetilde{J}_1(z) - \widetilde{J}_1(u)\widetilde{J}_2(z)}{W(u)}, \tag{3.102}$$

where $W(z)$ is the Wronskian,

$$W(z) = \widetilde{J}_1(z)\widetilde{J}_2'(z) - \widetilde{J}_1'(z)\widetilde{J}_2(z), \tag{3.103}$$

and where we have set the upper integration limit to ∞ (which will turn out to be convenient for satisfying the boundary conditions of the full solution).

The general solution is then given by

$$\widetilde{J}(z) = c_1\widetilde{J}_1(z) + c_2\widetilde{J}_2(z) + J_p(z), \tag{3.104}$$

where c_1 and c_2 are integration constants. Above the threshold, the flux has to vanish. Because $\Delta(z) = 0$ for $z > z_T$, it follows that also $J_p(z) = 0$ for $z > z_T$. Both $\widetilde{J}_1(z)$ and $\widetilde{J}_2(z)$ are, however, in general non-zero, and because they are linearly independent, the only choice of integration constants that lead to a vanishing flux for $z > z_T$ is $c_1 = c_2 = 0$. Thus, the particular solution, eq. (3.102), already *is* the full solution.

In Appendix A.3, we show that eq. (3.102), evaluated at $z = 0$ (corresponding to the lowest possible voltage v_-), can be written as

$$\widetilde{J}(0) = -2\sigma c_W^{-1} \int_0^\infty du\ (k_- - i\omega)\widetilde{\Delta}_+(u)\mathcal{F}(u,\omega) + k_-\widetilde{\Delta}_-(u)\mathcal{G}(u,\omega), \tag{3.105}$$

where c_W is a constant that will later drop out when setting $\widetilde{J}(0) = 0$ and where $\mathcal{F}(z,\omega)$ and $\mathcal{G}(z,\omega)$ are given in terms of the hypergeometric functions

$$\mathcal{F}(z,\omega) := {}_2F_1\left(-i\omega, k_+ + k_- - i\omega; k_- - i\omega; z\right), \tag{3.106}$$

$$\mathcal{G}(z,\omega) := {}_2F_1\left(-i\omega, k_+ + k_- - i\omega; 1 + k_- - i\omega; z\right). \tag{3.107}$$

Eq. (3.105) is one of the central results of this section. The reason is that up to here, we have not relied on the specific form of $\widetilde{\Delta}_+(z)$ and $\widetilde{\Delta}_-(z)$ (in the derivation in Appendix A.3, we only use that they vanish at 0 and ∞). Thus, we will be able to re-use eq. (3.105) for various inhomogeneities in the calculation of the susceptibility below.

For larger ω, it can be numerically advantageous to evaluate $\mathcal{F}(z,\omega)$ and $\mathcal{G}(z,\omega)$ using their alternative forms (Abramowitz and Stegun, 1972, 15.3.3),

$$\mathcal{F}(z,\omega) = (1-z)^{i\omega-k_+}{}_2F_1\left(k_-, -k_+; k_- - i\omega; z\right), \tag{3.108}$$

$$\mathcal{G}(z,\omega) = (1-z)^{1+i\omega-k_+}{}_2F_1\left(1+k_-, 1-k_+; 1+k_- - i\omega; z\right). \tag{3.109}$$

In order to calculate the spike-triggered rate $\widetilde{m}(\omega)$, we use the condition that the total flux vanishes at the lower boundary $v = v_-$, ($z = 0$).

With the inhomogeneities,

$$\begin{aligned}
\widetilde{\Delta}_+(z) &= \widetilde{m}(\omega)\frac{1}{2\sigma}\left[e^{i\omega\tau_{\text{ref}}}P_{+|+}(\tau_{\text{ref}})\delta(z-z_R) - \delta(z-z_T)\right] + \frac{1}{2\sigma}e^{i\omega\tau_{\text{ref}}}P_{+|+}(\tau_{\text{ref}})\delta(z-z_R),\\
\widetilde{\Delta}_-(z) &= \widetilde{m}(\omega)\frac{1}{2\sigma}e^{i\omega\tau_{\text{ref}}}P_{-|+}(\tau_{\text{ref}})\delta(z-z_R) + \frac{1}{2\sigma}e^{i\omega\tau_{\text{ref}}}P_{-|+}(\tau_{\text{ref}})\delta(z-z_R),
\end{aligned} \tag{3.110}$$

where $z_R := (v_R - \mu + \sigma)/(2\sigma)$ and $z_T := (v_T - \mu + \sigma)/(2\sigma)$, eq. (3.105) is readily inte-

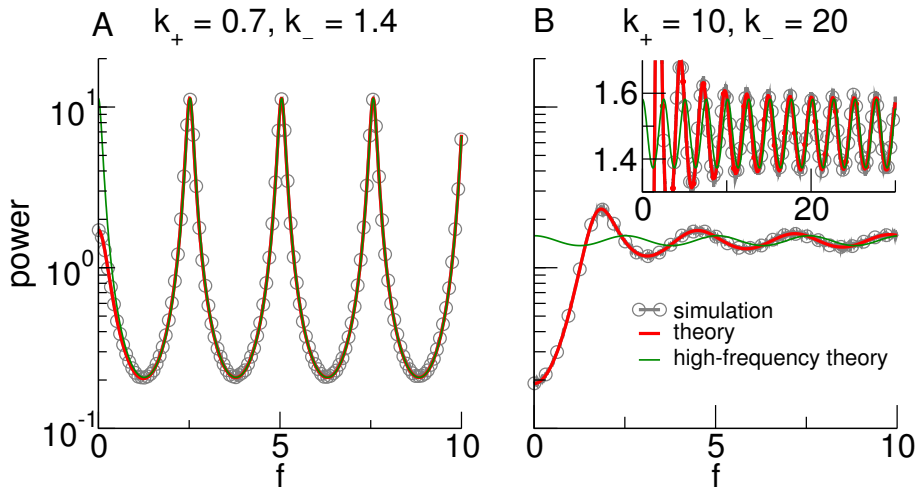

Figure 3.7.: Power spectrum of an LIF driven by dichotomous noise at different switching rates. The exact theory (eq. (3.112), thick red lines) is compared to simulation results (gray lines with circles) and the expression for the high-frequency behavior (eq. (3.116), thin green lines). The inset in B illustrates the ongoing oscillations over a wider frequency range. Parameters: $\mu = 1.5, \sigma = 2.4, v_R = 0, v_T = 1, \tau_{\text{ref}} = 0.1$.

grated and solved for $\widetilde{m}(\omega)$. One obtains the spike-triggered rate

$$\widetilde{m}(\omega) = \left[\frac{(k_+ + k_-)e^{-i\omega\tau_{\text{ref}}}\mathcal{F}(z_T,\omega)}{(k_+ e^{-\frac{\tau_{\text{ref}}}{\tau_c}} + k_-)\mathcal{F}(z_R,\omega) + \frac{k_+k_-}{k_- - i\omega}(1 - e^{-\frac{\tau_{\text{ref}}}{\tau_c}})\mathcal{G}(z_R,\omega)} - 1 \right]^{-1}, \tag{3.111}$$

which can be used to calculate the power spectrum via

$$\begin{aligned} S_{xx}(\omega) &= r_0\,(1 + 2\Re[\widetilde{m}(\omega)]) \\ &= r_0 \frac{\left|e^{-i\omega\tau_{\text{ref}}}\mathcal{F}(z_T,\omega)\right|^2 - \left|P_{+|+}(\tau_{\text{ref}})\mathcal{F}(z_R,\omega) + \frac{k_-}{k_- - i\omega}P_{-|+}(\tau_{\text{ref}})\mathcal{G}(z_R,\omega)\right|^2}{\left|e^{-i\omega\tau_{\text{ref}}}\mathcal{F}(z_T,\omega) - P_{+|+}(\tau_{\text{ref}})\mathcal{F}(z_R,\omega) - \frac{k_-}{k_- - i\omega}P_{-|+}(\tau_{\text{ref}})\mathcal{G}(z_R,\omega)\right|^2}. \end{aligned} \tag{3.112}$$

This is the main result of this section.

In the limit of a vanishing refractory period (but finite noise correlation time; see the discussion in Chapter 4, Sec. 4.2), the spike-triggered rate simplifies to

$$\widetilde{m}(\omega) = \left[\frac{\mathcal{F}(z_T,\omega)}{\mathcal{F}(z_R,\omega)} - 1 \right]^{-1}, \tag{3.113}$$

and the power spectrum can be compactly written as

$$S_{xx}(\omega) = r_0 \frac{|\mathcal{F}(z_T,\omega)|^2 - |\mathcal{F}(z_R,\omega)|^2}{|\mathcal{F}(z_T,\omega) - \mathcal{F}(z_R,\omega)|^2}. \tag{3.114}$$

In Fig. 3.7, we plot the power spectrum for different values of k_+ and k_- and compare it to spectra obtained in simulations. To someone familiar with spike train power spectra, especially the spectrum at low switching rates must look peculiar because it does not converge to the stationary firing rate for high ω but instead displays stable, ongoing oscillations. That the oscillations are indeed undamped is confirmed by examining the high-frequency behavior of eq. (3.112). Using (Abramowitz and Stegun, 1972, 15.7.1) and the deterministic time that the voltage needs to go from reset to threshold in the "+" state,

$$T_d^+ = \ln\left(\frac{\mu+\sigma-v_R}{\mu+\sigma-v_T}\right) + \tau_{\text{ref}} = \ln\left(\frac{1-z_R}{1-z_T}\right) + \tau_{\text{ref}}, \tag{3.115}$$

the high-frequency behavior of the power spectrum can be written as:

$$S_{xx}(\omega \gg 1) = \\ r_0 \frac{1 - P_{+|+}^2(\tau_{\text{ref}}) e^{-2k_+(T_d^+ - \tau_{\text{ref}})}}{1 + P_{+|+}^2(\tau_{\text{ref}}) e^{-2k_+(T_d^+ - \tau_{\text{ref}})} - 2P_{+|+}(\tau_{\text{ref}}) e^{-k_+(T_d^+ - \tau_{\text{ref}})} \cos(\omega T_d^+)}. \tag{3.116}$$

It is apparent that the $\cos(\omega T_d^+)$ term leads to undamped oscillations with a period that corresponds to the inverse time from reset to threshold in the "+" state. A plot of eq. (3.116) is included in Fig. 3.7. Especially for slow switching rates (Fig. 3.7A), the power spectrum is dominated by the oscillatory high frequency behavior described by eq. (3.116); here, differences between eq. (3.112) and eq. (3.116) are only discernible for frequencies smaller than the firing rate in the "+" state.

The ongoing oscillations are weaker but still present for higher switching rates (see Fig. 3.7B). Taking eq. (3.116) to the Gaussian white-noise limit $\tau_c \to 0$ with $k = 1/(2\tau_c)$ and $\sigma = \sqrt{D/\tau_c}$, one finds $S_{xx}(\omega \gg 1) \to r_0$, as expected.

What is the reason for these peculiar spectra? Consider first slow switching, in the sense that a single "+" state contains many ISIs. These ISIs will be all of the same (deterministic) length T_d^+, and consequently, the spike-triggered rate will contain δ peaks at multiples of T_d^+. When transforming to Fourier space, these δ peaks transform to an oscillatory contribution. Even for fast switching, there is still a finite probability for "+" states that are long enough to contain one or more ISIs of deterministic length. Thus, the δ peaks persist, albeit reduced in weight, leading to oscillations of smaller amplitude. Essentially, the undamped oscillations in the spectrum are therefore a consequence of the lack of further stochasticity within the two noise states. As evident from this explanation, the oscillations are not dependent on a particular neuron model; they have also been observed in the power spectrum of DMP-driven PIF neurons (Müller-Hansen et al.,

2015).

Fourier transform of the first-passage-time density

In Fourier space, the FPT density $\widetilde{\rho}(\omega)$ can be calculated using the same approach as for the spike-triggered rate by dropping the reset term at v_R. This means one may re-use eq. (3.105) with different inhomogeneities,

$$\begin{aligned}\widetilde{\Delta}_+(z) &= -\widetilde{\rho}(\omega)\frac{\delta(z-z_T)}{2\sigma} + e^{i\omega\tau_{\text{ref}}}P_{+|+}(\tau_{\text{ref}})\frac{\delta(z-z_R)}{2\sigma},\\ \widetilde{\Delta}_-(z) &= e^{i\omega\tau_{\text{ref}}}P_{-|+}(\tau_{\text{ref}})\frac{\delta(z-z_R)}{2\sigma}.\end{aligned} \tag{3.117}$$

Solving this for $\widetilde{\rho}(\omega)$ yields

$$\widetilde{\rho}(\omega) = \frac{(k_- - i\omega)P_{+|+}(\tau_{\text{ref}})\mathcal{F}(z_R,\omega) + k_- P_{-|+}(\tau_{\text{ref}})\mathcal{G}(z_R,\omega)}{e^{-i\omega\tau_{\text{ref}}}(k_- - i\omega)\mathcal{F}(z_T,\omega)}. \tag{3.118}$$

For the parameter regime we considered, the neuronal spike train is a renewal process. One could thus alternatively calculate the power spectrum using the formula (Stratonovich, 1967)

$$S_{xx}(\omega) = r_0\frac{1-|\widetilde{\rho}(\omega)|^2}{|1-\widetilde{\rho}(\omega)|^2}. \tag{3.119}$$

Plugging eq. (3.118) into eq. (3.119) yields the same result for the spectrum as above.

Inverting the Fourier transform to obtain the FPT density in the time domain is impracticable, but one could in principle use eq. (3.118) to obtain the moments of the FPT density by differentiation with respect to ω. Differentiation of hypergeometric functions with respect to their parameters a, b, and c is, however, non-trivial, resulting in generalized Kampé de Fériet functions (Ancarani and Gasaneo, 2008).

3.5.2. Susceptibility

The aim of this section is to calculate how the firing rate $r(t)$ of an LIF neuron driven by dichotomous noise responds to a weak additive signal $\epsilon s(t)$, where $\epsilon \ll 1$. A standard approach is to apply linear response theory, i.e. to assume that the modulation of the firing rate is captured by convolution of the signal with a linear response kernel $K(\tau)$,

$$r(t) \approx r_0 + \epsilon \int_{-\infty}^{\infty} d\tau\, K(\tau)s(t-\tau), \tag{3.120}$$

where $K(\tau)$ is causal ($K(\tau < 0) = 0$). The Fourier transform of $K(\tau)$ is the susceptibility,

$$\chi(\omega) = \int_{-\infty}^{\infty} d\tau \; e^{i\omega\tau} K(\tau), \tag{3.121}$$

and in Fourier space, where the convolution becomes a multiplication, one has, for $\omega > 0$,

$$\widetilde{r}(\omega) \approx \epsilon \chi(\omega) \widetilde{s}(\omega). \tag{3.122}$$

In order to calculate $\chi(\omega)$, it is sufficient to consider the response to a sinusoidal stimulus with frequency ω. This can be seen by plugging, for instance, $s(t) = \cos(\omega t)$ into eq. (3.120), which yields

$$r(t) \approx r_0 + \epsilon \, |\chi(\omega)| \cdot \cos\Big(\omega t - \arg\left[\chi(\omega)\right]\Big). \tag{3.123}$$

In words: in linear order, the firing rate response to a sinusoidal signal with frequency ω is itself sinusoidal; the amplitude of the rate modulation is determined by the absolute value of the susceptibility and the phase lag between signal and response by its argument. Thus, how the system responds to sinusoidal signals determines – in linear response – how it responds to arbitrary signals; this is simply a consequence of the assumed linearity and the fact that any signal can be constructed from sinusoids via Fourier synthesis.

For convenience, we may also choose a complex-valued stimulus $s(t) = e^{-i\omega t}$, which, plugged into eq. (3.120), leads to

$$r(t) = r_0 + \chi(\omega) \epsilon e^{-i\omega t}. \tag{3.124}$$

The master equations then read

$$\begin{aligned} \partial_t P_+(v,t) = &-\partial_v \Big[(\mu - v + \epsilon e^{-i\omega t} + \sigma) P_+(v,t)\Big] \\ &- k_+ P_+(v,t) + k_- P_-(v,t) \\ &+ r(t - \tau_{\text{ref}}) P_{+|+}(\tau_{\text{ref}}) \delta(v - v_R) - r(t) \delta(v - v_T), \end{aligned} \tag{3.125}$$

$$\begin{aligned} \partial_t P_-(v,t) = &-\partial_v \Big((\mu - v + \epsilon e^{-i\omega t} - \sigma) P_-(v,t)\Big) \\ &+ k_+ P_+(v,t) - k_- P_-(v,t) \\ &+ r(t - \tau_{\text{ref}}) P_{-|+}(\tau_{\text{ref}}) \delta(v - v_R). \end{aligned} \tag{3.126}$$

It is advantageous to make a change of variables that transforms away the oscillatory

driving at the cost of introducing time-dependent threshold and reset voltages. Setting

$$x := v + \epsilon \frac{1}{i\omega - 1} e^{-i\omega t} \tag{3.127}$$

maps the stochastic differential equation eq. (3.75) (with $s(t) = e^{-i\omega t}$) to

$$\dot{x} = \mu - x + \eta(t), \tag{3.128}$$

where now, however, reset and threshold are varying in time,

$$x_R(t) = v_R + \epsilon \frac{1}{i\omega - 1} e^{-i\omega t}, \quad x_T(t) = v_T + \epsilon \frac{1}{i\omega - 1} e^{-i\omega t}. \tag{3.129}$$

The new master equations read

$$\begin{aligned} \partial_t P_+(x,t) = &-\partial_x \left((\mu - x + \sigma) P_+(x,t) \right) - k_+ P_+(x,t) + k_- P_-(x,t) \\ &+ r(t - \tau_{\text{ref}}) P_{+|+}(\tau_{\text{ref}}) \delta(x - x_R(t)) - r(t) \delta(x - x_T(t)), \end{aligned} \tag{3.130}$$

$$\begin{aligned} \partial_t P_-(x,t) = &-\partial_x \left((\mu - x - \sigma) P_-(x,t) \right) + k_+ P_+(x,t) - k_- P_-(x,t) \\ &+ r(t - \tau_{\text{ref}}) P_{-|+}(\tau_{\text{ref}}) \delta(x - x_R(t)). \end{aligned} \tag{3.131}$$

In the steady state, one expects that the only time-dependency in $P(x,t)$ is periodic with frequency ω. One thus makes the following ansatz for $P_\pm(x,t)$,

$$P_\pm(x,t) = P_{\pm,0}(x) + \epsilon e^{-i\omega t} P_{\pm,1}(x,\omega) + \mathcal{O}(\epsilon^2). \tag{3.132}$$

This *cyclostationary* solution consists of the stationary solution $P_{\pm,0}(x)$ and a weak periodic modulation, oscillating at the frequency of the signal with a certain phase lag (contained in the complex phase of $P_{\pm,1}(x,\omega)$).

Plugging in this ansatz as well as the one for $r(t)$ (eq. (3.124)) into the master equation eqs. (3.130, 3.131), taylor-expanding the delta functions for small ϵ, and considering only the terms linear in ϵ, yields

$$\begin{aligned} -i\omega P_{+,1}(x) = &-\partial_x \left((\mu - x + \sigma) P_{+,1}(x) \right) - k_+ P_{+,1}(x) + k_- P_{-,1}(x) \\ &+ \chi(\omega) \left[e^{i\omega \tau_{\text{ref}}} P_{+|+}(\tau_{\text{ref}}) \delta(x - v_R) - \delta(x - v_T) \right] \\ &- \frac{r_0}{i\omega - 1} \left[P_{+|+}(\tau_{\text{ref}}) \delta'(x - v_R) - \delta'(x - v_T) \right], \end{aligned} \tag{3.133}$$

$$\begin{aligned}-i\omega P_{-,1}(x) = &-\partial_x\left((\mu - x - \sigma)P_{-,1}(x)\right) + k_+ P_{+,1}(x) - k_- P_{-,1}(x) \\ &+ \chi(\omega)e^{i\omega\tau_{\text{ref}}}P_{-|+}(\tau_{\text{ref}})\delta(x - v_R) \\ &- \frac{r_0}{i\omega - 1}P_{-|+}(\tau_{\text{ref}})\delta'(x - v_R).\end{aligned} \tag{3.134}$$

This can be seen to have the same structure as eq. (3.82) and eq. (3.83) with different inhomogeneities. Thus, if we consider the flux

$$J(x,t) = J_0(x) + \epsilon e^{-i\omega t}J_1(x), \tag{3.135}$$

then $J_1(v_-)$ is given by eq. (3.105) if the inhomogeneities $\widetilde{\Delta}_\pm(x)$ are appropriately chosen. Also in this signal-driven situation, the flux at the lowest attainable voltage $J(v_-)$ should vanish, and the susceptibility can thus be determined from demanding $J_1(z = 0) = 0$.

With the inhomogeneities

$$\begin{aligned}\widetilde{\Delta}_+(z) = &\frac{\chi(\omega)}{2\sigma}\left[e^{i\omega\tau_{\text{ref}}}P_{+|+}(\tau_{\text{ref}})\delta(x - v_R) - \delta(x - v_T)\right] \\ &- \frac{1}{4\sigma^2}\frac{r_0}{i\omega - 1}\left[P_{+|+}(\tau_{\text{ref}})\delta'(x - v_R) - \delta'(x - v_T)\right],\end{aligned} \tag{3.136}$$

$$\widetilde{\Delta}_-(z) = \frac{\chi(\omega)}{2\sigma}e^{i\omega\tau_{\text{ref}}}P_{-|+}(\tau_{\text{ref}})\delta(x - v_R) - \frac{1}{4\sigma^2}\frac{r_0}{i\omega - 1}P_{-|+}(\tau_{\text{ref}})\delta'(x - v_R), \tag{3.137}$$

the susceptibility is given by

$$\chi(\omega) = -\frac{r_0}{2\sigma}\frac{1}{i\omega - 1}\frac{\mathcal{F}'(z_T,\omega) - P_{+|+}(\tau_{\text{ref}})\mathcal{F}'(z_R,\omega) - \frac{k_- P_{-|+}(\tau_{\text{ref}})}{k_- - i\omega}\mathcal{G}'(z_R,\omega)}{\mathcal{F}(z_T,\omega) - e^{i\omega\tau_{\text{ref}}}\left[P_{+|+}(\tau_{\text{ref}})\mathcal{F}(z_R,\omega) + \frac{k_- P_{-|+}(\tau_{\text{ref}})}{k_- - i\omega}\mathcal{G}(z_R,\omega)\right]}, \tag{3.138}$$

where the transition probabilities of the DMP are given in eqs. (3.4, 3.5) and the derivatives of $\mathcal{F}(z)$ and $\mathcal{G}(z)$ are (Abramowitz and Stegun, 1972, 15.2.1)

$$\begin{aligned}\mathcal{F}'(z) &= \frac{-i\omega(k_+ + k_- - i\omega)}{k_- - i\omega}{}_2F_1\left(1 - i\omega, 1 + k_+ + k_- - i\omega; 1 + k_- - i\omega; z\right) \\ &= \frac{-i\omega(k_+ + k_- - i\omega)}{k_- - i\omega}(1 - z)^{i\omega - k_+ - 1}{}_2F_1\left(k_-, -k_+; 1 + k_- - i\omega; z\right),\end{aligned} \tag{3.139}$$

$$\begin{aligned}\mathcal{G}'(z) &= \frac{-i\omega(k_+ + k_- - i\omega)}{1 + k_- - i\omega}{}_2F_1\left(1 - i\omega, 1 + k_+ + k_- - i\omega; 2 + k_- - i\omega; z\right) \\ &= \frac{-i\omega(k_+ + k_- - i\omega)}{1 + k_- - i\omega}(1 - z)^{i\omega - k_+}{}_2F_1\left(1 + k_-, 1 - k_+; 2 + k_- - i\omega; z\right).\end{aligned} \tag{3.140}$$

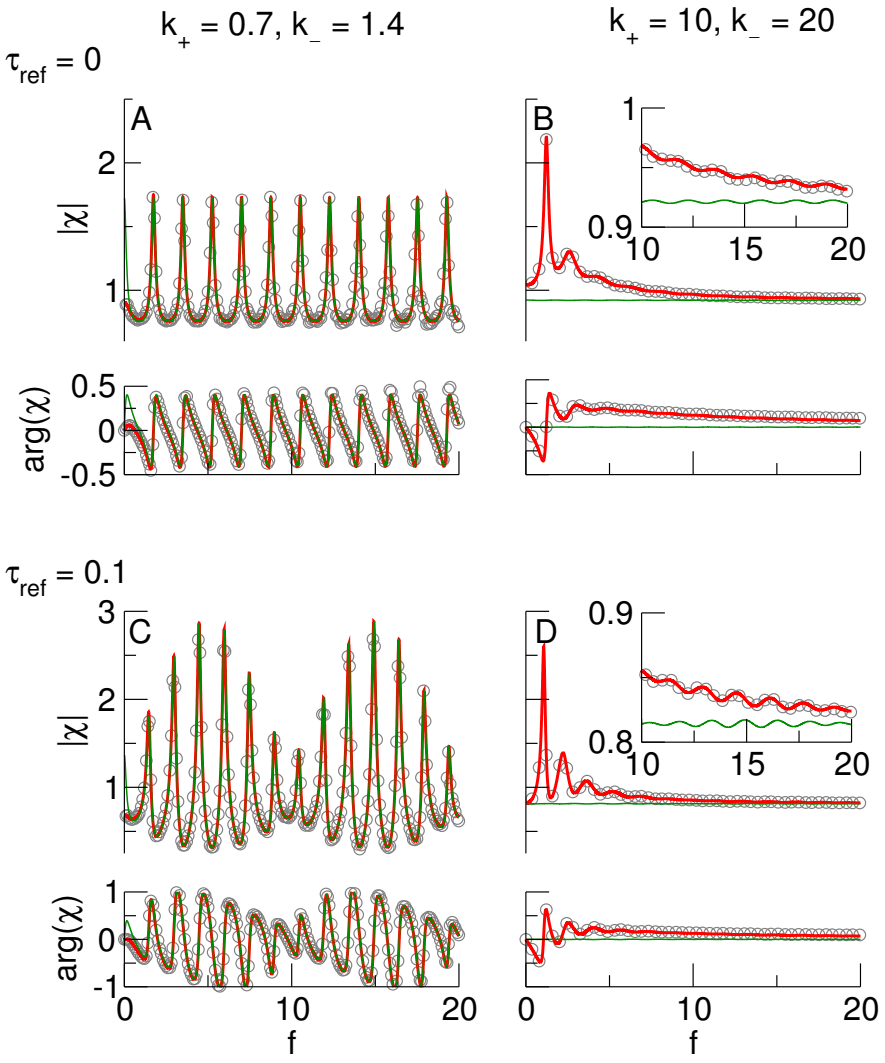

Figure 3.8.: Susceptibility of a DMP-driven LIF neuron to a current modulation. We compare our theory, eq. (3.138), (thick red lines) to simulations (circles). Also shown is the expression for the high-frequency behavior, eq. (3.142), (thin green lines). We contrast two combinations of switching rates at two values of the absolute refractory period. The inset in B and D is a zoomed version of the same curves at higher frequencies. Remaining parameters: $\mu = 1.5, \sigma = 0.8, v_R = 0, v_T = 1$.

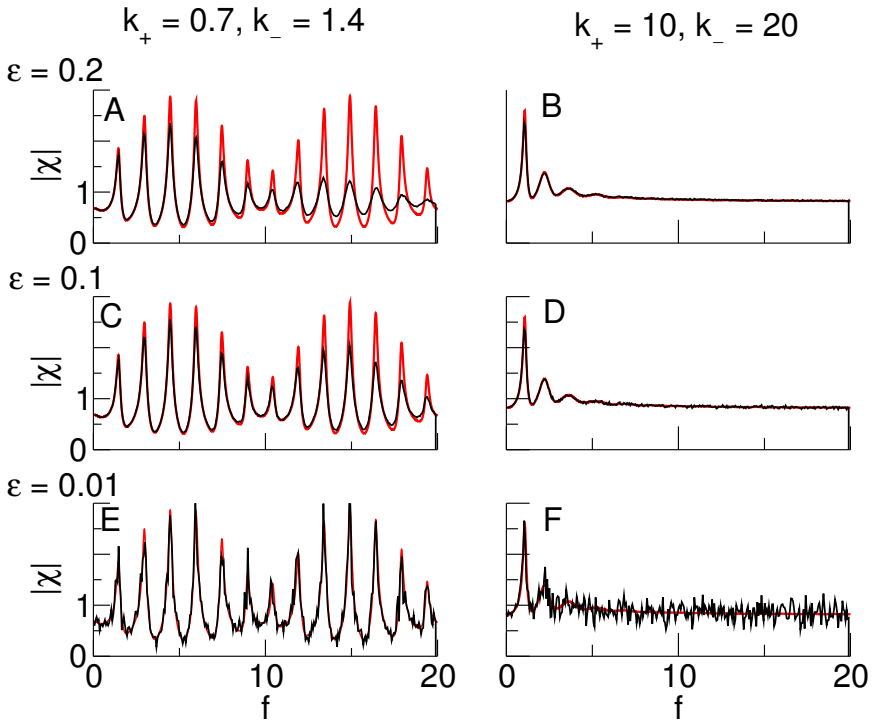

Figure 3.9.: Theory for the susceptibility (red lines) compared to simulations (black lines) in which the susceptibility was measured via the response to a broadband signal with cutoff frequency $f_c = 20$. Shown are three different signal amplitudes, again for either slow or fast switching noise. Remaining parameters: $\mu = 1.5, \sigma = 0.8, v_R = 0, v_T = 1$.

For vanishing absolute refractory period at non-vanishing noise-correlation time, the susceptibility simplifies to

$$\chi(\omega) = -\frac{r_0}{2\sigma}\frac{1}{i\omega - 1}\frac{\mathcal{F}'(z_T,\omega) - \mathcal{F}'(z_R,\omega)}{\mathcal{F}(z_T,\omega) - \mathcal{F}(z_R,\omega)}. \tag{3.141}$$

In Fig. 3.8, we plot the susceptibility for different parameter combinations. Again, as for the power spectrum, one observes an undamped oscillatory component. Indeed, one can derive an expression for the high-frequency behavior of the susceptibility,

$$\chi(\omega \gg 1) = \frac{r_0}{2\sigma}\frac{1 - P_{+|+}(\tau_{\text{ref}})e^{-(k_+ +1)(T_d^+ - \tau_{\text{ref}})}e^{i\omega(T_d^+ - \tau_{\text{ref}})}}{(1 - z_T)\left(1 - P_{+|+}(\tau_{\text{ref}})e^{-k_+(T_d^+ - \tau_{\text{ref}})}e^{i\omega T_d^+}\right)}, \tag{3.142}$$

which contains oscillatory terms, $e^{i\omega(T_d^+ - \tau_{\text{ref}})}$ and $e^{i\omega T_d^+}$. A non-vanishing absolute refractory period leads to a slight discrepancy in the frequencies of these terms, which manifests itself as a beating (see Fig. 3.8C, D). For higher switching rates, the sustained oscillations are less prominent (Fig. 3.8B, D) but still present (see insets). Here, the susceptibility settles into a (hardly perceptible) oscillation around a constant real value for large frequencies. Thus, in contrast to a white-noise-driven LIF, a high-frequency signal

may be transmitted instantaneously, i.e. without a phase lag. This has also been observed for LIFs driven by a different colored noise, an Ornstein-Uhlenbeck process (Brunel et al., 2001; Fourcaud and Brunel, 2002).

In Fig. 3.8, simulation results at a given frequency were obtained by considering the response of the LIF neuron to a cosine stimulus with that frequency. However, the susceptibility allows to describe the (linear) response to an arbitrary stimulus. In particular, broadband stimuli are often used in modeling, but also to probe the susceptibility experimentally. In Fig. 3.9, we compare our theory to simulation results where the neuron was stimulated with a broadband signal (a band-limited Gaussian white noise with $f_0 = 0, f_c = 20$). We consider three different values for the signal amplitude ϵ. For the case of a slowly switching DMP, it is apparent that at $\epsilon = 0.2$ (Fig. 3.9A), the theory breaks down at higher frequencies, and also at $\epsilon = 0.1$ (Fig. 3.9C), there are clear deviations. This is in contrast to stimulation by a sinusoidal stimulus, in which these amplitudes pose no problem.

It is plausible that a broadband signal destroys the ongoing oscillations in the susceptibility (or, for that matter, the power spectrum), because, as we have argued, they are a consequence of the absence of stochasticity within a given noise state. Here, the signal itself provides this stochasticity. For sufficiently weak signals ($\epsilon = 0.01$ in Fig. 3.9E) or if switching rates are high (Fig. 3.9B, D, F), the theory matches simulations well also for the broadband signal.

3.5.3. Susceptibility with respect to the modulation of a switching rate

Here, we briefly derive an expression for the susceptibility with respect to a modulation of one of the switching rates. This result will be used in Chapter 4, where we will take it to the shot noise limit.

Instead of a current modulation as above, we consider a time-dependent rate of switching from the "-" to the "+" state,

$$k_-(t) = k_- \cdot \left(1 + \epsilon e^{-i\omega t}\right). \tag{3.143}$$

In this case, the master equations read

$$\begin{aligned}
\partial_t P_+(v,t) &= -\partial_v \left[(\mu - v + \sigma) P_+(v,t)\right] \\
&\quad - k_+ P_+(v,t) + \left(k_-[1 + \epsilon e^{-i\omega t}]\right) P_-(v,t) \\
&\quad + r(t - \tau_{\text{ref}}) P_{+|+}(t, t - \tau_{\text{ref}}) \delta(v - v_R) - r(t)\delta(v - v_T), \\
\partial_t P_-(v,t) &= -\partial_v \left((\mu - v - \sigma) P_-(v,t)\right) \\
&\quad + k_+ P_+(v,t) - \left(k_-[1 + \epsilon e^{-i\omega t}]\right) P_-(v,t) \\
&\quad + r(t - \tau_{\text{ref}}) P_{-|+}(t, t - \tau_{\text{ref}}) \delta(v - v_R).
\end{aligned} \tag{3.144, 3.145}$$

Here, the DMP transition probabilities,

$$P_{\pm|+}(t, t-\tau_{\text{ref}}) = \Pr\Big(\eta(t) = \pm\sigma \;\Big|\; \eta(t-\tau_{\text{ref}}) = +\sigma\Big), \tag{3.146}$$

are also modulated by the signal and thus explicitly depend on time. They can be obtained by solving the DMP master equations, eqs. (3.1, 3.2), with the time-dependent switching rate $k_-(t)$ [eq. (3.143)]. Here, we give the solution for $P_{+|+}(t, t_0)$; $P_{-|+}(t, t-\tau_{\text{ref}}) = 1 - P_{+|+}(t, t-\tau_{\text{ref}})$ then follows. One obtains ($\tau_{\text{ref}} > 0$)

$$P_{+|+}(t, t-\tau_{\text{ref}}) = k_+ \int_{t-\tau_{\text{ref}}}^{t} ds\ \exp\left[(k_+ + k_-)(s-t) + \frac{ik_-\epsilon}{\omega}\left(e^{-i\omega s} - e^{-i\omega t}\right)\right]. \tag{3.147}$$

We are only interested in the order linear in ϵ, for which the integration can be carried out, yielding

$$\begin{aligned} P_{+|+}(t, t-\tau_{\text{ref}}) = {} & \frac{k_+ e^{-(k_+ + k_-)\tau_{\text{ref}}} + k_-}{k_+ + k_-} \\ & - \epsilon e^{-i\omega t} \cdot \frac{ik_+k_-}{\omega}\left[\frac{1 - e^{-(k_+ + k_-)\tau_{\text{ref}}} e^{i\omega\tau_{\text{ref}}}}{k_+ + k_- - i\omega} - \frac{1 - e^{-(k_+ + k_-)\tau_{\text{ref}}}}{k_+ + k_-}\right] + \mathcal{O}(\epsilon^2) \end{aligned} \tag{3.148}$$

and $P_{-|+}(t, t-\tau_{\text{ref}}) = 1 - P_{+|+}(t, t-\tau_{\text{ref}})$. Noting that the only t dependence is in the $e^{-i\omega t}$ term, we introduce the notation

$$P_{\pm|+}(t, t-\tau_{\text{ref}}) =: P_{\pm|+,0}(\tau_{\text{ref}}) + \epsilon e^{-i\omega t} P_{\pm|+,1}(\tau_{\text{ref}}) + \mathcal{O}(\epsilon^2). \tag{3.149}$$

Inserting eq. (3.149) along with the ansatz for the cyclostationary solution [eq. (3.132)] and the firing rate [eq. (3.124)] into the master equation eqs. (3.144, 3.145) and keeping only terms of order ϵ, one obtains

$$\begin{aligned} -i\omega P_{+,1}(v) = {} & -\partial_v\left((\mu - v + \sigma)P_{+,1}(v)\right) - k_+ P_{+,1}(v) + k_- P_{-,1}(v) \\ & + k_- P_{-,0}(v) + r_0 P_{+|+,1}(\tau_{\text{ref}})\delta(v - v_R) \\ & + \chi(\omega)\left[e^{i\omega\tau_{\text{ref}}} P_{+|+,0}(\tau_{\text{ref}})\delta(v - v_R) - \delta(v - v_T)\right], \end{aligned} \tag{3.150}$$

$$\begin{aligned} -i\omega P_{-,1}(v) = {} & -\partial_v\left((\mu - v - \sigma)P_{-,1}(v)\right) + k_+ P_{+,1}(v) - k_- P_{-,1}(v) \\ & - k_- P_{-,0}(v) - r_0 P_{+|+,1}(\tau_{\text{ref}})\delta(v - v_R) \\ & + \chi(\omega) e^{i\omega\tau_{\text{ref}}}\left[1 - P_{+|+,0}(\tau_{\text{ref}})\right]\delta(v - v_R). \end{aligned} \tag{3.151}$$

One can use eq. (3.105) with the inhomogeneities

$$\widetilde{\Delta}_+(z) = \frac{k_- P_{-,0}(z) + r_0 P_{+|+,1}(\tau_{\text{ref}})\delta(z-z_R) + \chi(\omega)\left[e^{i\omega\tau_{\text{ref}}} P_{+|+,0}(\tau_{\text{ref}})\delta(z-z_R) - \delta(z-z_T)\right]}{2\sigma}, \tag{3.152}$$

$$\widetilde{\Delta}_-(z) = \frac{-[k_- P_{-,0}(z) + r_0 P_{+|+,1}(\tau_{\text{ref}})\delta(z-z_R)] + \chi(\omega) e^{i\omega\tau_{\text{ref}}} P_{-|+,0}(\tau_{\text{ref}})\delta(z-z_R)}{2\sigma}, \tag{3.153}$$

to obtain the susceptibility

$$\chi_{k_-}(\omega) = \frac{\int_0^\infty du\ \left[k_- P_{-,0}(u) + r_0 P_{+|+,1}(\tau_{\text{ref}})\delta(u-z_R)\right] \cdot \left[(k_- - i\omega)\mathcal{F}(u,\omega) - k_-\mathcal{G}(u,\omega)\right]}{(k_- - i\omega)\left[\mathcal{F}(z_T,\omega) - e^{i\omega\tau_{\text{ref}}} P_{+|+,0}(\tau_{\text{ref}})\mathcal{F}(z_R,\omega)\right] - k_- e^{i\omega\tau_{\text{ref}}} P_{-|+,0}(\tau_{\text{ref}})\mathcal{G}(z_R,\omega)}. \tag{3.154}$$

3.6. Summary

In this chapter, we have developed a theory for integrate-and-fire neurons driven by asymmetric dichotomous noise. For general IF neurons, we have derived an expression for the stationary density in Sec. 3.3. This density displays several important differences to the density for the case of IF neurons driven by Gaussian white noise: it has bounded support, takes a finite value at the threshold voltage v_T, and changes qualitatively as a function of the absolute refractory period. Further, it may diverge at FPs of the "-" dynamics. We have discussed in detail how a solution needs to be constructed when such FPs are present.

In Sec. 3.4, we have derived recursive relations that allow to calculate the ISI moments for general IF neurons. Owing to our focus on signal transmission, we have refrained from a detailed discussion of these results and refer the interested reader to the extensive analysis in (Droste and Lindner, 2014).

In Sec. 3.5.1, we have derived the power spectrum for LIF neurons driven by dichotomous noise. We have found that the spectrum exhibits an undamped periodicity that can be explained by the absence of further stochasticity within each of the two noise states. The same periodicity appears in the susceptibility of DMP-driven LIFs with respect to a current modulation, which we have calculated in Sec. 3.5.2. As has been previously observed for other kinds of colored noise, this susceptibility does not decay to zero in the high-frequency limit, allowing for instantaneous signal transmission. Finally, in Sec. 3.5.3, we have given an expression for the susceptibility with respect to a modulation of one of the switching rates. This will be of use in the shot-noise limit, which we discuss in the following chapter.

Chapter 4.

IF neurons driven by excitatory shot noise with exponentially distributed weights

A neuron receives input from other neurons in the form of presynaptic action potentials (APs). In a somewhat simplified picture which neglects conductance dynamics, a presynaptic AP causes a jump in the postsynaptic membrane potential, the height of which corresponds to the weight of the synapse. Theoretical studies of neuronal firing statistics or signal transmission properties have often made use of the assumption that the height of each individual jump is small and that the constant bombardment by thousands of presynaptic neurons leads to a superposition of many such jumps in a short time interval. This suggests modeling the input as a Gaussian process, which becomes exact in the limit of vanishing synaptic weights and diverging input rate. If one additionally assumes white input, then this is the so-called diffusion approximation (DA).

Synaptic weights can be measured experimentally, by identifying synaptically connected pairs of cells and then stimulating one cell while recording from the other. The excitatory postsynaptic potentials (EPSPs), i.e. the voltage excursions, caused by a single presynaptic AP, can then be used to obtain the statistics of synaptic weights. Experimentalists have reported mean peak heights of EPSPs in the range of 1-2 mV (Thomson et al., 1993; Markram et al., 1997; Song et al., 2005; Lefort et al., 2009). The distributions of EPSPs has been reported to be highly skewed (Song et al., 2005; Lefort et al., 2009), with individual EPSP amplitudes ranging up to 8-10 mV (Thomson et al., 1993; Lefort et al., 2009; Loebel et al., 2009). Thus, EPSPs are not small when compared to the distance from resting potential to threshold, which for pyramidal neurons is reported to lie between 10 and 20 mV (Badel et al., 2008; Lefort et al., 2009). Rather, on average between 5 and 20 EPSPs can be sufficient to make the neuron fire, and in individual instances, even a single strong EPSP may be enough.

In many cases, it may be thus be advisable to explicitly take the non-Gaussian nature of the synaptic background noise into account. Specifically, one is dealing with a shot noise (SN), in which individual events have weights that are drawn from a skewed distribution.

Studying integrate-and-fire neurons driven by shot noise has a long history (going back to the work of Stein (1965), see the books by Holden (1976) and Tuckwell (1988) for an account of early works). Studies that explicitly contrast SN drive to the DA have focused mainly on the voltage distribution in spiking LIF neurons (Sirovich et al., 2000; Sirovich, 2003; Richardson, 2004; Helias et al., 2010a,b, 2011) or in conductance based, but non-spiking [1] neurons (Richardson, 2004; Richardson and Gerstner, 2005, 2006; Wolff and

[1] Here, non-spiking means that the threshold is assumed to be at infinity; i.e. the effect of the fire-and-reset

Lindner, 2008, 2010). Various works have considered signal transmission properties (Helias et al., 2010b, 2011; Richardson and Swarbrick, 2010); here, it was found that signals encoded in a SN process can be faithfully transmitted even at high frequencies, unlike signals that enter as a current modulation.

Exact analytical results for SN-driven spiking neurons are rare. Stein et al. (1972) derived the ISI density and the power spectrum of a PIF neuron driven by excitatory Poisson shot noise with constant weights. Recently, Richardson and Swarbrick (2010) have considered LIF neurons driven by excitatory and inhibitory Poissonian shot noise with exponentially distributed weights. Using Laplace transforms of the master equations, they were able to give analytical expressions for the output firing rate, the susceptibility with respect to a modulation of the input rate, and the power spectrum.

There exist some analytical results for the first-passage-time (FPT) density of SN-driven systems which were derived without an explicit reference to neuroscience but which translate directly to the ISI distribution of (mostly leaky) IF neurons: For a linear system driven by purely excitatory SN with exponentially distributed weights, the Laplace transformed FPT density was given by Tsurui and Osaki (1976) (for the special case where the ratio of some parameters is an integer) as an infinite series, and, more recently, by Novikov et al. (2005) in terms of confluent hypergeometric functions. The mean first passage time of a (potentially nonlinear) system driven by excitatory SN with either exponentially distributed or constant weights was calculated by Masoliver (1987). For linear systems subject to both excitatory and inhibitory SN (with weight distributions that are linear combinations of exponentials), the Laplace-transformed FPT density was derived by Jacobsen and Jensen (2007).

Here, we make use of the shot-noise limit of dichotomous noise, which has been known in the statistical physics literature for a long time (Van Den Broeck, 1983), but which has, to our knowledge, never been applied to the problem of finite spike weights in neuroscience. In this limit, dichotomous noise turns into a Poissonian shot noise (either excitatory *or* inhibitory) with exponentially distributed weights. It thus allows us to use the formulas which we have derived in the previous chapter to obtain exact analytical expressions for IF neurons driven by excitatory shot noise.

For the susceptibility and the power spectrum, we obtain expressions in terms of confluent hypergeometric functions that provide alternative expressions to those calculated by Richardson and Swarbrick (2010) (if one turns off inhibition in their setup); we also provide a novel expression for the susceptibility with respect to a current modulation. Further, while the spectral quantities are restricted to LIF neurons, we obtain exact expressions for the stationary density and the ISI moments of general IF neurons driven by excitatory shot noise.

Our goal is to better understand the effect of non-Gaussian synaptic noise on information transmission. We contrast it to a Gaussian white noise background, i.e. the DA. We outline the model and explain how its parameters relate to the DA in Sec. 4.1, before introducing the shot-noise limit of dichotomous noise in Sec. 4.2. In Sec. 4.3, we derive expressions for the stationary voltage distribution and the firing rate of SN-driven IF neurons. The probability density will be needed later for the calculation of the susceptibility to a rate-coded signal, while the behavior of the firing rate will help to interpret differ-

rule on the voltage distribution is neglected.

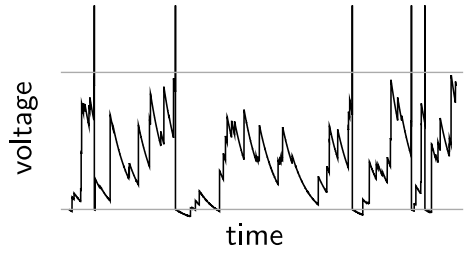

Figure 4.1.: Example voltage trace of an LIF neuron driven by excitatory shot noise with exponentially distributed weights.

ences between power spectrum, susceptibility, and coherence in the SN and the DA case. In Sec. 4.4 and Sec. 4.5 we give expressions for the power spectrum and susceptibility (both with respect to a current and a rate modulation) of a SN-driven LIF neuron and compare them to the DA. Finally, we use these quantities in Sec. 4.6 to study the coherence and the mutual information rate between the signal and the output spike train.

4.1. Model

We consider an IF neuron

$$\tau_{\mathrm{m}}\dot{v} = f(v) + \epsilon_\mu s(t) + \tau_{\mathrm{m}} X_{\mathrm{in}}(t) \tag{4.1}$$

with the usual fire-and-reset rule (if $v = v_T$, it is reset to v_R) and an absolute refractory period τ_{ref} after each spike. We use the membrane time constant $\tau_{\mathrm{m}} = 10\,\mathrm{ms}$. For most of this chapter, we will assume LIF neurons, i.e. $f(v) = \mu - v$; however, the results in Sec. 4.3 apply to general IF neurons. The synaptic input

$$X_{\mathrm{in}}(t) = \sum_i a_i \delta(t - t_i). \tag{4.2}$$

now consists of delta spikes with spike times $\{t_i\}$ and weights a_i. We model the weights to be independently drawn from an exponential distribution with $\langle a_i \rangle = a$ and the spike times to follow an inhomogeneous Poisson process with rate

$$\left\langle \sum_i \delta(t - t_i) \right\rangle = R(t) = r_{\mathrm{in}}[1 + \epsilon_R s(t)]. \tag{4.3}$$

The shot noise $X_{\mathrm{in}}(t)$ is only excitatory; the effect of inhibition can be roughly approximated by using a base current $\mu < v_R$.

The focus of this chapter is on information transmission with a shot-noise background. To this end, we consider the transmission of a signal $s(t)$, which we assume to have unit variance and zero mean. We contrast two cases: The signal either enters the neuronal dynamics directly as a current modulation ($\epsilon_\mu > 0; \epsilon_R = 0$) or it modulates the input rate ($\epsilon_\mu = 0; \epsilon_R > 0$). We assume that both modulation amplitudes are sufficiently small for

linear response theory to be applicable.

We assume that $\mu < v_R$ (except for Fig. 4.4). The reason for this choice is the limited range of validity of the expressions for spectral quantities derived in Chapter 3. It is not an unreasonable choice, as μ is supposed to capture the inhibitory input to the cell, while excitatory input is explicitly modeled. Note that $\mu_{\rm eff}(t)$, the effective mean input set by $\mu + \langle \tau_{\rm m} X_{\rm in}(t) \rangle$, can of course be larger than v_R.

Diffusion approximation

In order to judge the effect of finite spike weights on information transmission, it is useful to contrast results to the DA, i.e. the limit of vanishing spike weights at infinite input rate. In this case, the input can be modeled as Gaussian white noise. We can then apply the known formulas for firing rate $\breve{r}_0$ (Ricciardi and Sacerdote, 1979), power spectrum $\breve{S}_{xx}(\omega)$ (Lindner et al., 2002), and the susceptibility with respect to current modulation $\breve{\chi}_\mu(\omega)$ (Brunel et al., 2001; Lindner and Schimansky-Geier, 2001) or noise modulation $\breve{\chi}_D(\omega)$ (Lindner and Schimansky-Geier, 2001), which are summarized in Appendix B.1. Here and in the following, $\breve{\cdot}$ refers to a DA quantity.

The expressions given in the appendix refer to the (non-dimensionalized) dynamics

$$\dot{v} = \breve{\mu} - v + \breve{\epsilon}_\mu s(t) + \sqrt{2[\breve{D} + \breve{\epsilon}_D s(t)]}\xi(t), \tag{4.4}$$

with a Gaussian white noise $\xi(t)$ with $\langle \xi(t) \rangle = 0$ and $\langle \xi(t_1)\xi(t_2) \rangle = \delta(t_1 - t_2)$. The task at hand is thus to relate $\breve{\mu}, \breve{D}, \breve{\epsilon}_\mu$, and $\breve{\epsilon}_D$ to $\mu, r_{\rm in}, a, \epsilon_\mu$ and ϵ_R. In eq. (4.1), the mean input to the neuron is

$$\begin{aligned} \mu_{\rm eff}(t) &= \mu + \epsilon_\mu s(t) + \langle \tau_{\rm m} X_{\rm in}(t) \rangle = \mu + \epsilon_\mu s(t) + a\tau_{\rm m} R(t) \\ &= \mu + a\tau_{\rm m} r_{\rm in} + (\epsilon_\mu + a\tau_{\rm m} r_{\rm in} \epsilon_R) s(t), \end{aligned} \tag{4.5}$$

and the noise intensity of the input is

$$\begin{aligned} D_{\rm eff}(t) &= \tau_{\rm m}^2 \int_0^\infty d\tau \ \langle X_{\rm in}(t) X_{\rm in}(t+\tau) \rangle - \langle X_{\rm in}(t) \rangle^2 \\ &= a^2 \tau_{\rm m}^2 R(t) + \mathcal{O}(\epsilon_R^2) = a^2 \tau_{\rm m}^2 r_{\rm in}[1 + \epsilon_R s(t)] + \mathcal{O}(\epsilon_R^2). \end{aligned} \tag{4.6}$$

Note that $D_{\rm eff}(t)$ differs from the case with fixed spike weights, in which it would be $a^2 \tau_{\rm m} R(t)/2$. Comparing with eq. (4.4) and keeping in mind that $D_{\rm eff}(t)$ has to be properly scaled if time is measured in units of $\tau_{\rm m}$, one obtains

$$\breve{\mu} = \mu + a\tau_{\rm m} r_{\rm in}, \tag{4.7}$$

$$\breve{D} = a^2 \tau_{\rm m} r_{\rm in}, \tag{4.8}$$

$$\breve{\epsilon}_\mu = \epsilon_\mu + a\tau_{\rm m} r_{\rm in} \epsilon_R, \tag{4.9}$$

$$\breve{\epsilon}_D = a^2 \tau_{\rm m} r_{\rm in} \epsilon_R. \tag{4.10}$$

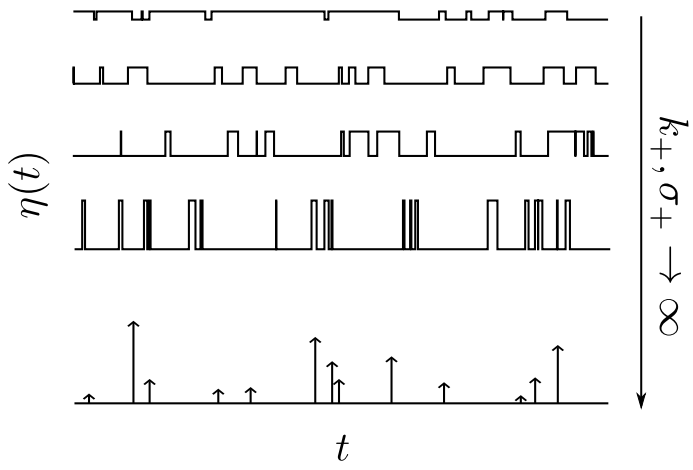

Figure 4.2.: Sketch of the shot-noise limit of dichotomous noise. Letting both k_+ and σ_+ tend to ∞ while keeping their ratio – the mean area under each excursion – constant results in a Poissonian shot noise with exponentially distributed weights.

(4.11)

It is apparent that a modulation of the presynaptic firing rate leads to a modulation of both the mean as well as the noise in the DA. Below, we consider either current modulation ($\epsilon_\mu > 0, \epsilon_R = 0$) *or* rate modulation ($\epsilon_R > 0, \epsilon_\mu = 0$). In the first case, the DA susceptibility is

$$\check{\chi}(\omega) = \check{\chi}_\mu(\omega), \tag{4.12}$$

while in the latter,

$$\check{\chi}(\omega) = a\tau_{\mathrm{m}} r_{\mathrm{in}} \check{\chi}_\mu(\omega) + a^2 \tau_{\mathrm{m}} r_{\mathrm{in}} \check{\chi}_D(\omega), \tag{4.13}$$

with $\check{\chi}_\mu(\omega)$ and $\check{\chi}_D(\omega)$ as given in eqs. (B.4, B.5) [p. 147].

4.2. The shot-noise limit of dichotomous noise

Consider an asymmetric dichotomous Markov process (DMP) $\eta(t)$, jumping between the amplitudes σ_+ and $\sigma_- = 0$ with rates k_+ and k_- (see Fig. 4.2). The area under each excursion from $\eta(t) = 0$ is given by the product of σ_+ with the residence time in the "+" state, which is exponentially distributed with mean $1/k_+$. Letting k_+ and σ_+ tend to ∞, while keeping $a = \sigma_+/k_+$ (the mean area under an excursion) constant, leads to a train of δ-spikes. Before taking the limit, the area under each excursion was an exponentially-distributed random number, so that now the weights of the δ-peaks are exponentially distributed with mean a (Van Den Broeck, 1983). The rate at which spikes occur is simply given by k_-, the rate of leaving the "-" state. Performing this shot-noise limit in the formulas derived in the previous chapter yields exact expressions for ISI moments, stationary distribution, power spectrum, and susceptibility of the system eq. (4.1).

Taking the limit is in most cases rather straightforward: First, one needs to replace $f(v)$ by $f(v) + (\sigma_+ + \sigma_-)/2$ and σ by $(\sigma_+ - \sigma_-)/2$. One may set $\sigma_- = 0$ and rename k_- to r_{in}, highlighting its role as the input firing rate. One then needs to replace σ_+ by $a \cdot k_+$, before performing the limit $k_+ \to \infty$.

If one wants to consider the limit of vanishing refractory period τ_{ref} at the same time, it is important to note that the order in which the two limits are taken does matter: Looking, for instance, at the initial conditions eqs. (3.20, 3.21) (pg. 45), it is apparent that after performing $k_+ \to \infty$ at a non-vanishing τ_{ref}, all trajectories start in the "-" state. This is the desirable behavior for shot noise – the input spike that made the neuron cross the threshold should not have an effect after the reset. In contrast, if one would have first taken $\tau_{\text{ref}} \to 0$ and then $k_+ \to \infty$, a fraction α of all trajectories would start out in "+" state.

In the previous chapter, we have given expressions for power spectrum and susceptibilities of LIF neurons in terms of Gauss' hypergeometric functions (Abramowitz and Stegun, 1972). As shown in Appendix B.2, they turn into confluent hypergeometric functions in the shot-noise limit. In particular,

$$\lim_{k_+\to\infty} \mathcal{F}(v,\omega) = {}_1F_1\left(-i\omega\tau_{\text{m}}; (r_{\text{in}} - i\omega)\tau_{\text{m}}; \frac{v-\mu}{a}\right) =: \widehat{\mathcal{F}}(v,\omega), \tag{4.14}$$

$$\lim_{k_+\to\infty} \mathcal{G}(v,\omega) = {}_1F_1\left(-i\omega\tau_{\text{m}}; 1 + (r_{\text{in}} - i\omega)\tau_{\text{m}}; \frac{v-\mu}{a}\right) =: \widehat{\mathcal{G}}(v,\omega), \tag{4.15}$$

$$\begin{aligned}\lim_{k_+\to\infty} \mathcal{F}'(v,\omega) &= \frac{-i\omega}{a(r_{\text{in}} - i\omega)} {}_1F_1\left(1 - i\omega\tau_{\text{m}}; 1 + (r_{\text{in}} - i\omega)\tau_{\text{m}}; \frac{v-\mu}{a}\right) \\ &= \widehat{\mathcal{F}}'(v,\omega),\end{aligned} \tag{4.16}$$

$$\begin{aligned}\lim_{k_+\to\infty} \mathcal{G}'(v,\omega) &= \frac{-i\omega\tau_{\text{m}}}{a(1 + [r_{\text{in}} - i\omega]\tau_{\text{m}})} {}_1F_1\left(1 - i\omega\tau_{\text{m}}; 2 + (r_{\text{in}} - i\omega)\tau_{\text{m}}; \frac{v-\mu}{a}\right) \\ &= \widehat{\mathcal{G}}'(v,\omega),\end{aligned} \tag{4.17}$$

where ${}_1F_1\,(a;b;z)$ is the confluent hypergeometric function (Abramowitz and Stegun, 1972). Here and in the following, we use $\widehat{\cdot}$ to denote a quantity that has been taken to the shot-noise limit.

As an example, consider the Fourier-transformed ISI density of an LIF neuron driven by a DMP, which we have calculated in the previous chapter (eq. (3.118) [p. 67]):

$$\widetilde{\rho}(\omega) = \frac{(k_- - i\omega)P_{+|+}(\tau_{\text{ref}})\mathcal{F}(z_R,\omega) + k_- P_{-|+}(\tau_{\text{ref}})\mathcal{G}(z_R,\omega)}{e^{-i\omega\tau_{\text{ref}}}(k_- - i\omega)\mathcal{F}(z_T,\omega)}. \tag{4.18}$$

Noting that

$$\lim_{k_+\to\infty} P_{+|+}(\tau_{\text{ref}}) = 0\,, \quad \lim_{k_+\to\infty} P_{-|+}(\tau_{\text{ref}}) = 1, \tag{4.19}$$

replacing k_- by r_{in}, and using eqs. (4.14, 4.15), the shot noise limit of eq. (4.18) is

$$\widehat{\widetilde{\rho}}(\omega) = e^{i\omega\tau_{\text{ref}}} \frac{r_{\text{in}}}{r_{\text{in}} - i\omega} \frac{\widehat{\mathcal{G}}(v_R, \omega)}{\widehat{\mathcal{F}}(v_T, \omega)}. \tag{4.20}$$

This recovers the result of Novikov et al. (2005, eq. (9)) if one sets $\tau_{\text{ref}} = 0$, $\mu = 0$. Expressions for the shot-noise limit of the stationary density, the firing rate, the power spectrum, and the susceptibility are obtained in the same way; they are given and discussed in detail below.

4.3. Stationary density and firing rate

As in the previous chapter, the stationary density needs to be given in N intervals delimited by threshold v_T, fixed points of the "-" dynamics (which here simply correspond to $f(v) = 0$), and the lowest attainable voltage v_-. Taking the SN limit of eq. (3.57) [p. 54], the stationary density in the ith interval is given by

$$\begin{aligned} \widehat{P}_0^i(v) = \tau_{\text{m}} \widehat{r}_0 \frac{e^{-\widehat{\phi}(v)}}{f(v)} \Bigg(& - \Big[\theta(c_i - v_R) - \theta(v - v_R)\Big] e^{\widehat{\phi}(v_R)} \\ & + \frac{1}{a} \int_{c_i}^{v} dx \ \left[\theta(x - v_R) - \theta(x - v_T)\right] e^{\widehat{\phi}(x)} \Bigg), \end{aligned} \tag{4.21}$$

where

$$c_i = \begin{cases} v_R^{\rightarrow} & \text{if } i = 0 \text{ and } f(v_T) > 0, \\ v_U & \text{if one of the interval boundaries is an unstable FP at } v_U, \\ v_T^{\leftarrow} & \text{if } i = N \text{ and } f(v_T) < 0, \end{cases} \tag{4.22}$$

and

$$\widehat{\phi}(v) = \frac{v}{a} + \tau_{\text{m}} r_{\text{in}} \int^{v} dx \ \frac{1}{f(x)} \tag{4.23}$$

(specific expressions for $\widehat{\phi}(v)$ for various choices of $f(v)$ are given in Appendix B.3). The fraction of trajectories crossing the threshold directly due to an input spike is

$$\widehat{\alpha} = 1 - \left[\theta(v_R - c_N) e^{\widehat{\phi}(v_R) - \widehat{\phi}(v_T)} + \frac{1}{a} \int_{c_N}^{v_T} dx \ \theta(x - v_R) e^{\widehat{\phi}(x) - \widehat{\phi}(v_T)} \right]. \tag{4.24}$$

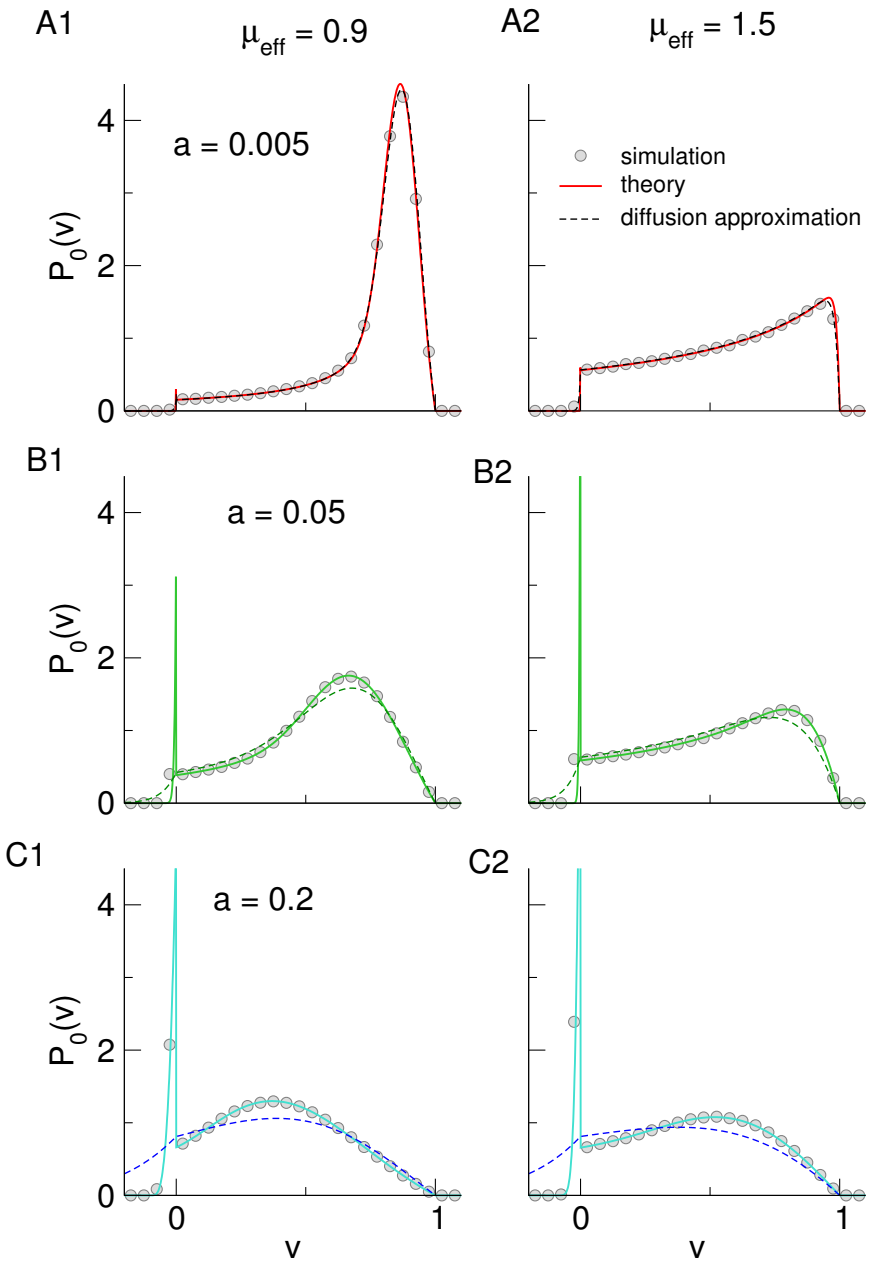

Figure 4.3.: Stationary voltage distribution of a SN-driven LIF neuron compared to the DA. Shown are distributions for different mean spike weights a, where the mean input $\mu_{\text{eff}} = \mu + \tau_{\text{m}} a r_{\text{in}}$ is fixed either at a subthreshold value ($\mu_{\text{eff}} = 0.9$; A1, B1, C1) or a suprathreshold value ($\mu_{\text{eff}} = 1.5$; A2, B2, C2). Theory (solid lines) is compared to simulation results (circles) and the DA (dashed lines). $\mu = -0.1, v_R = 0, v_T = 1, \tau_{\text{ref}} = 0.1 \times \tau_{\text{m}}$.

The stationary firing rate is given by

$$\tau_{\mathrm{m}}\widehat{r}_0 = \left[\frac{1}{a}\sum_{i=1}^{N}\int_{l_i}^{r_i} dx \int_{x}^{\bar{c}_i} dy\, \theta(x-v_R)\frac{e^{\widehat{\phi}(x)-\widehat{\phi}(y)}}{f(y)} + \int_{v_R}^{\bar{c}_1} dx\, \frac{e^{\widehat{\phi}(v_R)-\widehat{\phi}(x)}}{f(x)} + \frac{\tau_{\mathrm{ref}}}{\tau_{\mathrm{m}}}\right]^{-1}, \qquad (4.25)$$

where $\bar{c}_i$ is the interval boundary opposite of c_i. Note that v_R may not be a fixed point of the "-" dynamics for the theory to work (otherwise $e^{\widehat{\phi}(v_R)}$ in eq. (4.21) would diverge). In particular, this means that for an LIF neuron, the theory breaks down for $\mu = 0$. This is no severe restriction, however, as one may choose a non-vanishing but arbitrarily small value for μ.

Of course, the shot-noise limit can also be taken in the recursive relations for higher ISI moments, resulting for instance in exact expressions for the CV of SN-driven IF neurons. As we focus on information transmission here, we refer the reader interested in those expressions to Appendix B.4.

For LIF neurons driven by both excitatory and inhibitory shot noise (also with exponentially distributed weights), Richardson and Swarbrick (2010) have calculated the firing rate using a different approach, starting from the master-equations for shot noise and using Laplace transforms. In Appendix B.5, we show that their expression is equivalent to ours if one sets the inhibitory input rate in their expression to zero.

In Fig. 4.3, we plot the stationary density of an LIF neuron for different values of the mean input spike weight a at fixed mean input $\mu_{\mathrm{eff}} = \mu + a\tau_{\mathrm{m}}r_{\mathrm{in}}$. Our theoretical expression eq. (4.21) (solid lines) is compared to simulations (circles) and the DA (dashed lines). We show a sub- and a suprathreshold regime ($\mu_{\mathrm{eff}} = 0.9$ and $\mu_{\mathrm{eff}} = 1.5$, respectively). Note that varying a at fixed μ_{eff} implies changing also the noise intensity: At fixed μ_{eff}, a larger value of a corresponds to a larger D_{eff}. This is a consequence of the fact that our theory only allows for excitatory input; if also inhibitory input is present, both mean input and noise intensity can be fixed (Richardson and Swarbrick, 2010).

In contrast to the case of dichotomous noise input with a finite correlation time, the probability now goes to zero at the threshold v_T. Note that this only applies as long as the voltage can only be crossed due to incoming spikes. If, by contrast, $f(v_T) > 0$ (trajectories can also drift over the threshold), then $c_N < v_T$ in eq. (4.21), resulting in a finite value for $\widehat{P}_0^N(v_T)$.

For small spike weights $a = 0.005$, the shot-noise theory is hardly distinguishable from the DA. However, already at $a = 0.05$, corresponding to an average of 22 spikes needed to go from the resting potential to the threshold, there are noticeable differences. For instance, the voltage cannot be lower than $v_- = \mu$, in contrast to the Gaussian case, which in principle allows for arbitrarily negative voltages. The most prominent difference is a peak at v_R, where $\widehat{P}_0(v)$ exhibits a discontinuity which is not present in the DA (eq. (B.3) [p. 147]).

The peak at v_R is most easily understood by considering the case $\mu = 0$ (at which the theory breaks down, see above): In this case, trajectories that have crossed the threshold and have been reset remain at v_R for a finite amount of time, until the next input spike kicks them away from it. There is thus a non-vanishing probability to find the voltage

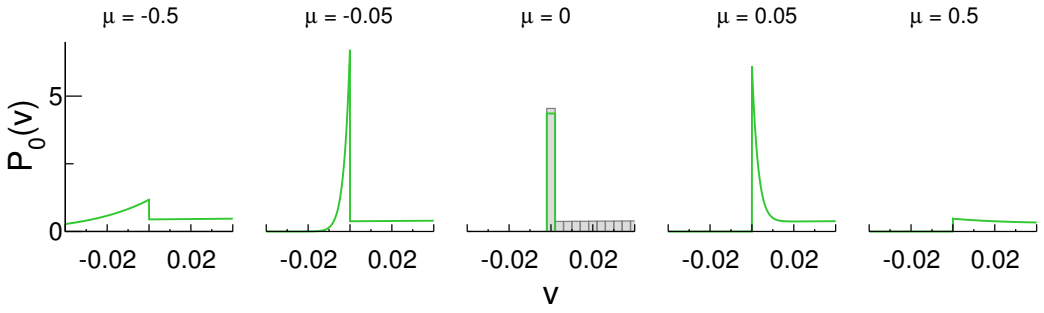

Figure 4.4.: Zoom into the voltage probability density near the reset voltage v_R for different values of μ. For $\mu = 0$, reset trajectories remain at v_R until the next input spike, leading to a δ-peak in $\widehat{P}_0(v)$ with weight $\widehat{r}_0/r_{\text{in}}$. For $\mu = 0$ we plot a binned version of the histogram (bin width $\Delta v = 0.004$) and compare the zeroth bin to $\widehat{r}_0/(r_{\text{in}}\Delta v)$. The slight discrepancy is due to the fact that at finite Δv, not all probability in the bin is due to the δ-peak. At negative (positive) μ, the voltage drifts to lower (higher) values after reset and there is no longer a finite probability to find the neuron at v_R (and thus no δ-peak). Parameters: $a = 0.05, \mu_{\text{eff}} = 0.9, v_R = 0, v_T = 1, \tau_{\text{ref}} = 0.1 \times \tau_{\text{m}}$.

exactly at v_R, corresponding to a δ-peak in the density (see Fig. 4.4). The weight of this δ-peak is $\widehat{r}_0/r_{\text{in}}$ and thus goes to zero as one approaches the DA ($r_{\text{in}} \to \infty$). For $\mu \neq 0$, the peak is no longer a divergence; rather, $\widehat{P}_0(v)$ now exhibits a jump at v_R: Reset trajectories either drift to lower voltages ($\mu < 0$) or higher voltages ($\mu > 0$) before the next input spike.

Figure 4.5 shows the firing rate of an LIF neuron as a function of the mean input μ_{eff}. We compare the theory for shot-noise input to the DA for different values of a. For small a, the curves coincide, as expected, while for moderate to large a, there are marked differences: For high mean input, the DA yields higher firing rates than the shot noise, but for small mean input, the situation is reversed and firing rates are higher for shot-noise input.

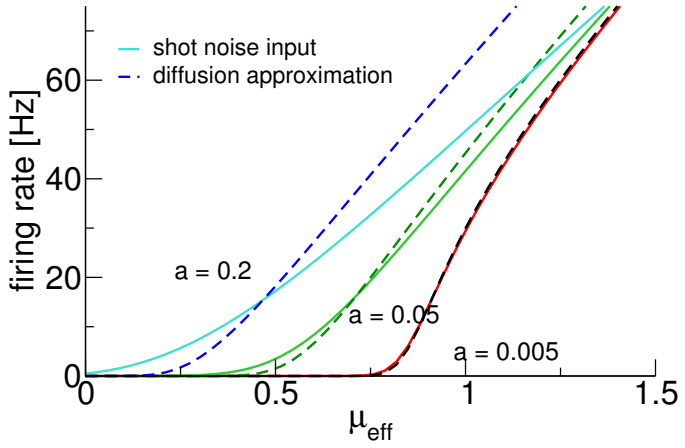

Figure 4.5.: Firing rate of an LIF neuron for shot-noise input with different mean input spike weights a over the mean input $\mu_{\text{eff}} = ar_{\text{in}}$ (solid lines), compared to the DA (dashed lines). Note that the noise intensity D_{eff} (as it enters the DA) increases linearly with μ_{eff}. Remaining parameters: $\mu = -0.1, v_R = 0, v_T = 1, \tau_{\text{ref}} = 0.1 \times \tau_{\text{m}}$.

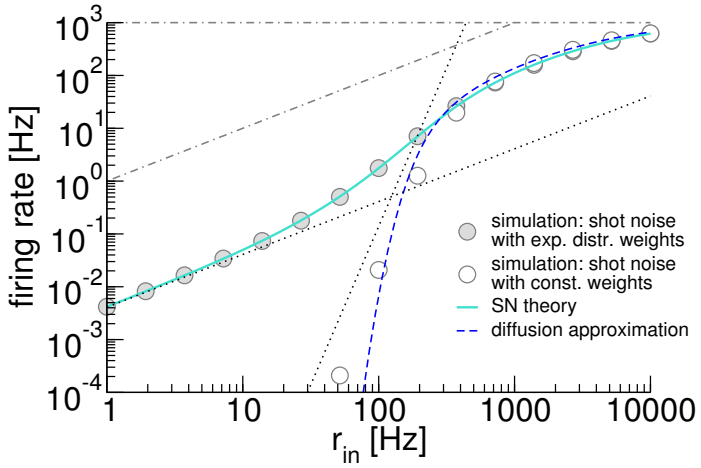

Figure 4.6.: Firing rate for an LIF neuron with shot-noise input (solid line) over the input rate, compared to the DA (dashed line) and simulations for shot noise with exponentially distributed weights (gray circles) and constant weights (white circles). The black dotted lines show the asymptotics for shot-noise input with exponential weights and with fixed weights, the gray dash-dotted lines delimit the maximal possible firing rate, which is given by $\min(r_{\text{in}}, 1/\tau_{\text{ref}})$. Parameters: $a = 0.2, \mu = -0.1, v_R = 0, v_T = 1, \tau_{\text{ref}} = 0.1 \times \tau_{\text{m}}$.

Why shot-noise input can lead to higher output firing rates can be understood in the limit of low input rates: Consider that spike weights are drawn randomly from an exponential distribution. Thus, for any given input spike, there is a finite probability that it makes the neuron fire. If we assume very sparse input (the voltage decays to μ between input spikes), then the probability that a single input spike brings the neuron across threshold is given by

$$\int_{v_T-\mu}^{\infty} dx \, \frac{e^{-\frac{x}{a}}}{a} = e^{-\frac{v_T-\mu}{a}}. \tag{4.26}$$

Thus, in this limit, the output firing rate is linear in the input rate

$$\widehat{r}_0 \approx r_{\text{in}} e^{-\frac{v_T-\mu}{a}}. \tag{4.27}$$

What if the input spikes all had the same weight? In this case, one may obtain a rough estimate of the output firing rate at low input rates by assuming that in a short time window τ_{m} (the membrane time constant), at least

$$N_c = \left\lceil \frac{v_T - \mu}{a} \right\rceil \tag{4.28}$$

input spikes have to coincide to produce an output spike, where $\lceil \cdot \rceil$ denotes the ceiling function. Using the Poisson nature of the input and assuming sparse input, $r_{\text{in}}\tau_{\text{m}} \ll 1$,

this assumption can be shown (see Appendix B.6) to yield the asymptotic firing rate

$$\widehat{r}_0 \approx \frac{(\tau_\mathrm{m} r_\mathrm{in})^{N_c}}{\tau_\mathrm{m} N_c \Gamma(N_c)}. \tag{4.29}$$

In Fig. 4.6, we plot both these asymptotics as well as the theory for shot noise with exponentially distributed weights as well as the DA as a function of the input rate. We compare the theory to simulations for shot noise with exponentially distributed weights (gray circles) and constant weights (white circles). Both shot-noise cases can be seen to yield higher output firing rates at low input rates, compared to the DA, which can be made plausible by considering the asymptotic behavior. Note that the plotted DA curve is for the case of exponentially distributed weights; the effective noise for the fixed weights is lower by a factor of two such that the corresponding DA would be even lower.

4.4. Power spectrum for LIF neurons

For LIF neurons, we start from eq. (3.112) [p. 65] to obtain an expression for the power spectrum. It reads

$$\widehat{S}_{xx}(\omega) = \widehat{r}_0 \frac{\left| e^{-i\omega\tau_\mathrm{ref}} \widehat{\mathcal{F}}(v_T, \omega) \right|^2 - \left| \frac{r_\mathrm{in}}{r_\mathrm{in} - i\omega} \widehat{\mathcal{G}}(v_R, \omega) \right|^2}{\left| e^{-i\omega\tau_\mathrm{ref}} \widehat{\mathcal{F}}(v_T, \omega) - \frac{r_\mathrm{in}}{r_\mathrm{in} - i\omega} \widehat{\mathcal{G}}(v_R, \omega) \right|^2}. \tag{4.30}$$

Note that, due to the restricted range of parameters considered in the previous chapter, this expression is only valid for $\mu < v_R$.

The most striking feature of the power spectrum of a DMP-driven LIF neuron was its unusual high-frequency behavior. Here, knowing that

$$\lim_{b\to\infty} {}_1F_1(a; b; z) = 1, \tag{4.31}$$

it can be seen that

$$\lim_{\omega\to\infty} \widehat{S}_{xx}(\omega) = \widehat{r}_0. \tag{4.32}$$

In words, the peculiar undamped oscillations have disappeared. This is due to the fact that shot-noise effectively leads to a reset from the "+" state to the "-" state. One can enforce this reset rule also in the original case of a DMP with non-vanishing correlation time (a quick way is to set $\tau_\mathrm{ref} = 0, P_{++}(\tau_\mathrm{ref}) = 0$ and $P_{-+}(\tau_\mathrm{ref}) = 1$ in eq. (3.112) [p. 65]) to obtain the same high-frequency behavior. The explanation is rather simple: When resetting to the "-" state, the noise has to switch at least once before the threshold can be crossed. This renders deterministic ISIs, which were responsible for the undamped oscillations, impossible.

In Fig. 4.7, we plot the power spectrum for different values of a at constant mean in-

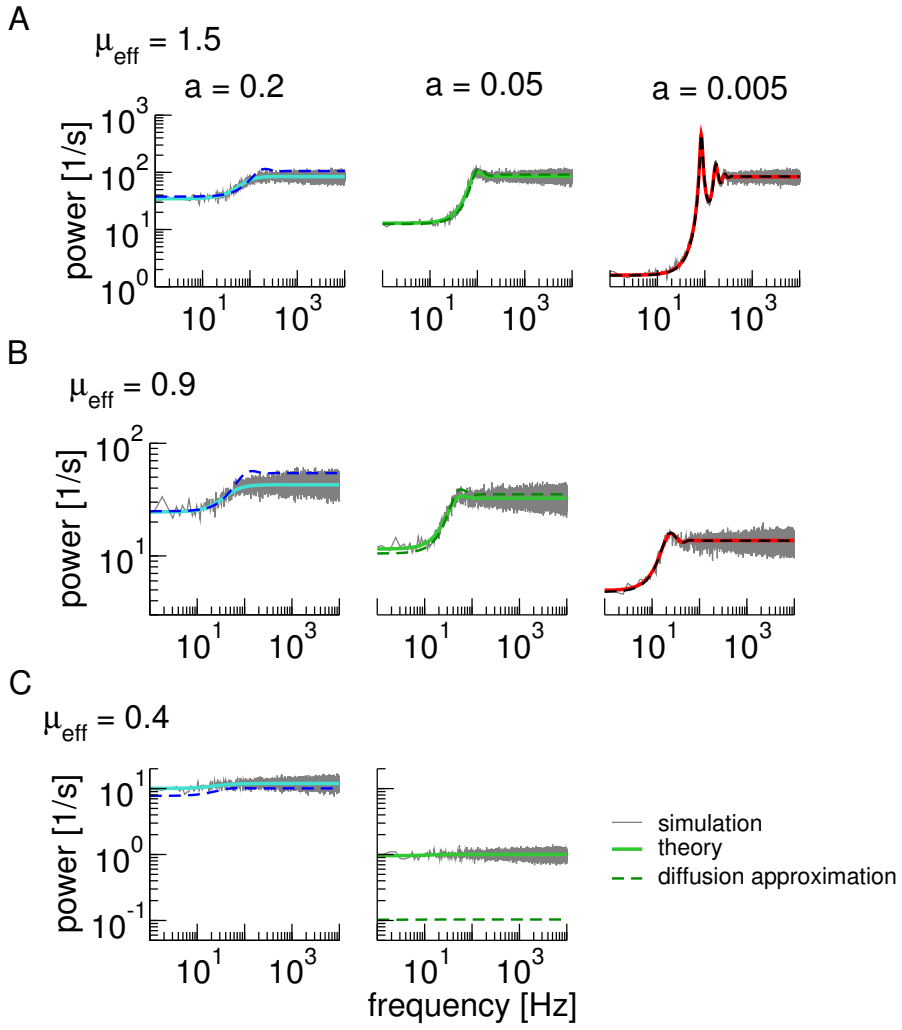

Figure 4.7.: Power spectra for the shot-noise-driven LIF compared to simulations and the DA. Shown are spectra for different mean synaptic weights a at a constant mean input that is either suprathreshold (A), mildly subthreshold (B) or far subthreshold (C).Theory (red/green/blue solid lines) is compared to the DA (dashed lines) and simulated spectra (gray solid lines). For C, $a = 0.005$ yields very low firing rates; this case has been omitted. Remaining parameters: $\mu = -0.1, v_R = 0, v_T = 1, \tau_{\text{ref}} = 0.1 \times \tau_{\text{m}}, \tau_{\text{m}} = 0.01\,\text{s}$.

put. In addition to the suprathreshold (Fig. 4.7A) and subthreshold (Fig. 4.7B) regimes considered in Fig. 4.3, we plot a regime that is further subthreshold (Fig. 4.7C, $\mu_{\text{eff}} = 0.4$). This is motivated by the above finding that the firing rate may be higher for shot-noise input than for the DA when the mean input is low.

A prominent effect of changing a at a constant μ_{eff} is a change in noise intensity D_{eff}. This is reflected in the power spectra, which become characteristic of more regular spike trains as a decreases (small low-frequency limit, more prominent oscillations).

The main effect of shot noise on the spectra (when compared to the DA) seems to be due to the difference in firing rate: The high-frequency limit of the SN spectra is suppressed compared to the DA in the supra- and moderate subthreshold regimes (A, B), while in a far-subthreshold regime, the shot-noise spectra are higher than the DA.

4.5. Susceptibility for LIF neurons

Taking the SN limit in eq. (3.138) [p. 70] and using eqs. (4.16, 4.17), the susceptibility with respect to a current modulation reads for the shot-noise case

$$\widehat{\chi}_\mu(\omega) = -\frac{\widehat{r}_0}{i\tau_{\text{m}}\omega - 1} \frac{\widehat{\mathcal{F}}'(v_T,\omega) - \frac{r_{\text{in}}}{r_{\text{in}} - i\omega}\widehat{\mathcal{G}}'(v_R,\omega)}{\widehat{\mathcal{F}}(v_T,\omega) - e^{i\omega\tau_{\text{ref}}}\frac{r_{\text{in}}}{r_{\text{in}} - i\omega}\widehat{\mathcal{G}}(v_R,\omega)}. \tag{4.33}$$

Calculating the high frequency behavior (see above) yields

$$\begin{aligned} |\widehat{\chi}_\mu(\omega \gg 1)| &= \frac{\widehat{r}_0}{a\tau_{\text{m}}\omega}, \\ \arg[\widehat{\chi}_\mu(\omega \gg 1)] &= \frac{\pi}{2}. \end{aligned} \tag{4.34}$$

This is in contrast to the high-frequency transmission properties of LIF neurons driven by Gaussian white noise, for which the susceptibility decays like $1/\sqrt{\omega}$, with an asymptotic phase shift of $\pi/4$ (see, e.g. (Fourcaud-Trocmé et al., 2003)).

In Fig. 4.8, we compare eq. (4.33) to simulations and the DA. Owing to the qualitative difference in high-frequency behavior, the differences between the shot-noise case and the DA are much more pronounced than for the power spectra. For supra- and moderately subthreshold mean input, the DA always has a higher susceptibility than the shot-noise case (unsurprisingly, as the firing rate is higher and the shot-noise susceptibility decays faster). However, for further subthreshold mean input, the SN susceptibility can be larger than the DA susceptibility over a wide frequency range. Again, this can be explained by the difference in firing rate.

We can also derive an expression for the susceptibility in the case that the signal enters as a modulation of the presynaptic firing rate ($\epsilon_R > 0$). Taking the SN limit of eq. (3.154)

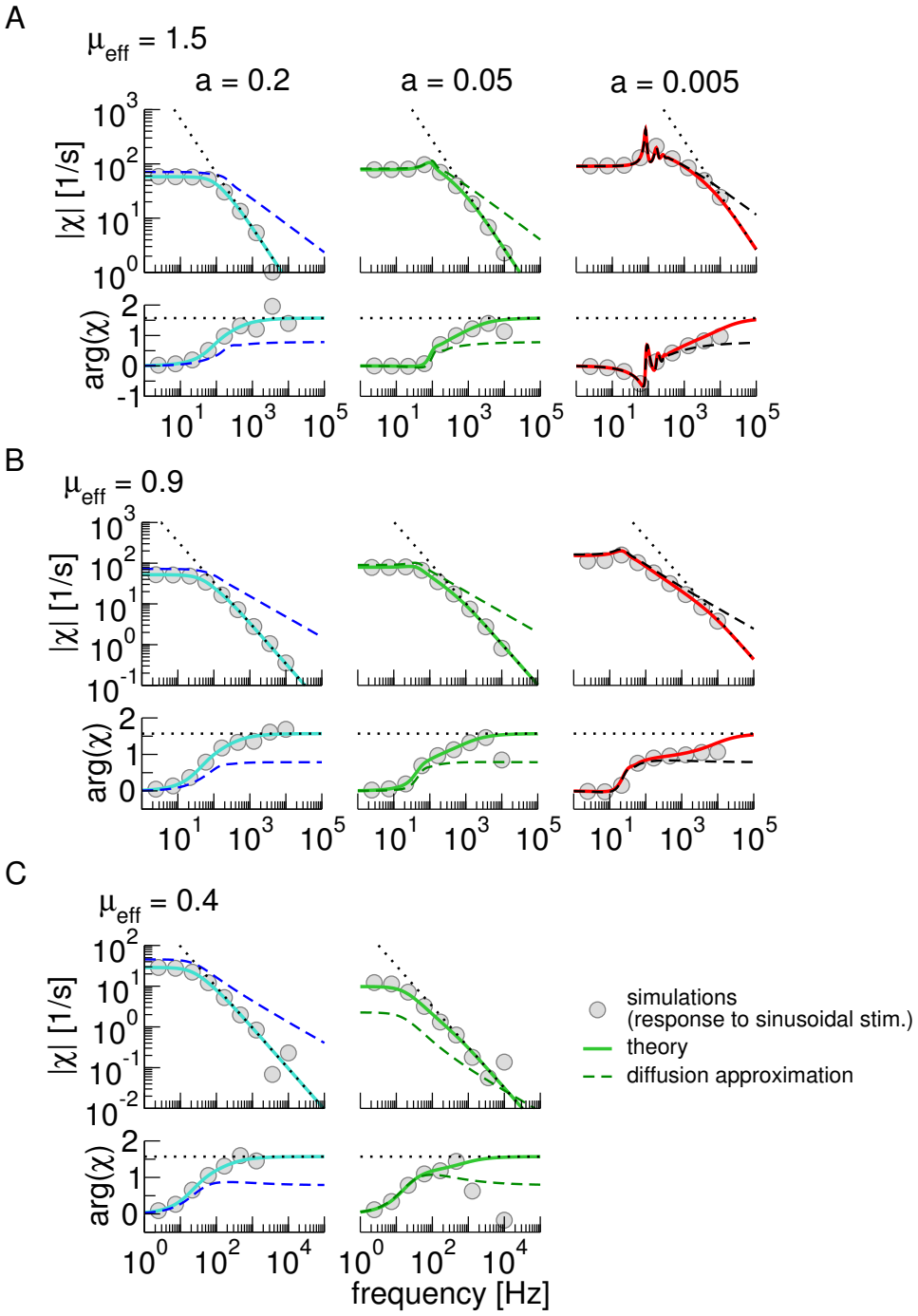

Figure 4.8.: Susceptibility $\widehat{\chi}_\mu(\omega)$ of an LIF neuron driven by excitatory shot noise with respect to a modulation of the base current. Theory (eq. (4.33), solid lines) compared to the DA (dashed lines) and simulation results (circles). Dotted lines show the asymptotic behavior of the shot-noise theory (eq. (4.34)). Shown are different values of a, with the mean input μ_{eff} in a suprathreshold (A), moderately subthreshold (B), and far subthreshold regime (C). Remaining parameters: $\mu = -0.1, v_R = 0, v_T = 1, \tau_{\text{ref}} = 0.1 \times \tau_{\text{m}}, \tau_{\text{m}} = 0.01\,\text{s}$.

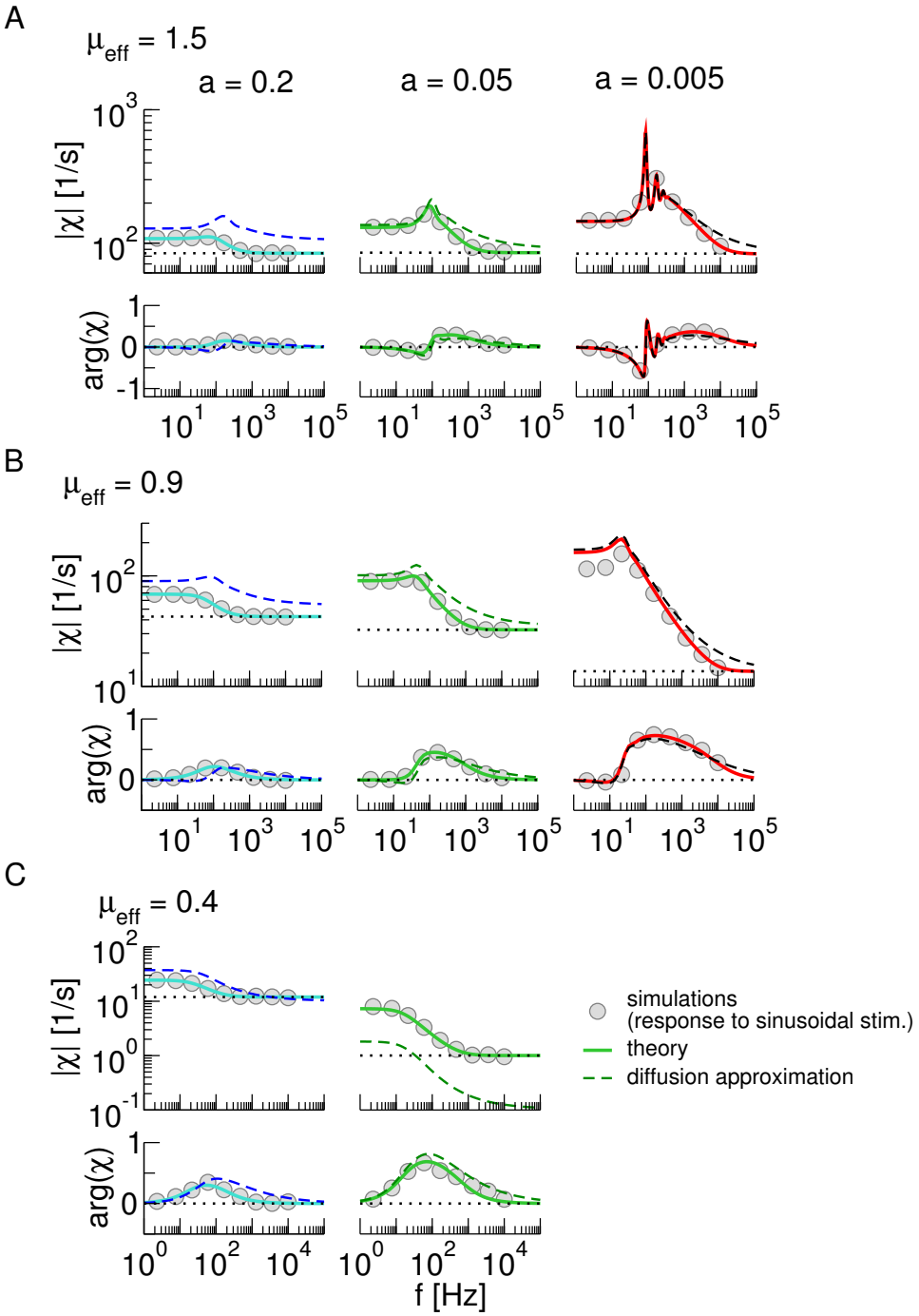

Figure 4.9.: Susceptibility $\widehat{\chi}_R(\omega)$ of an LIF neuron driven by excitatory shot noise with respect to a modulation of the presynaptic firing rate. Theory (eq. (4.35), solid lines) compared to the DA (dashed lines) and simulations (circles). Dotted lines show the asymptotic behavior of the shot-noise theory (eq. (4.37)). Shown are different values of a, with the mean input μ_{eff} in a suprathreshold (A), moderately subthreshold (B), and far subthreshold regime (C). Remaining parameters: $\mu = -0.1, v_R = 0, v_T = 1, \tau_{\text{ref}} = 0.1 \times \tau_{\text{m}}, \tau_{\text{m}} = 0.01\,\text{s}$.

[p. 75], we obtain

$$\widehat{\chi}_R(\omega) = \frac{\int_{v_-}^{v_T} dv\, r_{\text{in}} \widehat{P}_0(v) \left[(r_{\text{in}} - i\omega)\widehat{\mathcal{F}}(v,\omega) - r_{\text{in}}\widehat{\mathcal{G}}(v,\omega) \right]}{(r_{\text{in}} - i\omega)\widehat{\mathcal{F}}(v_T,\omega) - r_{\text{in}} e^{i\omega\tau_{\text{ref}}}\widehat{\mathcal{G}}(v_R)}, \tag{4.35}$$

where we have used that in the shot-noise limit, trajectories are in the "-" state virtually all the time, so that $\widehat{P}_{-,0}(v) = \widehat{P}_0(v)$.

Let us consider the high-frequency behavior of eq. (4.35),

$$\lim_{\omega\to\infty} \widehat{\chi}_R(\omega) = \frac{\int_{v_-}^{v_T} dv\, r_{\text{in}} \widehat{P}_0(v) \exp\left[\frac{v-\mu}{a}\right]}{\exp\left[\frac{v_T-\mu}{a}\right]} = r_{\text{in}} \int_{v_-}^{v_T} dv\, \widehat{P}_0(v) \exp\left[\frac{v-v_T}{a}\right]. \tag{4.36}$$

The rightmost expression can be identified as the input rate times the probability that an incoming AP causes the unperturbed neuron to spike, so that we can write

$$\lim_{\omega\to\infty} \widehat{\chi}_R(\omega) = \widehat{r}_0. \tag{4.37}$$

This high-frequency limit is consistent with the one obtained by Richardson and Swarbrick (2010). In stark contrast to current modulation, modulation of the input rate leads to a non-vanishing high-frequency response with zero phase lag (Richardson and Swarbrick, 2010).

In Fig. 4.9, we plot the susceptibility for rate modulation for different combinations of a and r_{in}, along with the respective asymptotics given by eq. (4.37). It is apparent that for large ω, the magnitude of the susceptibility does indeed approach a constant value, while the phase lag decays to zero. Again, the susceptibility may be higher for the SN case when the neuron is far subthreshold.

4.6. Information transmission

In order to judge how information transmission is affected by the shot-noise nature of the synaptic noise/the spikes carrying the signal, we make use of the coherence between the signal $s(t)$ and the output spike train $x(t)$,

$$\widehat{C}_{sx}(\omega) = \frac{|\widehat{S}_{sx}(\omega)|^2}{\widehat{S}_{xx}(\omega) S_{ss}(\omega)}, \tag{4.38}$$

where $S_{ss}(\omega)$ is the power spectrum of the signal. In linear response, the squared cross spectrum is

$$|\widehat{S}_{sx}(\omega)|^2 = |\widehat{\chi}(\omega)|^2 \epsilon^2 S_{ss}^2(\omega), \tag{4.39}$$

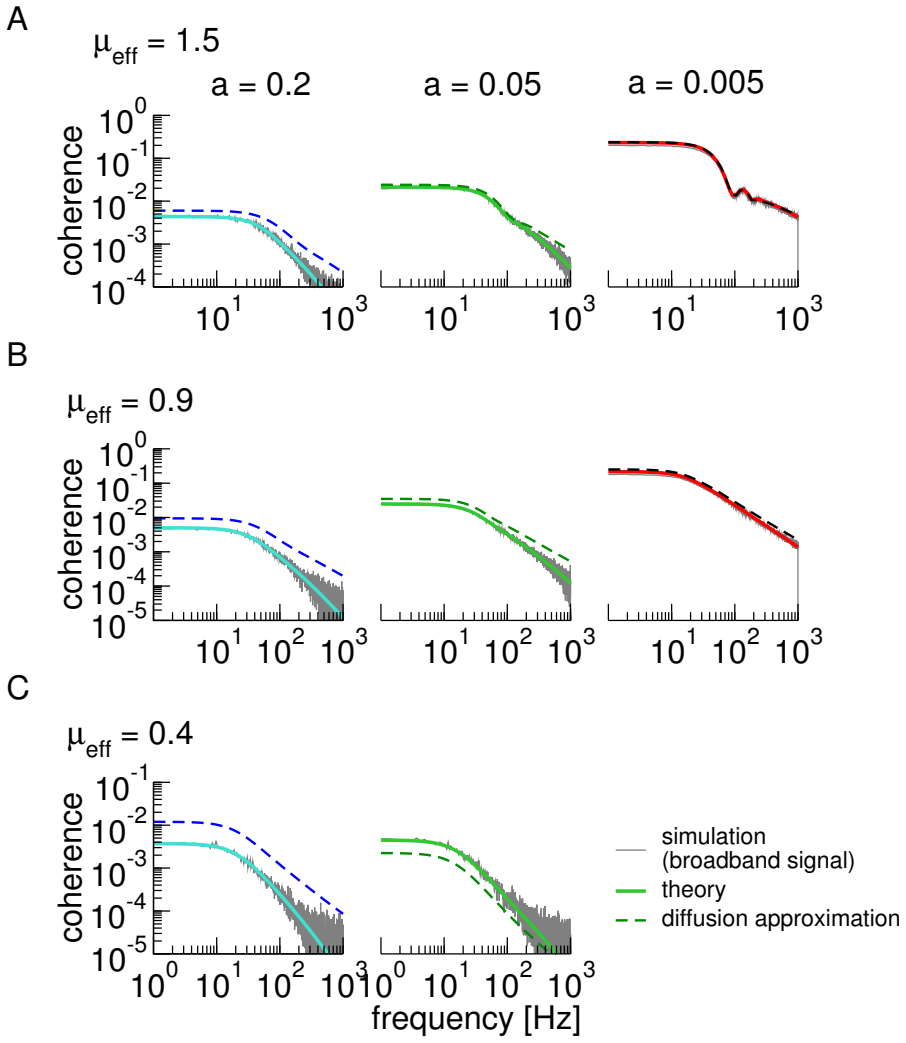

Figure 4.10.: Coherence between signal and output spike train when the signal enters as a current modulation. Theory (solid colored lines) compared to the DA (dashed lines) and simulations (solid gray lines). $\epsilon_\mu = 0.3$, $f_0 = 0\,\mathrm{Hz}$, $f_c = 1000\,\mathrm{Hz}$. Remaining parameters: $\mu = -0.1, v_R = 0, v_T = 1, \tau_{\mathrm{ref}} = 0.1 \times \tau_{\mathrm{m}}, \tau_{\mathrm{m}} = 0.01\,\mathrm{s}$

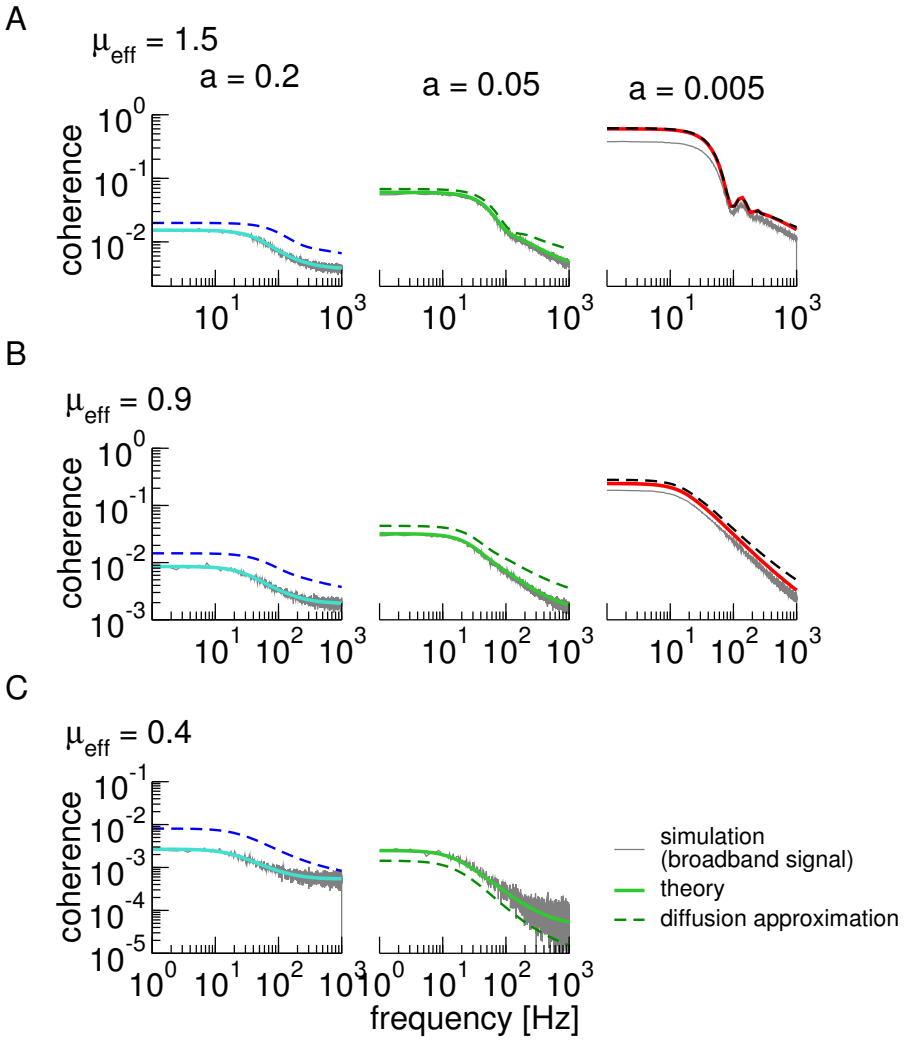

Figure 4.11.: Coherence between signal and output spike train when the signal enters as a rate modulation. Theory (solid colored lines) compared to the DA (dashed lines) and simulations (solid gray lines). $\epsilon_R = 0.3$, $f_0 = 0\,\mathrm{Hz}$, $f_c = 1000\,\mathrm{Hz}$. Remaining parameters: $\mu = -0.1, v_R = 0, v_T = 1, \tau_{\mathrm{ref}} = 0.1 \times \tau_{\mathrm{m}}, \tau_{\mathrm{m}} = 0.01\,\mathrm{s}$

where one either has $\epsilon = \epsilon_\mu$ and $\widehat{\chi}(\omega) = \widehat{\chi}_\mu(\omega)$ [eq. (4.33)], or $\epsilon = \epsilon_R$ and $\widehat{\chi}(\omega) = \widehat{\chi}_R(\omega)$ [eq. (4.35)]. We further assume that the signal is weak enough that we can use the unperturbed power spectrum (given in eq. (4.30), where we have assumed $\epsilon_\mu = \epsilon_R = 0$).

In Fig. 4.10, we plot the coherence for modulation of the base current; in Fig. 4.11, for a modulation of the presynaptic rate. In both cases, we compare it to the DA and simulations in the regimes considered above. First of all, the coherence is low pass in all cases, as known for Gaussian-white-noise-driven IF models with a current-modulated signal (Vilela and Lindner, 2009). In both scenarios, the coherence is higher for the DA in the suprathreshold regime (the dashed coherence curve is above the solid line).

For subthreshold input, in contrast, it can be advantageous to have finite spike weights: both for the additive signal as well as the rate-coded signal, the coherence curve for shot-noise input can be above the DA. This is further illustrated in Fig. 4.12, where we plot the lower bound for the mutual information rate (eq. (1.38) [p. 17]) between the signal

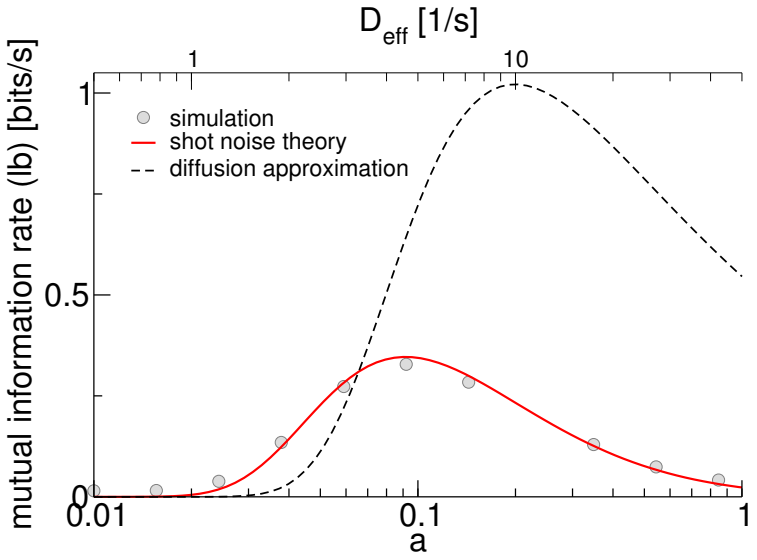

Figure 4.12.: Lower bound for the mutual information rate between a current-modulated signal and output spike train for different mean spike weights a (corresponding also to different effective noise intensities D_{eff}. Other parameters like in Fig. 4.10C.

(entering as a current modulation) and the output spike train for varying mean spike weight a at fixed mean input $\mu_{\text{eff}} = 0.4$. Different values of a correspond to different noise intensities (see the alternative x axis in Fig. 4.12). It is thus not surprising that one observes a stochastic resonance (SR) peak in the mutual information rate (both for SN as well as DA). Remarkably, the non-Gaussian nature of the noise may shift the SR peak towards lower noise intensities. Thus, there is a range of noise intensities where – compared to the DA – a background with finite synaptic weights and spikes arriving at a finite rate is favorable to information transmission.

4.7. Summary

In this chapter, we studied an LIF neuron driven by excitatory shot noise with exponentially distributed weights. By taking the shot-noise limit of dichotomous noise, we could use the results of the previous chapter to derive exact expressions for the stationary voltage distribution, the ISI moments, the power spectrum of spontaneous activity, and the susceptibility. The results for the probability density and the ISI moments apply to general IF neurons and are novel. For the special case of an LIF neuron, an expression for the firing rate has previously been derived for the case of excitatory *and* inhibitory shot noise (Richardson and Swarbrick, 2010). This expression agrees with the one we have derived when the rate of inhibitory input is set to zero. For the power spectrum and the susceptibility with respect to a rate-coded signal, expressions in terms of integrals have been derived by Richardson and Swarbrick (2010). Here, our results provide alternative formulations in terms of confluent hypergeometric functions (note that our expression for the susceptibility also involves an integration that has to be carried out numerically). The susceptibility with respect to current modulation, for which we give an expression in terms of confluent hypergeometric functions, is again a novel result. Here, we find that

it deviates qualitatively from the high-frequency behavior of LIF neurons with (either white or colored) Gaussian noise.

We compare our results to the diffusion approximation for different mean spike weights. Specifically, for the firing rate we find that at low input rates, shot-noise input can yield higher firing rates than the DA with the same mean input and noise intensity. This translates to the spectral quantities, and ultimately the coherence, in a subthreshold regime. Information transmission at low input rates can thus be enhanced by this kind of non-Gaussian noise.

Chapter 5.

Approximations for integrate-and-fire neurons driven by slow dichotomous noise with additional fast fluctuations

The exact results we have derived in Chapter 3 describe (leaky) integrate-and-fire neurons that are driven by a dichotomous Markov process (DMP), i.e. two-state input for which the dynamics within one state is entirely deterministic. In a real neuron, there are many sources of stochasticity, so that such a situation will never occur. And even without intrinsic noise, if the firing rate of a presynaptic population were to jump between two constant values (up and down states), the resulting input to the neuron would be stochastic within a state, due to its shot noise nature.

In Chapter 3, we found power spectrum and susceptibility of LIF neurons driven by purely dichotomous noise to exhibit undamped periodicity. This phenomenon can be traced to the absence of further stochasticity within a state of the dichotomous process. We thus expect these spectral quantities (and, with them, the cell's information transmission properties) to change qualitatively once additional stochasticity is taken into account.

The aim of this chapter is to derive approximations for the interspike interval (ISI) moments, the power spectrum and the susceptibility of IF neurons driven by a DMP with additional fast fluctuations. These approximations (for the case of LIF neurons) will then be used in Chapter 6, where we study the effect of network up-down states on information transmission. Here, we consider two sources of additional stochasticity (see Fig. 5.1): The fast fluctuations are either introduced by adding weak Gaussian white noise (GWN), or by considering inhomogeneous Poissonian shot noise (SN). In the latter case, the DMP enters as a rate modulation.

In the first scenario, the dynamics of the neuron is described by

$$\dot{v} = f(v) + \epsilon s(t) + \eta(t) + \sqrt{2D}\xi(t), \tag{5.1}$$

where $f(v)$ is a potentially nonlinear function, $\epsilon s(t)$ is a weak signal, $\eta(t)$ is a DMP that jumps between σ_+ and σ_- at rates k_+ ("+" to "-") and k_- ("-" to "+"), $\xi(t)$ is Gaussian white noise [$\langle\xi(t)\rangle = 0$, $\langle\xi(t)\xi(t')\rangle = \delta(t-t')$] and D is the noise intensity. We will refer to this scenario using the abbreviation DMP+GWN.

For the shot noise scenario (DMP+SN), the dynamics is governed by

$$\dot{v} = f(v) + \epsilon s(t) + X_{\text{in}}(t), \tag{5.2}$$

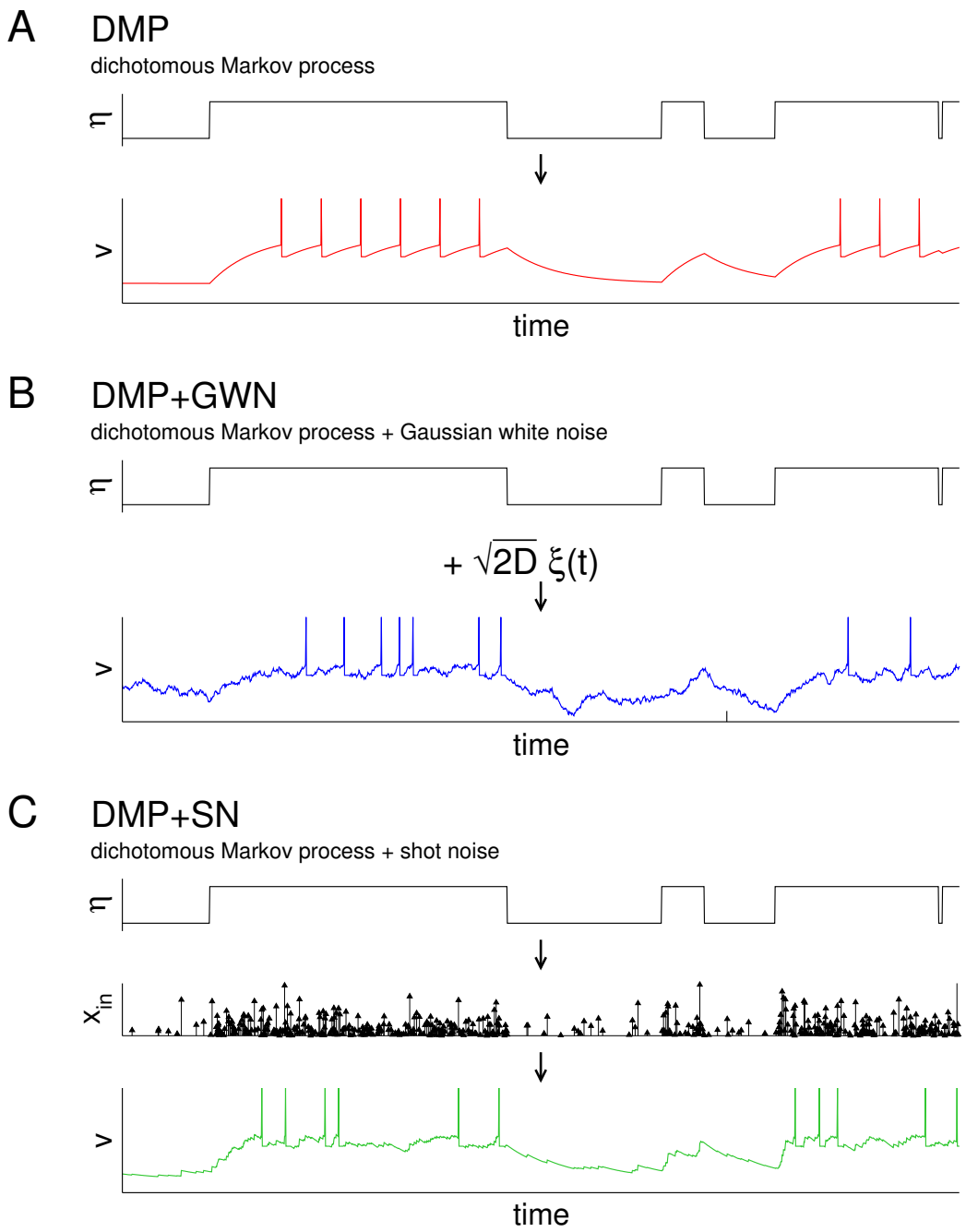

Figure 5.1.: Exemplary realizations of $\eta(t)$ and $v(t)$ for the scenarios considered in this chapter. In addition to the case of purely dichotomous noise (DMP), we investigate a case with additive Gaussian white noise (DMP+GWN) as well as the case of an excitatory inhomogeneous Poisson input — delta-spikes with exponentially distributed weights that occur at a rate given by a dichotomous process that jumps between r_{up} and r_{down} (DMP+SN). Note that spikes are not dynamically generated by the model but drawn for illustration purposes at the times of threshold crossings. Parameters: $\epsilon = 0, k_+ = 0.3, k_- = 0.5, \sigma_+ = 4.8, \sigma_- = 0.6, \mu = -2.9, \tau_{\text{ref}} = 0.1$ (all panels), $D = 0.48$ (B) and $a = 0.1$, meaning $r_{\text{up}} = 48, r_{\text{down}} = 6$ (C).

with the input spike train

$$X_{\text{in}}(t) = \sum_i a_i \delta(t - t_i), \tag{5.3}$$

where the sum runs over all incoming spikes; t_i is the time of the ith spike and a_i its weight, drawn from an exponential distribution with mean a. Spikes occur at a time-dependent rate $R(t)$, which jumps between r_{up} and r_{down} according to the dichotomous process $\eta(t)$,

$$R(t) = \max\left(0, \frac{\eta(t)}{a}\right). \tag{5.4}$$

Thus, $r_{\text{up}} = \sigma_+ / a$, while $r_{\text{down}} = \sigma_- / a$ if $\sigma_- > 0$ and 0 otherwise.

We contrast these two scenarios to a third one, the case of purely dichotomous input (denoted just by DMP), which corresponds to setting $D = 0$ in eq. (5.1). In all cases, time is measured in units of the membrane time constant and the evolution equation for the voltage is supplemented by the fire-and-reset rule: when the voltage reaches v_T, it is reset to v_R, where it remains clamped for a refractory period τ_{ref}.

There are two principal firing regimes that can be distinguished: The neuron either fires *almost* only when the DMP is in the "+" state (this is the situation depicted in Fig. 5.1), or it fires in both states. This distinction is clear-cut for the pure DMP scenario with $\epsilon = 0$, where firing within the "-" state happens only if $f(v) + \sigma_- > 0$ for all $v \in [v_R, v_T]$ (see the discussion in Chapter 3, Sec. 3.2). With additional fast fluctuations or in the presence of a signal, this is no longer strictly true. However, we assume that these fluctuations are sufficiently weak that the probability of spiking is very low if the mean input in the "-" state is subthreshold. Most of the approximations we develop in this chapter assume that firing only happens in the "+" state. This is the relevant case for modeling up-down input in Chapter 6, which is usually strongly hyperpolarizing in the down state (Steriade et al., 2001). Only for the ISI moments, approximations are also derived in the regime where the neuron fires in both states.

We develop analytical approximations for ISI moments, power spectrum and susceptibility under the assumption that the DMP is slow. By slow we mean, roughly speaking, that the time spent in either noise state is much larger than a typical ISI. For such an input, one may calculate quantities of interest for fixed noise values and average over the different possible values afterwards; this is a quasistatic approximation. Such approximations have been employed to study PIF (Middleton et al., 2003) and LIF neurons (Schwalger and Schimansky-Geier, 2008) driven by slow Ornstein-Uhlenbeck processes. In the present case, the two-state nature of the DMP considerably simplifies things. Similar approximations for slow switching between two point processes have been employed by Schwalger et al. (2012); Kromer et al. (2014); Müller-Hansen et al. (2015). We have used the approximation for the ISI moments with purely dichotomous input for LIF and QIF neurons in (Droste and Lindner, 2014).

While we consider different approximations below, they all share the same basic approach: We express the quantities of interest by the corresponding quantities of a neuron where the DMP $\eta(t)$ is *fixed* either in the "+" or the "-" state. We denote these quantities by a "+" or "-" superscript. Take, for example, the case of the firing rate r_0 in a parameter

regime where the neuron only fires in the "+" state. It is plausible that, neglecting transients at the onset of "+" states, this can be approximated by a weighted version of the firing rate of a neuron for which the DMP is always in the "+" state,

$$r_0 = \frac{k_-}{k_+ + k_-} r_0^+, \tag{5.5}$$

where the prefactor gives the stationary probability that $\eta(t)$ is in the "+" state. Below, we will derive this intuitive result in a slightly more systematic way that generalizes to higher ISI moments and the power spectrum.

The approximations developed in this chapter are in principle valid for IF neurons with arbitrary $f(v)$. However, many of the needed expressions for quantities at fixed $\eta(t)$, such as the Fourier-transformed ISI density $\widetilde{\rho}^+(\omega)$, the power spectrum $S_{xx}^+(\omega)$, or the susceptibility $\chi^+(\omega)$, are only available for PIF and LIF neurons. Below, we will therefore concentrate on the LIF model, setting

$$f(v) = \mu - v. \tag{5.6}$$

Note, however, that there exist efficient schemes to obtain the needed quantities for nonlinear models numerically (Richardson, 2007, 2008).

For the DMP+GWN scenario, we use the known results for LIF neurons in the diffusion approximation with noise intensity D and a base current $\mu + \sigma_+$, which are summarized in Appendix B.1. For the DMP+SN scenario, we use the expressions derived in Chapter 4, for which we choose the mean spike weight a such that the noise intensity in the "+" state matches that of the DMP+GWN scenario: $a^2 r_{\mathrm{up}} = D$ (see Chapter 4, Sec. 4.1). Note that the mean input in the "+" state is already the same by construction:

$$\mu + \langle X_{\mathrm{in}}(t) \rangle = \mu + a r_{\mathrm{up}} = \mu + \sigma_+. \tag{5.7}$$

The outline of this chapter is as follows: We first develop an approximation for the ISI density, which we then use to obtain approximations for the first two ISI moments (Sec. 5.1). As our focus lies on approximating the spectral quantities which are relevant for the study of information transmission, we illustrate these results only briefly for firing rate and CV of an LIF neuron driven by purely dichotomous input. In Sec. 5.2, we turn to the power spectrum. This can either be approximated using the results for the ISI density, or via an approach based on an approximation of the spike train's auto-correlation function. Finally, in Sec. 5.3, we use a similar approach (based on an approximation of the impulse response in the time domain) to obtain an expression for the susceptibility.

5.1. Approximation for the ISI density and its moments

The main assumption of our approximation is that the duration of "+" and "-" states is large enough that most ISIs can clearly be assigned to either a "+" or a "-" state. We first consider the situation that the neuron only fires when the DMP is in the "+" state. This situation is sketched in Fig. 5.2. ISIs are either short and fall entirely into a "+" state, or

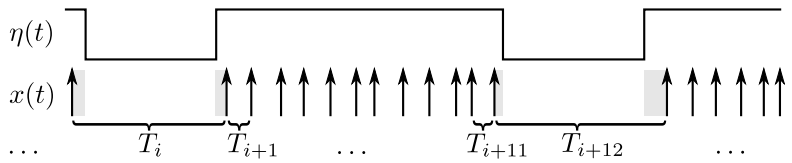

Figure 5.2.: Sketch of the output spike train $x(t)$ for slowly switching dichotomous noise (in a regime where the neuron fires only during "+" dynamics). Most ISIs are short and fall entirely into a "+" state; each "-" state leads to one long ISI. The grey bars show the error made by using the duration of "-" states for long ISIs.

they are long and coincide *almost* entirely with a "-" state. We then assume that long ISIs are distributed like the duration of "-" states (neglecting effects at the boundaries). For the short ISIs in the "+" state, we assume that their distribution $\rho^+(T)$ equals that of a neuron where the DMP is fixed in the "+" state (i.e. $\eta(t) \equiv \sigma_+$).

For the pure DMP scenario, all ISIs during "+" dynamics have the same length, so that

$$\rho^+(T) = \delta(T - T_d^+), \tag{5.8}$$

where T_d^+ is the deterministic time from reset to threshold, eq. (3.115) [p. 66]. For the two scenarios with additional stochasticity, no explicit expressions are known for $\rho^+(T)$. However, in order to calculate spectral quantities or ISI moments, we will only need either the Fourier transform $\widetilde{\rho}^+(\omega)$ or the moments $\langle T^{+n} \rangle$. For an LIF driven by Gaussian white noise (needed for DMP+GWN), ISI moments and Fourier-transformed ISI density are known (Siegert, 1951; Darling and Siegert, 1953; Ricciardi and Sacerdote, 1979; Lindner et al., 2002) (summarized in Appendix B.1). For the case of excitatory shot noise input (needed for DMP+SN), we have derived these quantities in the previous chapter.

The ISI distribution is approximated by a weighted average of the distributions of long and short intervals,

$$\rho(T) \approx P_\mathrm{s} \rho^+(T) + P_\mathrm{l} k_- e^{-k_- T}, \tag{5.9}$$

where P_s is the probability that a randomly chosen ISI is a short one, i.e. occurs in a "+" state, and $P_\mathrm{l} = 1 - P_\mathrm{s}$. P_s can be approximated as follows: On average, the time spent in the "+" state is $1/k_+$. The mean duration of a short ISI is $\langle T^+ \rangle$. Thus, there are $1/(\langle T^+ \rangle k_+)$ intervals in an average "+" state. Each "+" state is followed by one long interval. The probability that a given interval is a short one is thus

$$P_\mathrm{s} \approx \frac{\frac{1}{k_+}\frac{1}{\langle T^+ \rangle}}{\frac{1}{k_+}\frac{1}{\langle T^+ \rangle} + 1} = \frac{1}{1 + \langle T^+ \rangle k_+}. \tag{5.10}$$

Expressions for the first two ISI moments are readily calculated using eq. (5.9).

$$\langle T \rangle \approx \frac{k_+ + k_-}{k_-} \frac{1}{\frac{1}{\langle T^+ \rangle} + k_+} \approx \frac{k_+ + k_-}{k_-} \langle T^+ \rangle, \tag{5.11}$$

where in the last step we have used that $k_+ \ll 1/\langle T^+ \rangle$. This means that the firing rate of the neuron is simply approximated by the firing rate of a neuron fixed in the "+" state, weighted by the probability for the DMP to be in the "+" state. For the second moment, one obtains

$$\langle T^2 \rangle \approx \frac{\left\langle T^{+2} \right\rangle + \frac{2k_+}{k_-^2} \langle T^+ \rangle}{1 + k_+ \langle T^+ \rangle} \approx \left\langle T^{+2} \right\rangle + \frac{2k_+}{k_-^2} \langle T^+ \rangle . \tag{5.12}$$

We now turn to the parameter regime where the neuron may also fire during "-" dynamics. In this case, a similar approximation is possible, with the difference that we no longer assume ISIs occurring during "-" state to be exponentially distributed. Instead, we assume that their distribution is well described by $\rho^-(T)$, the ISI density of a neuron where $\eta(t)$ is fixed in the "-" state. The ISI density is approximated by

$$\rho(T) \approx P_\mathrm{s} \rho^+(T) + P_\mathrm{l} \rho^-(T), \tag{5.13}$$

where P_s and $P_\mathrm{l} = 1 - P_\mathrm{s}$ are different from the case treated above; we approximate

$$P_\mathrm{s} \approx \frac{k_- \langle T^- \rangle}{k_+ \langle T^+ \rangle + k_- \langle T^- \rangle}, \tag{5.14}$$

because there are on average $1/(k_- \langle T^- \rangle)$ ISIs in a "-" state.

As in the previous chapter, we restrict ourselves to the first parameter regime for the approximations to power spectrum and susceptibility. Before we turn to those quantities, we conclude this section by briefly illustrating the approximation for firing rate and CV for the pure DMP scenario.

Firing rate and CV of IF neurons driven by purely dichotomous noise

If $f(v) + \sigma_- < 0$ for some $v \in [v_R, v_T]$, then eqs. (5.11, 5.12) apply and rate and CV read

$$r_0 \approx \frac{k_-}{k_+ + k_-} \frac{1}{T_d^+}, \tag{5.15}$$

$$C_V \approx \sqrt{\frac{2k_+}{(k_+ + k_-)^2} \frac{1}{T_d^+}}. \tag{5.16}$$

If, on the other hand, $f(v) + \sigma_- > 0$ for all $v \in [v_R, v_T]$, one has via eq. (5.13)

$$r_0 \approx \frac{k_- \frac{1}{T_d^+} + k_+ \frac{1}{T_d^-}}{k_+ + k_-}, \tag{5.17}$$

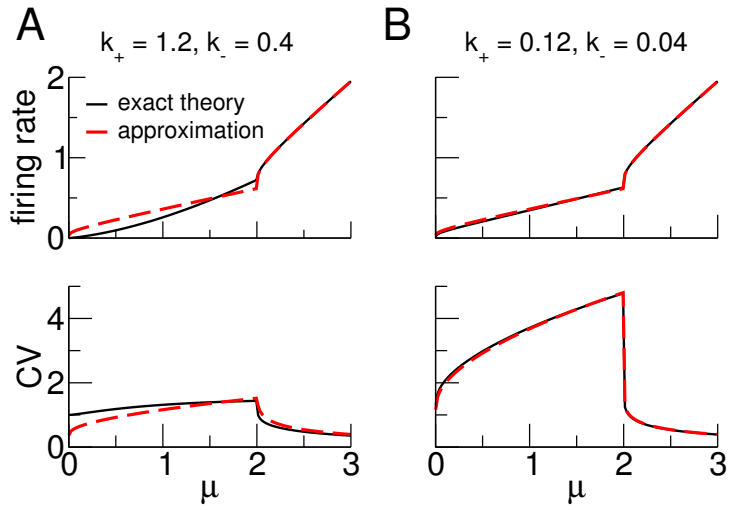

Figure 5.3.: Firing rate and CV of an LIF neuron in the pure DMP scenario for different values of the base current μ at two different pairs of switching rates. Compared are the exact theory (black solid lines) and the quasistatic approximation (red dashed line). Parameter values are $k_+ = 1.2, k_- = 0.4$ (A) and $k_+ = 0.12, k_- = 0.04$ (B). Remaining parameters; $\sigma_+ = 1, \sigma_- = -1, v_R = 0, v_T = 1$, and $\tau_{\text{ref}} = 0$.

$$C_V \approx \sqrt{\frac{k_+ k_-}{(k_+ + k_-)^2} \frac{(T_d^+ - T_d^-)^2}{T_d^+ T_d^-}}. \tag{5.18}$$

Here, T_d^- is the deterministic time from reset to threshold during "-" dynamics.

In Fig. 5.3, we compare the approximations for firing rate and CV to the exact expressions derived in Chapter 3 for two combinations of switching rates. The most prominent feature is the kink at $\mu = 2$. Here, the stable fixed point moves across the threshold and firing becomes possible in the "-" state as well. This leads to an increase in firing rate and, most importantly, to a drastic drop in firing variability. The approximation can be seen to decently capture the qualitative behavior, even if switching rates are rather high. It becomes quantitatively better the higher μ, as with higher base current, ISIs become shorter relative to the noise residence times.

5.2. Approximation for the power spectrum

In the remainder of this chapter, we consider the regime in which the neuron only fires in the "+" state. In this case, its output spike train is a renewal process and the power spectrum is related to the ISI density (see, e.g., Stratonovich (1967)),

$$\begin{aligned} S_{xx}(\omega) &= r_0 \frac{1 - |\widetilde{\rho}(\omega)|^2}{|1 - \widetilde{\rho}(\omega)|^2} \\ &\approx \frac{k_-}{k_+ + k_-} r_0^+ \frac{1 - |P_s \widetilde{\rho}^+(\omega) + P_1 \frac{k_-}{i\omega - k_-}|^2}{|1 - P_s \widetilde{\rho}^+(\omega) + P_1 \frac{k_-}{i\omega - k_-}|^2}, \end{aligned} \tag{5.19}$$

where in the second line, we have used the quasistatic approximation, eq. (5.9). For purely dichotomous input ($\widetilde{\rho}^{+}(\omega) = \exp[i\omega T_d^+]$), the approximation to the power spectrum can be expressed in terms of elementary functions,

$$S_{xx}(\omega) \approx r_0 \frac{1 - P_s^2 - \frac{k_-^2 P_1^2 + 2k_- P_1 P_s \left[k_- \cos(\omega T_d^+) + \omega \sin(\omega T_d^+)\right]}{\omega^2 + k_-^2}}{1 - 2P_s \cos(\omega T_d^+) + P_s^2 + \frac{k_-^2 P_1^2 - 2k_-^2 P_1 + 2k_- P_1 P_s \left[k_- \cos(\omega T_d^+) + \omega \sin(\omega T_d^+)\right]}{\omega^2 + k_-^2}}. \tag{5.20}$$

For high frequencies $\omega \gg 1$, this exhibits the same undamped oscillatory behavior as the exact expression, eq. (3.116) [p. 66],

$$S(\omega \gg 1) \approx \frac{1 - P_s^2}{1 - 2P_s \cos(\omega T_d^+) + P_s^2}. \tag{5.21}$$

The quasistatic approximation assumes that the DMP is slow compared to the mean ISI, i.e.

$$\langle T \rangle \ll \frac{1}{k_+}, \quad \langle T \rangle \ll \frac{1}{k_-}. \tag{5.22}$$

The first inequality means that the mean number of ISIs in a "+" state is supposed to be large. In the following, when discussing results for particular switching rates, we thus always give the mean number of ISIs in a "+" state, calculated as $1/(\langle T \rangle k_+)$. Note that this is of course already an approximation, which, neglecting boundary effects, will in general overestimate the number of ISIs.

In order to assess the quality of the approximation, we plot power spectra for three different values of k_+ (and the three scenarios: DMP, DMP+GWN, and DMP+SN) and compare them to simulations in Fig. 5.4. For $k_+ = 0.8$, the approximation severely overestimates the power spectrum. Such a marked deviation is not surprising, as the assumption of many ISIs per "+" state is far from being met (the mean number of ISIs in a "+" state is roughly 2). For $k_+ = 0.2$, the approximation already yields decent results. This is remarkable, as there are only about 7 ISIs in an average "+" state. For $k_+ = 0.04$ (33 ISIs in a "+" state), the approximation's assumptions are well met and the approximation matches the simulated spectra.

In Fig. 5.4, it is already apparent that additional stochasticity destroys the undamped periodicity in the spectrum. This is further illustrated in Fig. 5.5, where we plot the approximation for the power spectrum for the three scenarios and different noise intensities: purely dichotomous input (red lines, Fig. 5.5A), additional Gaussian white noise (thin blue lines; $D = 5 \times 10^{-4}$ in Fig. 5.5B and $D = 0.05$ in Fig. 5.5C) and inhomogeneous Poisson input (thick green lines; $a = 1.04 \times 10^{-4}$, meaning $D = 5 \times 10^{-4}$ in Fig. 5.5B and $a = 0.010417$, meaning $D = 0.05$ in Fig. 5.5C). It can be seen that already weak additional stochasticity (compared to the intensity of the dominating DMP, $D_{\mathrm{DMP}} = 8.27$ [see eq. (3.12) [p. 41]]) abolishes the undamped periodicity [1]. In contrast, the low-frequency

[1] Note, however, that due to the DMPs long correlation time, comparing noise intensities is probably not

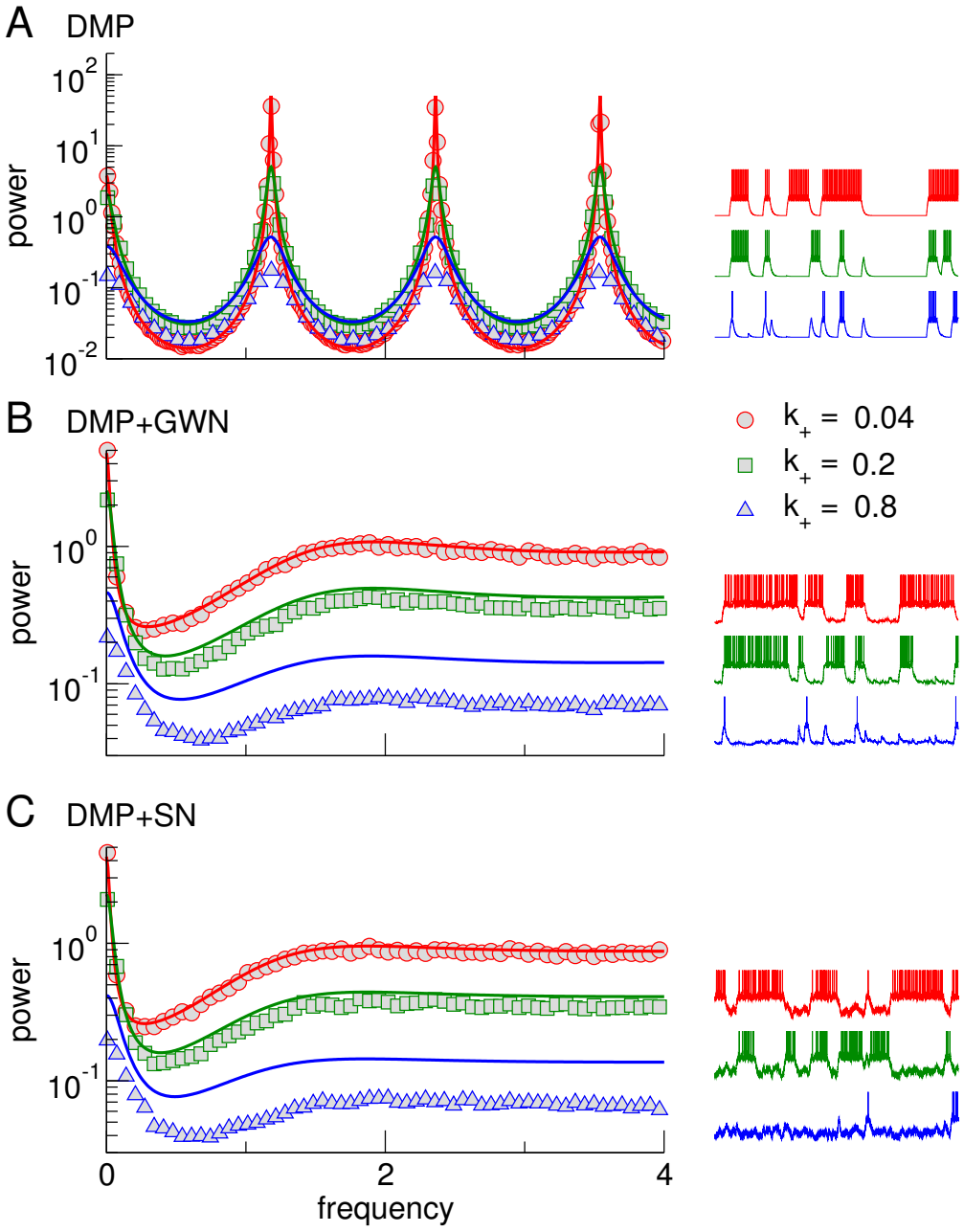

Figure 5.4.: Approximation for the power spectrum at different values of the switching rate k_+ in the three scenarios. We compare the approximation eq. (5.19) (lines) to simulations (symbols). Also shown are exemplary voltage trajectories (spikes added for illustration) at the different switching rates. For $k_+ = 0.04$ (red), the mean number of intervals per "+" state is about 33 (for A, B, and C), for $k_+ = 0.2$ (green), it is 7, and for $k_+ = 0.8$ (blue), it is 2. Remaining parameters are $k_- = 0.1, \mu = -2.9, \sigma_+ = 4.8, \sigma_- = 0.6, v_R = 0, v_T = 1, \tau_{\text{ref}} = 0.1$ (all panels), $D = 0.24$ (B) and $a = 0.05$, meaning $r_{\text{up}} = 96, r_{\text{down}} = 12$ (C).

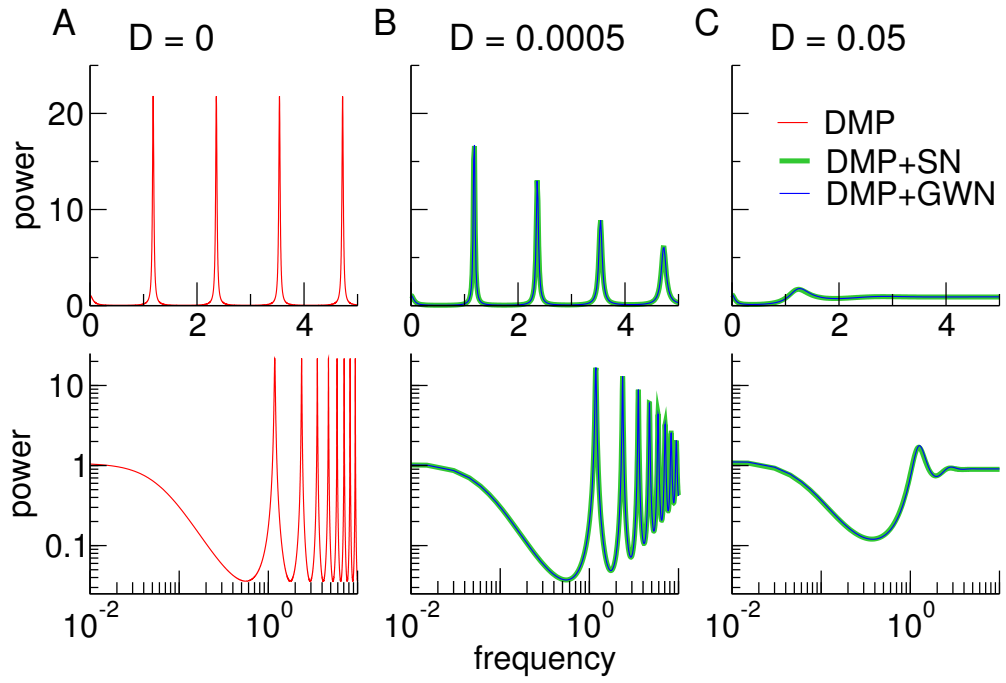

Figure 5.5.: Effect of fast fluctuations on the power spectrum. We show the analytical approximations, eq. (5.19). We compare the pure DMP scenario (A) to the DMP+GWN scenario with $D = 5 \times 10^{-4}$ (B) and $D = 0.05$ (C), as well as the DMP+SN scenario with $a = 1.04 \times 10^{-4}$ ($r_{\text{up}} = 4.61 \times 10^4, r_{\text{down}} = 5760$) (B) and $a = 0.010417$ ($r_{\text{up}} = 460.8, r_{\text{down}} = 57.6$) (C). The second row shows log-log plots of the same curves. Remaining parameters are $k_+ = 0.1, k_- = 0.3, \mu = -2.9, \sigma_+ = 4.8, \sigma_- = 0.6$ and $\tau_{\text{ref}} = 0.1$ (all panels).

behavior remains qualitatively unchanged.

Alternative approximation for the power spectrum

It is instructive to consider a different way to approximate the power spectrum. This approach is based on an approximation for the spike train auto-correlation function,

$$\mathcal{K}_{xx}(\tau) = \langle x(t_0)x(t_0+\tau)\rangle - \langle x(t_0)\rangle^2 . \tag{5.23}$$

Suppose that one wants to estimate this quantity in a numerical simulation for given t_0 and τ. Let us consider how different realizations contribute to the second moment. Realizations in which the DMP is in a "-" state either at time t_0 or at time $t_0 + \tau$ do not contribute, as $x(t_0)x(t_0+\tau)$ can only be zero in this case ($x(t)$ is a train of δ spikes). The contributing realizations thus fall into two categories: Those in which, at $t_0 + \tau$, the DMP is in the same "+" state as at t_0, and those where it is in a different one. Of those realizations that contribute, the fraction that belongs to the first category is given by

$$\Pr\left(\text{same "+" at } t_0+\tau \;\middle|\; \text{"+" at } t_0\right) = e^{-k_+|\tau|} \tag{5.24}$$

particularly insightful.

(the residence times in a DMP are exponentially distributed), while the fraction belonging to the second category is

$$\begin{aligned}
&\Pr\left(\text{different "+" at } t_0+\tau \;\middle|\; \text{"+" at } t_0\right) \\
&= \Pr\left(\text{any "+" at } t_0+\tau \;\middle|\; \text{"+" at } t_0\right) - \Pr\left(\text{same "+" at } t_0+\tau \;\middle|\; \text{"+" at } t_0\right) \\
&= \frac{k_+ e^{-(k_++k_-)|\tau|}+k_-}{k_++k_-} - e^{-k_+|\tau|},
\end{aligned} \tag{5.25}$$

where, in the last line, we have used eq. (3.4) [p. 40].

We now assume that within one "+" state, the spiking statistics are well described by those of a neuron with the DMP fixed in the "+" state. This means that we neglect transients at the "+" state's onset. Under this assumption, the average of $x(t_0)x(t_0+\tau)$ over all the realizations that belong to the first category can be expressed via the spike train auto-correlation function of a neuron fixed in the "+" state,

$$\left\langle x(t_0)x(t_0+\tau)\middle|\text{"+" at } t_0,\ \text{same "+" at } t_0+\tau\right\rangle \approx \mathcal{K}^+_{xx}(\tau)+{r_0^+}^2. \tag{5.26}$$

For realizations belonging to the second category, we assume that spikes in different "+" states are independent – they are, after all, separated by at least one long "-" state of stochastic duration. Thus, their averaged contribution is

$$\left\langle x(t_0)x(t_0+\tau)\middle|\text{"+" at } t_0,\ \text{different "+" at } t_0+\tau\right\rangle \approx {r_0^+}^2. \tag{5.27}$$

Weighting eq. (5.26) and eq. (5.27) by the fractions of realizations that contribute, we obtain

$$\begin{aligned}
\mathcal{K}_{xx}(\tau) &\approx \frac{k_-}{k_++k_-}\left[e^{-k_+\tau}\left(\mathcal{K}^+_{xx}(\tau)+{r_0^+}^2\right)+\left(\frac{k_+e^{-(k_++k_-)|\tau|}+k_-}{k_++k_-}-e^{-k_+|\tau|}\right){r_0^+}^2\right]-r_0^2 \\
&\approx \frac{k_-}{k_++k_-}e^{-k_+|\tau|}\mathcal{K}^+_{xx}(\tau)+\frac{k_+k_-e^{-(k_++k_-)|\tau|}}{(k_++k_-)^2}{r_0^+}^2,
\end{aligned} \tag{5.28}$$

where, in the last line, we have used that $r_0 \approx k_-/(k_++k_-)r_0^+$, where r_0^+ is the firing rate during "+" states. For the power spectrum, this means

$$S_{xx}(\omega) \approx \frac{k_-}{k_++k_-}\left[\frac{1}{\pi}\frac{k_+}{\omega^2+k_+^2} * S^+_{xx}(\omega)\right]+\frac{2k_+k_-}{k_++k_-}\frac{{r_0^+}^2}{\omega^2+(k_++k_-)^2}. \tag{5.29}$$

Eq. (5.29) has an intuitive interpretation: The first additive term is a downscaled convolution of a Lorentzian with the power spectrum of a neuron for which the DMP is fixed in the "+" state. Much like in spectroscopy, where the finite lifetime of an excited state leads to a broadening of spectral lines that has Lorentzian shape, the finite lifetime of the "+" state leads to a similar broadening of peaks in the spike train power spectrum. The downscaling by the probability to find the noise in the "+" state reflects the reduction in overall firing rate. The second additive term accounts for the additional power introduced into the system: it is the power spectrum of a dichotomous process that jumps between the values 0 and r_0^+ (cf. eq. (3.13) [p. 41]).

If the envelope of the correlation function $\mathcal{K}_{xx}^+(\tau)$ decays fast compared to the typical residence time in the "+" state (this can be achieved by making "+" states sufficiently long or by making the noise within the "+" state sufficiently strong), then eq. (5.29) can be replaced by a simpler approximation,

$$S_{xx}(\omega) \approx \frac{k_-}{k_+ + k_-} S_{xx}^+(\omega) + \frac{2k_+k_-}{k_+ + k_-} \frac{{r_0^+}^2}{\omega^2 + (k_+ + k_-)^2}. \tag{5.30}$$

In Fig. 5.6, we compare the three approximations for the shot noise scenario (the case of Gaussian white noise is not qualitatively different). We refer to the eq. (5.19) as the "FPT approximation", to eq. (5.29) as the "convolution approximation" and to eq. (5.30) as the "simple approximation". We compare each approximation to simulations for low noise (A1, B1, C1) and for higher noise (A2, B2, C2). Irrespective of the noise level, the mean number of ISIs per "+" state is roughly 12 for $k_+ = k_- = 0.1$, 3 for $k_+ = k_- = 0.4$, and 2 for $k_+ = k_- = 0.7$.

Both the FPT approximation (Fig. 5.6A) and the convolution approximation (Fig. 5.6B) yield similar results. As expected, they match simulations well for low switching rates, but even for higher switching rates with a rather low number of ISIs per "+" state, they perform decently. For higher switching rates, the convolution approximation yields better results for low frequencies (this is especially apparent for higher noise). As expected, the simple approximation performs worse when the noise is weak and spiking in the "+" state is very regular (Fig. 5.6C1), where it misses the broadening of the peak. For higher noise intensities, differences between the simple approximation (Fig. 5.6C2) and the other two are minor, as discussed above.

5.3. Approximation for the susceptibility

In order to approximate the susceptibility, we use an approach similar to the convolution approximation to the power spectrum. Recall that the inverse Fourier transform of the susceptibility $\chi(\omega)$ is the convolution kernel $K(\tau)$ in the linear response ansatz

$$r(t) = r_0 + \epsilon \int_{-\infty}^{\infty} d\tau\, K(\tau) s(t-\tau). \tag{5.31}$$

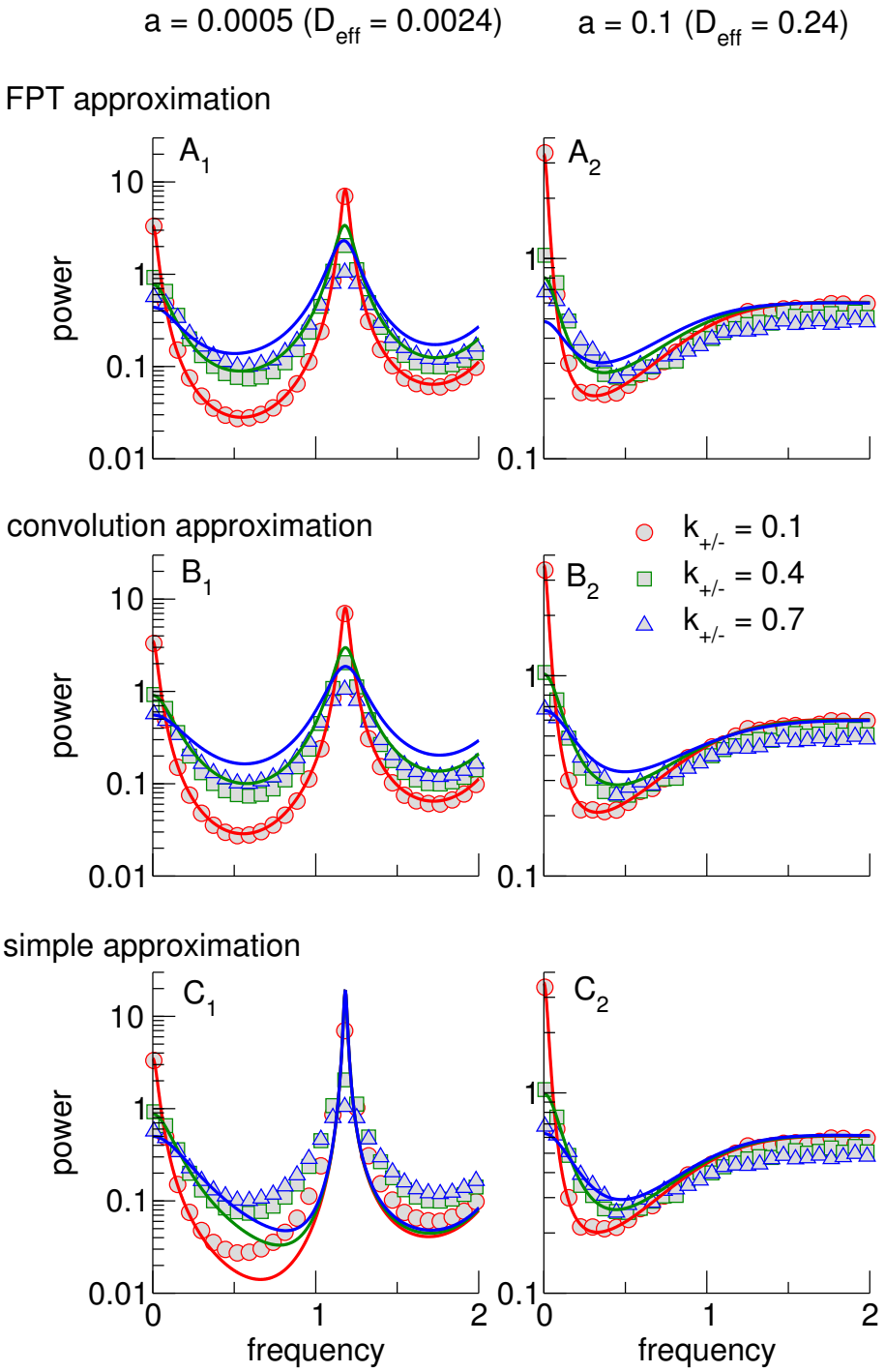

Figure 5.6.: Comparison of the different approximations for the power spectrum at different switching rates of the DMP for the DMP+SN scenario. The FPT approximation (eq. (5.19)); lines in A), convolution approximation (eq. (5.29); lines in B) and the simple approximation (eq. (5.30), lines in C) are compared to simulations (symbols) for two different mean spike weights $a = 5 \times 10^{-4}$ (A1, B1, C1) and $a = 0.1$ (A2, B2, C2), corresponding to two different effective noise intensities. Other parameters as in Fig. 5.5.

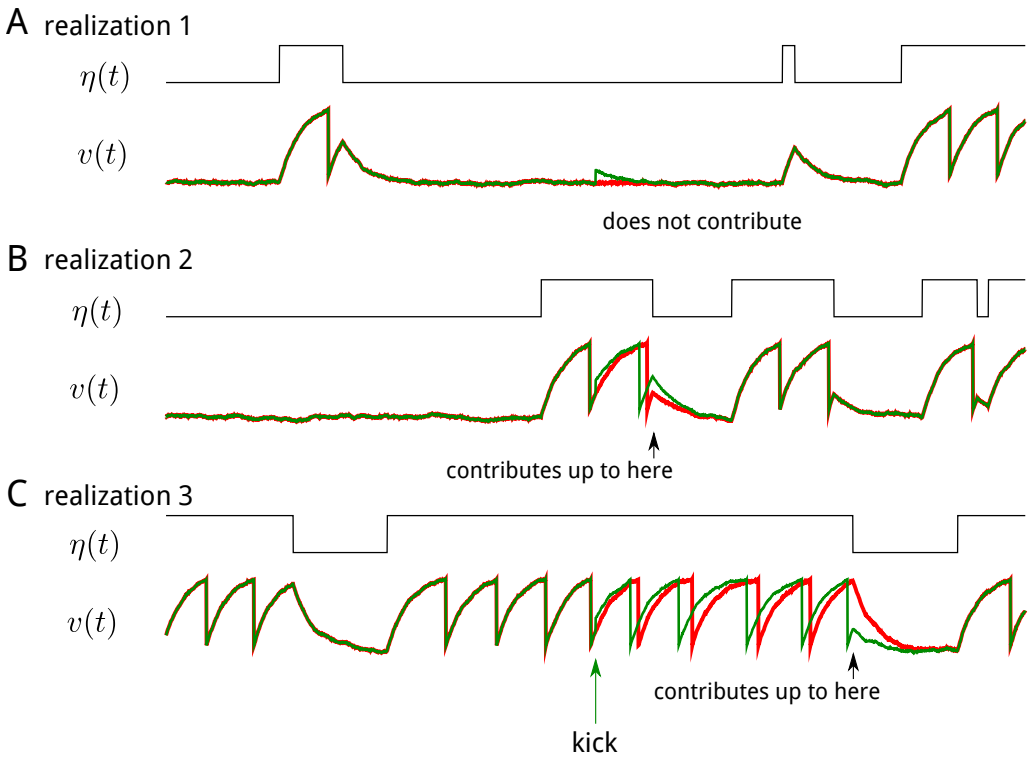

Figure 5.7.: Contribution of individual realizations to the calculation of the impulse response. Red lines are unperturbed trajectories, green lines show the trajectory if a kick to the voltage is delivered at the instant marked by the green arrow (with the same noise realizations). Spiking activity is only influenced if the kick is delivered during a "+" state (realizations 2 and 3) and only as long as the DMP stays in the same "+" state.

One way to measure $K(\tau)$ is to measure the firing rate response to an impulse $s(t) = \delta(t - t_0)$ (which makes the voltage jump by ϵ). Plugging this into eq. (5.31) directly yields

$$r(t) = r_0 + \epsilon K(t - t_0). \tag{5.32}$$

The linear response kernel is thus given by the so-called *impulse response*.

Suppose now that we want to measure the impulse response of an LIF driven by a slow DMP (potentially with additional stochasticity). We discretize the time axis, kick the voltage at a given time t_0, and register for each subsequent time bin whether a spike occurred. We then repeat this for many realizations to estimate the time-dependent firing rate from the binned spike counts. The difference between this time dependent rate and the stationary firing rate yields an estimate of the impulse response.

Consider now how different realizations contribute to the impulse response. In realizations where we deliver the impulse during a "-" state, its effect decays quickly before the next "+" state and it does not affect spiking (see Fig. 5.7A). If the impulse is delivered during a "+" state, it may influence subsequent spiking (Fig. 5.7B and C). The fraction of such realizations is

$$\Pr(\text{"+" at } t_0) = \frac{k_-}{k_+ + k_-}. \tag{5.33}$$

However, once the "+" state ends, the voltage quickly decays and the impulse cannot influence spiking in the next "+" state. The probability that a realization contributes to the impulse response at time $t_0 + \tau$ thus corresponds to the probability that the DMP was in a "+" state at time t_0 and still is in the *same* "+" state at time $t_0 + \tau$,

$$\Pr\Big(\text{"+" at } t_0 \text{ , same "+" at } t_0 + \tau\Big) = \frac{k_-}{k_+ + k_-} e^{-k_+|\tau|}. \tag{5.34}$$

Within a "+" state, we neglect transients and assume that the effect the pulse has on spiking activity is the same as for a neuron where the DMP is fixed in the "+" state ($\eta(t) \equiv \sigma_+$) . Weighting the different contributions, the impulse response can thus be approximated by

$$\begin{aligned} K(\tau) &\approx \Pr\Big(\text{"+" at } t_0 \text{ , same "+" at } t_0 + \tau\Big) K^+(\tau) \\ &= \frac{k_-}{k_+ + k_-} e^{-k_+|\tau|} K^+(\tau), \end{aligned} \tag{5.35}$$

where $K^+(\tau)$ is the impulse response of the system fixed in "+" state. In Fourier space, this product turns into a convolution,

$$\chi(\omega) \approx \frac{k_-}{k_+ + k_-} \left[\frac{1}{\pi} \frac{k_+}{\omega^2 + k_+^2} * \chi^+(\omega) \right], \tag{5.36}$$

where $\chi^+(\omega)$ is the susceptibility of the system fixed in "+" state (eq. (B.4) [p. 147] for the DMP+GWN scenario, eq. (4.33) [p. 90] for the DMP+SN scenario).

If the envelope of the impulse repose $K^+(\tau)$ decays quickly compared to the time the DMP stays in the "+" state, then the weighting by the probability that the DMP is still in the same "+" state at $t_0 + \tau$ can be neglected — for any τ with non-vanishing $K^+(\tau)$, almost all realizations are still in the "+" state anyway. In such a situation, which arises either when k_+ is sufficiently small (long "+" states) or the additional noise is sufficiently large (quickly decaying impulse response), we may thus use the simple approximation

$$\chi(\omega) \approx \frac{k_-}{k_+ + k_-} \chi^+(\omega). \tag{5.37}$$

In Fig. 5.8, we compare these approximations to simulations for different values of k_+. We plot both the convolution approximation eq. (5.36) and the simple approximation eq. (5.37). For $k_+ = 1.3$, the approximations significantly overestimate the magnitude of the susceptibility (due to the low number of roughly 1 ISI per "+" state). For $k_+ = 0.2$ (~ 6 ISIs), the convolution approximation already yields quite good results, while the simple approximation is still far off. For $k_+ = 0.02$ (~ 59 ISIs), both approximations agree well with the simulation results.

To further illustrate the difference between the two approximations, we zoom onto the

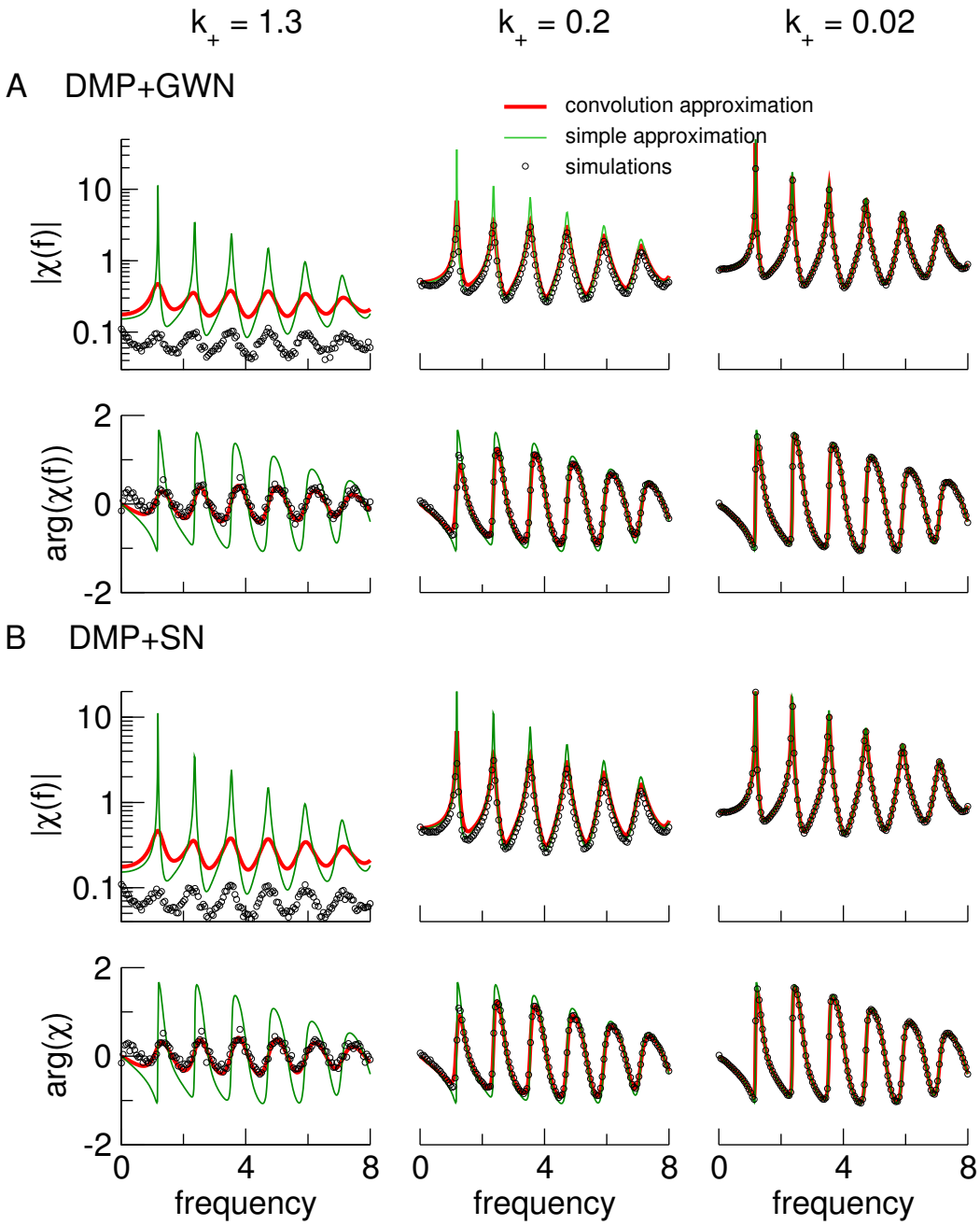

Figure 5.8.: Approximations for the susceptibility compared to simulations for various values of k_+ in both scenarios of additional stochasticity. Circles correspond to simulation results (stimulation with a sinusoidal stimulus), thick red lines to the convolution approximation eq. (5.36) and thin green lines to the simple approximation eq. (5.37). A: DMP+GWN scenario ($D = 6 \times 10^{-4}$). B: DMP+SN scenario ($a = 1.25 \times 10^{-4}$ [$r_{\text{up}} = 3.84 \times 10^4$, $r_{\text{down}} = 4800$]). For $k_+ = 1.3$, a "+" state contains an average of roughly 1 ISI, for $k_+ = 0.2$, the average is 6 ISIs and for $k_+ = 0.02$, the average is 59 ISIs. Remaining parameters are $k_- = 0.3, \mu = -2.9, \sigma_+ = 4.8, \sigma_- = 0.6, v_R = 0, v_T = 1, \tau_{\text{ref}} = 0.1$ (all panels).

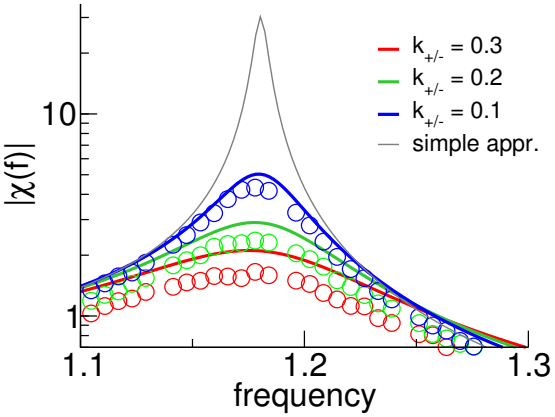

Figure 5.9.: Zoom into the first peak of the susceptibility for the shot-noise scenario for three different combinations of k_+/k_- (other parameters as in Fig. 5.8). The simple approximation (grey line) is compared to the convolution approximation (red, green and blue lines).

first peak in the susceptibility for the DMP+SN scenario in Fig. 5.9. Here, we compare different combinations of k_+ and k_-. While the simple approximation eq. (5.37) is independent of the switching rates as long as their ratio stays constant, the convolution approximation captures the flattening of the peaks with increasing switching rates.

5.4. Summary

In this chapter, we have derived approximations for two-state input with additional stochasticity. These approximations are valid for long correlation times. Specifically, we have considered a dichotomous noise with additional weak Gaussian white noise, and inhomogeneous Poissonian shot noise with a time-dependent rate given by a dichotomous noise. For these cases, we have derived expressions for the stationary firing rate and the CV, as well as for the power spectrum and the susceptibility with respect to a current modulation. For both spectral quantities, we have derived expressions in the form of a convolution of the respective quantities for a neuron fixed in the "+" state by a Lorentzian, as well as simpler multiplicative expressions that become valid for longer residence times.

We have critically compared the approximations in all scenarios to simulations for different switching rates of the DMP. While we have assumed in the derivation of the expressions that the number of ISIs in a "+" state is large on average, we find that the approximations yield decent results already for small number of around 5 ISIs per "+" state.

The expressions for inhomogeneous Poisson input with a two state rate will form the basis for the analytical approach to signal transmission in the presence of up-down states, which is carried out in the following chapter.

Chapter 6.

Signal transmission in the presence of up/down states

How a cortical neuron transmits information about a sensory signal depends heavily on background activity. This background consists of the spiking activity of the (typically thousands of) cells that make synaptic connections to the neuron in question but do not encode the signal. Depending on cortical state, the background input may occur at a rate that is (approximately) constant in time, or it may exhibit a temporal structure.

Input spikes occur at a constant rate if the presynaptic network is in a so-called *asynchronous-irregular* (AI) regime (Brunel, 2000). Here, irregular refers to the activity of individual cells, which are assumed to fire approximately Poisson-like, and asynchronous refers to the cross-correlation between cells, which is assumed to vanish. In this scenario, analytical approaches to information transmission are well established. Usually, they rely on the diffusion approximation: the superposition of many presynaptic spikes arriving in a short time-window is often modeled as a white Gaussian process.

AI regimes are typically associated with attentive wakefulness. A drastically different network state can observed under anesthesia, during slow-wave sleep, or in quiet wakefulness: In this regime, network activity jumps abruptly between an active state (the *up state*), in which firing rates are comparable to those in the AI regime or higher, and a quiescent state (the *down state*), in which neurons fire at low rates or not at all (Steriade et al., 2001). Compared to the transitions between up and down states, which take place on a timescale of hundreds of milliseconds, the network state changes on a much slower time scale; in the present chapter, we assume it to be static.

While traditionally, the occurrence of up-down states has been strongly linked to anesthesia or slow-wave sleep, more and more evidence is accumulating that they also occur during quiet wakefulness, e.g. when an animal is passively perceiving a stimulus (Petersen et al., 2003; Zagha et al., 2013; Luczak et al., 2013). For this reason, a growing number of experimental studies have studied how the response to a sensory stimulus depends on the network background (Arieli et al., 1996; Petersen et al., 2003; Sachdev et al., 2004; Goard and Dan, 2009; Marguet and Harris, 2011; Luczak et al., 2013; Zagha et al., 2013). Reported effects vary across studies; it has been reported that a stimulus is less (Petersen et al., 2003; Sachdev et al., 2004) or more (Shu et al., 2003) likely to evoke spikes in an up state than in a down state, that information transmission is worse with an UD than an AI background (Goard and Dan, 2009; Marguet and Harris, 2011; Zagha et al., 2013), and it has been hypothesized that up states gate sensory input (Luczak et al., 2013).

Theoretical works have mostly been concerned with modeling the mechanism that

generates up/down transitions (Destexhe, 2009; Millman et al., 2010; Mejias et al., 2010; Holcman and Tsodyks, 2006); models for the response to a stimulus with an UD background are rare (Curto et al., 2009). We are not aware of previous analytical approaches to signal transmission with an UD background.

Recently, Vyazovskiy and Harris (2013) have hypothesized on a functional role of up-down transitions: They suggest that a major role of sleep is to allow cellular maintenance, such as the degradation or repair of damaged proteins and the replenishment of synaptic vesicles, to occur. These processes, according to the authors, necessitate a reduction in the overall presynaptic firing rate in the form of down states. While an individual down state is too short to complete restorative processes, they argue that "brief pauses [...] reduce cellular energy consumption and synaptic activity sufficiently to allow [...] processes that occur over a much longer timescale".

The idea that down states enable cellular maintenance through an overall decrease in input firing rate does, however, beg the following question: Why should a lower firing rate be attained by introducing pauses – the down states – instead of moving the system into another asynchronous-irregular state with a lower firing rate? One possible answer is that below a certain firing rate, asynchronous-irregular activity can no longer be sustained, leading to short-lived periods of network activity interspersed with pauses. In this case, the occurrence of up and down states would simply be a consequence of network dynamics, rather than of functional relevance. In this chapter, by contrast, we hypothesize on a different answer: When the overall input firing rate is low, a network background that undergoes transitions between up and down states may be advantageous to information transmission.

We study a neuron that receives a weak signal while it is subject to input from a background population. The signal can be thought of as a sensory input (from the thalamus or lower cortical areas; *bottom-up* input), the background as input from higher cortical areas (top-down input). We ask how the transmission of the signal depends on the network state of the background population, as quantified by the coherence and the mutual information rate. After detailing this setup in Sec. 6.1, we introduce two main effects of an UD background in Sec. 6.2: Such a background can lead to a band-pass filtering of information, and it can be advantageous to information transmission when the mean input rate is low. We explore these two effects in detail in Sec. 6.3 and Sec. 6.4. Finally, we discuss in Sec. 6.5 the question whether such a beneficial effect could also occur at a fixed output firing rate.

6.1. Setup

The setup we consider is sketched in Fig. 6.1A. We consider a LIF neuron, with voltage dynamics given by

$$\tau_{\mathrm{m}}\dot{v} = \mu - v + \epsilon s(t) + \tau_{\mathrm{m}} \sum_{i=0}^{N} a_i X_{\mathrm{in},i}(t), \tag{6.1}$$

with the usual fire-and-reset rule: if $v = v_T$, it is reset to v_R and dynamics continue after an absolute refractory period τ_{ref}. Here, $\epsilon s(t)$ is the weak signal, which we model as

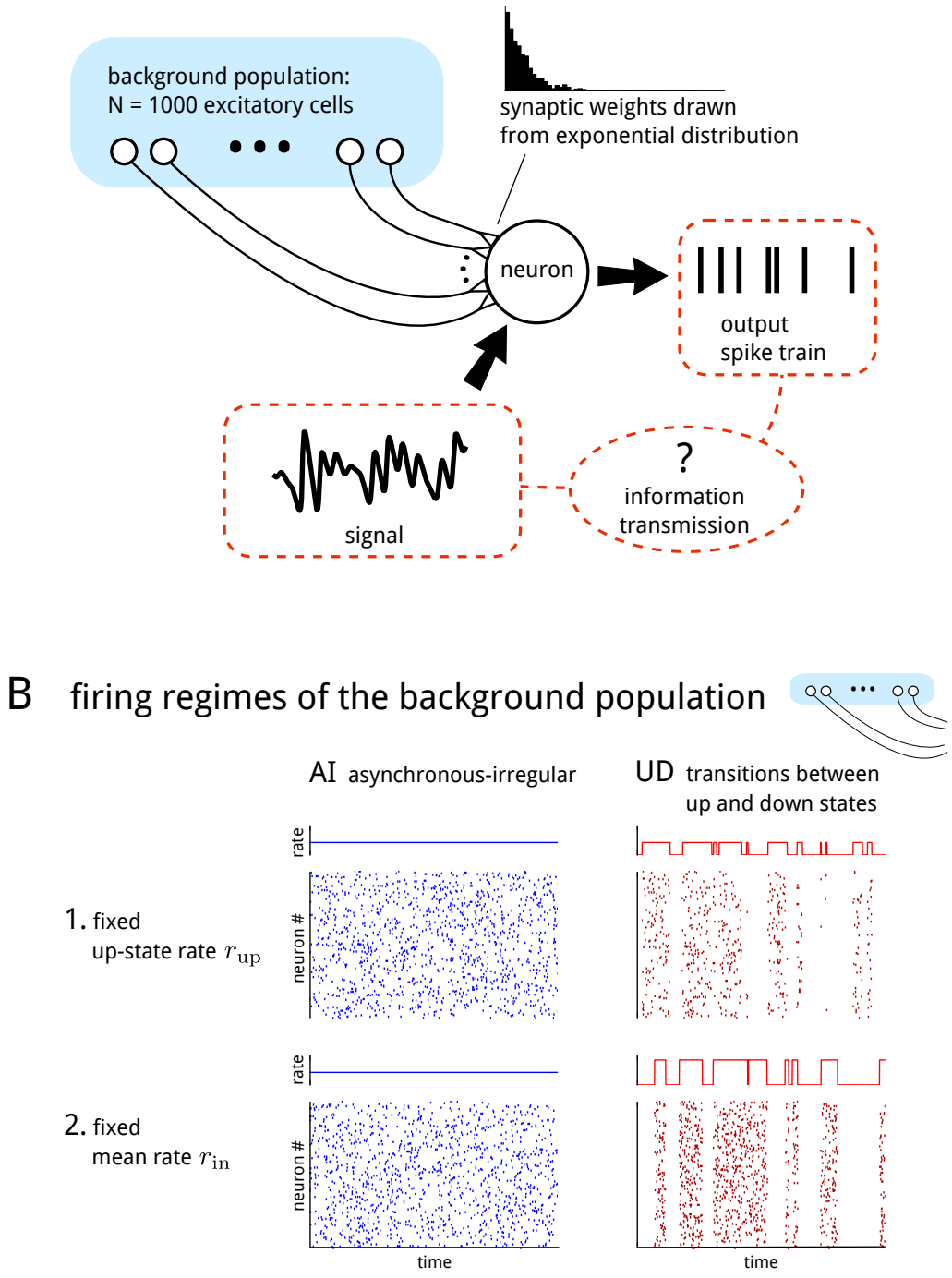

Figure 6.1.: A: **Sketch of the setup we consider.** A neuron receives a sensory signal, as well as input from a background population, connected via synapses with exponentially distributed weights. We ask how the transmission of information about the signal is affected by the network state of the background population. B: **We contrast two firing regimes of the background population:** asynchronous-irregular firing (AI) and transitions between up and down states (UD). We compare these regimes when the rate in the up state is held constant (B1) and when the mean firing rate is held constant (B2).

Parameter	Value	Description
N	1000	number of presynaptic neurons
a	0.05	mean synaptic weight
τ_{m}	0.01 s	membrane time constant
μ	0	base current
v_R	0	reset voltage
v_T	1	threshold voltage
τ_{ref}	0.001 s	refractory period
f_0	0 Hz	lower signal cutoff
f_c	1000 Hz	upper signal cutoff
ϵ	0.4	signal amplitude
k_+	10 Hz	rate of leaving the up state
k_-	10 Hz	rate of leaving the down state

Table 6.1.: Parameters used in this chapter and their values, where nothing else is indicated.

band-limited Gaussian white noise with variance ϵ^2 and power between f_0 and f_c. The sum runs over all N neurons in the background population; a_i is the weight of the ith synapse, and

$$X_{\mathrm{in},i}(t) = \sum_j \delta(t - t^*_{i,j}) \tag{6.2}$$

the spike train of the ith background neuron, where $\{t^*_{i,j}\}$ is the respective set of spike times. The weights for each synapse are drawn from an exponential distribution with mean a once when the network is set up.

The background population consists of neurons that fire as inhomogeneous Poisson processes with a common rate, $\langle X_{\mathrm{in},i}(t)\rangle = R(t)$. We consider two firing regimes: The background population is either in an asynchronous-irregular state (AI), in which the firing rate is constant,

$$R(t) = r_{\mathrm{in}}, \tag{6.3}$$

or it switches between up states and quiescent down states (UD) (see Fig. 6.1B). In this case, we model the firing rate as a dichotomous Markov process (DMP) that jumps between r_{up} and 0 with the constant rates k_+ (rate of leaving the up state) and k_- (rate of leaving the down state).

The model parameters and their default values are summarized in Table 6.1.

In the following, we contrast the two regimes for two choices of baseline firing rates (see Fig. 6.1B): We either set $r_{\mathrm{up}} = r_{\mathrm{in}}$, i.e. the firing rate during an up state equals that during the AI state, or we choose r_{up} such that the mean firing rates in both regimes are equal. The first choice can be thought of as introducing pauses in the AI activity, the second one as keeping the number of spikes fixed but redistributing them to form up states.

We use the analytical expressions developed in the two previous chapters: For the AI case, we use the theory for excitatory (homogeneous) Poissonian shot noise derived in Chapter 4, while for the UD case, we use the approximation for shot noise with a two-state firing rate developed in Chapter 5. Note that the spike weights in both cases were

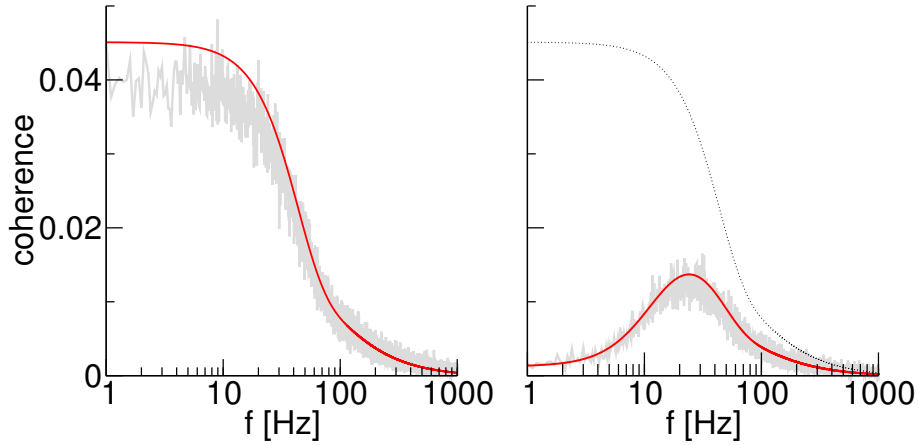

Figure 6.2.: Coherence curves for AI background (left) and UD background (right). Simulations (grey lines) are compared to the approximation eq. (6.4) (red lines). The coherence with AI background is also plotted in the right panel for easier comparison (dotted line). Parameters are $r_{\mathrm{up}} = 2.5\,\mathrm{Hz}$ for both panels, $k_+ = 10\,\mathrm{Hz}, k_- = 10\,\mathrm{Hz}$ for the right panel.

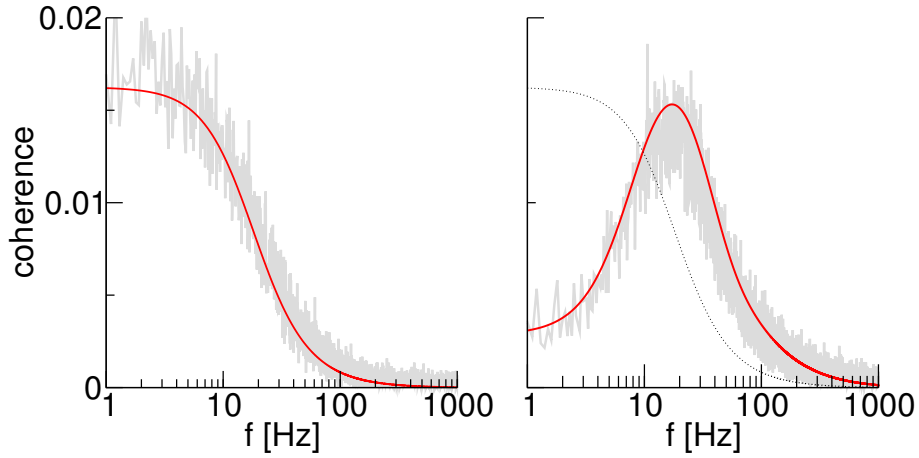

Figure 6.3.: Coherence curves for AI background (left) and UD background (right), both with the same mean input rate $r_{\mathrm{in}} = 1\,\mathrm{Hz}$ (this corresponds to an up-state-rate $r_{\mathrm{up}} = 2\,\mathrm{Hz}$ in the right panel). All other parameters as in Fig. 6.2.

assumed to be drawn from an exponential distribution for each incoming spike, while here, each synaptic weight is chosen only once; all spikes from a particular presynaptic neuron are then endowed with the same weight. Thus, we expect even the expressions for the AI case to be only an approximation (that becomes better the larger the number of presynaptic neurons).

6.2. Main observations

As a measure for the system's information transmission properties, we use the coherence between the signal and the output spike train. Using the approximations developed in the previous chapter, eq. (5.29) [p. 109] and eq. (5.36) [p. 113], an analytical expression

for the coherence in the UD regime is

$$\begin{aligned} C_{sx}(f) &= \frac{|S_{sx}(f)|^2}{S_{xx}(f)S_{ss}(f)} \\ &\approx \frac{k_-}{k_+ + k_-} \frac{\left| \frac{2k_+}{(2\pi f)^2 + k_+^2} * \chi^+(f) \right|^2}{\left(\frac{2k_+}{(2\pi f)^2 + k_+^2} * S_{xx}^+(f) \right) + \frac{2k_+ r_0^{+2}}{(2\pi f)^2 + (k_+ + k_-)^2}} S_{ss}(f), \end{aligned} \tag{6.4}$$

here, $\chi^+(f)$, $S_{xx}^+(f)$ and r_0^+ are the susceptibility, power spectrum, and firing rate during up states, which equal the respective quantities for the AI case.

In Fig. 6.2, we plot the coherence for an AI network background (A) and for a background that switches between up and down states (B); we choose the up state firing rate in the UD case to equal the firing rate in the AI case, $r_{\text{up}} = r_{\text{in}}$. First of all, we find that simulation results are well described by the approximation eq. (6.4). For an asynchronous-irregular background, the coherence is low-pass, as known for IF neuron models driven by Gaussian white noise (e.g. Vilela and Lindner (2009)) and as observed in Chapter 4. When the background activity is interrupted by down states, in contrast, the coherence curves are qualitatively different; they now exhibit a peak. In this case, the system (i.e. the neuron along with its top-down input) constitutes a band-pass filter for information.

The occurrence of a peak in the coherence does not come unexpected. It is plausible that signal transmission is hampered at low frequencies, because the spontaneous transitions between up and down states dominate the time dependence of the cell's firing rate on a slow timescale. In other words: The dichotomous process underlying the up/down input has power at low frequencies, which leads to a decreased signal-to-noise ratio in this range.

In Fig. 6.2, the coherence with an UD background is, for all frequencies, smaller than the coherence with an AI background. This is not surprising; it is, however due to a somewhat unfair comparison: with an UD background for which $r_{\text{up}} = r_{\text{in}}$, the time-averaged input to the neuron is significantly smaller than r_{in}. Recall that one motivating question we asked above was why introducing pauses – down states – should be a preferable way of attaining a lower overall input firing rate, rather than realizing *the same* input firing rate with an AI background. To address this question, one should thus compare the two cases for the same total input rate. One way to think about this is to start from the UD case and redistribute the spikes uniformly across the time axis. This conserves the total number of input spikes, but the resulting firing rate is lower than the firing rate *within* an up state,

$$r_{\text{in}} = \frac{k_-}{k_+ + k_-} r_{\text{up}}. \tag{6.5}$$

In Fig. 6.3, we compare the coherence curves again, this time with the same total input rate. Remarkably, the coherence with an UD background is now higher than with an AI background over a wide range of frequencies (note the log scale).

The rather surprising finding that an UD background can be advantageous to information transmission is reminiscent of stochastic resonance (SR) – after all, introducing up/down states amounts to introducing an additional noise source (in our model the DMP). Indeed, as for SR, the beneficial effect of an UD background can again be linked to an increase in firing rate: At a low overall input rate, the neuron hardly fires at all with an AI background (and consequently cannot transmit much information about the signal). In such a situation, grouping the few input spikes into up states may allow the threshold to be crossed an lead to a significantly higher output firing rate.

In the remainder of this chapter, we aim at a better understanding of the two effects described above, specifically their dependence on parameters. We first take a closer look at the band-pass behavior in Sec. 6.3. There, we do not adjust r_{up} to keep the overall input constant when we vary parameters; our goal is to first understand the direct effect these parameters have on the band-pass-nature of the coherence. In Sec. 6.4, we explore the beneficial effect that an UD background may have on signal transmission when the total input rate is low. To quantify this effect, we use the lower bound for the mutual information rate. Here, we also discuss the relation of the effect to stochastic resonance.

6.3. Band-pass nature of the coherence

To better understand how the shape of the coherence depends on parameters, it is useful to simplify eq. (6.4) even more by using the "simple" approximations for the susceptibility and power spectrum (eq. (5.30) [p. 110], eq. (5.37) [p. 113]). As we have argued in the previous chapter, they become valid if up states are sufficiently long (compared to an ISI) or if spiking is sufficiently irregular. Using these approximations allows us to get rid of the convolutions in eq. (6.4) and to express the coherence in terms of the the AI coherence $C_{sx}^{+}(f)$,

$$\begin{aligned} C_{sx}(f) &\approx \frac{k_-}{k_+ + k_-} \cdot \frac{\left|\chi^+(f)\right|^2}{S_{xx}^+(f) + \frac{2k_+ {r_0^+}^2}{(2\pi f)^2 + (k_+ + k_-)^2}} S_{ss}(f) \\ &= \frac{k_-}{k_+ + k_-} \cdot \frac{1}{1 + \frac{1}{S_{xx}^+(f)} \frac{2k_+ {r_0^+}^2}{(2\pi f)^2 + (k_+ + k_-)^2}} \cdot C_{sx}^+(f). \end{aligned} \tag{6.6}$$

The first term in eq. (6.6) shows that an UD background leads to a frequency-independent down-scaling of the coherence. This down-scaling only depends on the ratio of switching rates and not their absolute values; it reflects the fact that the neuron can now only transmit information a fraction of the time.

The frequency-dependent down-scaling that is responsible for the appearance of a peak is described by the second term, a multiplication of the (low-pass) AI coherence

with

$$\lambda(f) := \frac{1}{1 + \frac{1}{S^+_{xx}(f)} \frac{2k_+ {r_0^+}^2}{(2\pi f)^2 + (k_+ + k_-)^2}}. \tag{6.7}$$

The function $\lambda(f)$ is monotonically increasing and tends to 1 as $f \to \infty$.

As a quantitative measure for the band-pass effect, we use the *quality factor* (Erchova et al., 2004) [1],

$$Q := \frac{\max(C_{sx}(f))}{C_{sx}(0)}. \tag{6.8}$$

For a low-pass coherence, this measure equals 1 (the maximum is at zero frequency); higher values are indicative of a band-pass.

We note that Q is related to the separation factor Γ introduced in Chapter 2, eq. (2.38) [p. 31] when the coherence is high-pass; the two measures then differ by one, $Q = \Gamma + 1$. For a low-pass coherence, however, $Q = 1$ while Γ quantifies how pronounced the low pass is.

Exploiting that the AI coherence $C^+(f)$ is low-pass, eq. (6.6) allows us to calculate an upper bound for the quality factor (within the validity of the approximation),

$$\begin{aligned} Q \leq \lambda(\infty)/\lambda(0) &= 1 + \frac{1}{S^+_{xx}(0)} \frac{2k_+ {r_0^+}^2}{(k_+ + k_-)^2} \\ &= 1 + \frac{1}{{C_V^+}^2} \frac{2k_+ r_0^+}{(k_+ + k_-)^2}, \end{aligned} \tag{6.9}$$

where, in the last line, we have used that $S^+_{xx}(0) = r_0^+ {C_V^+}^2$ (because we are dealing with a renewal spike train).

In Fig. 6.4, we plot the coherence for the UD background at various values of k_+, the rate of leaving the up state (solid lines). For comparison, we also show the coherence for the AI case (dotted line). In the inset, we plot the quality factor Q over k_+ (solid line; circles mark values of k_+ for which coherence lines are shown) as well as the upper bound, eq. (6.9), (dashed line). With increasing k_+, we observe a drop in overall coherence. At first, this goes along with an increase in quality – the coherence curves become more peaked. However, the quality is not monotonously increasing with k_+; at larger values, it decreases again and coherence curves eventually again approach a low pass.

The drop in coherence with increasing k_+ is plausible: For higher k_+, down states become more frequent and the fraction of time in which information can be transmitted decreases. Mathematically, this is reflected in the decreasing prefactor in eq. (6.6).

[1] Note that this is not what is usually understood as a quality factor in the physics literature but a much simpler measure; it does not take the width of the peak into account and does not distinguish between a band- and a high-pass.

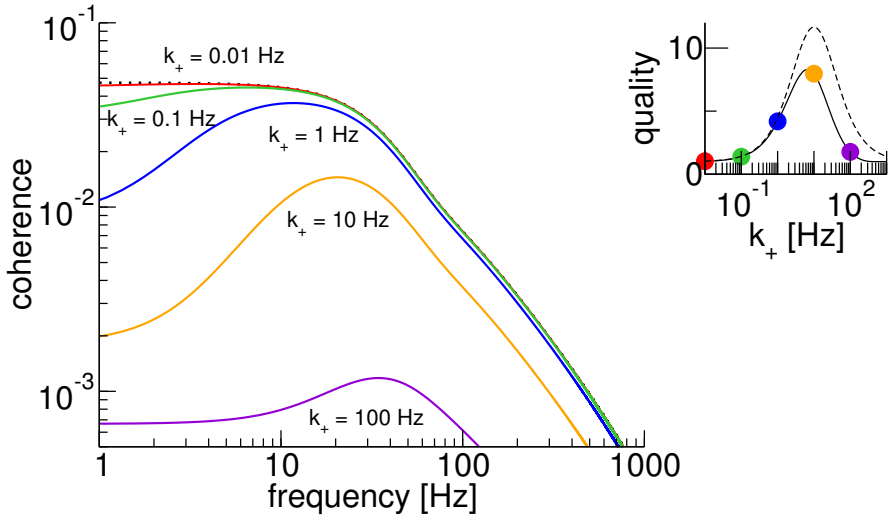

Figure 6.4.: Coherence (theory) with an UD background for various values of k_+ (eq. (6.4), solid colored lines). For comparison, we also show the AI coherence (dotted line). In the inset, we plot the quality factor over k_+; the k_+ values corresponding to the coherence curves in the main plot are marked by circles. The dashed line here marks the upper bound for Q, eq. (6.9). Remaining parameters: $k_- = 10\,\mathrm{Hz}, r_{\mathrm{up}} = 2.2\,\mathrm{Hz}, \mu = 0, a = 0.05, \tau_m = 0.01\,\mathrm{s}, v_R = 0, v_T = 1, \epsilon = 0.4, f_c = 1000\,\mathrm{Hz}$.

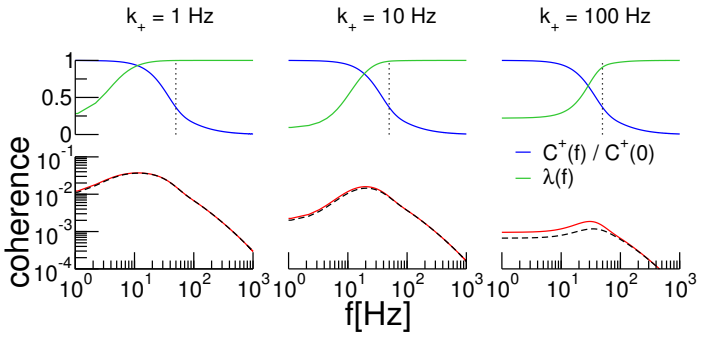

Figure 6.5.: Coherence curves for different values of k_+ (bottom row). Solid red lines correspond to convolution approximation eq. (6.4), dashed lines to the simple approximation eq. (6.6). Above, we plot $\lambda(f)$ and $C^+_{sx}(f)/C^+_{sx}(0)$. The dotted line marks r^+_0, the firing rate in the up state. Remaining parameters as in Fig. 6.4.

To understand how the shape of the coherence depends on k_+, it is instructive to look first at the upper bound for the quality factor, eq. (6.9): For $k_+ = 0$, the quality cannot be greater than 1, corresponding to a low-pass coherence. The same is true for the limit $k_+ \to \infty$, where the quadratic term dominates. [2] However, for finite k_+, the upper bound

[2] One should be cautious not to over-interpret the limit of very large k_+ for two reasons: First, for large k_+, eq. (6.4) can no longer be trusted to be a good approximation to the system's coherence, and second, a vanishingly small coherence can not be resolved in simulations (much less experimentally), so that question about its low- or band-pass nature are moot.

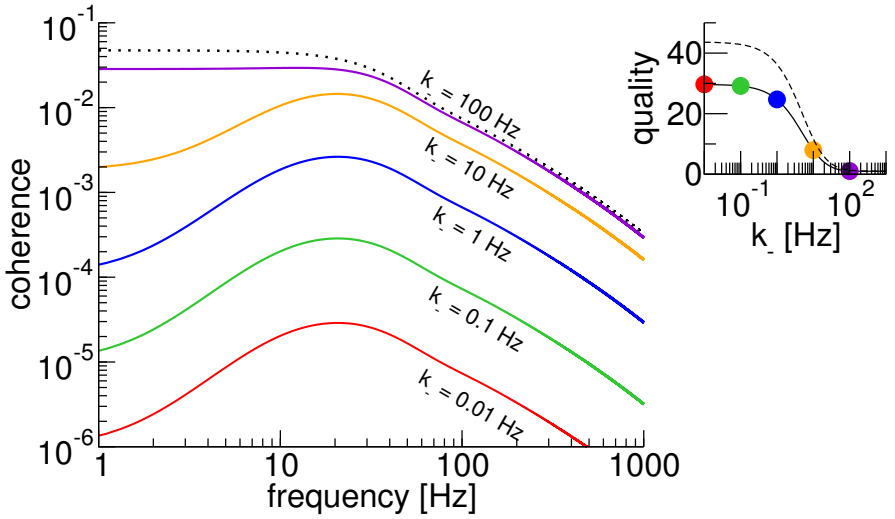

Figure 6.6.: Coherence curves for different values of k_- (eq. (6.4), solid colored lines). $k_+ = 10\,\mathrm{Hz}$, remaining parameters like in Fig. 6.4.

for the quality factor is larger than one, attaining its maximum,

$$1 + \frac{r_0^+}{2C_V^{+2}k_-}, \tag{6.10}$$

at symmetric switching rates, $k_+ = k_-$. The actual maximal quality factor is lower than this upper bound, and is attained at smaller k_+. The reason for this is illustrated in Fig. 6.5, where we plot coherence curves for three values of k_+. Also shown are $\lambda(f)$ and the AI coherence $C^+(f)/C^+(0)$ (normalized for the purpose of illustration), as the product of these two functions determines the shape of the UD coherence. As k_+ is increased, the inflection point of $\lambda(f)$ moves to higher frequencies. Because $C_{sx}^+(f)$ itself falls off at higher frequencies (a rough cut-off is given by the up state firing rate), increasing k_+ leads to a coherence with a flatter peak.

Despite the above considerations, the upper bound is still useful to make qualitative statements about the peakedness of the coherence: From eq. (6.10), for instance, one can conclude that the band-pass effect becomes more pronounced the larger the rate and regularity of up state firing and the longer the duration of down states.

Figure 6.6 again shows the coherence, this time for varying k_-. We observe that the overall coherence increases for increasing k_-, as more time spent in up states allows more information to be transmitted. Interestingly, the shape of the coherence is independent of k_- as long as the latter is small. This is reflected in the quality factor (inset of Fig. 6.6), which exhibits a plateau at small k_-. As k_- is increased, the quality eventually decreases as coherences get closer to the (low-pass) AI case. Note that even when $k_- \to \infty$, the analytical approximation for the UD coherence never converges exactly to the AI coherence, as one would expect. This is because the assumption of small k_- (compared to the up state firing rate) is grossly violated in this limit. Turning again to the upper bound for the quality factor, one finds that its maximum is attained at $k_- = 0$.

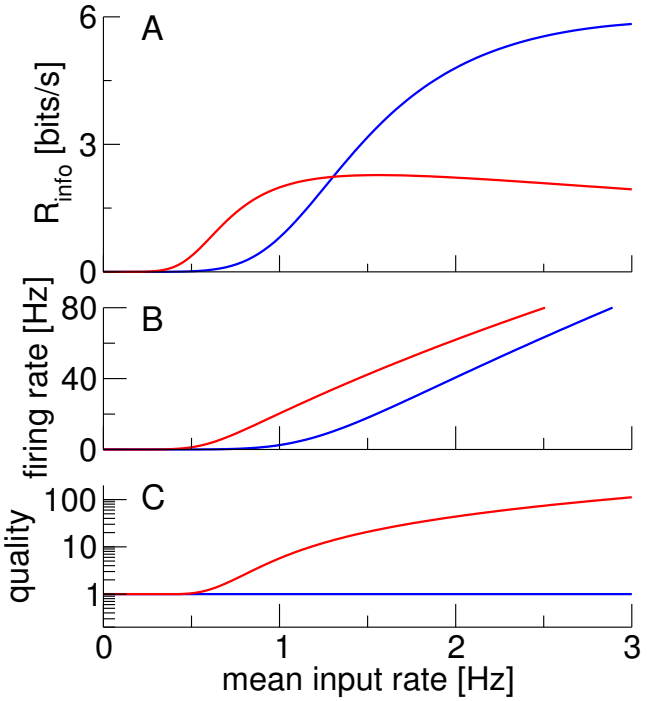

Figure 6.7.: Mutual information rate (lower bound, theory) between signal and output spike train as a function of the mean input. With an UD background (red line), more information can be transmitted than with an AI background (blue line) at low mean input rates (A). This is because with UD input, the same mean input rate yields a higher output firing rate (B). Higher mean input leads to a higher quality factor (i.e. a more pronounced band-pass coherence) in the UD case (C). Parameters: $k_+ = 10\,\mathrm{Hz}, k_- = 10\,\mathrm{Hz}$.

6.4. Effect of an up-down background on the mutual information rate

In order to quantify the effect of an UD background on information transmission, we compare in Fig. 6.7A the mutual information rate between signal and output spike train for AI and UD input. The two scenarios are compared at the same mean input rate, i.e. we set

$$r_{\mathrm{up}} = \frac{k_+ + k_-}{k_-} r_{\mathrm{in}}. \tag{6.11}$$

For high input rates, the mutual information rates are much higher with an AI background compared to those with an UD background. The situation is drastically different for low mean input. Here, an UD background allows information to be transmitted at input rates for which the mutual information rate with an AI background has, for all practical purposes, gone to zero. As shown in Fig. 6.7B, this goes along with a firing rate that is higher for the UD case. At low mean input, the neuron hardly fires at all in the AI case, while spikes arriving concentrated in up states still elicit a significant firing rate. In Fig. 6.7C, we plot the quality factor of the coherence. While the AI background is always low pass, the UD background leads to a band-pass effect. The quality increases

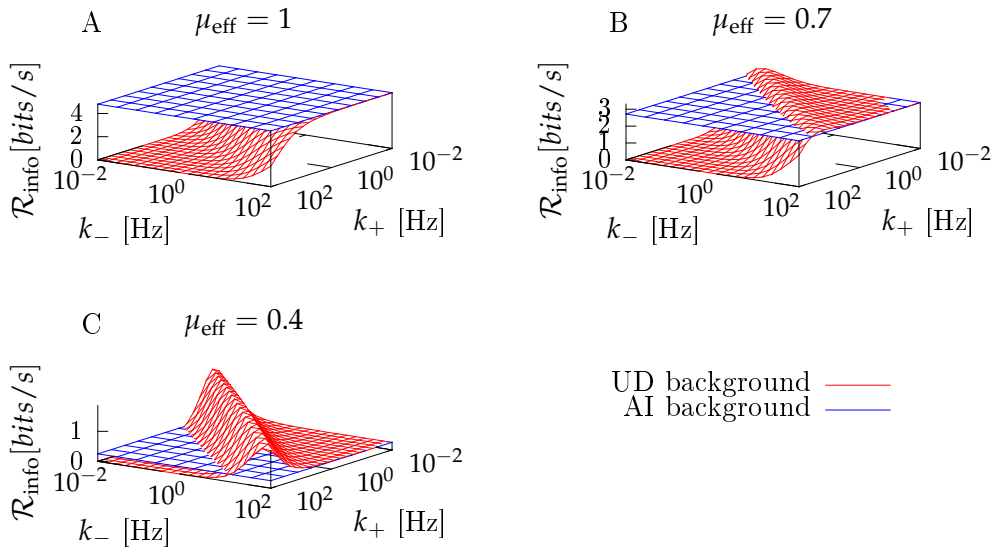

Figure 6.8.: Mutual information rate (lower bound, theory) between signal and output spike train with an UD background as a function of the switching rates k_+ and k_-, compared to the AI case at the same mean input rate. Different panels correspond to different mean inputs (A: $\mu_{\text{eff}} = 1$, corresponding to $r_{\text{in}} = 2\,\text{Hz}$; B: $\mu_{\text{eff}} = 0.7$, corresponding to $r_{\text{in}} = 1.4\,\text{Hz}$; C: $\mu_{\text{eff}} = 0.4$, corresponding to $r_{\text{in}} = 0.8\,\text{Hz}$).

with the mean input rate; this is in line with the results obtained in the previous section, as a higher mean input also leads to a higher output rate.

In Fig. 6.8, we plot the mutual information rate for the UD case over the switching rates k_+ and k_- (red surface) and compare it to the AI case (blue surface). The phenomenon shown in Fig. 6.7A for one particular combination of k_+ and k_- is also reflected here: At a mean input of $\mu_{\text{eff}} = 1$ (Fig. 6.8A), the information transmission rate with an AI background is always higher than in the UD case, but for $\mu_{\text{eff}} = 0.7$ (Fig. 6.8B), an UD background is already slightly advantageous for some switching rate combinations, and for $\mu_{\text{eff}} = 0.4$ (Fig. 6.8C), there is a wide range of switching rates for which the mutual information rate with an UD background is significantly higher than in the AI case.

For large k_-, up states become more frequent, and for small k_+ they become longer; it is thus plausible that in both limits, the mutual information rate with an UD background approaches that with an AI background in all panels in Fig. 6.8. Similarly, for small k_-/large k_+, the presynaptic population spends almost all the time in the down state, where no firing occurs and no information can be transmitted, and $\mathcal{R}_{\text{info}}$ goes to zero in all panels. In Fig. 6.8B, C, the position of the local maxima seems to occur at a constant ratio of k_+ and k_- and their value increases with decreasing k_+ and k_-. To explain these observations, below we take two complementary perspectives on the beneficial effects of an UD background.

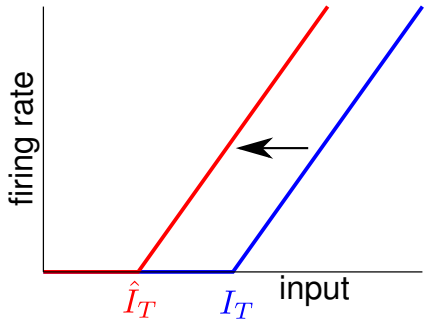

Figure 6.9.: A simple piecewise linear caricature of an FI curve. Input from an UD background (red line) effectively shifts the curve to lower input values compared to the AI case (blue line).

UD background as an effective shifting of the threshold

Effectively, the UD input can be thought of as leading to a reduced firing threshold. To see this, consider the caricature of a neuron as a static nonlinearity that acts upon an adiabatically slow input. In this case, the neuron is characterized by its *FI curve*, the relationship between input current and output firing rate. The most simplistic FI curve that captures the presence of a hard threshold is piecewise linear (see Fig. 6.9):

$$r(I) = \begin{cases} 0 & I < I_T, \\ g \cdot (I - I_T) & I \geq I_T, \end{cases} \tag{6.12}$$

where the gain g is a constant and I_T is threshold input beyond which the neuron starts to fire. In the AI case (approximated by a constant input I_{AI}), one would thus, in the supra-threshold regime, have the rate

$$r_{\mathrm{AI}} = g \cdot (I_{\mathrm{AI}} - I_T)\,. \tag{6.13}$$

For sufficiently slow UD input with the same total input rate, one can approximate the output rate during up states by

$$r^{+}_{\mathrm{UD}} = g \cdot \left(\frac{k_+ + k_-}{k_-} I_{\mathrm{AI}} - I_T \right), \tag{6.14}$$

and, as no firing occurs during down states, the overall rate is

$$\begin{aligned} r_{\mathrm{UD}} &= g \cdot \left(\frac{k_+ + k_-}{k_-} I_{\mathrm{AI}} - I_T \right) \frac{k_-}{k_+ + k_-}. \\ &= g \cdot \left(I_{\mathrm{AI}} - \widehat{I}_T \right). \end{aligned} \tag{6.15}$$

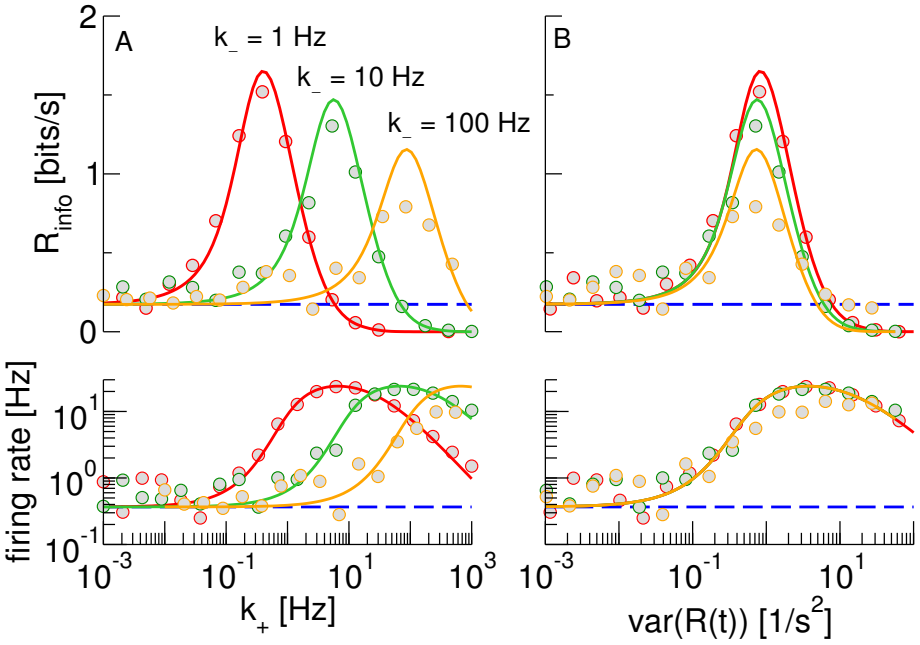

Figure 6.10.: The beneficial effect of UD input as a stochastic resonance phenomenon. Mutual information rates and firing rates for three different values of k_- are plotted over k_+ (A) and $\mathrm{var}[R(t)] = r_{\mathrm{in}}^2 k_+/k_-$ (B). Solid lines are theory for the UD background, dashed lines for the AI case, circles are results from simulations. Mean input $r_{\mathrm{in}} = 0.75$, other parameters as in the previous figures.

This has the same form as the curve in the AI case, but with a reduced effective threshold

$$\widehat{I}_T = \frac{k_-}{k_+ + k_-} I_T. \tag{6.16}$$

In principle, the effective threshold can be shifted to values arbitrarily close to zero by increasing the duration of down states (i.e. decreasing k_-).

UD background as a noise source inducing stochastic resonance

The beneficial effect of an UD background can also be interpreted as a SR effect. In other words, information transmission is optimal at a finite noise level of the two-state process $R(t)$.

First, we need to clarify what we mean by noise level. Traditionally, SR refers to the enhancement of signal transmission at a finite intensity of Gaussian white noise. However, for colored noise, the appropriate measure depends also on the correlation time: For short correlation times, D is a good characterization, while for long correlation times, the variance may be more appropriate (see (Droste and Lindner, 2014) for a discussion). Here, by construction, up and down states are assumed to be on average much longer than the mean up state ISI, so that the correlation time of $R(t)$ is large. We thus have to ask whether a finite value of the variance of $R(t)$ yields an optimum in the mutual information rate.

The variance of the dichotomously-fluctuating rate $R(t)$ is (eq. (3.10) [p. 41])

$$\mathrm{var}(R(t)) = \frac{r_{\mathrm{up}}^2 k_+ k_-}{(k_+ + k_-)^2} = r_{\mathrm{in}}^2 \frac{k_+}{k_-}. \tag{6.17}$$

We can thus change the variance by varying either k_+ or k_-.

In Fig. 6.10A (top panel), we plot the mutual information rate (lower bound) when k_+ is varied for three different values of k_-. It starts already at a finite value for $k_+ \to 0$, because for the parameters chosen here, already AI input can make the neuron fire at a low rate. The mutual information rate then increases with k_+ up to an optimal value, after which it decays. When plotting these curves over the variance of $R(t)$ (Fig. 6.10B), they collapse approximately onto into one curve (albeit with different peak heights). This means that information transmission is indeed optimized at a specific finite value of the variance of $R(t)$.

In the bottom panels of Fig. 6.10, we plot the corresponding firing rate curves. In contrast to the traditional case of SR, where the firing rate monotonically increases with the noise, they also exhibit a maximum at finite noise. This is because, along with changing the variance of the process, we simultaneously decrease its correlation time: While the input rate during an up state grows, the duration of up states decreases, leading essentially to shot-noise-like input. As the target neuron cannot fire at arbitrarily high rates due to its absolute refractory period, its output firing rate during an up state saturates, and as up states become shorter, the total firing rate goes down.

When plotted as a function of the input rate variance, the firing rate curves for the three cases collapse into the same curve. This reflects that in our approximation, the firing rate is independent of the correlation time of $R(t)$ when the variance is fixed. This can be explicitly seen by rewriting the expression for the firing rate,

$$r_0 = \frac{k-}{k_+ + k_-} r_0^+ \Big|_{a, r_{\mathrm{up}}} = \frac{r_{\mathrm{in}}^2}{r_{\mathrm{in}}^2 + \mathrm{var}(R(t))} r_0^+ \Big|_{a, \frac{\mathrm{var}(R(t))}{r_{\mathrm{in}}} + r_{\mathrm{in}}}. \tag{6.18}$$

In Fig. 6.10, we also plot simulation results (circles). While, as expected, the curves no longer collapse perfectly, the results of the approximation are confirmed qualitatively, even for parameter values that are outside of the approximation's assumptions ($k_- = 100\,\mathrm{Hz}$ at high k_+, i.e. short up and down states).

6.5. Information transmission in the AI vs. the UD case at fixed output rate

As we have seen above, the beneficial effect that an UD background may have on the transmission of a weak signal is due to an increase in output firing rate. This raises the question whether switching between up and down states can also be advantageous if the mean *output* rate of the neuron is kept fixed. For the sake of simplicity, let us consider up and down states of symmetric length. Under which circumstances can it be advantageous

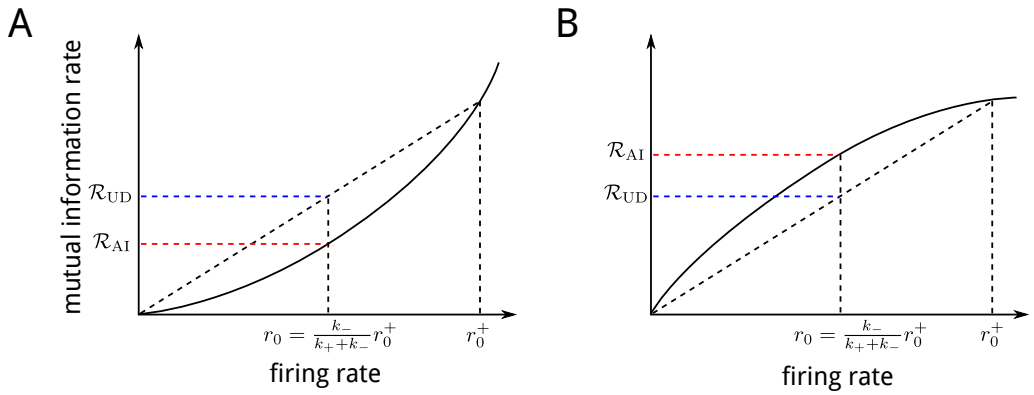

Figure 6.11.: Whether information transmission at a given mean output firing rate r_0 may benefit from adiabatically slow switching between two rates r_0^+ and $r_0^- = 0\,\mathrm{Hz}$ is determined by the shape of the AI mutual information curve over the output firing rate. If the curve is convex (A), switching between the two rates may provide an advantage, while for a concave function (B), switching is always detrimental to information transmission.

to switch between $r_0^+ = 2r_0$ and $r_0^- = 0\,\mathrm{Hz}$ instead of keeping the firing rate constant at r_0? We expect (and have observed above) that the slower the switching, the higher the information transmission rate. We should thus consider adiabatically slow switching — if switching between two firing rates is not beneficial to information transmission in this case, it should be even less so for finite up and down state duration. One will gain from adiabatically slow switching if the AI information transmission rate $\mathcal{R}_{\mathrm{info}}$ at $2r_0$ is *more* than two times as high as that at r_0 (as now, information can only be transmitted half of the time). This means that $\mathcal{R}_{\mathrm{info}}(r_0)$ needs to be convex (see sketch in Fig. 6.11).

In Fig. 6.12, we plot $\mathcal{R}_{\mathrm{info}}$ for the AI case as a function of the output firing rate. The highest output firing rate is given by the inverse refractory period; at this rate, firing no longer contains any information about the stimulus. For this reason, $\mathcal{R}_{\mathrm{info}}(r_0)$ is not a monotonic function but, after an initial rise, goes to zero as $r_0 \to 1/\tau_{\mathrm{ref}}$ (see inset). It can be seen that $\mathcal{R}_{\mathrm{info}}(r_0)$ is concave, leading us to conclude that up-down switching can not enhance information transmission at a fixed output firing rate. For an (arbitrarily chosen) up state firing rate $r_0^+ = 17.9\,\mathrm{Hz}$, we also plot the maximally possible mutual information rate that can be achieved by switching between r_0^+ and 0 Hz (dashed line). The symbols (red triangles and circles) show mutual information rates for an UD background at given switching rates k_+ and k_-. While unrealistically slow switching (triangles) comes close to the theoretical optimum, an UD background at more realistic switching rates (circles) performs considerably worse.

To understand how far the convex shape of $\mathcal{R}_{\mathrm{info}}(r_0)$ is a general property of neuronal information transmission, we consider a simpler model for the encoding of a signal in a spike train: an inhomogeneous Poisson process with the instantaneous firing rate given by

$$R(t) = r_0[1 + \epsilon s(t)]. \tag{6.19}$$

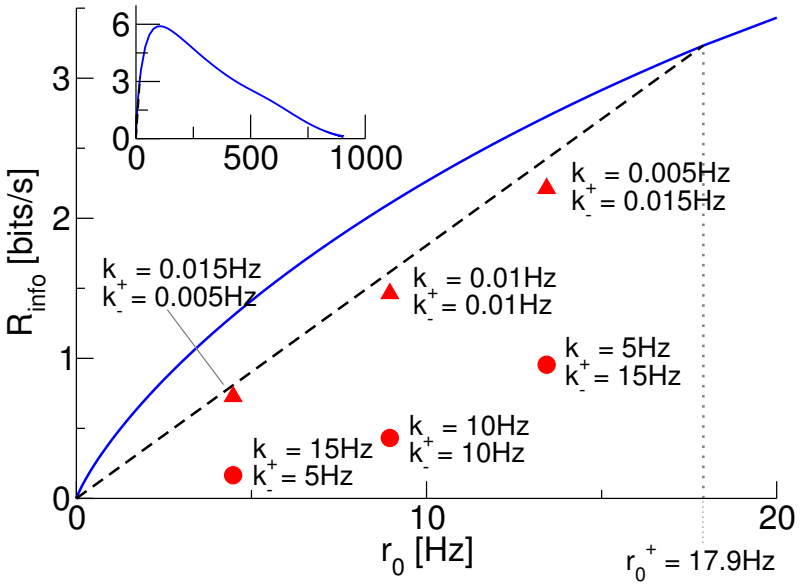

Figure 6.12.: Mutual information rate between the signal and the output spike train over the output firing rate for an AI background (blue line, theory). The inset shows $\mathcal{R}_{\text{info}}$ for higher output firing rates. The dashed line marks the optimal possible information rate that can be achieved at that output firing rate by switching between $r_0^+ = 17.9\,\text{Hz}$ and $0\,\text{Hz}$ (with the ratio k_+/k_- chosen to keep the mean at r_0). Symbols represent analytical results for the UD case for a particular combination of k_+ and k_-.

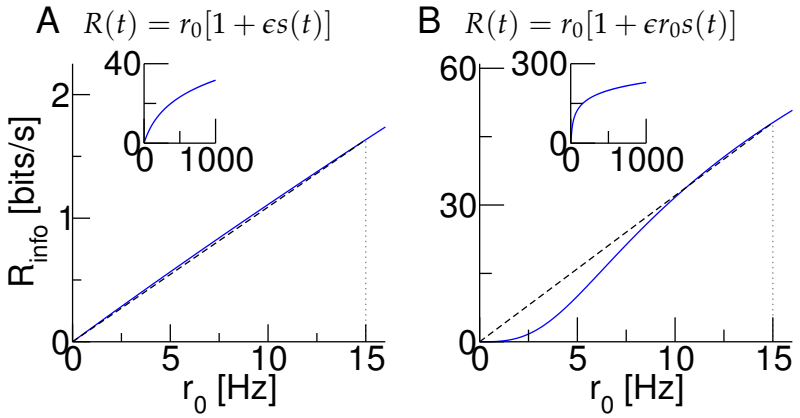

Figure 6.13.: Mutual information rate between a signal and an inhomogeneous Poisson process that encodes that signal, plotted as a function of the baseline firing rate r_0. While for the usual ansatz (rate modulation goes linearly with the baseline rate), the function is concave (A), it may be convex for a range of r_0 values if the rate modulation has, for instance, a quadratic dependence on the baseline rate (B). Parameters: $r_0^+ = 15\,\text{Hz}, \epsilon = 0.4, f_c = 10\,\text{Hz}$.

For this case, the lower bound to the mutual information rate is given by

$$\mathcal{R}_{\text{info}}(r_0) = -\int_0^\infty df\ \log_2\left[\frac{1}{1+r_0\epsilon^2 S_{ss}(f)}\right]. \tag{6.20}$$

The second derivative of $\mathcal{R}_{\text{info}}(r_0)$,

$$\frac{d^2}{dr_0^2}\mathcal{R}_{\text{info}}(r_0) = -\frac{1}{\ln(2)}\int_0^\infty df\ \frac{\epsilon^4 S_{ss}^2(f)}{(1+\epsilon^2 r_0 S_{ss}(f))^2}, \tag{6.21}$$

is always negative and hence the function always concave (illustrated in Fig. 6.13A). It is, however, possible to come up with ways to encode the signal in the rate for which this is no longer the case. For example, if the rate modulation due to the signal goes quadratically with the baseline rate r_0 (see Fig. 6.13B), then $\mathcal{R}_{\text{info}}(r_0)$ may be convex over a certain range — here, the information transmission would benefit from a (sufficiently slow) switching between up and down states. Whether such a form of firing rate modulation may arise from physiologically inspired considerations is an open question.

6.6. Summary and discussion

In this chapter, we have studied the transmission of a weak signal by a neuron that receives background input from a population that is either in an asynchronous-irregular state or undergoes transitions between up and down states. We have found two main effects of using UD input: First, in contrast to the low-pass coherence observed for an AI background, UD input can yield a band-pass coherence. Second, when the mean input rate is low, an UD background can be advantageous to information transmission.

We have studied how the band-pass effect depends on the input parameters and found it to be most pronounced for approximately symmetric switching rate k_+ and k_- and for a high rate of regularity of the target cell's firing during up states.

Further, we have discussed the mechanism responsible for the beneficial effect of an UD background, which can be understood as a down-scaling of the effective firing threshold. At the same time, one may also consider the beneficial effect of UD input a stochastic resonance phenomenon: we have shown that, regardless of the particular choice of switching rates, information transmission is maximized at a finite noise variance of the firing rate.

We have demonstrated that the beneficial effect of an UD background relies on an increase in firing rate and that, in our setup, such a background does not help information transmission if the output firing rate is held fixed.

The analysis carried out in this chapter is but a step in developing a theoretical understanding of the role of UD states in information transmission. In our opinion, there are three main questions that need to be addressed in future research:

Does a DMP capture the statistics of real up-down states?

In this chapter, we assumed that a DMP is as suitable model for the rate of a population of neurons undergoing up-down transitions. This implies that the residence times of up or down states are exponentially distributed and independent, which is certainly an approximation. However, the duration of up and down states has been reported as rather irregular and "nonrhythmic" (Mochol et al., 2015) and their distribution as gamma-like, with serial correlation coefficients between 0.1 and 0.2 for neighboring U-D or D-U intervals (Jercog, 2013). On a coarse level, using a DMP thus seems a decent first approximation.

Still, it is an interesting question how the results in this chapter would change with different, potentially more realistic rate dynamics. For a sufficiently irregular two-state process with small or vanishing correlations between subsequent up and down states, we expect the qualitative results to hold: A process with most of its power at low frequencies should again lead to a coherence that is essentially a band-pass. The beneficial effect of an UD background at low mean input should be even more robust. As we demonstrated, it can be interpreted as a SR effect; it should thus work in principle for any sufficiently variable rate modulation (although with potentially large quantitative differences).

Several authors have investigated dichotomous noise (Rozenfeld et al., 2000) or other processes switching between discrete levels (Danziger and Grill, 2015) in the context of stochastic resonance (SR). Rozenfeld et al. (2000) showed that a weak DMP can enhance the SR induced by a Gaussian white noise. More recently, Danziger and Grill (2015) demonstrated that rectangular pulses can induce SR in a model neuron and report it to be more effective than an OU noise. A thorough investigation of how information transmission with a DMP-modulated background rate compares to other kinds of rate modulations (discrete or continuous) constitutes an interesting task for future research.

What do our results mean for transient inputs?

Above, we found that the rate of information transmission in the presence of an UD background is higher the lower the switching rates (the longer the duration of up and down states). In our framework, which considers stationary stimuli, this is plausible: The slower the switching of the DMP, the narrower the frequency range in which it has power and thus disturbs the transmission of the signal. However, a real organism has to be able to respond to short, transient signals. It is of little use if, thanks to UD switching, its brain transmits signals better *on average* when firing rates are low, but a crucial stimulus is missed because it happens to fall into a long down state.

Various authors have observed that a stimulus onset can induce an up state (Shu et al., 2003; Luczak et al., 2013); such an interaction between the stimulus and the background network, which is not covered in our simple setup, might mitigate the problem of missing transients. Another possible way around this problem lies in the UD dynamics themselves: While it makes sense to model a relatively small population as being simultaneously either in an up or a down state, this is probably no longer true when one considers, say, the entire auditory cortex. It is thus imaginable that, while some neurons are in a down state, others are in an up state and can transmit information. Indeed, several recent works have argued that up states propagate cortex as a traveling wave (Massimini

et al., 2004; Luczak et al., 2007; Keane and Gong, 2015).

Do our results apply to recurrent networks?

In our setup, the presynaptic neurons provide the background input (AI or UD) but are not involved in the transmission of the signal. Signal transmission is, by contrast, performed by a second population (out of which we considered one neuron in this chapter), which receives its dominant input from the background population. A more realistic picture might be that the same network that generates the UD activity also receives sensory input. When singling out one neuron out of such a population, the situation would be, at first glance, similar to the setup studied in this chapter: The neuron would receive a sensory (bottom-up) signal, but a large part of its input would be recurrent, i.e. from other cells in the network, either in an AI or an UD regime. However, there would be one important difference: Assuming a homogeneous network, self-consistency demands that the firing rate of the cell in question equals that of the cells from which it receives input. The beneficial effect of an UD background (compared to AI) that we discussed above relied on achieving a higher output firing rate at the same mean input rate. In Sec. 6.5, we argued that at a fixed output firing rate, information transmission may benefit from UD switching if the mutual information rate is a convex function of the output firing rate. For our setup, however, we found it to be concave. Under which conditions a convex curve can be achieved and whether this is possible in a realistic recurrent network is an exciting question for future research.

Chapter 7.

Concluding remarks

In this thesis, we have studied information transmission in stochastic neuron models in which the background noise is non-white, non-Gaussian, or neither white nor Gaussian. We have concentrated on three specific scenarios: Signal transmission in the presence of a second signal, of shot noise, and of a background network that transitions between up and down states. We chose such specific examples because we find them physiologically interesting and relevant, but also out of necessity: There is no framework in which non-Gaussian and non-white noise could be studied in general, and even if there was, the huge space of possible processes would probably give rise to a vast variety of effects, too diverse to be briefly summarized. Still, it seems important to trace commonalities and point out differences between our scenarios. Here, we give a brief summary of our results and, where applicable, discuss whether they should be interpreted as effects of the color of the background noise or its non-Gaussian nature.

In Chapter 2, we considered the interplay of two signals in a neuron with heterogeneous short-term plasticity (STP). We observed two main effects: 1: In the presence of a second signal, information transmission is no longer broadband; instead, the neuron preferentially encodes information about slow components of the signal that enters through facilitating synapses and fast components of the signal that enters through depressing synapses. 2: The system can display a new kind of stochastic resonance (SR), in which the role of the helpful noise is played by the second signal. In this scenario, the noise is colored for three reasons: First, the signals themselves are limited to a band between 0 and 10 Hz, second, they are filtered by STP (low-pass for facilitating, high-pass for depressing synapses), and third, they are low-pass filtered by the conductance dynamics. It is clearly this color of the noise that is responsible for the frequency dependence of the coherence that we called a spectral separation of information. The signal-mediated stochastic resonance (SR) effect does not rely on the noise being colored: As we demonstrated, it is also observed for static synapses and would even become more effective if the second signal was spread out over a wider frequency range. While, strictly speaking, the noise in the setup is non-Gaussian (shot noise), we expect both effects to occur also with a Gaussian colored noise with suitably chosen spectrum (a setup in which STP input is modeled by a Gaussian process has recently been explored by Schwalger et al. (2015)).

We turned to a both colored (exponentially correlated) and non-Gaussian (two-valued) noise in Chapter 3, in which we studied integrate-and-fire (IF) neurons driven by asymmetric dichotomous noise. We derived analytical expressions for the stationary density, the moments of the ISI density, the power spectrum, and the susceptibility. In contrast to the case of Gaussian white noise, the stationary density does not vanish at the threshold and its shape does depend on the absolute refractory period; these are effects of the noise

color that would, for instance, also be observed with an Ornstein-Uhlenbeck (OU) process. In contrast, the bounded support of the probability density and the fact that it may show (integrable) divergences are a consequence of the (rather particular) stationary distribution of the noise. The same goes for the undamped periodicity which we observed in the spectral measures – it is a consequence of the fact that the noise is non-Gaussian; however, it relies on a rather particular type of non-Gaussian noise and would not appear for non-Gaussian noises with continuous distributions (as explored in Chapter 5). Finally, we also found that the susceptibility does not vanish in the high-frequency limit, even with a current-modulated signal. This is again an effect of the noise color, closely related to the non-vanishing stationary probability density at the threshold.

In Chapter 4, we considered the case of white shot noise (SN) with exponentially distributed weights. For such input, we were able to obtain exact expressions for the stationary voltage distribution and the ISI moments of IF neurons as well as the power spectrum and susceptibility (both with respect to a rate and a current modulation) of LIF neurons. We found that such noise can lead to a firing rate that is, depending on the mean input, either higher or lower than in the diffusion approximation (DA). This difference in firing rate is reflected in differences of the power spectra, the susceptibilities, and, ultimately, information transmission. Additionally, the susceptibility with respect to a current modulation shows a qualitatively different high-frequency behavior: It decays slower, with $1/f$ instead of $1/\sqrt{f}$. As the SN considered here is white, all differences to the DA are due to its non-Gaussian distribution.

In Chapter 5, we considered a neuron driven by a two-state process with additional fast fluctuations within the states. This represents a colored Gaussian noise with a continuous distribution. Making use of a quasistatic approximation (assuming the two-state noise to be slow), we could derive various approximations for the ISI moments, the power spectrum, and the susceptibility. These expressions relate quantities in the full system to known expressions for a neuron that is fixed in one of the two states, i.e. where switching is turned off. We compared different approximation approaches and found some of them to perform well even if states were rather short, i.e. if they contained only a few interspike intervals; this made them suitable for use in a simple model of a neuron driven by a network in an up-down (UD) regime.

How information transmission in a single neuron is affected by a background network in an UD regime was explored in Chapter 6. We observed two main effects of such a background on signal transmission: First, it leads to a coherence that has a peak; it can thus be seen as a band-pass filter for information. This is an effect of the (low-pass) power of the two-state process, i.e. of the noise color. Second, compared to a background where the firing rate is constant in time, an UD regime can lead to higher mutual information rates through an increase in firing rate. As we have shown, this effect, which occurs when the overall input rate is low, can be also understood as an SR effect. We would thus expect the effect as such to occur with a Gaussian noise as well; how a continuous rate modulation (say by an OU process) would change information transmission rates is an open question that should be explored in follow-up work.

Especially the second result could help to elucidate the functional role of up-down states: It has been argued that they are needed to allow for cellular maintenance via a reduction in overall firing rate (Vyazovskiy and Harris, 2013). It is not immediately clear, however, why such a reduction should be achieved by switching between active and

silent periods, instead of by lowering the overall firing rate in an extended active period. Our findings hint at a possible explanation: At a lower firing rate, an UD regime might be more effective with respect to information transmission.

Appendix A.

IF neurons driven by dichotomous noise

A.1. $\phi(v)$ in some common cases

Here, we give closed-form expressions for

$$\phi(v) := k_+ \int^v du\ \frac{1}{f(u)+\sigma} + k_- \int^v du\ \frac{1}{f(u)-\sigma}. \tag{A.1}$$

Note that the lower integration boundary can be chosen arbitrarily as one always deals with pairs

$$e^{-\phi(v_1)} \cdot e^{\phi(v_2)} \tag{A.2}$$

so that an integration constant would drop out.

- PIF ($f(v) = \mu$):

$$\phi(v) = v\left(\frac{k_+}{\mu+\sigma} + \frac{k_-}{\mu-\sigma}\right). \tag{A.3}$$

- LIF ($f(v) = \mu - v$):

$$\phi(v) = -k_+ \ln(|\mu - v + \sigma|) - k_- \ln(|\mu - v - \sigma|). \tag{A.4}$$

- QIF ($f(v) = \mu + v^2$):

$$\begin{aligned}\phi(v) = {} & \frac{k_+}{\sqrt{\mu+\sigma}} \arctan\left(\frac{v}{\sqrt{\mu+\sigma}}\right) \\ & + \frac{k_-}{\sqrt{|\mu-\sigma|}} \begin{cases} \arctan\left(\frac{v}{\sqrt{\mu-\sigma}}\right) & \mu > \sigma \\ -\operatorname{arctanh}\left(\frac{v}{\sqrt{-\mu+\sigma}}\right) & -\sqrt{-\mu+\sigma} < v < \sqrt{-\mu+\sigma}\,. \\ -\operatorname{arccoth}\left(\frac{v}{\sqrt{-\mu+\sigma}}\right) & \text{otherwise} \end{cases}\end{aligned} \tag{A.5}$$

A.2. Transformation of the master equations to a second-order ODE for the flux

We start from eqs. (3.82, 3.83) [p. 61]:

$$-i\omega\widetilde{P}_+(v,\omega) = -\frac{d}{dv}\Big[(\mu - v + \sigma)\widetilde{P}_+(v,\omega)\Big] - k_+\widetilde{P}_+(v,\omega) + k_-\widetilde{P}_-(v,\omega) + \widetilde{\Delta}_+(v,\omega), \tag{A.6}$$

$$-i\omega\widetilde{P}_-(v,\omega) = -\frac{d}{dv}\Big[(\mu - v - \sigma)\widetilde{P}_-(v,\omega)\Big] + k_+\widetilde{P}_+(v,\omega) - k_-\widetilde{P}_-(v,\omega) + \widetilde{\Delta}_-(v,\omega). \tag{A.7}$$

These can be expressed in terms of the fluxes

$$\widetilde{J}_\pm(v,\omega) = (\mu - v \pm \sigma)\widetilde{P}_\pm(v,\omega). \tag{A.8}$$

To unburden notation, we omit the ω for the time being and understand derivatives as taken w.r.t. v. One has

$$0 = -\widetilde{J}_+'(v) - \gamma_1(v)\widetilde{J}_+ + \gamma_2(v)\widetilde{J}_- + \widetilde{\Delta}_+(v), \tag{A.9}$$

$$0 = -\widetilde{J}_-'(v) + \gamma_3(v)\widetilde{J}_+ - \gamma_4(v)\widetilde{J}_- + \widetilde{\Delta}_-(v), \tag{A.10}$$

where we have used the abbreviations

$$\gamma_1(v) := \frac{k_+ - i\omega}{\mu - v + \sigma}, \tag{A.11}$$

$$\gamma_2(v) := \frac{k_-}{\mu - v - \sigma}, \tag{A.12}$$

$$\gamma_3(v) := \frac{k_+}{\mu - v + \sigma}, \tag{A.13}$$

$$\gamma_4(v) := \frac{k_- - i\omega}{\mu - v - \sigma}. \tag{A.14}$$

Writing eqs. (A.9, A.10) in terms of the total flux, $\widetilde{J}(v) = \widetilde{J}_+(v) + \widetilde{J}_-(v)$, as well as the difference of fluxes, $\widetilde{L}(v) := \widetilde{J}_+(v) - \widetilde{J}_-(v)$, and adding (subtracting) the second equation to (from) the first one yields

$$0 = -\widetilde{J}(v)' + \alpha_1(v)\widetilde{J}(v) + \alpha_2(v)\widetilde{L}(v) + \widetilde{\Delta}_+(v) + \widetilde{\Delta}_-(v), \tag{A.15}$$

$$0 = -\widetilde{L}(v)' + \alpha_3(v)\widetilde{J}(v) + \alpha_4(v)\widetilde{L}(v) + \widetilde{\Delta}_+(v) - \widetilde{\Delta}_-(v), \tag{A.16}$$

where

$$\alpha_1(v) := \frac{-\gamma_1(v) + \gamma_2(v) + \gamma_3(v) - \gamma_4(v)}{2} = \frac{i\omega(\mu - v)}{(\mu - v)^2 - \sigma^2}, \tag{A.17}$$

$$\alpha_2(v) := \frac{-\gamma_1(v) - \gamma_2(v) + \gamma_3(v) + \gamma_4(v)}{2} = \frac{-i\omega\sigma}{(\mu - v)^2 - \sigma^2}, \tag{A.18}$$

$$\begin{aligned}\alpha_3(v) &:= \frac{-\gamma_1(v) + \gamma_2(v) - \gamma_3(v) + \gamma_4(v)}{2} \\ &= \frac{-k_+(\mu - v - \sigma) + k_-(\mu - v + \sigma) - i\omega\sigma}{(\mu - v)^2 - \sigma^2},\end{aligned} \tag{A.19}$$

$$\begin{aligned}\alpha_4(v) &:= \frac{-\gamma_1(v) - \gamma_2(v) - \gamma_3(v) - \gamma_4(v)}{2} \\ &= \frac{-k_+(\mu - v - \sigma) - k_-(\mu - v + \sigma) + i\omega(\mu - v)}{(\mu - v)^2 - \sigma^2}.\end{aligned} \tag{A.20}$$

We solve eq. (A.15) for $\widetilde{L}(v)$,

$$\widetilde{L}(v) = \frac{\widetilde{J}'(v) - \alpha_1(v)\widetilde{J}(v) - \widetilde{\Delta}_+(v) - \widetilde{\Delta}_-(v)}{\alpha_2(v)} \tag{A.21}$$

and plug the result into eq. (A.16). After multiplication by $\alpha_2(v)$ and sorting, it reads

$$\begin{aligned}0 = &-\widetilde{J}''(v) + \left(\frac{\alpha_2'(v)}{\alpha_2(v)} + \alpha_1(v) + \alpha_4(v)\right)\widetilde{J}'(v) \\ &+ \left(\alpha_1'(v) - \frac{\alpha_1(v)\alpha_2'(v)}{\alpha_2(v)} + \alpha_2(v)\alpha_3(v) - \alpha_4(v)\alpha_1(v)\right)\widetilde{J}(v) \\ &+ \left(-\alpha_4(v) - \frac{\alpha_2'(v)}{\alpha_2(v)}\right)\left[\widetilde{\Delta}_+(v) + \widetilde{\Delta}_-(v)\right] + \alpha_2(v)\left[\widetilde{\Delta}_+(v) - \widetilde{\Delta}_-(v)\right] \\ &+ \widetilde{\Delta}_+'(v) + \widetilde{\Delta}_-'(v)\end{aligned} \tag{A.22}$$

Using the above definitions of $\alpha_1(v)$ - $\alpha_4(v)$, one finds, after some simplification, the form given in eq. (3.86) [p. 62]:

$$\begin{aligned} 0 = {} & \widetilde{J}''(v) + p(v)\widetilde{J}'(v) + q(v)\widetilde{J}(v) \\ & - \left(p(v) + \frac{i\omega}{\mu - v + \sigma}\right)\widetilde{\Delta}_+(v) - \left(p(v) + \frac{i\omega}{\mu - v - \sigma}\right)\widetilde{\Delta}_-(v) \\ & - \widetilde{\Delta}'_+(v) - \widetilde{\Delta}'_-(v), \end{aligned} \tag{A.23}$$

where

$$p(v) := -\frac{(\mu - v)\,(2 - k_+ - k_- + 2i\omega) + \sigma\,(k_+ - k_-)}{(\mu - v)^2 - \sigma^2}, \tag{A.24}$$

$$q(v) := \frac{i\omega\,(1 - k_+ - k_- + i\omega)}{(\mu - v)^2 - \sigma^2}. \tag{A.25}$$

A.3. Simplifying the expression for $\widetilde{J}(0)$

Here, we simplify, the expression

$$\widetilde{J}(0) = \int_0^\infty du\; \widetilde{\Delta}(u)\frac{\widetilde{J}_2(u)\widetilde{J}_1(0) - \widetilde{J}_1(u)\widetilde{J}_2(0)}{W(u)}, \tag{A.26}$$

where $\widetilde{J}_1(z)$ and $\widetilde{J}_2(z)$ are the two linearly independent solutions to eq. (3.90) [p. 62], given in terms of hypergeometric functions in eq. (3.100) [p. 63], and $W(z)$ is their Wronskian. For the inhomogeneity,

$$\widetilde{\Delta}(z) = 2\sigma\left[\left(p(z) + \frac{i\omega}{1 - z}\right)\widetilde{\Delta}_+(z) + \left(p(z) - \frac{i\omega}{z}\right)\widetilde{\Delta}_-(z) + \widetilde{\Delta}'_+(z) + \widetilde{\Delta}'_-(z)\right], \tag{A.27}$$

we only use that $\widetilde{\Delta}_+(z)$ and $\widetilde{\Delta}_-(z)$ vanish at 0 and ∞.

From the properties of hypergeometric functions (Abramowitz and Stegun, 1972), one easily finds

$$\widetilde{J}_1(0) = 1, \quad \widetilde{J}_2(0) = 0. \tag{A.28}$$

Thus, one deals with the problem of integrating

$$\begin{aligned}\widetilde{J}(0) = 2\sigma \int_0^\infty du \Bigg[&\left(p(u) + \frac{i\omega}{1-u} \right) \widetilde{\Delta}_+(u) + \left(p(u) - \frac{i\omega}{u} \right) \widetilde{\Delta}_-(u) \\ &+ \widetilde{\Delta}'_+(u) + \widetilde{\Delta}'_-(u) \Bigg] f(u)\end{aligned} \tag{A.29}$$

with the the abbreviation $f(z) := \widetilde{J}_2(z)/W(z)$.

Next, the Wronskian can be considerably simplified. Differentiating eq. (3.103) [p. 63] and plugging in the homogeneous ODE yields

$$\begin{aligned}W'(z) &= \widetilde{J}_1(z) \left[-p(z)\widetilde{J}'_2(z) - q(z)\widetilde{J}_2(z) \right] \\ &\quad - \left[-p(z)\widetilde{J}'_1(z) - q(z)\widetilde{J}_1(z) \right] \widetilde{J}_2(z)\end{aligned} \tag{A.30}$$

$$= -p(z)W(z). \tag{A.31}$$

Thus,

$$W(z) = c_W \cdot e^{-\int^z dw\, p(w)} = c_W \cdot (1-z)^{k_+ - 1 - i\omega} \cdot z^{k_- - 1 - i\omega}, \tag{A.32}$$

where c_W is a constant that will later drop out of the final result.

Noting that

$$f'(z) = \frac{\widetilde{J}'_2(z) + p(z)\widetilde{J}_2(z)}{W(z)}, \tag{A.33}$$

the integral can be further simplified through integration by parts,

$$\begin{aligned}\widetilde{J}(0) = 2\sigma \Bigg[&[\widetilde{\Delta}_+(u) f(u) + \widetilde{\Delta}_-(u) f(u)]_0^\infty \\ &+ \int_0^\infty du\, \frac{\widetilde{\Delta}_+(u)}{W(u)} \left(\frac{i\omega}{1-u} \widetilde{J}_2(u) - \widetilde{J}'_2(u) \right) - \frac{\widetilde{\Delta}_-(u)}{W(u)} \left(\frac{i\omega}{u} \widetilde{J}_2(u) + \widetilde{J}'_2(u) \right) \Bigg].\end{aligned} \tag{A.34}$$

The integrands can be further simplified by exploiting known relations about hypergeometric functions. Using (Abramowitz and Stegun, 1972, 15.2.4),

$$\begin{aligned}\widetilde{J}'_2(z) &= \left[z^{k_- - i\omega} \cdot {}_2F_1\left(k_-, 1-k_+; 1+k_- - i\omega; z\right) \right]' \\ &= (k_- - i\omega) \cdot z^{k_- - i\omega - 1} \cdot {}_2F_1\left(k_-, 1-k_+; k_- - i\omega; z\right)\end{aligned} \tag{A.35}$$

and thus (Abramowitz and Stegun, 1972, 15.2.25),

$$\frac{i\omega}{1-z}\widetilde{J}_2(z) - \widetilde{J}_2'(z) = -z^{k_- - i\omega - 1}(1-z)^{-1}(k_- - i\omega)\cdot {}_2F_1\left(k_-, -k_+; k_- - i\omega; z\right), \quad \text{(A.36)}$$

and (Abramowitz and Stegun, 1972, 15.2.17)

$$\frac{i\omega}{z}\widetilde{J}_2(z) + \widetilde{J}_2'(z) = z^{k_- - i\omega - 1}k_- \cdot {}_2F_1\left(1+k_-, 1-k_+; 1-k_- - i\omega; z\right). \quad \text{(A.37)}$$

Plugging in eq. (A.32) for the Wronskian and using (Abramowitz and Stegun, 1972, 15.3.3), one finds

$$\frac{1}{W(z)}\left(\frac{i\omega}{1-z}\widetilde{J}_2(z) - \widetilde{J}_2'(z)\right) \quad \text{(A.38)}$$

$$= -c_W^{-1}(k_- - i\omega)\cdot {}_2F_1\left(-i\omega, k_+ + k_- - i\omega; k_- - i\omega; z\right) \quad \text{(A.39)}$$

and

$$\frac{1}{W(z)}\left(\frac{i\omega}{z}\widetilde{J}_2(z) + \widetilde{J}_2'(z)\right) \quad \text{(A.40)}$$

$$= c_W^{-1}k_- \cdot {}_2F_1\left(-i\omega, k_+ + k_- - i\omega; 1 + k_- - i\omega; z\right) \quad \text{(A.41)}$$

For the flux at $z = 0$, we thus have

$$\widetilde{J}(0) = -2\sigma c_W^{-1}\int_0^\infty du\ (k_- - i\omega)\widetilde{\Delta}_+(u)\mathcal{F}(u,\omega) + k_-\widetilde{\Delta}_-(u)\mathcal{G}(u,\omega), \quad \text{(A.42)}$$

with

$$\mathcal{F}(z,\omega) := {}_2F_1\left(-i\omega, k_+ + k_- - i\omega; k_- - i\omega; z\right), \quad \text{(A.43)}$$

$$\mathcal{G}(z,\omega) := {}_2F_1\left(-i\omega, k_+ + k_- - i\omega; 1 + k_- - i\omega; z\right). \quad \text{(A.44)}$$

Appendix B.

Shot noise

B.1. Formulas for Gaussian white noise

Here, we list known results for an LIF neuron in the diffusion approximation (DA). We consider the non-dimensionalized voltage dynamics

$$\dot{v} = \check{\mu} - v + \check{\epsilon}_\mu s(t) + \sqrt{2[\check{D} + \check{\epsilon}_D s(t)]}\xi(t), \tag{B.1}$$

with the usual fire and reset rule and a refractory period τ_{ref}. Here, $\xi(t)$ is Gaussian white noise [$\langle\xi(t)\rangle = 0, \langle\xi(t)\xi(t')\rangle = \delta(t-t')$], $s(t)$ is a signal which enters either as a current modulation ($\check{\epsilon}_\mu > 0$) or a noise modulation ($\check{\epsilon}_D > 0$).

- Firing rate (for $\check{\epsilon}_\mu = \check{\epsilon}_D = 0$) (Ricciardi and Sacerdote, 1979):

$$\check{r}_0 = \left(\tau_{\text{ref}} + \sqrt{\pi} \int_{(\check{\mu}-v_T)/(2\check{D})}^{(\check{\mu}-v_R)/(2\check{D})} dz\, e^{z^2} \text{erfc}(z) \right)^{-1}, \tag{B.2}$$

  where erfc(z) is the complementary error function (Abramowitz and Stegun, 1972).
- Stationary probability density ($\check{\epsilon}_\mu = \check{\epsilon}_D = 0$, see e.g. (Lindner, 2002)):

$$\check{P}_0(v) = \frac{\check{r}_0}{\check{D}} e^{-(v-\check{\mu})^2/(2\check{D})} \begin{cases} \int_{v_R}^{v_T} dy\, e^{(y-\check{\mu})^2/(2\check{D})} & v < v_R \\ \int_{v}^{v_T} dy\, e^{(y-\check{\mu})^2/(2\check{D})} & v_R < v < v_T \end{cases}. \tag{B.3}$$

- Susceptibility with respect to current modulation ($\check{\epsilon}_\mu > 0, \check{\epsilon}_D = 0$) (Brunel et al., 2001; Lindner and Schimansky-Geier, 2001)

$$\check{\chi}_\mu(\omega) = \frac{\check{r}_0 i\omega}{\sqrt{\check{D}}(i\omega - 1)} \frac{\mathcal{D}_{i\omega-1}\left(\frac{\check{\mu}-v_T}{\sqrt{\check{D}}}\right) - e^{\frac{v_R^2 - v_T^2 + 2\check{\mu}(v_T - v_R)}{4\check{D}}} \mathcal{D}_{i\omega-1}\left(\frac{\check{\mu}-v_R}{\sqrt{\check{D}}}\right)}{\mathcal{D}_{i\omega}\left(\frac{\check{\mu}-v_T}{\sqrt{\check{D}}}\right) - e^{\frac{v_R^2 - v_T^2 + 2\check{\mu}(v_T - v_R)}{4\check{D}}} e^{i\omega\tau_{\text{ref}}} \mathcal{D}_{i\omega}\left(\frac{\check{\mu}-v_R}{\sqrt{\check{D}}}\right)}, \tag{B.4}$$

where $\mathcal{D}_n(z)$ is the parabolic cylinder function (Abramowitz and Stegun, 1972).

- Susceptibility with respect to noise modulation ($\check{\epsilon}_\mu = 0, \check{\epsilon}_D > 0$) (Lindner and Schimansky-Geier, 2001):

$$\check{\chi}_D(\omega) = \frac{\check{r}_0 i\omega(i\omega-1)}{\check{D}(2-i\omega)} \frac{\mathcal{D}_{i\omega-2}\left(\frac{\check{\mu}-v_T}{\sqrt{\check{D}}}\right) - e^{\frac{v_R^2-v_T^2+2\check{\mu}(v_T-v_R)}{4\check{D}}}\mathcal{D}_{i\omega-2}\left(\frac{\check{\mu}-v_R}{\sqrt{\check{D}}}\right)}{\mathcal{D}_{i\omega}\left(\frac{\check{\mu}-v_T}{\sqrt{\check{D}}}\right) - e^{\frac{v_R^2-v_T^2+2\check{\mu}(v_T-v_R)}{4\check{D}}}e^{i\omega\tau_{\mathrm{ref}}}\mathcal{D}_{i\omega}\left(\frac{\check{\mu}-v_R}{\sqrt{\check{D}}}\right)}. \tag{B.5}$$

- Fourier-transformed ISI density ($\check{\epsilon}_\mu = \check{\epsilon}_D = 0$) (Darling and Siegert, 1953; Lindner et al., 2002):

$$\check{\tilde{\rho}}(\omega) = \exp\left[\frac{1}{4\check{D}}\left(v_R^2 - v_T^2 + 2\check{\mu}(v_T - v_R)\right)\right] \frac{\mathcal{D}_{i\omega}\left(\frac{\check{\mu}-v_R}{\sqrt{\check{D}}}\right)}{\mathcal{D}_{i\omega}\left(\frac{\check{\mu}-v_T}{\sqrt{\check{D}}}\right)}. \tag{B.6}$$

- Power spectrum ($\check{\epsilon}_\mu = \check{\epsilon}_D = 0$) (Lindner et al., 2002):

$$\check{S}_{xx}(\omega) = \check{r}_0 \frac{\left|\mathcal{D}_{i\omega}\left(\frac{\check{\mu}-v_T}{\sqrt{\check{D}}}\right)\right|^2 - e^{2\frac{v_R^2-v_T^2+2\check{\mu}(v_T-v_R)}{4\check{D}}}\left|\mathcal{D}_{i\omega}\left(\frac{\check{\mu}-v_R}{\sqrt{\check{D}}}\right)\right|^2}{\left|\mathcal{D}_{i\omega}\left(\frac{\check{\mu}-v_T}{\sqrt{\check{D}}}\right) - e^{i\omega\tau_{\mathrm{ref}}+\frac{v_R^2-v_T^2+2\check{\mu}(v_T-v_R)}{4\check{D}}}\mathcal{D}_{i\omega}\left(\frac{\check{\mu}-v_R}{\sqrt{\check{D}}}\right)\right|^2}. \tag{B.7}$$

B.2. Shot-noise limit of the expressions involving hypergeometric functions

Here, we calculate the shot-noise limit of

$$\mathcal{F}(z,\omega) = {}_2F_1\left(-i\omega, k_+ + k_- - i\omega; k_- - i\omega; z\right). \tag{B.8}$$

This means expressing σ by σ_+ and σ_-, setting $\sigma_- = 0$ and $\sigma_+ = ak_+$, renaming k_- to r_{in} and then taking the limit $k_+ \to \infty$. Recall that a system switching between the flows $\mu \pm \sigma$ can be written as one switching between the flows $\mu' + \sigma_\pm$ (Sec. 3.2) by setting

$$\sigma = \frac{\sigma_+ - \sigma_-}{2}, \tag{B.9}$$

$$\mu = \mu' + \frac{\sigma_+ + \sigma_-}{2}, \tag{B.10}$$

and thus

$$z = \frac{v-\mu+\sigma}{2\sigma} = \frac{v-\mu'-\frac{\sigma_+}{2}+\frac{\sigma_+}{2}}{\sigma_+} = \frac{v-\mu}{ak_+}, \tag{B.11}$$

where in the last step, we have dropped the ′.

For a hypergeometric function

$$ {}_2F_1\left(a, \lambda + b; c; z/\lambda\right) = \sum_{n=0}^{\infty} \frac{(a)_n (\lambda + b)_n}{(c)_n} \frac{\left(\frac{z}{\lambda}\right)^n}{n!}. \tag{B.12} $$

It holds

$$ (\lambda + b)_n \left(\frac{z}{\lambda}\right)^n = \underbrace{(\lambda + b)(\lambda + b + 1) \ldots (\lambda + b + n - 1)}_{n \text{ terms}} \left(\frac{z}{\lambda}\right)^n \tag{B.13} $$

$$ = \lambda^n \left(\frac{z}{\lambda}\right)^n + \mathcal{O}\left(\frac{1}{\lambda}\right)^{n-1}, \tag{B.14} $$

so that we have

$$ \lim_{\lambda \to \infty} {}_2F_1\left(a, \lambda + b; c; z/\lambda\right) = \sum_{n=0}^{\infty} \frac{(a)_n}{(c)_n} \frac{z^n}{n!} = {}_1F_1\left(a; c; z\right), \tag{B.15} $$

where ${}_1F_1\left(a; c; z\right)$ is the confluent hypergeometric function (Abramowitz and Stegun, 1972). Thus

$$ \begin{aligned} \widehat{\mathcal{F}}(v, \omega) &= \lim_{k_+ \to \infty} \mathcal{F}(v, \omega) = \lim_{k_+ \to \infty} {}_2F_1\left(-i\omega, k_+ + r_{\text{in}} - i\omega; r_{\text{in}} - i\omega; \frac{v - \mu}{a k_+}\right) \\ &= {}_1F_1\left(-i\omega, r_{\text{in}} - i\omega; \frac{v - \mu}{a}\right). \end{aligned} \tag{B.16} $$

For numerical evaluation, it can be useful to further transform this using the Kummer transform (Abramowitz and Stegun, 1972),

$$ \begin{aligned} \widehat{\mathcal{F}}(v, \omega) &= {}_1F_1\left(-i\omega; r_{\text{in}} - i\omega; \frac{v - \mu}{a}\right) \\ &= \exp\left[\frac{v - \mu}{a}\right] {}_1F_1\left(r_{\text{in}}; r_{\text{in}} - i\omega; -\frac{v - \mu}{a}\right). \end{aligned} \tag{B.17} $$

The results for $\widehat{\mathcal{G}}(v, \omega)$, $\widehat{\mathcal{F}}'(v, \omega)$ and $\widehat{\mathcal{G}}'(v, \omega)$ are obtained analogously.

B.3. Expressions for $\widehat{\phi}(v)$ for various neuron models

Here, we list explicit expressions for

$$\widehat{\phi}(v) = \frac{v}{a} + \tau_{\mathrm{m}} r_{\mathrm{in}} \int^{v} dx \, \frac{1}{f(x)} \tag{B.18}$$

for PIF, LIF and QIF neurons (cf. Appendix A.1).

- PIF ($f(v) = \mu$):

$$\widehat{\phi}(v) = v \left(\frac{1}{a} + \frac{\tau_{\mathrm{m}} r_{\mathrm{in}}}{\mu} \right). \tag{B.19}$$

- LIF ($f(v) = \mu - v$):

$$\widehat{\phi}(v) = \frac{v}{a} - \tau_{\mathrm{m}} r_{\mathrm{in}} \ln(|\mu - v|). \tag{B.20}$$

- QIF ($f(v) = \mu + v^2$):

$$\widehat{\phi}(v) = \frac{v}{a} + \frac{\tau_{\mathrm{m}} r_{\mathrm{in}}}{\sqrt{|\mu|}} \begin{cases} \arctan\left(\frac{v}{\sqrt{\mu}}\right) & \mu > 0 \\ -\operatorname{arctanh}\left(\frac{v}{\sqrt{-\mu}}\right) & -\sqrt{-\mu} < v < \sqrt{-\mu} \\ -\operatorname{arccoth}\left(\frac{v}{\sqrt{-\mu}}\right) & \text{otherwise} \end{cases}. \tag{B.21}$$

B.4. Recursive relations for the FPT moments

Here, we give the shot-noise limit of the recursive relations that allow to calculate the ISI moments, eq. (3.70) [p. 57] and eq. (3.71) [p. 57]. They read:

$$\widehat{\mathcal{J}}_n(v) = \sum_{i=1}^{i(v)} \int_{l_i}^{\min(v, r_i)} dx \, n \frac{\widehat{\mathcal{M}}^i_{n-1}(x)}{f(x)} + \left(\frac{\tau_{\mathrm{ref}}}{\tau_{\mathrm{m}}} \right)^n \delta(x - v_R), \tag{B.22}$$

$$\widehat{\mathcal{M}}^i_n(v) = e^{-\widehat{\phi}(v)} \int_{c_i}^{v} dx \, e^{\widehat{\phi}(x)} \left(n \frac{\widehat{\mathcal{M}}^i_{n-1}(x)}{f(x)} + \frac{\widehat{\mathcal{J}}_n(x)}{a} + \left(\frac{\tau_{\mathrm{ref}}}{\tau_{\mathrm{m}}} \right)^n \delta(x - v_R) \right). \tag{B.23}$$

where $i(v)$ denotes the interval that contains v. The nth ISI moment is then given by $\left\langle \widehat{T}^n \right\rangle = \widehat{\mathcal{J}}_n(v_T)$.

First ISI moment

One finds

$$\widehat{\mathcal{J}}_0(v) = \theta(v - v_R) \tag{B.24}$$

$$\widehat{\mathcal{M}}_0(v) = e^{-\widehat{\phi}(v)} \int_{c_i}^{v} dx\, e^{\widehat{\phi}(x)} \frac{\theta(x - v_R)}{a} + e^{\widehat{\phi}(v_R) - \widehat{\phi}(v)} \left[\theta(v - v_R) - \theta(c_i - v_R)\right], \tag{B.25}$$

and thus

$$\begin{aligned} \left\langle \widehat{T} \right\rangle = \widehat{\mathcal{J}}_1(v_T) = \sum_{i=1}^{N} \Bigg[\int_{l_i}^{r_i} dx \int_{c_i}^{x} dy\, \frac{e^{\widehat{\phi}(y) - \widehat{\phi}(x)}}{a f(x)} \theta(y - v_R) \\ + \int_{l_i}^{r_i} dx\, \frac{e^{\widehat{\phi}(v_R) - \widehat{\phi}(x)}}{f(x)} \left[\theta(x - v_R) - \theta(c_i - v_R)\right] \Bigg] + \frac{\tau_{\text{ref}}}{\tau_{\text{m}}}. \end{aligned} \tag{B.26}$$

The order of integration in the double integral can be changed and the second integral can be rewritten by noting that it can only contribute in the first interval (in which v_R is always contained), yielding expression given in eq. (4.25) [p. 85]

$$\left\langle \widehat{T} \right\rangle = \frac{1}{a} \sum_{i=1}^{N} \int_{l_i}^{r_i} dx \int_{x}^{\bar{c}_i} dy\, \theta(x - v_R) \frac{e^{\widehat{\phi}(x) - \widehat{\phi}(y)}}{f(y)} + \int_{v_R}^{\bar{c}_1} dx\, \frac{e^{\widehat{\phi}(v_R) - \widehat{\phi}(x)}}{f(x)} + \frac{\tau_{\text{ref}}}{\tau_{\text{m}}}, \tag{B.27}$$

where $\bar{c}_i$ is the interval boundary opposite of c_i.

B.5. Equivalence of our expression for the LIF firing rate and the one given by Richardson and Swarbrick (2010)

Richardson and Swarbrick (2010) give the firing rate of an LIF (with $\mu = 0$ and $\tau_{\text{ref}} = 0$) driven by excitatory and inhibitory shot noise with exponentially distributed weights in terms of a single integral,

$$\tau_{\text{m}} \widehat{r}_0 = \left[\int_{0}^{1/a_e} dc\, \frac{(1 - a_e c)^{\tau_{\text{m}} r_{\text{in}}^e} (1 - a_i c)^{\tau_{\text{m}} r_{\text{in}}^i}}{c} \left(\frac{e^{c v_T}}{1 - a_e c} - e^{c v_R} \right) \right]^{-1}, \tag{B.28}$$

where a_e (a_i) and r_{in}^e (r_{in}^i) are weight and input rate of excitatory (inhibitory) input. Our expression for the firing rate of a general IF neuron driven by purely excitatory shot noise, eq. (4.25) [p. 85], involves a two-dimensional integral. We thus need to show that for an

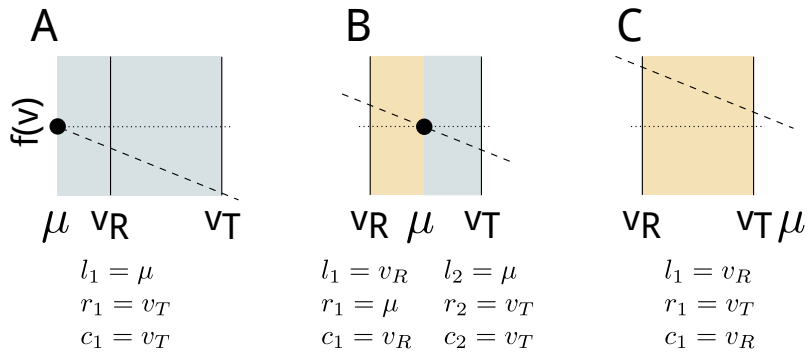

Figure B.1.: Sketch of the three different parameter regimes for a (excitatory-shot-noise-driven) LIF neuron that lead to different solution intervals or different choices of integration constants c_i. Here, $f(v) = \mu - v$.

LIF neuron, this can be reduced to the one-dimensional integral in eq. (B.28), if one sets $a_i = r_{\text{in}}^i = 0$ there. Using eq. (B.20) and settig $\tau_{\text{ref}} = 0$, our expression, eq. (4.25) [p. 85], becomes

$$\tau_{\text{m}}\widehat{r}_0 = \Bigg[\overbrace{\frac{1}{a}\sum_{i=1}^{N} \int_{l_i}^{r_i} dx \int_{x}^{\bar{c}_i} dy\, \theta(x - v_R) \frac{e^{\frac{x}{a}} |\mu - x|^{-\tau_{\text{m}} r_{\text{in}}} \cdot e^{-\frac{y}{a}} |\mu - y|^{\tau_{\text{m}} r_{\text{in}}}}{\mu - y}}^{=:I_i} + \underbrace{\int_{v_R}^{\bar{c}_1} dx\, \frac{e^{\frac{v_R}{a}} |\mu - v_R|^{-\tau_{\text{m}} r_{\text{in}}} \cdot e^{-\frac{x}{a}} |\mu - x|^{\tau_{\text{m}} r_{\text{in}}}}{\mu - x}}_{=:J_1} \Bigg]^{-1}. \tag{B.29}$$

The main task consists in simplifying the double integral I_i.

Richardson and Swarbrick (2010) set $\mu = 0$; however, we cannot simply take $\mu \to 0$ in eq. (B.29). We will thus simplify the full expression and then take $\mu \to 0$ in the end. A particular choice of μ has consequences for the number of intervals N and the values of the constants c_i (illustrated in Fig. B.1). We consider here the case depicted in Fig. B.1B, i.e. $v_R < \mu < v_T$. As, in the end, we let $\mu \to 0$, it should not make a difference if we started from the case depicted in Fig. B.1A.

Changing the order of integration and swapping the symbols x and y, the double integral I_i can be written as

$$I_i = \int_{l_i}^{r_i} dx \int_{c_i}^{x} dy\, \frac{e^{-\frac{x}{a}} |\mu - x|^{\tau_{\text{m}} r_{\text{in}}} \cdot e^{\frac{y}{a}} |\mu - y|^{-\tau_{\text{m}} r_{\text{in}}}}{\mu - x}, \tag{B.30}$$

where we have already used that for the considered parameter regime, the Heaviside

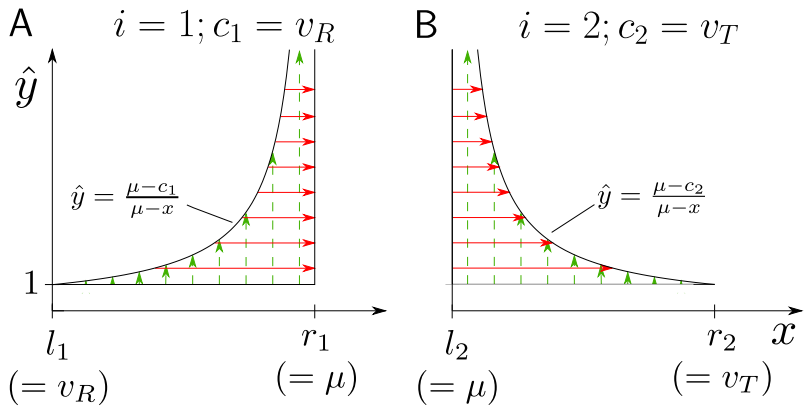

Figure B.2.: Sketch of how the order of integration is changed from eq. (B.32) (green dashed arrows) to eq. (B.33) (red solid arrows). The panels A and B correspond to the different solution intervals.

function is always 1. Making the substitution

$$\widehat{y} := \frac{\mu - y}{\mu - x}, \tag{B.31}$$

the integral reads

$$I_i = \int_{l_i}^{r_i} dx \int_{1}^{(\mu - c_i)/(\mu - x)} d\widehat{y}\ \exp\left[-\frac{(x-\mu)(1-\widehat{y})}{a}\right] \widehat{y}^{-\tau_m r_{in}}. \tag{B.32}$$

After changing the order of integration (see Fig. B.2), one obtains for the two intervals

$$I_i = \begin{cases} \int_1^{\infty} d\widehat{y} \int_{-(\mu - v_R)/\widehat{y} + \mu}^{\mu} dx\ \exp\left[-\frac{(x-\mu)(1-\widehat{y})}{a}\right] \widehat{y}^{-\tau_m r_{in}} & \text{if } i = 1, \\ \int_1^{\infty} d\widehat{y} \int_{\mu}^{-(\mu - v_T)/\widehat{y} + \mu} dx\ \exp\left[-\frac{(x-\mu)(1-\widehat{y})}{a}\right] \widehat{y}^{-\tau_m r_{in}} & \text{if } i = 2. \end{cases} \tag{B.33}$$

This can be written somewhat more compactly,

$$I_i = (\delta_{i,1} - \delta_{i,2}) \cdot \int_1^{\infty} d\widehat{y} \int_{-(\mu - c_i)/\widehat{y}}^{0} d\widehat{x}\ \exp\left[-\frac{\widehat{x}(1-\widehat{y})}{a}\right] \widehat{y}^{-\tau_m r_{in}}, \tag{B.34}$$

where $\delta_{i,j}$ is the Kronecker-δ and where we have substituted $\widehat{x} = x - \mu$. Carrying out the

integration over $\widehat{x}$ leads to

$$I_i = (\delta_{i,1} - \delta_{i,2}) \cdot \int_1^\infty d\widehat{y}\, \frac{a\widehat{y}^{-\tau_\mathrm{m} r_\mathrm{in}}}{1-\widehat{y}} \left(\exp\left[\frac{(\mu - c_i)(1-\widehat{y})}{a\widehat{y}} \right] - 1 \right). \tag{B.35}$$

Going back at eq. (B.29), we rewrite the second integral, J_1, by substituting

$$\widehat{y} = \frac{\mu - v_R}{\mu - x}, \tag{B.36}$$

yielding

$$J_1 = \int_1^\infty d\widehat{y}\, \widehat{y}^{-\tau_\mathrm{m} r_\mathrm{in} - 1} \exp\left[\frac{(\mu - v_R)(1-\widehat{y})}{a\widehat{y}} \right]. \tag{B.37}$$

Plugging eqs. (B.35, B.37) into eq. (B.29), we obtain

$$\tau_\mathrm{m} \widehat{r}_0 = \left[\int_1^\infty d\widehat{y}\, \widehat{y}^{-\tau_\mathrm{m} r_\mathrm{in}} \left(e^{\frac{(\mu - v_R)(1-\widehat{y})}{a\widehat{y}}} \left[\frac{1}{\widehat{y}} + \frac{1}{1-\widehat{y}} \right] - e^{\frac{(\mu - v_T)(1-\widehat{y})}{a\widehat{y}}} \frac{1}{1-\widehat{y}} \right) \right]^{-1} \tag{B.38}$$

Finally, substituting

$$c := -\frac{1-\widehat{y}}{a\widehat{y}}, \tag{B.39}$$

the integral becomes

$$\tau_\mathrm{m} \widehat{r}_0 = \left[\int_0^{1/a} dc\, \frac{1}{c} (1 - ac)^{\tau_\mathrm{m} r_\mathrm{in}} \left(\frac{e^{c(v_T - \mu)}}{1 - ac} - e^{c(v_R - \mu)} \right) \right]^{-1}. \tag{B.40}$$

For $\mu = 0$ (the parameter choice in (Richardson and Swarbrick, 2010)), this can be seen to be identical to eq. (B.28) with $r^e_\mathrm{in} = r_\mathrm{in}, a_e = a, r^i_\mathrm{in} = a_i = 0$.

B.6. Firing rate for shot noise with constant weights at low input rates

Here, we give an approximation for a neuron's firing rate at low input rates if the synaptic weights are finite and constant.

We assume that for the neuron to spike in the time interval τ_m (the membrane time constant), at least N_c spikes have to arrive within that time interval. As the input is

Poisson, the probability to spike in the interval is

$$\begin{aligned}\Pr\left(\text{spike within } \tau_{\mathrm{m}}\right) &= \sum_{k=N_c}^{\infty} \frac{(\tau_{\mathrm{m}} r_{\mathrm{in}})^k}{k!} e^{-\tau_{\mathrm{m}} r_{\mathrm{in}}} \\ &= 1 - e^{-\tau_{\mathrm{m}} r_{\mathrm{in}}} \sum_{k=0}^{N_c-1} \frac{(\tau_{\mathrm{m}} r_{\mathrm{in}})^k}{k!} \\ &= 1 - e^{-\tau_{\mathrm{m}} r_{\mathrm{in}}} e_{N_c-1}\left(\tau_{\mathrm{m}} r_{\mathrm{in}}\right),\end{aligned} \tag{B.41}$$

where $e_n(a)$ is the exponential sum function,

$$e_n(x) := \sum_{k=0}^{n} \frac{x^k}{k!}. \tag{B.42}$$

Using (Abramowitz and Stegun, 1972, 6.5.13, 6.5.2, 6.5.3), we can write

$$e_{n-1}(x) = e^x \frac{\Gamma(n, x)}{\Gamma(n)}, \tag{B.43}$$

where $\Gamma(n)$ is the $(\Gamma(n, x))$ is the (upper incomplete) gamma function, and thus

$$\Pr\left(\text{spike}\right) = 1 - \frac{\Gamma(N_c, \tau_{\mathrm{m}} r_{\mathrm{in}})}{\Gamma(N_c)} = (\tau_{\mathrm{m}} r_{\mathrm{in}})^{N_c} \gamma^*(N_c, \tau_{\mathrm{m}} r_{\mathrm{in}}), \tag{B.44}$$

with $\gamma^*(n, x)$ as defined in (Abramowitz and Stegun, 1972, 6.5.4). If $\tau_{\mathrm{m}} r_{\mathrm{in}} \ll 1$, one has (Abramowitz and Stegun, 1972, 6.5.29),

$$\gamma^*(N_c, \tau_{\mathrm{m}} r_{\mathrm{in}}) = \frac{1}{a\Gamma(N_c)} + \mathcal{O}(\tau_{\mathrm{m}} r_{\mathrm{in}}), \tag{B.45}$$

so that

$$\Pr\left(\text{spike within } \tau_{\mathrm{m}}\right) \approx \frac{(\tau_{\mathrm{m}} r_{\mathrm{in}})^{N_c}}{N_c \Gamma(N_c)} \tag{B.46}$$

The rate is then given by

$$\widehat{r}_0 \approx \frac{1}{\tau_{\mathrm{m}}} \frac{(\tau_{\mathrm{m}} r_{\mathrm{in}})^{N_c}}{N_c \Gamma(N_c)}. \tag{B.47}$$

What is the critical number of spikes? A crude assumption is that the voltage does not decay between the input spikes that arrive within the time window and that the needed

number is thus

$$N_c = \left\lceil \frac{v_T - \mu}{a} \right\rceil , \tag{B.48}$$

where $\lceil \cdot \rceil$ is the ceiling function.

Bibliography

Abbott, L. F. and Regehr, W. G. Synaptic computation. *Nature*, 431(7010):796–803, 2004.

Abbott, L. F., Varela, J. A., Sen, K., and Nelson, S. B. Synaptic depression and cortical gain control. *Science*, 275:220, 1997.

Abramowitz, M. and Stegun, I. A. *Handbook of mathematical functions: with formulas, graphs, and mathematical tables*. Dover, New York, 1972.

Adrian, E. and Zotterman, Y. The impulses produced by sensory nerve-endings: Part II. The response of a Single End-Organ. *J. Physiol.*, 61(2):151, 1926.

Allen, C. and Stevens, C. F. An evaluation of causes for unreliability of synaptic transmission. *Proc. Natl. Acad. Sci.*, 91(22):10380–10383, 1994.

Ancarani, L. and Gasaneo, G. Derivatives of any order of the confluent hypergeometric function. *J. Math. Phys.*, 49:063508, 2008.

Arieli, A., Sterkin, A., Grinvald, A., and Aertsen, A. Dynamics of ongoing activity: explanation of the large variability in evoked cortical responses. *Science*, 273(5283):1868–1871, 1996.

Badel, L., Lefort, S., Brette, R., Petersen, C. C., Gerstner, W., and Richardson, M. J. Dynamic IV curves are reliable predictors of naturalistic pyramidal-neuron voltage traces. *J. Neurophysiol.*, 99(2):656–666, 2008.

Bair, W. and Koch, C. Temporal precision of spike trains in extrastriate cortex of the behaving macaque monkey. *Neural Comput*, 8(6):1185–1202, 1996.

Balakrishnan, V. and Chaturvedi, S. Persistent diffusion on a line. *Physica*, 148A:581, 1988.

Balakrishnan, V. and Lakshmibala, S. On the connection between biased dichotomous diffusion and the one-dimensional Dirac equation. *New J. Phys.*, 7(1):11, 2005.

Banitt, Y., Martin, K. A. C., and Segev, I. A biologically realistic model of contrast invariant orientation tuning by thalamocortical synaptic depression. *J. Neurosci.*, 27(38): 10230–10239, 2007.

Barlow, H. B. Summation and inhibition in the frog's retina. *J. Physiol.*, 119(1):69–88, 1953.

Bauermeister, C., Schwalger, T., Russell, D. F., Neiman, A. B., and Lindner, B. Characteristic effects of stochastic oscillatory forcing on neural firing: analytical theory and comparison to paddlefish electroreceptor data. *PLoS Comput. Biol.*, 9(8):e1003170, 2013.

Beck, J. M., Ma, W. J., Pitkow, X., Latham, P. E., and Pouget, A. Not noisy, just wrong: the role of suboptimal inference in behavioral variability. *Neuron*, 74(1):30–39, 2012.

Bena, I., Van den Broeck, C., Kawai, R., and Lindenberg, K. Nonlinear response with dichotomous noise. *Phys. Rev. E*, 66:045603, 2002.

Bena, I. Dichotomous Markov noise: exact results for out-of-equilibrium systems. *Int. J. Mod. Phys. B*, 20(20):2825–2888, 2006.

Benzi, R., Sutera, A., and Vulpiani, A. The mechanism of stochastic resonance. *J. Phys. A*, 14:L453, 1981.

Benzi, R., Parisi, G., Sutera, A., and Vulpiani, A. Stochastic resonance in climatic change. *Tellus*, 34:10, 1982.

Bernardi, D. and Lindner, B. A frequency-resolved mutual information rate and its application to neural systems. *J. Neurophysiol.*, 113(5):1342–1357, 2015.

Bialek, W., DeWeese, M., Rieke, F., and Warland, D. Bits and brains: Information flow in the nervous system. *Physica A*, 200(1):581–593, 1993.

Bird, A. D. and Richardson, M. J. Long-term plasticity determines the postsynaptic response to correlated afferents with multivesicular short-term synaptic depression. *Front. Comput. Neurosci.*, 8, 2014.

Borst, A. and Theunissen, F. Information theory and neural coding. *Nat. Neurosci.*, 2: 947–958, 1999.

Boudreau, C. E. and Ferster, D. Short-term depression in thalamocortical synapses of cat primary visual cortex. *J. Neurosci.*, 25(31):7179–7190, 2005.

Brunel, N. Dynamics of sparsely connected networks of excitatory and inhibitory spiking neurons. *J. Comput. Neurosci.*, 8(3):183–208, 2000.

Brunel, N. and Latham, P. E. Firing rate of the noisy quadratic integrate-and-fire neuron. *Neural Comput.*, 15(10):2281–2306, 2003.

Brunel, N. and Sergi, S. Firing frequency of leaky intergrate-and-fire neurons with synaptic current dynamics. *J. Theor. Biol.*, 195(1):87–95, 1998.

Brunel, N., Chance, F. S., Fourcaud, N., and Abbott, L. F. Effects of Synaptic Noise and Filtering on the Frequency Response of Spiking Neurons. *Phys. Rev. Lett.*, 86:2186–2189, 2001.

Bulsara and Zador. Threshold detection of wideband signals: A noise-induced maximum in the mutual information. *Phys. Rev. E*, 54(3):R2185–R2188, 1996.

Burkitt, A. N. A review of the integrate-and-fire neuron model: I. Homogeneous synaptic input. *Biol. Cybern.*, 95(1):1–19, 2006a.

Burkitt, A. N. A review of the integrate-and-fire neuron model: II. Inhomogeneous synaptic input and network properties. *Biol. Cybern.*, 95(2):97–112, 2006b.

Collins, J., Chow, C., and Imhoff, T. Aperiodic stochastic resonance in excitable systems. *Phys. Rev. E*, 1995.

Curto, C., Sakata, S., Marguet, S., Itskov, V., and Harris, K. D. A simple model of cortical dynamics explains variability and state dependence of sensory responses in urethane-anesthetized auditory cortex. *J. Neurosci.*, 29(34):10600–10612, 2009.

Danziger, Z. and Grill, W. M. A neuron model of stochastic resonance using rectangular pulse trains. *J Comput Neurosci*, 38(1):53–66, 2015.

Darling, D. A. and Siegert, A. J. F. The first passage problem for a continuous Markov process. *Ann. Math. Stat.*, 24:624, 1953.

Dayan, P. and Abbott, L. F. *Theoretical Neuroscience*. MIT Press, Cambridge, MA, 2001.

de Ruyter van Steveninck, R. R., Lewen, G. D., Strong, S. P., Koberle, R., and Bialek, W. Reproducibility and variability in neural spike trains. *Science*, 275(5307):1805–1808, 1997.

Deneve, S., Latham, P. E., and Pouget, A. Efficient computation and cue integration with noisy population codes. *Nat. Neurosci.*, 4(8):826–831, 2001.

Destexhe, A., Rudolph, M., Fellous, J. M., and Sejnowski, T. J. Fluctuating synaptic conductances recreate in vivo-like activity in neocortical neurons. *Neuroscience*, 107(1): 13–24, 2001.

Destexhe, A. Self-sustained asynchronous irregular states and up–down states in thalamic, cortical and thalamocortical networks of nonlinear integrate-and-fire neurons. *J. Comput. Neurosci.*, 27(3):493–506, 2009.

Destexhe, A. and Rudolph-Lilith, M. *Neuronal noise*. Springer, Heidelberg, 2012.

Diesmann, M., Gewaltig, M.-O., and Aertsen, A. Stable propagation of synchronous spiking in cortical neural networks. *Nature*, 402:529, 1999.

Dimitrov, A. G., Lazar, A. A., and Victor, J. D. Information theory in neuroscience. *J. Comput. Neurosci.*, 30(1):1–5, 2011.

Dittman, J., Kreitzer, A., and Regehr, W. Interplay between facilitation, depression, and residual calcium at three presynaptic terminals. *J. Neurosci.*, 20(4):1374–1385, 2000.

Driver, J. and Noesselt, T. Multisensory Interplay Reveals Crossmodal Influences on 'Sensory-Specific' Brain Regions, Neural Responses, and Judgments. *Neuron*, 57(1): 11–23, 2008.

Droste, F. and Lindner, B. Integrate-and-fire neurons driven by asymmetric dichotomous noise. *Biol. Cybern.*, 108(6):825–843, 2014.

Droste, F., Schwalger, T., and Lindner, B. Interplay of two signals in a neuron with heterogeneous synaptic short-term plasticity. *Front. Comp. Neurosci.*, 7, 2013.

Elliott, T., Kuang, X., Shadbolt, N. R., and Zauner, K.-P. Adaptation in multisensory neurons: Impact on cross-modal enhancement. *Network Comp. Neural.*, 20(1):1–31, 2009.

Erchova, I., Kreck, G., Heinemann, U., and Herz, A. Dynamics of rat entorhinal cortex layer II and III cells: characteristics of membrane potential resonance at rest predict oscillation properties near threshold. *J. Physiol.*, 560(Pt 1):89, 2004.

Faisal, A. A., Selen, L. P. J., and Wolpert, D. M. Noise in the nervous system. *Nat. Rev. Neurosci.*, 9:292, 2008.

Fisch, K., Schwalger, T., Lindner, B., Herz, A. V. M., and Benda, J. Channel noise from both slow adaptation currents and fast currents is required to explain spike-response variability in a sensory neuron. *J. Neurosci.*, 32(48):17332–17344, 2012.

Fitzhugh, R. Statistical properties of the asymmetric random telegraph signal, with applications to single-channel analysis. *Math. Biosci.*, 64(1):75–89, 1983.

Fortune, E. S. and Rose, G. J. Short-term synaptic plasticity as a temporal filter. *Trends Neurosci.*, 24:381, 2001.

Fourcaud, N. and Brunel, N. Dynamics of the firing probability of noisy integrate-and-fire neurons. *Neural Comput.*, 14(9):2057–2110, 2002.

Fourcaud-Trocmé, N., Hansel, D., Van Vreeswijk, C., and Brunel, N. How spike generation mechanisms determine the neuronal response to fluctuating inputs. *J. Neurosci.*, 23(37):11628–11640, 2003.

Foxe, J. J., Morocz, I. A., Murray, M. M., Higgins, B. A., Javitt, D. C., and Schroeder, C. E. Multisensory auditory-somatosensory interactions in early cortical processing revealed by high-density electrical mapping. *Cogn. Brain. Res.*, 10(1-2):77–83, 2000.

Fuhrmann, G., Segev, I., Markram, H., and Tsodyks, M. Coding of temporal information by activity-dependent synapses. *J. Neurophysiol.*, 87(1):140–148, 2002.

Gammaitoni, L., Hänggi, P., Jung, P., and Marchesoni, F. Stochastic resonance. *Rev. Mod. Phys.*, 70:223, 1998.

Gardiner, C. W. *Handbook of Stochastic Methods*. Springer, Heidelberg, 1985.

Gerstein, G. L. and Mandelbrot, B. Random walk models for the spike activity of a single neuron. *Biophys. J.*, 4:41, 1964.

Gerstner, W., Kistler, W. M., Naud, R., and Paninski, L. *Neuronal dynamics: from single neurons to networks and models of cognition*. Cambridge University Press, Cambridge, 2014.

Ghazanfar, A. A. and Schroeder, C. E. Is neocortex essentially multisensory? *Trends Cogn. Sci.*, 10(6):278–285, 2006.

Giard, M. and Peronnet, F. Auditory-visual integration during multimodal object recognition in humans: a behavioral and electrophysiological study. *J. Cognitive Neurosci.*, 11 (5):473–490, 1999.

Goard, M. and Dan, Y. Basal forebrain activation enhances cortical coding of natural scenes. *Nat. Neurosci.*, 12(11):1444–1449, 2009.

Goldman, M. S., Maldonado, P., and Abbott, L. F. Redundancy reduction and sustained firing with stochastic depressing synapses. *J. Neurosci.*, 22:584, 2002.

Goychuk, I. and Hänggi, P. Stochastic resonance in ion channels characterized by information theory. *Phys. Rev. E*, 61:4272–4280, 2000.

Gupta, A., Wang, Y., and Markram, H. Organizing principles for a diversity of GABAergic interneurons and synapses in the neocortex. *Science*, 287(5451):273–278, 2000.

Hartley, R. V. Transmission of information. *Bell Syst. Tech. J.*, 7(3):535–563, 1928.

Helias, M., Deger, M., Diesmann, M., and Rotter, S. Equilibrium and Response Properties of the Integrate-and-Fire Neuron in Discrete Time. *Front Comput Neurosci*, 3:29, 2010a.

Helias, M., Deger, M., Rotter, S., and Diesmann, M. Instantaneous non-linear processing by pulse-coupled threshold units. *PLoS Conput. Biol.*, 6(9):e1000929, 2010b.

Helias, M., Deger, M., Rotter, S., and Diesmann, M. Finite post synaptic potentials cause a fast neuronal response. *Front Neurosci*, 5:19, 2011.

Heneghan, Chow, Collins, Imhoff, Lowen, and Teich. Information measures quantifying aperiodic stochastic resonance. *Phys. Rev. E*, 54(3):R2228–R2231, 1996.

Hodgkin, A. and Huxley, A. A quantitative description of membrane current and its application to conduction and excitation in nerve. *J. Physiol.*, 1952.

Holcman, D. and Tsodyks, M. The emergence of up and down states in cortical networks. *PLoS Comput. Biol.*, 2(3):e23, 2006.

Holden, A. V. *Models of the Stochastic Activity of Neurones*. Springer, Heidelberg, 1976.

Horsthemke, W. and Lefever, R. *Noise induced transitions*. Springer, Heidelberg, 1984.

Hubel, D. H. and Wiesel, T. N. Receptive fields, binocular interaction and functional architecture in the cat's visual cortex. *J. Physiol.*, 160(1):106–154, 1962.

Hänggi, P. Stochastic resonance in biology. How noise can enhance detection of weak signals and help improve biological information processing. *ChemPhysChem*, 3(3):285–290, 2002.

Jacobsen, M. and Jensen, A. T. Exit times for a class of piecewise exponential Markov processes with two-sided jumps. *Stoch. Proc. Appl.*, 117(9):1330–1356, 2007.

Jercog, D. A. *Dynamics of spontaneous activity in the cerebral cortex across brain states*. PhD thesis, Universitat de Barcelona, 2013.

Johnston, D., Wu, S. M.-S., and Gray, R. *Foundations of cellular neurophysiology*. MIT press, Cambridge, MA, 1995.

Kandel, E., Schwartz, J., and Jessell, T. *Principles of Neural Scicence*. McGraw-Hill, New York, 2000.

Katz, B. and Miledi, R. The role of calcium in neuromuscular facilitation. *J. Physiol.*, 195 (2):481–492, 1968.

Keane, A. and Gong, P. Propagating waves can explain irregular neural dynamics. *J. Neurosci.*, 35(4):1591–1605, 2015.

Klyachko, V. and Stevens, C. F. Excitatory and feed-forward inhibitory hippocampal synapses work synergistically as an adaptive filter of natural spike trains. *PLoS Biol.*, 4: 1187, 2006.

Kromer, J. A., Pinto, R. D., Lindner, B., and Schimansky-Geier, L. Noise-controlled bistability in an excitable system with positive feedback. *Europhys. Lett.*, 108(2):20007, 2014.

Kumar, A., Rotter, S., and Aertsen, A. Spiking activity propagation in neuronal networks: reconciling different perspectives on neural coding. *Nat. Rev. Neurosci.*, 11:615, 2010.

Lánský, P. and Lánská, V. Diffusion approximation of the neuronal model with synaptic reversal potentials. *Biol. Cybern.*, 56:19, 1987.

Lapicque, L. Recherches quantitatives sur l'excitation électrique des nerfs traitéecomme une polarization. *J. Physiol. Pathol. Gen.*, 9:620, 1907.

Larkum, M. E., Zhu, J. J., and Sakmann, B. A new cellular mechanism for coupling inputs arriving at different cortical layers. *Nature*, 398(6725):338–341, 1999.

Lefort, S., Tomm, C., Sarria, J.-C. F., and Petersen, C. C. The excitatory neuronal network of the C2 barrel column in mouse primary somatosensory cortex. *Neuron*, 61(2):301–316, 2009.

Levin, J. E. and Miller, J. P. Broadband neural encoding in the cricket cercal sensory system enhanced by stochastic resonance. *Nature*, 380:165, 1996.

Lewis, J. E. and Maler, L. Dynamics of electrosensory feedback: short-term plasticity and inhibition in a parallel fiber pathway. *J. Neurophysiol.*, 88:1695, 2002.

Lewis, J. E. and Maler, L. Synaptic dynamics on different time scales in a parallel fiber feedback pathway of the weakly electric fish. *J. Neurophysiol.*, 91:1064, 2004.

Lindner, B. *Coherence and Stochastic Resonance in Nonlinear Dynamical Systems*. PhD thesis, Humboldt-Universität zu Berlin, 2002.

Lindner, B. A brief introduction to some simple stochastic processes. In Laing, C. and Lord, G., editors, *Stochastic Methods in Neuroscience*. Oxford University Press, Oxford, 2009.

Lindner, B. and Schimansky-Geier, L. Transmission of Noise Coded versus Additive Signals through a Neuronal Ensemble. *Phys. Rev. Lett.*, 86:2934–2937, 2001.

Lindner, B., Schimansky-Geier, L., and Longtin, A. Maximizing spike train coherence or incoherence in the leaky integrate-and-fire model. *Phys. Rev. E.*, 66:031916, 2002.

Lindner, B., García-Ojalvo, J., Neiman, A., and Schimansky-Geier, L. Effects of noise in excitable systems. *Phys. Rep.*, 392:321, 2004.

Lindner, B., Gangloff, D., Longtin, A., and Lewis, J. Broadband coding with dynamic synapses. *J. Neurosci.*, 29(7):2076–2087, 2009.

Lindner, B. Interspike interval statistics of neurons driven by colored noise. *Phys. Rev. E*, 69(2):022901, 2004a.

Lindner, B. Moments of the first passage time under external driving. *J. Stat. Phys.*, 117 (3-4):703–737, 2004b.

Lindner, B. Superposition of many independent spike trains is generally not a Poisson process. *Phys. Rev. E*, 73(2):022901, 2006.

Lisman, J. E. Bursts as a unit of neural information: making unreliable synapses reliable. *Trends Neurosci.*, 20(1):38–43, 1997.

Loebel, A., Silberberg, G., Helbig, D., Markram, H., Tsodyks, M., and Richardson, M. J. Multiquantal release underlies the distribution of synaptic efficacies in the neocortex. *Front. Comput. Neurosci.*, 3, 2009.

London, M., Roth, A., Beeren, L., Häusser, M., and Latham, P. E. Sensitivity to perturbations in vivo implies high noise and suggests rate coding in cortex. *Nature*, 466(7302): 123–127, 2010.

Longtin, A. Stochastic resonance in neuron models. *J. Stat. Phys.*, 70:309, 1993.

Luczak, A., Barthó, P., Marguet, S. L., Buzsáki, G., and Harris, K. D. Sequential structure of neocortical spontaneous activity in vivo. *Proc. Natl. Acad. Sci.*, 104(1):347–352, 2007.

Luczak, A., Bartho, P., and Harris, K. D. Gating of sensory input by spontaneous cortical activity. *J. Neurosci.*, 33(4):1684–1695, 2013.

Ma, W. J. and Pouget, A. Linking neurons to behavior in multisensory perception: A computational review. *Brain Res.*, 1242:4–12, 2008.

Ma, W. J., Beck, J. M., Latham, P. E., and Pouget, A. Bayesian inference with probabilistic population codes. *Nat. Neurosci.*, 9(11):1432–1438, 2006.

Macaluso, E., Frith, C., and Driver, J. Modulation of human visual cortex by crossmodal spatial attention. *Science*, 289(5482):1206–1208, 2000.

Marguet, S. L. and Harris, K. D. State-dependent representation of amplitude-modulated noise stimuli in rat auditory cortex. *J. Neurosci.*, 31(17):6414–6420, 2011.

Markram, H., Lübke, J., Frotscher, M., Roth, A., and Sakmann, B. Physiology and anatomy of synaptic connections between thick tufted pyramidal neurones in the developing rat neocortex. *J. Physiol.*, 500(Pt 2):409, 1997.

Markram, H., Pikus, D., Gupta, A., and Tsodyks, M. Potential for multiple mechanisms, phenomena and algorithms for synaptic plasticity at single synapses. *Neuropharmacol.*, 37(4):489–500, 1998a.

Markram, H., Wang, Y., and Tsodyks, M. Differential signaling via the same axon of neocortical pyramidal neurons. *Proc. Natl. Acad. Sci.*, 95(9):5323–5328, 1998b.

Masoliver, J. First-passage times for non-Markovian processes: Shot noise. *Phys. Rev. A*, 35(9):3918, 1987.

Masquelier, T. Neural variability, or lack thereof. *Front. Comput. Neurosci.*, 7, 2013.

Massimini, M., Huber, R., Ferrarelli, F., Hill, S., and Tononi, G. The sleep slow oscillation as a traveling wave. *J. Neurosci.*, 24(31):6862–6870, 2004.

McDonnell, M. D. and Abbott, D. What is stochastic resonance? Definitions, misconceptions, debates, and its relevance to biology. *PLoS Comput. Biol.*, 5(5):e1000348, 2009.

McNamara, B., Wiesenfeld, K., and Roy, R. Observation of stochastic resonance in a ring laser. *Phys. Rev. Lett.*, 60:2626, 1988.

Mejias, J. F., Kappen, H. J., and Torres, J. J. Irregular dynamics in up and down cortical states. *PLoS One*, 5(11):e13651, 2010.

Meredith, M. and Stein, B. Interactions among converging sensory inputs in the superior colliculus. *Science*, 221(4608):389–391, 1983.

Merkel, M. and Lindner, B. Synaptic filtering of rate-coded information. *Phys. Rev. E*, 81 (4):041921, 2010.

Middleton, J., Chacron, M., Lindner, B., and Longtin, A. Firing statistics of a neuron model driven by long-range correlated noise. *Phys. Rev. E*, 68(2):021920, 2003.

Millman, D., Mihalas, S., Kirkwood, A., and Niebur, E. Self-organized criticality occurs in non-conservative neuronal networks during 'up' states. *Nat. Phys.*, 6(10):801–805, 2010.

Mochol, G., Hermoso-Mendizabal, A., Sakata, S., Harris, K. D., and de la Rocha, J. Stochastic transitions into silence cause noise correlations in cortical circuits. *Proc. Natl. Acad. Sci.*, 112(11):3529–3534, 2015.

Moreno, R., de La Rocha, J., Renart, A., and Parga, N. Response of spiking neurons to correlated inputs. *Phys. Rev. Lett.*, 89(28):288101, 2002.

Morse, P. M. and Feshbach, H. *Methods of Theoretical Physics*. 1953.

Moss, F., Ward, L. M., and Sannita, W. G. Stochastic resonance and sensory information processing: a tutorial and review of application. *Clin Neurophysiol*, 115(2):267–281, 2004.

Müller-Hansen, F., Droste, F., and Lindner, B. Statistics of a neuron model driven by asymmetric colored noise. *Phys. Rev. E*, 91:022718, 2015.

Novikov, A., Melchers, R., Shinjikashvili, E., and Kordzakhia, N. First passage time of filtered Poisson process with exponential shape function. *Prob. Eng. Mech.*, 20(1):57 – 65, 2005.

Nyquist, H. Certain factors affecting telegraph speed. *J. Am. Inst. Elec. Eng.*, 43:412–422, 1924.

Patton, P., Belkacem-Boussaid, K., and Anastasio, T. J. Multimodality in the superior colliculus: an information theoretic analysis. *Cogn. Brain Res.*, 14(1):10–19, 2002.

Petersen, C. C., Hahn, T. T., Mehta, M., Grinvald, A., and Sakmann, B. Interaction of sensory responses with spontaneous depolarization in layer 2/3 barrel cortex. *Proc. Natl. Acad. Sci.*, 100(23):13638–13643, 2003.

Renart, A., de la Rocha, J., Bartho, P., Hollender, L., Parga, N., Reyes, A., and Harris, K. D. The asynchronous state in cortical circuits. *Science*, 327(5965):587–590, 2010.

Ricciardi, L. M. and Sacerdote, L. The Ornstein-Uhlenbeck process as a model for neuronal activity. *Biol. Cybern.*, 35:1, 1979.

Richardson, M. J. E. Firing-rate response of linear and nonlinear integrate-and-fire neurons to modulated current-based and conductance-based synaptic drive. *Phys. Rev. E.*, 76:021919, 2007.

Richardson, M. J. E. Spike-train spectra and network response functions for non-linear integrate-and-fire neurons. *Biol. Cybern.*, 99:381, 2008.

Richardson, M. J. E. Effects of synaptic conductance on the voltage distribution and firing rate of spiking neurons. *Phys. Rev. E*, 69(5 Pt 1):051918, 2004.

Richardson, M. J. E. and Gerstner, W. Statistics of subthreshold neuronal voltage fluctuations due to conductance-based synaptic shot noise. *Chaos*, 16(2):026106, 2006.

Richardson, M. J. and Gerstner, W. Synaptic shot noise and conductance fluctuations affect the membrane voltage with equal significance. *Neural Comput.*, 17(4):923–947, 2005.

Richardson, M. J. and Swarbrick, R. Firing-rate response of a neuron receiving excitatory and inhibitory synaptic shot noise. *Phys. Rev. Lett.*, 105(17):178102, 2010.

Rieke, F., Warland, D., de Ruyter van Steveninck, R., and Bialek, W. *Spikes: Exploring the neural code*. MIT Press, Cambridge, Massachusetts, 1996.

Risken, H. *The Fokker-Planck Equation*. Springer, Heidelberg, 1989.

Rolls, E. T. and Deco, G. *The noisy brain: stochastic dynamics as a principle of brain function*. Oxford university press, Oxford, 2010.

Rosenbaum, R., Rubin, J., and Doiron, B. Short Term Synaptic Depression Imposes a Frequency Dependent Filter on Synaptic Information Transfer. *PLoS Comput. Biol.*, 8 (6), 2012.

Rotman, Z., Deng, P.-Y., and Klyachko, V. A. Short-Term Plasticity Optimizes Synaptic Information Transmission. *J. Neurosci.*, 31:14800, 2011.

Rowland, B., Stanford, T., Stein, B., et al. A model of the neural mechanisms underlying multisensory integration in the superior colliculus. *Perception*, 36(10):1431–1444, 2007.

Rozenfeld, R., Neiman, A., and Schimansky-Geier, L. Stochastic resonance enhanced by dichotomic noise in a bistable system. *Phys. Rev. E*, 62:R3031–R3034, 2000.

Rudolph, M. and Destexhe, A. Correlation Detection and Resonance in Neural Systems with Distributed Noise Sources. *Phys. Rev. Lett.*, 86:3662–3665, 2001.

Sachdev, R. N., Ebner, F. F., and Wilson, C. J. Effect of subthreshold up and down states on the whisker-evoked response in somatosensory cortex. *J. Neurophysiol.*, 92(6):3511–3521, 2004.

Salinas, E. and Sejnowski, T. J. Integrate-and-fire neurons driven by correlated stochastic input. *Neural Comput.*, 14(9):2111–2155, 2002.

Schmid, G., Goychuk, I., and Hänggi, P. Stochastic resonance as a collective property of ion channel assemblies. *Europhys. Lett.*, 56(1):22, 2001.

Schwalger, T. and Schimansky-Geier, L. Interspike interval statistics of a leaky integrate-and-fire neuron driven by Gaussian noise with large correlation times. *Phys. Rev. E*, 77 (3):031914, 2008.

Schwalger, T., Tiana-Alsina, J., Torrent, M., Garcia-Ojalvo, J., and Lindner, B. Interspike-interval correlations induced by two-state switching in an excitable system. *Europhys. Lett.*, 99(1):10004, 2012.

Schwalger, T., Droste, F., and Lindner, B. Statistical structure of neural spiking under non-Poissonian or other non-white stimulation. *J. Comput. Neurosci.*, 2015.

Sekuler, R., Sekuler, A., and Lau, R. Sound alters visual motion perception. *Nature*, 385 (6614):308–308, 1997.

Shams, L., Kamitani, Y., and Shimojo, S. What you see is what you hear. *Nature*, 408: 788–788, 2000.

Shannon, C. E. Communication in the presence of noise. *Proc. IRE*, 37:10, 1949.

Shannon, R. The Mathematical Theory of Communication. *Bell. Syst. Tech. J.*, 27:379, 1948.

Shimojo, S. and Shams, L. Sensory modalities are not separate modalities: plasticity and interactions. *Curr. Opin. Neurobiol.*, 11(4):505–509, 2001.

Shu, Y., Hasenstaub, A., and McCormick, D. A. Turning on and off recurrent balanced cortical activity. *Nature*, 423(6937):288–293, 2003.

Siegert, A. J. F. On the First Passage Time Probability Problem. *Phys. Rev.*, 81:617–623, 1951.

Sirovich, L., Omurtag, A., and Knight, B. Dynamics of neuronal populations: The equilibrium solution. *SIAM J. Appl. Math.*, 60(6):2009–2028, 2000.

Sirovich, L. Dynamics of neuronal populations: eigenfunction theory; some solvable cases. *Network*, 14(2):249–272, 2003.

Song, S., Sjöström, P. J., Reigl, M., Nelson, S., and Chklovskii, D. B. Highly nonrandom features of synaptic connectivity in local cortical circuits. *PLoS Biol.*, 3(3):e68, 2005.

Stein, B. and Stanford, T. Multisensory integration: current issues from the perspective of the single neuron. *Nat. Rev. Neurosci.*, 9(4):255–266, 2008.

Stein, R. B. A theoretical analysis of neuronal variability. *Biophys. J.*, 5:173, 1965.

Stein, R. B., French, A. S., and Holden, A. V. The frequency response, coherence, and information capacity of two neuronal models. *Biophys. J.*, 12:295, 1972.

Steriade, M., Timofeev, I., and Grenier, F. Natural waking and sleep states: a view from inside neocortical neurons. *J. Neurophysiol.*, 85(5):1969–1985, 2001.

Stratford, K. J., Tarczy-Hornoch, K., Martin, K. A., Bannister, N. J., and Jack, J. J. Excitatory synaptic inputs to spiny stellate cells in cat visual cortex. *Nature*, 382(6588):258–261, 1996.

Stratonovich, R. L. *Topics in the Theory of Random Noise*. Gordon and Breach, London, 1967.

Thomson, A. M., Deuchars, J., and West, D. C. Large, deep layer pyramid-pyramid single axon EPSPs in slices of rat motor cortex display paired pulse and frequency-dependent depression, mediated presynaptically and self-facilitation, mediated postsynaptically. *J. Neurophysiol.*, 70(6):2354–2369, 1993.

Torres, J., Marro, J., and Mejias, J. Can intrinsic noise induce various resonant peaks? *New J. Phys.*, 13:053014, 2011.

Tsodyks, M. V. and Markram, H. The neural code between neocortical pyramidal neurons depends on neurotransmitter release probability. *Proc. Natl. Acad. Sci.*, 94(2):719–723, 1997.

Tsurui, A. and Osaki, S. On a first-passage problem for a cumulative process with exponential decay. *Stoch. Proc. Appl.*, 4(1):79–88, 1976.

Tuckwell, H. C. *Introduction to theoretical neurobiology: Volume 2, nonlinear and stochastic theories*, volume 8. Cambridge University Press, Cambridge, 1988.

Van Den Broeck, C. On the relation between white shot noise, Gaussian white noise, and the dichotomic Markov process. *J. Stat. Phys.*, 31(3):467–483, 1983.

Vere-Jones, D. Simple stochastic models for the release of quanta of transmitter from a nerve terminal. *Aust. J. Stat.*, 8(2):53–63, 1966.

Vilela, R. D. and Lindner, B. Comparative study of different integrate-and-fire neurons: Spontaneous activity, dynamical response, and stimulus-induced correlation. *Phys. Rev. E*, 80:031909, 2009.

Vogels, T. P. and Abbott, L. F. Signal propagation and logic gating in networks of integrate-and-fire neurons. *J. Neurosci.*, 25:10786, 2005.

Vyazovskiy, V. V. and Harris, K. D. Sleep and the single neuron: the role of global slow oscillations in individual cell rest. *Nat. Rev. Neurosci.*, 14(6):443–451, 2013.

White, J. A., Rubinstein, J. T., and Kay, A. R. Channel noise in neurons. *Trends Neurosci.*, 23(3):131–137, 2000.

Wolff, L. and Lindner, B. Method to calculate the moments of the membrane voltage in a model neuron driven by multiplicative filtered shot noise. *Phys. Rev. E*, 77:041913, 2008.

Wolff, L. and Lindner, B. Mean, variance, and autocorrelation of subthreshold potential fluctuations driven by filtered conductance shot noise. *Neural Comput.*, 22(1):94–120, 2010.

Yamamoto, N., Yamada, K., Kurotani, T., and Toyama, K. Laminar specificity of extrinsic cortical connections studied in coculture preparations. *Neuron*, 9(2):217–228, 1992.

Zagha, E., Casale, A. E., Sachdev, R. N., McGinley, M. J., and McCormick, D. A. Motor cortex feedback influences sensory processing by modulating network state. *Neuron*, 79(3):567–578, 2013.

Zucker, R. and Regehr, W. Short-term synaptic plasticity. *Annu. Rev. Physiol.*, 64(1):355–405, 2002.

Danksagung / Acknowledgments

Diese Arbeit wäre ohne die engagierte Betreuung durch Prof. Dr. Benjamin Lindner nicht möglich gewesen. Dafür, dass er mir sehr viel beigebracht, immer ein offenes Ohr gehabt, und mich immer wieder ermutigt hat, möchte ich mich ganz herzlich bedanken!

Meine netten Kollegen haben die Arbeitsgruppe "Theorie komplexer Systeme und Neurophysik" zu einem angehmen Arbeitsplatz gemacht. Nicht zuletzt dank Nikola Schrenks organisatorischer Umsicht konnte ich mich hier ganz auf Neurophysik und Tischkicker konzentrieren.

Dem DFG-Graduiertenkolleg 1589/1 "Sensory Computation in Neural Systems" verdanke ich nicht nur ein Stipendium, sondern auch die Gelegenheit einen breiten Einblick in aktuelle Forschungsfelder der theoretischen Neurowissenschaft zu erhalten. Besonders sei hier Dr. Vanessa Casagrande, Margret Franke, Julia Schaeffer und Dr. Robert Martin gedankt, die durch ihre warme Art noch dem drögsten Verwaltungsakt den Schrecken genommmen haben.

Prof. Dr. Susanne Schreiber und Prof. Dr. Lutz Schimansky-Geier haben mir im Rahmen des Graduiertenkollegs regelmäßig Rückmeldung und hilfreiche Ratschläge gegeben. Dafür vielen Dank!

Dr. Tilo Schwalger hat mir, insbesondere in der Anfangszeit, mit großem Enthusiasmus und viel Geduld auf zahlreiche Fragen geantwortet und diese Arbeit nachhaltig beeinflusst.

Besonderer Dank gilt Davide Bernardi, Sven Blankenburg, Jens Doose, Hubert Droste, Jordi Giner Baldó, Alexandra Kruscha, Sergej Voronenko und Dr. Stefan Wieland. Sie haben Teile dieser Arbeit Korrektur gelesen und durch hilfreiche Kommentare sicher dazu beigetragen, sie zu verbessern.

Meinen Eltern Hubert Droste und Verena Fuchs möchte ich für die liebevolle Unterstützung danken. Das gilt auch für Alicia Dorado Corsino, die mich in schwierigeren Phasen immer wieder aufgerichtet und, vor allem, ertragen hat. Danke!

Selbständigkeitserklärung

Ich erkläre, dass ich die vorliegende Arbeit selbständig und nur unter Verwendung der angegebenen Literatur und Hilfsmittel angefertigt habe.

Berlin, den 2. September 2015 Felix Droste